DISPERSION MODELING OF OXIDES OF NITROGEN, SULFUR DIOXIDE AND $PM_{2.5}$ IN THE PROVINCE OF NOVA SCOTIA, CANADA

by

Soumita Kundu

Submitted in partial fulfilment of the requirements
for the degree of Master of Applied Science

at

Dalhousie University
Halifax, Nova Scotia
September 2011

DALHOUSIE UNIVERSITY

DEPARTMENT OF ENVIRONMENTAL ENGINEERING

The undersigned hereby certify that they have read and recommend to the Faculty of Graduate Studies for acceptance a thesis entitled "DISPERSION MODELING OF OXIDES OF NITROGEN, SULFUR DIOXIDE AND $PM_{2.5}$ IN THE PROVINCE OF NOVA SCOTIA, CANADA" by Soumita Kundu in partial fulfillment of the requirements for the degree of Master of Applied Science.

Dated: September 6, 2011

Supervisor: _____

Readers: _____

_____

DALHOUSIE UNIVERSITY

DATE: September 6, 2011

AUTHOR: Soumita Kundu

TITLE: DISPERSION MODELING OF OXIDES OF NITROGEN, SULFUR DIOXIDE AND $PM_{2.5}$ IN THE PROVINCE OF NOVA SCOTIA, CANADA

DEPARTMENT OR SCHOOL: Department of Environmental Engineering

DEGREE: MASc CONVOCATION: May YEAR: 2012

_____

Signature of Author

DEDICATION

This thesis is dedicated to the late Mr. A. K. Gundappa, who taught me to be competently self-dependent, and bold enough to pursue my goals in life. It is also dedicated to my respected mentor, Mr. Sunil Saha, who taught me the importance of self-learning, and that quality work is born out of dedication.

TABLE OF CONTENTS

LIST OF FIGURES

LIST OF TABLES

ABSTRACT

This study focuses on NO_x, $PM_{2.5}$ and SO_2 dispersion modeling in seven domains across the province of Nova Scotia. The emission sources of the above pollutants include major industrial sources and highways across the province. US EPA steady state Gaussian Plume model AERMOD is used to conduct the dispersion simulation study. Due to the limitation of AERMOD to compute the short range (<50km) dispersion, the domains are of size equal to or less than 50 km. Pollutant emission data, vehicle count and the emission source's characteristics were taken from the NPRI database. Although this study was aimed to conduct the dispersion modeling for a span of four year from 2004 to 2007, due to missing records in the database, simulations were carried out in different years in each domain depending upon maximum available data for model input. Meteorological data is obtained from Halifax International Airport, Sydney and Yarmouth MET stations. Elevations of the surface are obtained using Geotiff files from ArcGIS v9.3. Nova Scotia's Comprehensive Air Pollutant Emission Source Inventory is used to obtain emission source characteristics and total emissions per year. Modeling results demonstrate that dispersion of the pollutants is governed by the wind direction, ambient temperature and emission rate of the NO_x, $PM_{2.5}$ and SO_2. Modeling results of NO_x, $PM_{2.5}$ and SO_2 are compared with Environment Canada's monitored NAPS data during 2004. The comparison results show better agreement between monitored and modeled data in Sydney and Prohawksbury areas compared to Halifax. This phenomenon is caused by the exclusion of ship emission at Halifax harbor and automobile emission in downtown Halifax area. Overall the model showed reasonable agreement with the monitored values. Model performance can be improved by including more number of available emission sources and hourly emission rates.

LIST OF ABBREVIATIONS AND SYMBOLS USED

Air Dispersion Models- ADM

Air Quality Branch- AQB

Canada Wide Standard- CWS

Convective boundary layer- CBL

Criteria Air Contaminants- CAC

Digital Elevation Model- DEM

Emission rate- ER

Ground level concentration- GLC

Halifax- HFX

Halifax International Airport meteorological station- YHZM

Hydroxyl- OH

Light duty commercial vehicle- LDCV

Light duty passenger vehicle- LDPV

Lunenburg- LNN

Maximum- MAX

Minimum- MIN

Medium duty commercial vehicle- MDCV

Meteorology- MET

National Air Pollution Surveillance- NAPS

National Pollutant Release Inventory- NPRI

Nitrogen oxide- NO

Nitrous oxide- N_2O

Nitrogen dioxide- NO_2

Not Available- NA

Nova Scotia- NS

Nova Scotia Air Quality Branch- NSAQB

Oxides of Nitrogen- NO_x

Ozone- O_3

Particulate matter- PM

Particulate matter diameter size 2.5 micron or less- $PM_{2.5}$

Particulate matter diameter size 10 micron or less- PM_{10}

Pictou- PIC

Planetary Boundary Layer-PBL

Point Aconi- PTA

PortHawksbury- PRTHWKS

Stable Boundary Layer- SBL

Sulfur dioxide- SO_2

Sydney- SYD

Sydney meteorological station- SYDM

Total Particulate Matter- TPM

Truro- TRR

United States Environmental Protection Agency- US EPA

Volatile Organic Compounds- VOC

Weather Research Forecast- WRF

ACKNOWLEDGEMENT

It has been my distinct pleasure to have had the opportunity to work under the guidance of my research advisor, Dr. Mysore Satish. The fundamental ideas provided by Dr. Satish helped me to have a strong base for my entire thesis. His faith in me allowed me the confidence to carry out my independent research, and I owe him my deepest gratitude for always remaining positive throughout our time together.

Without the support of Mr. Johnny McPherson, and Mr. Will A. Green, from Nova Scotia Environment, this thesis would not have been possible. I am grateful to Mr. McPherson, and Mr. Green, for the extensive data resources they provided for computational purposes. My sincerest thank you to Ms. Barb Bryden, and Ms. Fran Deceasers, for the essential NAPS data required for model validation.

It has been an honor to have had Dr. Lei Liu, and Dr. Mark Gibson as teachers. The knowledge they provided gave me direction to begin my thesis, and their valuable review was essential for the successful completion of this research. I cannot find the words to thank Dr. Gibson for his crucial inputs.

It gives me great pleasure to acknowledge the support and instruction of Ms. Jennifer Strang, from the GIS Centre at Dalhousie University, and Mr. Gavin King, from Community Health and Epidemiology. Their comprehension of GIS data has been an immeasurable resource for mapping the simulated data.

I would also like to show my gratitude to the office staff of the Department of Civil and Resource Engineering and to my beloved brother Arunava Majumdar, my friends James Wilson, Jibril Olatunde, Matthew Cole and others who have been there in times of need and hardship.

A very special thank you is owed to Dr. Sudhakar. M Rao, Dr Subba Rao K.S and Dr. Rudrappa Shettally, for believing in me, and my potential to succeed in research work.

Finally I would like to express my heartfelt gratitude to late Mr. A. K. Gundappa as well as my parents, Dr. Shambhu Kundu, and Dr. Lapita Kundu, for their unconditional encouragement and support throughout my educational journey thus far.

CHAPTER 1: INTRODUCTION

Air pollutants such as oxides of nitrogen (NO_x), particulate matter with median aerodynamic diameter less than 2.5 micron ($PM_{2.5}$), sulfur dioxide (SO_2), volatile organic compounds (VOC) are described as the criteria air contaminants (CAC). Sources of $PM_{2.5,}$ NO_x and SO_2 include biogenic, geogenic, anthropogenic local and long-range emissions and secondary formations within the atmosphere (De Gouw et al., 2008; Harrison et al., 1997; Garcia et al., 2004; Atari, Luginaah, Xu, & Fung, 2008; M. D. Gibson et al., 2009; Dongarrà, Manno, Varrica, Lombardo, & Vultaggio, 2010; La Spina, Burton, & Salerno, 2010; Lu et al., 2006). The source contributions of $PM_{2.5,}$ NO_x and SO_2 to the atmosphere and impacts on receptors display diurnal and seasonal variability, driven by meteorology and influenced by local topography (Wagstrom & Pandis, 2011; M. D. Gibson et al., 2009; M. Gibson et al., 2010; Riga-Karandinos & Saitanis, 2005). CACs play a major role in degrading the natural resources such as vegetation, land and ecosystem. CACs can cause acid deposition which in turn depletes soil nutrient. Many studies have shown that acute and chronic exposure to $PM_{2.5}$, NO_x and SO_2 are significantly associated with increases in mortality (Dockery et al., 1993; Neupane et al., 2010;C.A. I. Pope, 2000; Stieb, Judek, & Burnett, 2002; Stieb et al., 2008; Krewski et al., 2005).

CACs travel regionally as well as globally, once they are emitted from the source of generation. The concentration of air pollutants reduces by various phenomena such as diffusion, advection, chemical loss and deposition. The movement of air pollutants governed by both advection and diffusion is referred as dispersion. Dispersion pattern of the air pollutants is influenced by different factors such as the meteorology; terrain condition, land cover type and characteristics of the emission sources. Dispersion is one of the most effective removal processes for CACs from the atmosphere along with removal by chemical reactions and deposition (Thad, 2004).

Air pollutant dispersion modeling can estimate the source contribution of point, line, volume and area sources to surface air quality in an airshed with given emission source characteristics, land use, terrain and meteorological data (Johnson, Isakov, Touma, Mukerjee, & Özkaynak, 2010).A commonly used regulatory air pollution dispersion model is the American Meteorological Society and U.S. Environmental Protection Agency Regulatory Model AERMOD (A. J. Cimorelli et al., 2005; (A. J. Cimorelli et al., 2003). AERMOD is a steady-state Gaussian plume

dispersion model aimed at short-range (< 50 km) dispersion from point, line area and volume sources (A. J. Cimorelli et al., 2003; A. J. Cimorelli et al., 2005). Dispersion models such as ISC-PRIME and ISCST3 work on Pasquill-Gifford stability class-based plume dispersion, whereas AERMOD View v6.2 (Lakes Environmental™, 450-2 Philip St, Waterloo, ON, N2L 5J2, Canada) uses PBL concept to incorporate meteorological data pre-processing (AERMET) (A. J. Cimorelli et al., 2003). AERMOD has been promulgated by the USEPA as a preferred air dispersion model to replace the ISCST3 (S. Lee & Keener, 2008).

In this study dispersion modeling of $PM_{2.5}$, NO_x and SO_2 is established in seven different domains across Nova Scotia (NS) in different years during 2004-2007 by using AERMOD View v6.2. Simulation year for each domain was chosen based upon maximum available model input data from the NPRI database. The main sources of $PM_{2.5}$, NO_x and SO_2 in NS, Canada are power generation, domestic and industrial space heating, construction activity, ship emissions, vehicle emissions, resuspended dust. The majority of long-range transport originates from the North East US and the Windsor - Québec corridor (M. D. Gibson, Guernsey et al., 2009; Waugh, 2006; Bryden, 2009).

The main interest of this study is to conduct dispersion modeling to delineate the airshed of Nova Scotia and help the provincial government to make decisions on rules and regulations to control the emission of air pollutants, well within permissible limits (Green, 2008). The modeling study was carried out based upon available emission data from a number of point and linear emission sources across the province. A comparison study between model predictions and NAPS data is conducted for the year 2004 in four different domains for NO_x, $PM_{2.5}$ and SO_2. An ArcGIS map (ESRI, 2008) of 1km is used as a base map for the modeling purpose to understand the population or property exposure to the air pollutants at specific receptor locations.

1.1 OBJECTIVES

The three main objectives of this research project are:

1. To determine the surface dispersion pattern of $PM_{2.5}$, NO_x and SO_2 from point and line emission sources in seven model domains across the province of NS.

2. To compare model performance with measured data from NAPS stations.

3. To prepare a database to provide information on community exposure to air pollutants, health risk assessment and airshed management.

Thesis Organization

This thesis contains five sections. The sections are as follows,

1. **Literature Review:** This section includes a brief description of air pollution history, effect of air pollution, factors affecting the air pollutant dispersion in the atmosphere, air pollutant dispersion modeling and previous studies using AERMOD.

2. **Dispersion Study Approach in the Province of Nova Scotia:** This section includes dispersion modeling approach in the province of Nova Scotia, description of the seven modeling domains across the province, information about point and linear emission source characteristics, methods of emission factor calculation and the method of comparing the NAPS observed and model predicted values. The results of preprocessed meteorological and terrain data using AERMET and AERMAP respectively are also given in this section.

3. **Results and Discussion:** This section includes results and discussion on AERMOD predicted GLCs and dispersion patterns of NO_x, SO_2 and $PM_{2.5}$ in seven modeling domains. Also comparison between the modeled and observed values of the above three pollutants are discussed in this section.

4. **Conclusions:** This section includes the summary and findings of the dispersion modeling of NO_x, SO_2 and $PM_{2.5}$ in the province of Nova Scotia.

5. **Recommendations:** This section includes the possible inclusion of a number of factors into the model that can improve the model performance.

CHAPTER 2: LITERATURE REVIEW

Air pollution is a common phenomenon since ancient times (Masters, 1997). In the Middle Ages smoke from coal burning was considered as a serious air pollution problem impacting health and the environment (Masters, 1997). Air pollution can be defined as the contamination of the atmosphere by gaseous, liquid and solid waste that is detrimental to the human health and environment. Air pollution control became a major concern after several serious air pollution episodes in the past. A four-day episode persisted over a small town in Donora, Pennsylvania, United States and was caused by settlement of anticyclonic inversion on the valley floor (Bell, Davis, & Fletcher, 2004). The town had a population of only 14000 and almost 6000 became ill due to the air pollution and 20 people died. Another major air pollution episode persisted in 1952 in London. On 5th December 1952, dense smog covered London city for a week. The smog caused 3000 more deaths than normal during this period (Bell et al., 2001). The analysis by Bell 2001 demonstrates that only a fraction of mortality was caused due to influenza and rest through the delayed effect of the smog. Study of Bell et al., 2001also showed that, death due to respiratory diseases in 1953 January and February was more highly correlated than the later weeks in 1952 December. The above incident implies that, London smog episode had not only the acute effect but also the chronic effect. Air pollution study was speeded up after the London smog episode due to excessive mortality and morbidity due to air pollution (Bell et al., 2004). The atmosphere serves as a sink for the air pollutants up to a certain limit. The capability of the atmosphere to carry away, dilute and scavenge air pollutants is termed fate and transport. Air pollutant transport in the atmosphere is governed by a number of factors such as meteorology and terrain effect (Bell & Davis, 2001). An important feature of air pollution transport is the dispersion of the pollutant release within the air mass as it is advected away from the source region (Masters, 1997) (Schnelle & Dey, 2000).

This section includes the review of the composition of the atmosphere, meteorological factors that affect the air dispersion of and air pollutant dispersion study using a Gaussian Plume steady state model AERMOD.

2.1 Composition of the Atmosphere

Earth's atmosphere is a mixture of number of gasses along with water vapor present in it. The main constituents of the atmosphere include nitrogen (78.01%), Oxygen (20.94%) and 1% of various other gases comprising xenon, carbon dioxide, hydrogen, argon, neon, helium, and krypton. The atmosphere also contains water vapor, pollen, dust, and other particles. Under high temperatures, nitrogen combines with oxygen to form nitrogen monoxide (NO), nitrous oxide (N_2O), and nitrogen dioxide (NO_2). The earth's atmosphere reaches nearly 600 kilometers from the Earth surface. The atmosphere is divided into four distinct layers (Figure 1) depending upon thermal characteristics, chemical composition, movement, and density.

The Troposphere, also known as the 'boundary layer' is the bottom most layer and penetrates to a height of 7 to 20 km above sea level starting at Earth's surface. Most of the weather conditions and pollution occurs within this layer. The layer between the Troposphere and Stratosphere is called as Tropopause. The Stratosphere lies above the Troposphere and below the Mesosphere with a thickness of 30km. This layer is relatively free from turbulence. The Mesosphere starts at 50 km above Earth's surface and extends vertically to 85 km. The temperature in this layer reduces with the height. The layer between the Mesosphere and the Thermosphere is known as Mesopause. It is the fourth layer of the Earth's atmosphere from the earth's surface. This layer is about 90 km thick. Gases stay in ionized form in this layer (Masters, 1997).

Figure 1 Vertical Structure of the Atmosphere

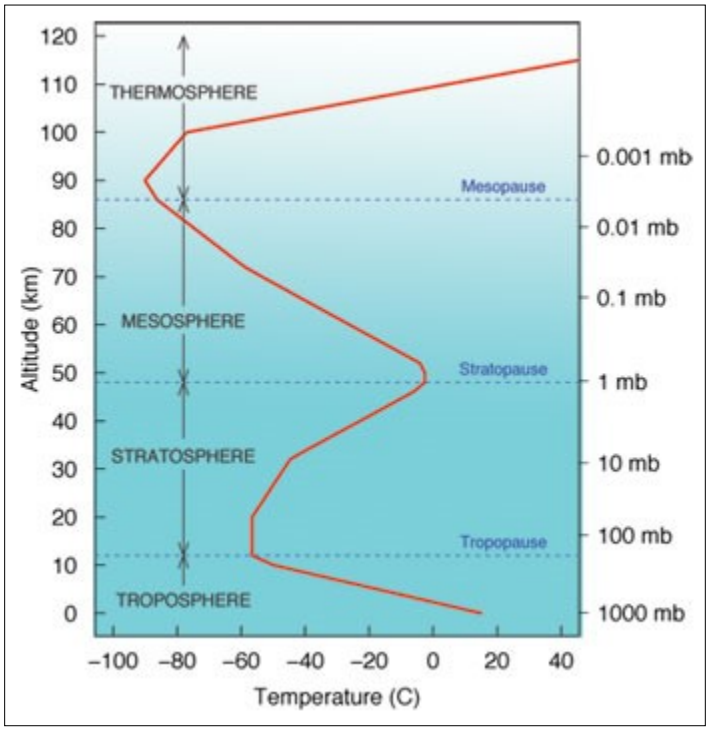

(Source**:** Steven C. Wofsy, 2006)

2.2 **Air Quality E**ffect on Human Health and the Environment

Air quality is a critical issue as it has important impacts on human health, vegetation, buildings and the economy. To reduce risks, it is essential to know, the types of air pollutants, their effect, source and their concentration at various locations.

Air contaminants are particulates or gaseous substances that originate from natural sources such a**s** dust, pollen, salt particles, and smoke from forest fires, volcanic eruptions and gases from organic wastes. Anthropogenic sources include combustion of fossil fuels, automobile emissions and construction activity. Volatile organic compounds (VOCs) from biogenic sources contribute the major portion of the pollution in the ambient atmosphere. Particulate matters consist of complex and varying mixtures of particles suspended in the ambient air. These particles vary in size and composition (Pöschl, 2005). The particles having a median aerodynamic diameter smaller than 2.5 micron and 10 micron are termed as $PM_{2.5}$ and PM_{10} respectively. The sources of these particulate matters are the energy generation, acid production and metallurgical operations.

Churg, 1996 suggested that the persistence of $PM_{2.5}$ in the lungs for a longer period of time results in respiratory diseases and deaths. Pope, 1996 demonstrated that PM_{10} is strongly associated with lower respiratory symptoms and cough. Perez et al., 2009 suggested that there is a higher mortality risk when PM_{10} interacts with soil particles.

Gaseous pollutants have major effect on the atmospheric composition changes. Gaseous pollutants such as NO_x, SO_2, VOC, ground level ozone (O_3) as secondary pollutant etc. are generated from the mobile and stationary combustion sources, which use fossil fuel (Katsouyanni, 2003 ; Kampa & Castanas, 2008). Katsouyanni, 2003 also demonstrated that NO rapidly reacts with ozone or radicals in the atmosphere forming NO_2. Free radicals of nitrogen species are detrimental to cellular lipids, proteins, and nuclear- or mitochondrial- DNA (Valko et al., 2007). Necrosis, cell death, lung diseases can be caused from chronic effect of the NO_x exposure (Bascom, 1996).

Another potential air pollutant is SO_2. Natural sources of SO_2 are volcanoes (Geogenic), oceans and anthropogenic sources such as combustion of sulfur-containing coal and heavy oils. Sandstrom's (1988) investigation demonstrated that an early exposure to SO_2 can cause eye irritations. SO_2 is also responsible for chronic effect such as immune system suppression, for an increased probability of bronchitis and may even lead to cancer (Bascom, 1996; Pearson, Watchel, & Ebi, 2000). Air quality in the vicinity of roadways can be seriously impacted by emission from heavy traffic flows. As a result, high concentration of air pollutants are frequently observed in the vicinity of roadways and have been shown to result in a range of health outcomes such as reduced lung function (Brunekreef et al., 1997), adverse respiratory symptoms (Venn, Lewis, Cooper, Hubbard, & Britton, 2001), asthma and mortality (Beelen et al., 2008). Dockery conducted a study on the association between the air quality and mortality in six US cities in year 1993. The study demonstrated that the fine particulates and sulfates were majorly generated from the long-term transport and mixing of combustion product in large scale. Fine inhalable and sulfate particles have more effect on mortality than the total particulate pollution. Relationship between the mortality and air pollution remain significantly unchanged when other factors such as cigarette smoking and occupational exposure to pollutants were not considered (Bell et al., 2004).

O_3 can interfere with biochemical and physiological processes in the plants (M. D. Gibson, Guernsey et al., 2009). As a result these can cause reduction in productivity and death of the plant. Material surfaces get damaged by SO_2 and sulfuric acid deposition (Tidblad, Kuvera, & Mikhailov, 1988). Sulfur is released as SO_2 and SO_3 when the sulfur containing fuel is burnt. SO_2 reacts with free OH radical and atmospheric oxygen to form sulfur trioxide. This sulfur trioxide reacts very quickly with the water to form sulfuric acid (Masters, 1997). Reactions 1 through 3 demonstrates the mechanism of sulfuric acid generation in the atmosphere,

$$SO_2 + OH \longrightarrow HOSO_2 \qquad [1]$$

$$HOSO_2 + O_2 \longrightarrow SO_3 + HO_2 \qquad [2]$$

$$SO_3 + H_2O \longrightarrow H_2SO_4 \qquad [3]$$

Aquatic and terrestrial ecosystems can be severely impacted by acid rain caused by H_2SO_4 wet and dry deposition (Masters, 1997). SO_2 can cause high yield reductions by interfering with crop's awn structure (Taylor, Ashmore, & Bell, 1986).

2.3 Air Pollutant Dispersion

Air Pollutants are released from ground level and elevated sources into the Planetary Boundary Layer (PBL) and directly affected by Earth's surface. They are subjected to atmospheric processes by increasing the volume of air both horizontally and vertically immediately after the release from sources. When the air pollutant moves into the atmosphere by both advection and diffusion, it is termed as dispersion. Dispersion causes dilution of the air pollutant concentration with distance in the downwind direction. Dilution of the air pollutants begin at the point of release from the continuously releasing stacks (Schnelle & Dey, 2000). Free dispersal of the air pollutants are affected by several factors which are discussed in the following paragraphs (Thad, 2004).

2.4 Effect of Wind on Air Pollutant Dispersion

P.Goyal et al. (2001) reported that plume dilution is inversely proportional to wind speed. In urban areas, due to high surface roughness the wind speed is lower which in turn affects the

relatively high ground level pollutant concentrations. Under low wind conditions the dispersion of pollutants becomes weak resulting in large GLC. The authors study found that the largest mean GLC due to elevated sources are typically found under daytime convective conditions with moderate to weak winds. A study of Okamoto & Shiozawa, 1978 for ground level sources showed that high GLC may occur due to weak horizontal dispersion.

Arya, 1995 defined the wind speed as low when the surface wind speed at 10 m level is less than 2 m s^{-1}. He showed that low winds pose a particular problem in Gaussian plume dispersion models, since concentration is inversely proportional to the wind speed, resulting in over prediction of concentration when wind speed approaches zero. Large pollutant concentrations might occur under convective low wind conditions due to elevated point sources (Moore, 1969). The Gaussian plume model produces unreasonable results when applied to diffusion in low wind cases as downwind diffusion is neglected in comparison to the advection (Bass, Benkley, Scire, & Mories, 1979); (Zannetti, 1986). The pollutant concentration is inversely proportional to wind speed and therefore, the concentration approaches infinity as the wind tends to zero and the average concentrations are stationary (Anfossi, Brusasca, & Tinarelli, 1990).

Wind direction has significant effect on air quality (Schnelle & Dey, 2000). Wind direction can change widely between 0 degree and 360 degrees in a short period of time. Downwind of point source where wind is relatively persistent experiences more of GLC than other areas at similar distance. Wind direction is important for dispersion of pollutants over a large geographical area. Southwesterly wind carries acid precursors from the United States to Northeastern states and Southeastern states of Canada (Schnelle & Dey, 2000).

2.5 Atmospheric Stability

Ashrafi & Hoshyaripour, 2010, have shown that atmospheric stability has significant influence over air contaminant dispersion. The degree of stability impacts the rate of air pollutant removal from the atmosphere. As atmospheric stability is dependent upon the ambient temperature, it changes with season and time of the day. During winter, night and early morning more stable conditions exist. The atmosphere is more unstable during summer and day time (Ashrafi & Hoshyaripour, 2010). Stability classification is made on the basis of popular schemes such as Pasquill-Gifford stability classification and Monin-Obukhov length (Agarwal& Tandon, 2010).

Their research demonstrated that the GLC is lowest for unstable and highest for stable atmospheric conditions. The most popular and oldest stability classification scheme is the Pasquil-Gifford stability classification. Pasquill classified the atmosphere in six stability classes such as A- very unstable, B- unstable, C-slightly unstable, D-neutral, E- slightly stable, F- stable depending upon his observation. The stability classes are influenced by the solar radiation and wind speed (Thad, 2004). It is assumed that stability in the layers near the ground is dependent on the net radiation (Vijay Bhaskar, Jeba, P, & Amit P, 2008). Incoming solar radiation on a cloud free day is dependent on solar altitude, which is a function of latitude, day of the year and time of the day. At night the radiation condition depends only upon cloud cover. Concentration of pollutants is greatest for a stable case and lowest for an unstable case at lower vertical heights. Under stable conditions, the horizontal plume dominates the advection of the pollutants, while a terrain characteristic is more important under neutral and unstable conditions (Vijay Bhaskar et al., 2008).

Temperature differences between boundary-layer air flow and the upwind surface air flow approaching an urban area affect air pollutant dispersion (Raman & Cermak, 1975). Petersen & Parce, 1993 demonstrated that the thermal effects on flow and dispersion over an urban area arise from heating and cooling of the surroundings. The nature and magnitude of the thermal effects are strongly dependent on meteorological factors, seasons, time of day, surface roughness and topographic features (Cermak, 1996). As discussed by Changnon (1992), significant local weather modifications have been attributed to large-scale effects. Gaussian plume dispersion models such as ISC-PRIME and ISCST3 are developed on the basis of Pasquill-Gifford stability classification (A. J. Cimorelli et al., 2003). Whereas US-EPA's most advanced dispersion model AERMOD uses the Monin-Obukhov PBL concept for computing the GLC of the air pollutants.

2.6 Mixing Height and Atmospheric Boundary Layer

The boundary layer height is assumed to be the same as the mixing height (Arya, 1988), which starts building up at 11 a.m. attaining a maximum at 1 p.m. and decreasing thereafter till 6 p.m. Average morning mixing heights range from 300 m to over 900 m above ground level (Holzworth, 1972). A study by Tie, Brasseur, & Ying, 2010, demonstrated that CO and NO_x concentrations have maximum values in early morning in Mexico City due to very shallow PBL

height. Diurnal pattern often causes smoke to be concentrated in basins and valleys during the morning and dispersed aloft in the afternoon. Simpson, Raman, Lundquist, & Leach, 2007 demonstrated that increased cloud cover causes lower mixing height and vice versa. The mixing heights at night range from 100m - 500m while they were generally around 400m during clear and calm conditions (A. J. Cimorelli et al., 2005). Under low wind condition, if pollutants are released into the stable or neutral PBL, the near field concentration could be less compared to far distances (Krautstrunk et al., 2000).

Dispersion patterns in Convective Boundary Layer (CBL) strongly vary both in time and space (Fedorovich, Kaiser, Rau, & Plate, 1996). The plume height, GLC, vertical and horizontal dispersion parameters and crosswind-integrated concentrations in the CBL are all affected by wind shear. Marques Filho et al (2006) demonstrated that the wind velocity, buoyancy and concentration of atmospheric constituents in the heart of the CBL do not change with height and time due to active mixing.

2.7 Air Pollutants Removal from the Atmosphere

Air pollutant residence time in the atmosphere ranges from few days to weeks and in rare cases up to months. The residence time of PM depends on its size and location. Larger particles settle to the ground quickly by the force of gravity than smaller particles. Smaller particles such as fine and ultrafine particulate matter sink by a number of processes such as washout and turbulence settling. Washout is a removal process in which aerosol acts as nuclei for the condensation of cloud droplets. Some of these aerosol droplets grow to a large size that fall (gravitationally settle) to the surface as rain drops. The Washout ratio W can be represented by Equation 1 (Colls, 2002),

$$\mathbf{W} = \frac{\textbf{Concentration per kg of rainwater}}{\textbf{Concentration per kg of air}} \qquad [1]$$

Gravitational settling is the simplest deposition process for removal of the particles from the atmosphere by gravity. Very large particles fall through the boundary layer with a terminal velocity. This terminal velocity can be calculated from Stokes' law. Turbulence is the most

effective dry vertical transport mechanism for the air pollutant movement in the boundary layer (Seinfeld & Pandis, 2006).

2.8 Air Pollutant Dispersion Modeling

Dispersion modeling uses mathematical formulations to characterize the atmospheric processes. Based on emissions and meteorological inputs and source information such as emission rates and stack height, dispersion models are designed to characterize primary pollutants that are emitted directly into the atmosphere**.** Dispersion models are important as they are widely used by agencies tasked with both identifying the emission source and assist in the design of effective strategies to reduce harmful air pollutants. These models can be used during the permitting process to verify that a new source will not exceed ambient air quality standards or, if necessary, determine appropriate additional control requirements. In addition, these models can also be used to predict future pollutant concentrations from multiple sources. There are a number of models that are used for dispersion simulations. One such dispersion model is the Box model and this model works on the principle of mass conservation. This model requires very simple meteorological and emission data. Examples of Box models are AURORA, CPB and PBM. Another type is the Gaussian model which is formulated based on Gaussian distribution of the plume in the vertical and horizontal directions under steady state conditions. Some of the Gaussian Plume models are CALINE4, HIWAY2, CAR-FMI, OSPM, CALPUFF, AEROPOL, AERMOD, UK-ADMS and SCREEN3. Another two dispersion models are Lagrangian model and Eulerian model. Lagrangian model follows the particle in a moving plume whereas Eulerian model follows the trajectory of an air parcel (Wikipedia, 2011). Examples of such models are GRAL, TAPM, and ARIA Regional. Computational Fluid Dynamic models solve Navier–Stokes equation using finite difference or finite volume methods in three dimensions to do the fluid flow analysis. Some of the CFD models are ARIA Local, MISKAM, and CRO-CALGRID (Holmes & Morawska, 2006). ADMs have been widely used to investigate the dispersion pattern behavior of air emission (Mehdizadeh & Rifai, 2004) and to assess the potential hazards to the human health in the nearby population (James, Cherry, & Stack, 1995; Zhou, Levy, Hammitt, & Evans, 2003). Point source emissions from various industrial sources have been studied by ADM. For example, ADM3.1 model has been used for SO_2 emission (Carruthers et al., 1997); (Carslaw & Beevers,

2002); (Bennett & Hunter, 1997), ISCST3 model for CO and NO_x (Venegas & Mazzeo, 2006). CALPUFF was used to study the dispersion of $PM_{2.5}$ by Zhou et al., (2003).

When the existing topography of a particular modeling domain experiences horizontally homogeneous wind flow and more or less steady-state meteorological conditions, there is no accumulation of pollutants (Benson, 1989). The author has demonstrated that AERMOD simulated maximum PM_{10} concentrations are seen in the summer season (March-May) and minimum concentrations during monsoon season (June-September) respectively. The highest concentration of particulate matter in summer might be described with photochemical reactions along with factors such as source strength and other meteorological parameters. The lowest concentration of PM_{10} in monsoon could be attributed to the scavenging of particulate pollutants from the atmosphere due to rainfall (Stern, 1976). AERMOD can under predict the pollutant GLC due to lack of accurate emission factors of transportation sources (Vijay Bhaskar et al., 2008). For a non-buoyant release from a small source in urban area where the receptors were located upwind of the dominant westerly wind direction, the highest concentrations are over estimated by AERMOD (Venkatram, 1980). Lakes environmental developed ISC AERMOD view has incorporated user-friendly options such as RMMET and AERMET meteorological data preprocessing software (Jesse, Cristiane, & Michael, 2000).

2.9 Gaussian Plume Model

The most widely used models for predicting the impact of CACs released from smokestacks and other sources are based on Gaussian diffusion. In Gaussian models, the spread of a plume in vertical and horizontal directions is assumed to occur by simple diffusion along the direction of the mean wind. The maximum ground level concentration is calculated by means of Equation 2 (Masters, 1997),

$$C_{(x,\,y)} = \frac{Q}{\pi u_H \sigma_y \sigma_z} exp[\frac{-H^2}{2{\sigma_z}^2}] exp[\frac{-y^2}{2{\sigma_y}^2}] \qquad [2]$$

Where,

$C_{(x,\,y)}$ = ground level concentration at the point (x, y), µg m^{-3}

Q = average emission rate of pollutants (µg sec^{-1})

x = distance directly downwind, (m)

y = horizontl distance from the plume centre line (m)

u_H = mean wind speed (m sec^{-1})

H = effective stack height (m) (H = h + Δh, where h = actual stack height and Δh = plume rise)

σ_y = horizontal dispersion coefficient (standard deviation) (m)

σ_z = vertical dispersion coefficient (standard deviation) (m)

Rao, Sistla, Keenan, & Wilson, 1980, carried out the evaluation of some commonly used dispersion models to quantify their predictive capacity and performance. Their study showed that despite several limitations and assumptions used in Gaussian Plume models, these models are comparatively more accurate and consistent with the random nature of turbulence in the atmosphere and are best suited for pollutant dispersion. Air dispersion models incorporating the parameterization for PBL, turbulence and dispersion in the convective boundary layer and terrain interactions of pollutant plume are suggested to be suited for estimation of spatial dispersion of pollutants (Otte et al., 2005).

2.10 Description of AERMOD

AERMOD is a steady state Gaussian plume model developed by the American Meteorological Society/Environmental Protection Agency Regulatory Model Improvement Committee (AERMIC) largely with the support of the United States Environmental Protection Agency (US EPA) (Perry et al., 1994). AERMOD modeling system (U.S. EPA., 1998) consists of a main processor, terrain preprocessor AERMAP and meteorological preprocessor AERMET. This model is designed to estimate nearfield concentrations (less than 50 km). AERMOD's concentration estimates are based on a steady state plume approach with significant improvements over commonly used regulatory dispersion models.

The dispersion of a pollutant is completely governed by the local meteorological parameters (A. J. Cimorelli et al., 2003). Therefore meteorological information is a crucial input for the dispersion models. AERMOD concentration algorithm considers the effects of vertical variation

of wind, temperature and turbulence profiles. These profiles are represented by equivalent values that are constructed by averaging over the planetary boundary layer (PBL) through which plume material travels directly from the source to the receptor (A. J. Cimorelli et al., 2003). The model uses the boundary layer parameters in conjunction with meteorological measurements to characterize the vertical structure profiles.

Perry et. al 2005 described the approaches and algorithms involved in AERMOD for air pollutant concentration predictions as follows,

- Algorithms for estimating PBL parameters
- Algorithms for developing vertical meteorological profiles
- An approach for handling PBL non homogeneity
- An approach to establish the influence of terrain
- The general structure of the dispersion model
- Dispersion algorithms
- Building downwash algorithms
- Treatment of the urban boundary layer

AERMET is the meteorological preprocessor of AERMOD. AERMET requires hourly surface and upper air observations for wind speed, wind direction, dry bulb temperature, ceiling heights and humidity. AERMET estimates the convective (Z_{ic}) and mechanical *(*Z_{im}) mixed layer heights respectively. AERMET defines the stability of the PBL using sensible heat flux (H) which depends upon the net solar radiation (convective for $H > 0$ and stable for $H < 0$). AERMET also calculates the PBL parameters in the convective boundary layer (CBL) such as friction velocity (u*), Monin-Obukhov length (L), convective velocity scale (w*), temperature scale (θ*), mixing height (zi), and sensible heat flux (H) along with the land use parameters in the form of Albedo, Bowen Ratio and surface roughness (U.S. EPA., 1998). Convective velocity scale is calculated as a function of the mixing height in AERMET. Convective velocity scale is utilized by

AERMOD to characterize the convective portion of the turbulence in the CBL. In the CBL, the plume is treated as Gaussian in horizontal direction but bi-Gaussian in vertical direction (A. J. Cimorelli et al., 2005).

AERMOD considers the effect of dispersion from vertical variation of PBL. The growth and structure of the PBL is driven by the heat fluxes and momentum. The depth of this layer and the dispersion of pollutants within it are influenced on a local scale by surface characteristics such as surface roughness, albedo and surface moisture (Bowen ratio). The vertical mixing of air pollutants depends on the depth and stratification of the PBL which is a function of sensible heat flux, large-scale vertical motion, horizontal advection and entrainment at the boundary layer surface. AERMOD's meteorological preprocessor AERMET characterizes the state of PBL by estimating sensible heat flux, friction velocity (u*) and the Monin-Obukhov length (L) during the convective conditions (Oke, 1978,). The sensible heat flux, friction velocity (u*) and the Monin-Obukhov length (L) help AERMET to calculate the mixing height (Zi) and the convective velocity scale (w*). Venkatram (1980) observed that temperature scale which sets the level of the temperature fluctuations in the surface layer can be used to determine the friction velocity (u*). AERMET calculates the heat flux in the stable boundary layer (SBL) and the total mixing height (Zi) with the help of u*. A set of routines within AERMOD known as the AERMOD interface uses similar relationships with the boundary layer parameters, the measured meteorological data and other site-specific information provided by AERMET to compute vertical profiles of wind direction, wind speed, temperature(θ), vertical potential temperature gradient, vertical turbulence (F_w) and lateral turbulence (F_v). As AERMOD is a steady-state plume model, it can use only a single value of each meteorological parameter to represent the layer through which these parameters are varying. Thus, the model converts the nonhomogeneous values into equivalent effective or homogeneous values for wind speed, dispersion coefficients and temperature gradients (A. J. Cimorelli et al., 2005).

Kesarkar, Dalvi, Kaginalkar, & Ojha, 2007, developed an offline preprocessor to couple WRF model with the AERMOD at the Centre for Development of Advanced Computing (C-DAC), Pune, India. The preprocessor initializes AERMOD by substituting the required hourly values of surface layer and PBL parameters with those derived from WRF outputs. These authors presented a discussion on coupling methodology and initial results from the WRF-AERMOD

simulations. The required coupler for WRF-AERMOD offline coupled system has been developed as a part of their work. This coupler derives the PBL and surface parameters for a given location from WRF model output and directly generates the AERMOD meteorological input files, by-passing the need for AERMET preprocessor and thus any observational data requirement. The authors suggested that the effect of the transient deviations between observed and simulated meteorological parameters can be better evaluated by comparing hourly AERMOD outputs with hourly monitored values (Kesarkar et al., 2007).

Buoyant plume mass that penetrates the stable elevated layer is tracked by AERMOD and allows it to re-enter the mixed layer at some downwind distance (W. H. Snyder et al., 1985). AERMOD accounts for the flow and dispersion of the air pollutants in the complex terrain in stably stratified conditions. The authors showed that AERMOD incorporates dividing streamline concept and the plume is modeled as a combination of terrain-impacting states. It handles all terrain in a consistent and continuous manner while considering the dividing streamline concept.

The terrain pre-processor AERMAP uses gridded terrain data to calculate a representative terrain-influence height (h_c) also known as terrain height scale (W. H. Snyder et al., 1985). The terrain height scale h_c, which is uniquely defined for each receptor location, is used to calculate the dividing streamline height. The gridded data required by AERMAP is selected from Digital Elevation Model (DEM) data. AERMAP is also used to create receptor grids. The elevation for each specified receptor is automatically assigned through AERMAP. For each receptor, AERMAP passes the information such as the receptor's location (x_r, y_r), its height above mean sea level (z_r), receptor specific terrain height scale (h_c), plume height and receptor elevation to AERMOD. For a receptor at elevation z_t and an effective plume height (h_e), the height that the streamlines must reach to be in the terrain-following state is given by (z_t+h_e).

AERMOD considers that the plume exists in two states, horizontal i.e. on flat terrain and the other on elevated terrain (Vijay Bhaskar et al., 2008). The concentration of any pollutant is calculated as the sum of these two. At horizontal state plume material stays below the streamline and on elevated terrain plume material stays above the streamline. Under stable atmospheric condition, the first state has a major effect and under unstable and neutral conditions the second

state has more effect. On flat terrain, the concentration equation reduces to the form of a single plume (Vijay Bhaskar et al., 2008). The general form is given in Equation 3,

$$C_t = f*C(x, y, z) + (1-f)*C(x, y, z_{eff}) \qquad [3]$$

Where,

C_t = concentration on flat terrain

C (x, y, z_{eff}) = Adjusted concentration on elevated terrain

Z = height of the receptor (this includes the height above local terrain)

f = weighting factor related to the fraction of plume material that is below the height

2.11 Sensitivity of AERMOD to Different Land Use Parameters

AERMOD calculates convective (daytime) turbulence based on the amount of solar heat available to drive the turbulent processes (Grosch & Lee, 1998). The land use parameters such as albedo, Bowen Ratio, and surface roughness length play significant roles to calculate the friction velocity and Monin-Obukhov length required by the AERMOD system to compute turbulent dispersion of air pollutants. Grosch & Lee, 1998 observed that the increased turbulence directly affects air pollutant concentrations by increasing dispersion and indirectly by causing the mixing height to increase by altering the wind speed profiles and turbulence. The authors suggested that the surface roughness affects wind flow due to surface drag. The surface drag creates shear by generating the turbulence which affects the mixing height and alters the profiles of various meteorological parameters. During stable (nighttime) conditions, only the effect of surface roughness length is considered by the model.

The authors of the above study have also shown that when surface parameters are altered at a time by selecting minimum and maximum values of albedo, Bowen Ratio, and surface roughness, the design concentrations can decrease up to 36% for any averaging period higher than 1hour. The highest design concentration occurs with the mid-range value of the albedo. The sensitivity of design concentrations to the surface roughness length appeared more complex. The

1-hour design concentration decreases by a factor of 2.4 as the roughness is increased from its minimum to its maximum value. The lowest design concentrations were observed with the lowest value of roughness length at 24 hour and design concentrations increase with roughness by a factor of 2 for the annual averaging. Highest GLC occurred on water and lowest at Conifer forest for the emission from surface sources in the study of Grosch & Lee, 1998. The authors demonstrated that surface roughness length has significant effect on the design concentration. Reducing the surface roughness by a factor of 4 resulted in a 52% increase in the predicted concentration.

The observation by Grosch & Lee, 1998 also demonstrates that the solar radiation plays major role in case of an elevated emission source. Solar radiation changes by a factor of 4 could lead up to 50% change in the predicted concentration. Volume sources are most sensitive to changes in surface roughness; surface roughness reduction by a factor of 4 can result in 85% increase in the predicted concentration (Grosch & Lee, 1998). Finally the authors have shown that the cloud cover data is another sensitive parameter. A 50% increase in cloud cover can lead to an 18 percent decrease in the predicted concentration.

According to S. Lee & Keener, 2008, limited analysis of varying land use parameters on concentration predictions indicates that the model performance may be significantly affected by the values of the surface roughness, albedo, and Bowen ratio in certain cases.

2.12 Building Downwash

AERMOD incorporates the Plume Rise Model Enhancements (PRIME) algorithms to handle plumes that are affected by building wakes (Schulman, Strimaitis, & Scire, 2000). PRIME partitions plume mass between a cavity and wake region are specified by the lateral and vertical separation streamlines. Dispersion of the mass that is initially captured within the cavity is based on building geometry and is assumed to be uniformly mixed. Beyond the cavity region, this mass is emitted into the wake where it is combined with un-captured plume mass and dispersed at an enhanced rate. A. J. Cimorelli et al., 2005 developed a numerical model that considers the effects of streamline deflection near the buildings, vertical wind speed shear, and enhanced dilution from the turbulent wake and velocity deficit. The authors suggested that specification of the

cavity extent, plume material height and spread is critical to appropriately simulate the downwash effect in case of both area and volume sources.

2.13 AERMOD Performances for Different Release Sources

Hanna, Chang, & Fernau, 1998, found that AERMOD's highest level of overall success were most likely due to the improved algorithms for convective conditions in reproducing the concentration distributions for buoyant, tall-stack releases in moderate to complex topography. AERMOD performs well in reproducing the upper end of the concentration distribution due to tall, buoyant stacks in flat terrain. The authors also reported the bi-Gaussian vertical concentration distribution in AERMOD results was much more appropriate for the treatment of the elevated plume material in convective conditions. In contrast, annual average comparisons implied that the model has difficulty in reproducing some of the lower concentration values, particularly in stable conditions. Study by Perry et al., (1994) showed that, AERMOD under predicts the GLC of pollutants released from non-buoyant area and volume sources.

2.14 AERMOD-Case Studies

Zou, Benjamin Zhan, Gaines Wilson, & Zeng, 2010 found that AERMOD performs better in simulating SO_2 concentration when both point and mobile sources are used as model inputs than using point or mobile emission sources alone in urban and rural areas with simple or complex topography. The model has the capacity to employ hourly sequential preprocessed meteorological data to estimate concentration of pollutant concentrations at receptor locations at different time scales ranging from 1hour to 12 months.

The study of Zou et al., 2010 represented that AERMOD simulates a plume as a weighted sum of concentrations from two extreme scenarios; 1. Horizontal plume under very stable conditions and 2. The plume accounts for varying elevation in the area. The model produced better simulation results in the above study for 8-hr, daily, monthly and annual scale than at time scales of 1-hr and 3-hr. Point source's emission rates were obtained from dividing the annual total emissions by the operation time period due to lack of accurate emission rates at specified time intervals. The authors followed the mobile emission rate calculation by proportionally allocating the mobile emissions to different parts of a road segment. Mobile emission rates could be

improved by considering factors such as traffic flows, vehicle and fuel types associated with different segments of a road network. The model did not have the capability to incorporate these factors by its own. Therefore, variations of mobile emissions during the 24 hour period also could not be reflected during the model simulations. Zou et al., 2010, suggested that photochemical effect and dispersion delay might affect the overall results.

Another study was conducted by Gildemeister, Graney, & Keeler, 2005, using AERMOD to understand the dispersion pattern of Total Gaseous Mercury (TGM) from four coal fired power plants in surrounding area of the Genesee site in Alberta Canada which is directly affected by the North West winds. A number of mercury concentrations monitoring had been performed near the coal-fired power plants in Genesee by D. S. Lee, Dollard, & Pepler, 1998 and Manolopoulos et al., 2007. In some cases the researcher's ability to identify a specific source is confounded by the presence of multiple sources from cities or industrial regions. AERMOD was run to simulate the effect of the power plants on the ambient TGM levels in Lake Wabmun area. The emission for each of the coal-fired power plants was estimated from an annual emissions inventory (NPRI 2006) and the hourly emission rates were calculated from yearly total emission. A 50km by 50km grid with 169 uniformly spaced receptors were centered over the region and terrain data Geo Base (Geo base 2008) was extracted using AERMAP (Mazur, Mintz, Lapalme, & Wiens, 2009). The diurnal variations of TGM concentrations at Meadows and Genesee agree with previous studies (Gabriel, Williamson, & Brooks, 2005; Kellerhals et al., 2003; D. Snyder, Dallmann, Schauer, Holloway, & Kleeman, 2008). Model predicted results demonstrated that the TGM emission under normal operating conditions can influence the GLC by 0.46 -1.19 ng m^{-3}. At later stages the mercury entered remote ecosystem through atmospheric dispersion. According to Temme et al., 2007 for a given emission rate, predicted GLC can be high due to extreme rare transient conditions. For example, maximum concentrations can occur in early spring and minimum in late summer.

CHAPTER 3: DISPERSION STUDY APPROACH IN THE PROVINCE OF NOVA SCOTIA

The AQB of NSE is responsible for monitoring the outdoor air quality and developing regulations and policies to protect Nova Scotia's environment and the health of its residents. The NSE AQB has planned to develop an airshed management framework in the province to manage the air resources. Nova Scotia Environment has gathered baseline information about the air pollutant release sources to develop the airshed management framework. Baseline information along with meteorological and land use type information are useful for simulation models to depict the provincial airshed.

There are some gaps in knowledge with regards to the CAC transport and its fate in the province. The concentration of the air pollutants are being measured at several NAPS stations across the province. However, the number of these stations is very limited to understand the air pollutant dispersion scenario. Air dispersion modeling study can serve the above purpose. Therefore, Lakes environmental Waterloo Ontario, Canada developed dispersion simulation software AERMOD view version 6.2 is utilized to conduct the dispersion modeling across the province along with other informations. Model simulations were carried out in yearly, monthly and hourly basis in different years during 2004 to 2007. The year of simulation for each domain was chosen based on maximum available model input data available from NPRI database.

This chapter includes the description of the seven modeling domains across the province, information about point and linear emission source characteristics, method of emission factor calculation. Also the method of comparing the NAPS observed and model predicted values are discussed in this section. The information about meteorological and terrain data used by AERMET and AERMAP respectively is described in this section.

3.1 Location and Topography of Nova Scotia

Nova Scotia is one of the maritime provinces in Canada, located on the south east coast, latitude between 43^{o}50'N and 46^{o}56'N and longitude between 62^{o}54'W and 64^{o}13'W with an area of 55,284 square kilometers. The province is surrounded by the Atlantic Ocean with numerous

bays, islands and uplands. Northern part of the province consists of uplands with an elevation ranging between 100-300m from the sea level. Lowland of the province exits at the northern part along with the uplands. This region is mainly covered with conifer forest along with some grassland. Both coastal area and low land are seen at the North West part of the province. Rest of the province is known as Atlantic interior which is mostly plain land with vegetation cover and urban areas (Wikipedia, 2011).

The main factors influencing Nova Scotia's climate are the westerly wind, interaction among the three main air masses which converge on the east coast, province's location on the route of the major eastward-moving storms and the modifying influence of the sea. The ocean is the major influence of Nova Scotia's warm summer and moderately cold winter. The temperature of the Atlantic Ocean moderates the climate of the south and east coasts of the province, whereas heavy ice build-up in the Gulf of Saint Lawrence causes cold winter in northern Nova Scotia (Wikipedia, 2011).

Nova Scotia's rainfall varies between 140 centimeters in the south and 100 centimeters elsewhere. Province experiences 196 foggy days per year on an average. The temperature of NS varies between a maximum and minimum of 28^{o}C and -20^{o}C during summer and winter respectively (Wikipedia, 2011).

3.2 Modeling Domains

AERMOD simulation studies were carried out in seven different domains that included the cities of Halifax, Lunenberg, Pictou, Port hawksbury, Sydney, Point Aconi and Truro in Nova Scotia. The seven modeling domains include peri-urban rural environments and complex coastal and valley topography. Figure 2 shows the locations of the Halifax,Lunenberg, Pictou, Port hawksbury ,Sydney, Point Aconi and Truro modeling domains.

Figure 2 Seven modeling domains across Nova Scotia

The above mentioned domains are less than 50km/50km but vary in dimensions due to availability of county wide Digital Elevation Models (DEM). Figures 3a through 3g describe the details of dimensions, receptor spacing, point and highway emission sources that are being used for the AERMOD simulation study.

The dimension of the Halifax Modeling Domain (HFX) is given in Table 1. Emission from 12 chimeny stacks ,1 flare and a section length of 207 km of highways 101,102,103 and main roads

107,111and 125 are used as input for HFX domain. The point sources include five chimney stacks and a flare source from Dartmouth Oil refinary (a,b,c,d,e,f), one from Dalhousie University Central facility, three from Capital health Halifax (a,b,c) and three from Tufts cove power generation (a,b,c) unit as shown in Figure 3a.

The geographical location of the Lunenberg domain (LNN) is given in the Table 1. This modeling domain is 48.3km long and 48.3km wide. The emission sources include a chimney stack from Brooklyn Energy Centre and a section lenth of 28.75 km of highway103, as shown in Figure 3b.

The dimension of Pictou domain (PIC) is given in Table 1. A Section length of 64.5 km of highways 104 and 106, and four point emission sources of Neenah Paper industry (a,b,c,d) were available for model inputs, as shown in Figure 3c.

The geographical location of the PortHawksbury domain (PRTHWKS) is given in the Table 1. Emissions from two chimeny stacks of New Page Paper and a section lenth of total 53.5 km of highways 104 and 106 were used as input inthe model as shown in Figure 3d.

The dimension of Pictou domain (PTA) is given in Table 1. This domain is 25 km long and 15 km wide. Emissions from a section length of 17.5 km of highway 105 and a chimney stack from Point Aconi generation station are used for model input, as shown in Figure 3e.

The geographical location of the Sydney domain (SYD) is given in the Table 1. The emission sources in SYD are the Lingan Generating Station and a section length of 23.5 km of highways respectively, as shown in Figure 3f.

The dimension of Truro domain (TRR) is given in Table 1. Two stacks from Brookfield Cement Plant and Truro Paper mill and a total section leagths of 118 km of highways 102 and 104 are used as emission sources for the siulation study, as shown in Figure 3g.

Table 1 Characteristics of the modeling domains

Domain	South-West Corner Coordinates in UTM (m)	North-East Corner Coordinates in UTM (m)	Length [east: west](km)	Length [north: south](km)	Maximum Elevation from the Mean Sea level (m)
Halifax (HFX)	432907.86: 4940306.88	482351.56: 4991354.16	50.58	48.55	185
Lunenburg (LNN)	326300.79: 4866992.21	374607.8: 4915299.22	48.3	48.3	139.6
Pictou (PIC)	492097.16: 5022396.44	539644.44: 5065136.59	47.01	42.65	320.4
Point Aconi (PTA)	692545.6: 510841.4	708045.6: 5133713.4	15.5	25.3	215.5
Porthawkesbury (PRTHWKS)	609805.32: 5024268.03	657403.62: 5073720.92	49.0	47.31	283.1
Sydney (SYD)	707486.23: 5104407.14	728994.84: 5125770.9	21.25	21.25	179.6
Truro (TRR)	463843.97: 4990779.86	509443.97: 5043267.34	45.6	52.48	315.2

Figures 3a-g Description of emission sources and receptor grid in four domains

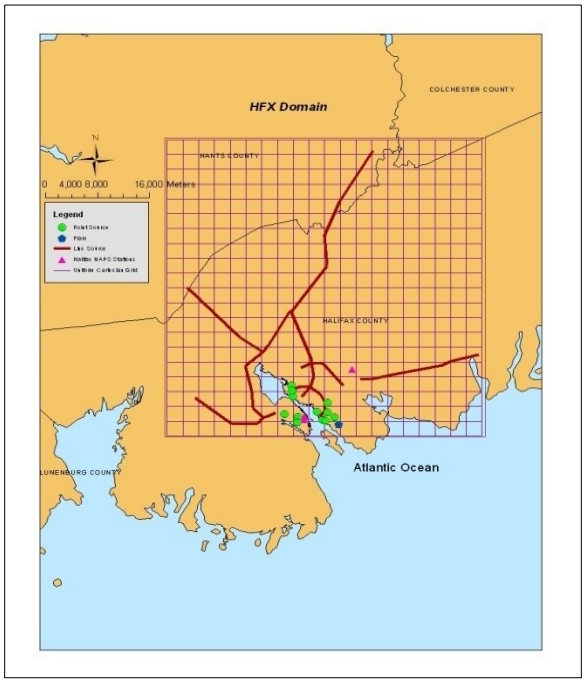

a. HFX domain

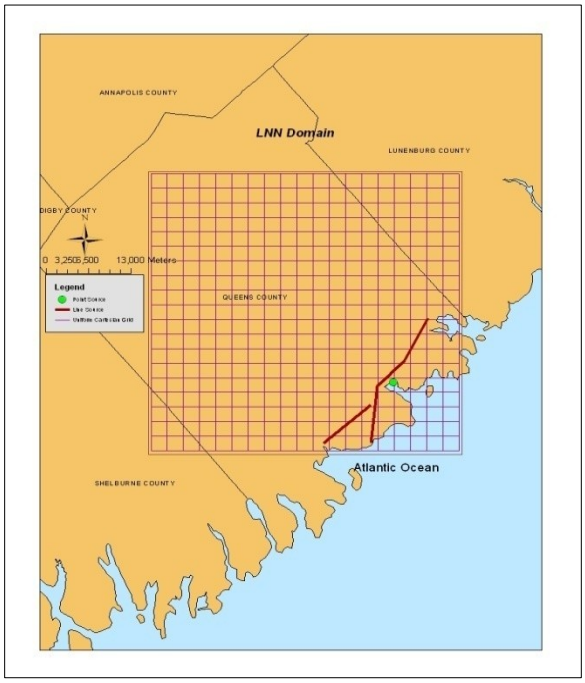

b. LNN domain

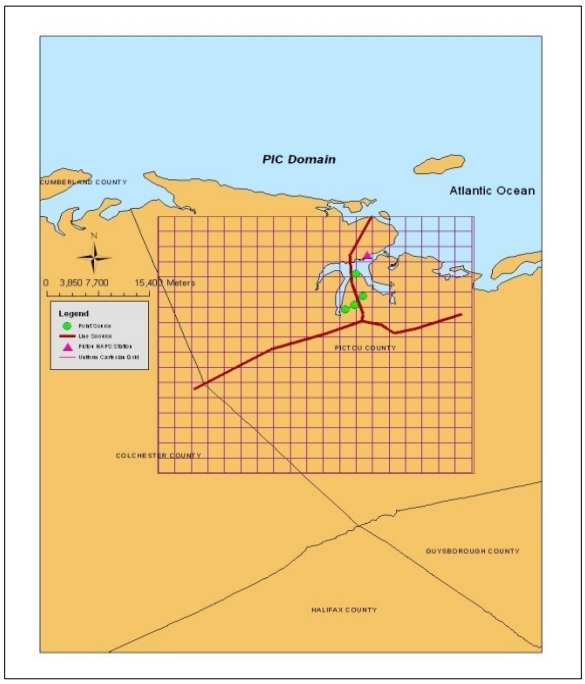

c. PIC domain

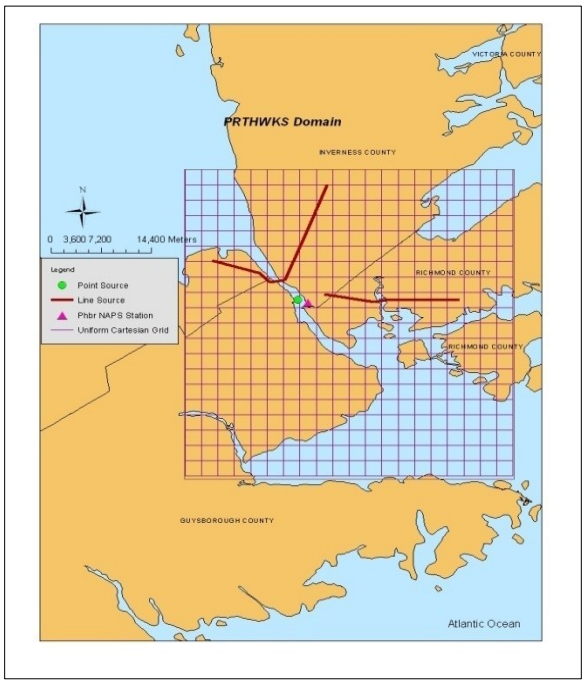

d. PRTHWKS domain

(Figures Cont'd)

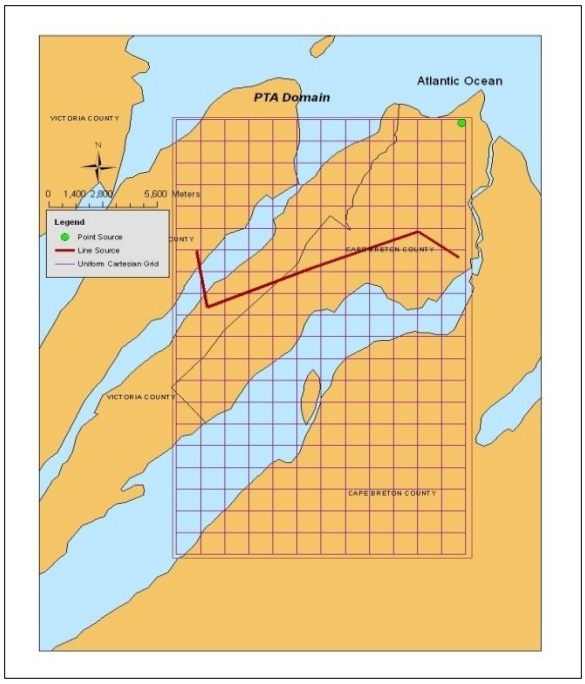

e. PTA domain

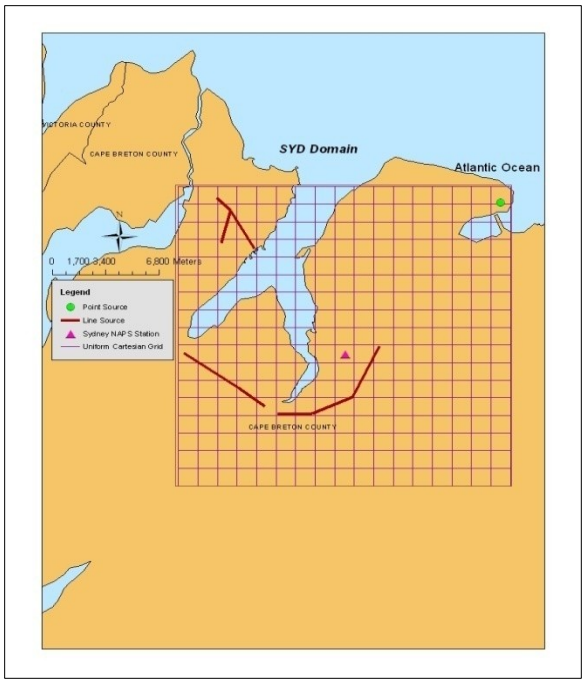

f. SYD domain

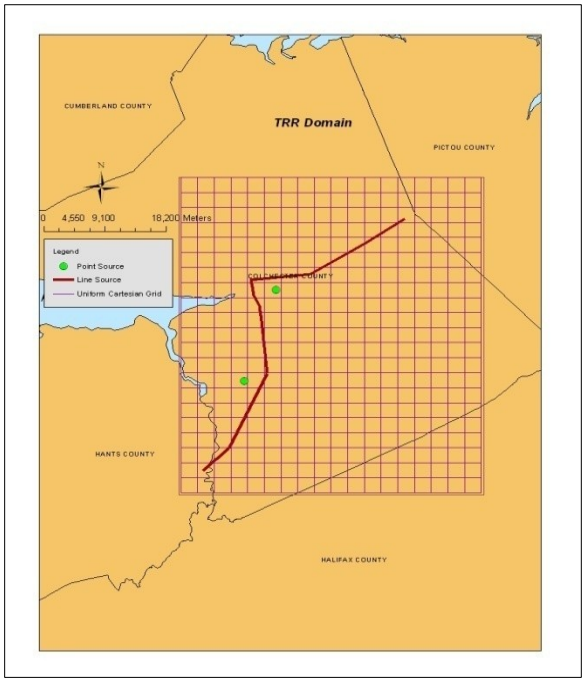

g. TRR domain

3.3 Description of Seven Pathways in AERMOD VIEW v6.2

There are seven different pathways to input the required data in the main module of AERMOD (Jesse, et al., 2000). These six pathways are described as follows,

1. Control pathway- It is used to specify the pollutant type, pollutant averaging periods, dispersion coefficients either rural or urban and regulatory options. The model run is controlled by this pathway.

2. Source pathway- Point, linear, volume, flare and area emission source's location coordinates, base elevation, release height, emission rate, dimension, exit velocity and exit temperature are assigned through source pathway. Also this pathway is used to stipulate the hourly emission rates and emission factors.

3. Meteorological pathway- This pathway is used to import the preprocessed surface and profile files from the AERMET preprocessor.

4. Receptor pathway- This pathway is used to define the geographical coordinates of the specific receptor locations along with their elevation.

5. Terrain Pathway- Terrain data in DEM format is used through this pathway to process the terrain elevation and hill heights using AERMAP.

6. Building Pathway- This pathway is utilized for specifying the building (if present at the vicinity of the modeling area) characteristics to calculate impacts on air pollutant dispersion.

7. Output Pathway- Output pathway is utilized for user specific result options of the model simulated dispersion data.

Running steps of AERMOD view v6.2 are given below. Flowchart 1 shows the steps to feed the input data to the model.

1. Modeling domain of dimensions less than or equal to 50km/50km is created.

2. Regulatory or non-regulatory options, averaging periods and dispersion coefficient are specified in control pathway.

3. Emission sources location, characteristics, source groups and emission factors are specified through source pathway.

4. Check for the presence of buildings, if there is any high rise building present which can influence the air pollutant dispersion, run BPIP and use the outputs as AERMOD input. If there is no building present running BPIP can be omitted.

5. Specify the receptor grid. Different types of receptors such as Uniform Cartesian, Polar, Nested and discrete receptors can be used depending upon the requirement of the user.

6. DEM data has to be imported on the modeling domain to run the AERMAP and generated elevations of the receptors that are used as AERMOD input.

7. Surface and profile files have to be chosen through the meteorological pathway from the preprocessed AERMET outputs. Also the maximum elevation of the modeling domain and the meteorological data reading period has to be specified in meteorological pathway.

8. AERMOD can be run once the above steps are performed successfully.

9. AERMOD generated outputs can be visualized and evaluated through output option in the model.

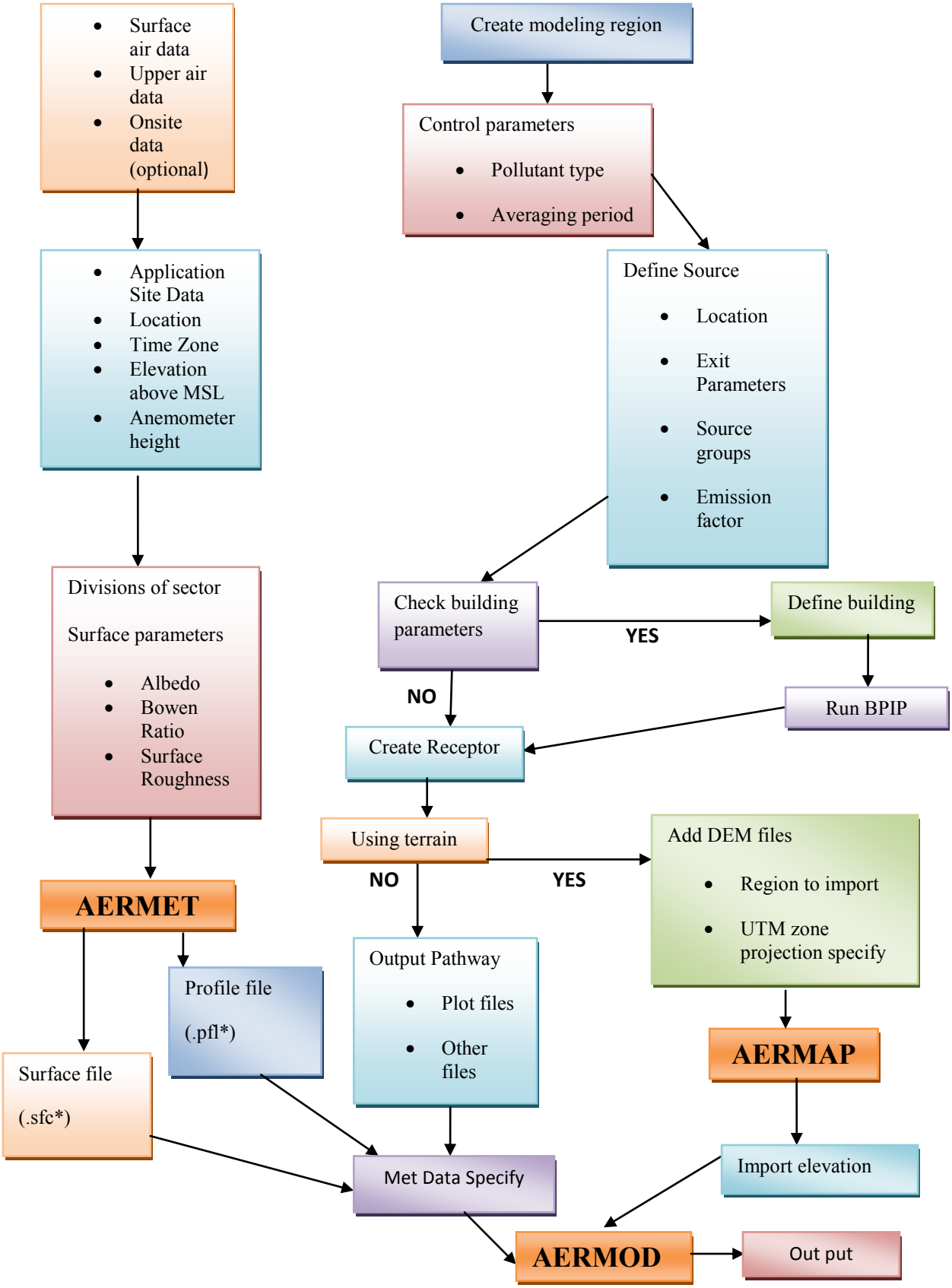

Flowchart 1 AERMOD Flowchart (Lakes Environmental, 2008)

3.4 Meteorological Data

Dispersion and GLC of any air pollutant depend on the meteorological parameters such as wind speed, wind direction, ambient temperature, turbulence and mixing height. The dispersion module of AERMOD uses the preprocessed meteorological data consisting of a 'surface' file and a 'profile' file and estimates of boundary layer parameters by AERMET. AERMET requires hourly surface air data including wind speed, wind direction, temperature, total cloud cover and upper air data obtained from Radiosonde observations. Hourly surface air data from the Halifax International Airport (YHZM) and Sydney (SYDM) and upper air data from Yarmouth MET stations are used for this study.

YHZM is located at x-459196.21m: y-4970120.17m, 35 km North East of Halifax Metro area (Figure 4a) and SYDM is located at x-716155.19m: y-5116377.04m (Figure 4b). Hourly surface air data (in CD-144 format) was obtained for four years (2004-2007) from both MET stations to conduct the simulations in seven domains. The upper air data (NCDC TD-6201 Fixed Length format) was obtained from Yarmouth MET station situated at x-250899.37m: y-4861736.2m to use in AERMET.

Land use characteristics such as albedo, Bowen ratio and surface roughness lengths are used by AERMET along with surface and upper air meteorological data to compute the boundary layer parameters. The values of land use characteristics vary with land cover types such as grassland, swamp, urban areas, water bodies, grassland and cultivated lands. The annual maximum and minimum values of albedo, Bowen ratio and surface roughness lengths of different land cover types are determined by referring the AERMOD Implementation Guide [29]. Land cover types such as urban areas, water bodies, grassland and cultivated lands are found in NS. Therefore, annual maximum and minimum values of albedo, Bowen Ration and surface roughness lengths of the above land use characteristics, given in Table 2 are used for this study.

Figures 4a-b Surface and upper air MET stations

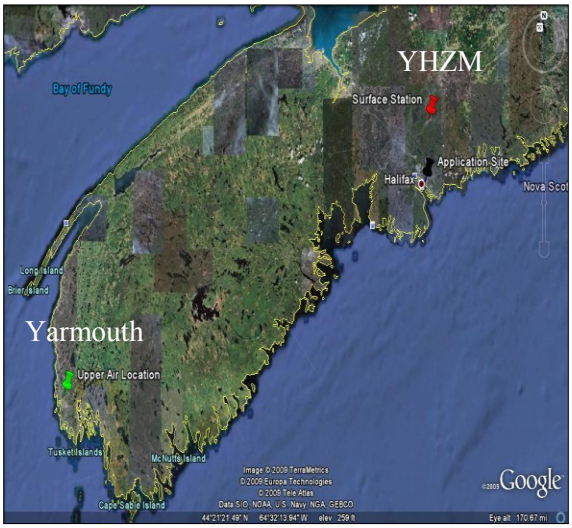

a. YHZM and Yarmouth MET stations

a. SYDM and Yarmouth MET stations

Table 2 Annual maximum and minimum values of Land use characteristics

Land cover Type	Values	Albedo	Bowen Ratio	Surface Roughness length
Urban areas	Max	0.35	1.5	1
	Min	0.14	1	1
Water bodies	Max	0.2	1.5	0.0001
	Min	0.1	0.1	0.0001
Grassland	Max	1.5	0.6	0.1
	Min	0.4	0.18	0.001
Cultivated Land	Max	0.6	0.3	0.01
	Min	0.14	1.5	0.2

Monthly average values of wind speed, temperature and cloud cover lengths obtained from YHZM MET station during 2004-2007 are given in Table 3.

Table 3 Monthly average values of Surface air parameters at YHZ MET station during 2004-2007

	2004			2005			2006			2007		
Month	Wind Speed ($m\ s^{-1}$)	Temp (K)	cloud cover (m)	Wind Speed ($m\ s^{-1}$)	Temp (K)	cloud cover (m)	Wind Speed ($m\ s^{-1}$)	Temp (K)	cloud cover (m)	Wind Speed ($m\ s^{-1}$)	Temp (K)	cloud cover (m)
Jan	7.3	263	8	7.2	270.4	10	9.5	274	9	9	269.85	7
Feb	9	265.6	10	6.45	267.9	6	9	269.2	5	9.5	264.2	8
Mar	5.9	270.4	7	9.25	268.8	4	6.4	272	6	9	269.85	10
Apr	6.35	283.25	5	6.7	277.9	4	9.48	280.4	8	7.7	280.9	4
May	7.2	284.5	9	7.45	281.45	9	5.75	285.95	7	6.2	287.55	8
Jun	7.42	290.4	6	5.9	287.9	7	7.7	289.75	9	4.92	288.45	9
Jul	5.72	291.45	7	4.9	291.2	9	8.25	292.45	4	5.65	292.35	5
Aug	6.52	289.95	6	5.4	292	3	6.36	290.9	3	6.7	290.9	8
Sep	7.3	286.42	8	5.9	287.9	10	5.6	287.35	6	6.2	289.75	5
Oct	7.3	282	5	6.45	284.7	5	8.25	284	9	8	283.4	8
Nov	8.3	277.8	9	7.7	278.45	8	8.8	278.2	7	12.85	277.4	10
Dec	10.05	270.9	8	13.4	273.95	6	5.5	272.9	5	10.05	270.05	7
Annual	7.4	281	8	9.25	279.2	8	9.5	278.4	6	8.02	276.4	5

With reference to Table 3 it is seen that during 2004-2007 maximum and minimum monthly average wind speed was recorded in winter and summer respectively with an exception for the year 2006. Wind speed ranged between 4.9 m s^{-1} and 13.4 m s^{-1} during the chosen four year period. Maximum and minimum annual average wind speed was recorded in December 2005 and July 2005 respectively. As expected the maximum and minimum monthly average temperature was recorded in summer and winter months. During this four years period, the ambient temperature ranged between 263.0 K and 292.4 K. Maximum and minimum annual average temperature was recorded in July 2006 and January 2004 respectively. Monthly maximum cloud cover lengths were observed during early and late winter months, whereas the minimum cloud cover lengths were observed during different months in summer.

Wind rose plot in Figure 5 demonstrates the directions of different wind speed categories at YZHM MET station during 2004-2007. As seen in the Figure 5, wind directions were from North, South, North West and South West. About 11% of the time wind was blowing from North West and South West, nearly 8% of the time wind was from north and South. Percentage of the wind blowing from North and South East was comparatively less. Maximum 4% of time wind was from North East. The resultant wind vector was found at 265^{o}. Calm hours existed for only 2.13% of the time.

Figure 5 Wind rose plot during 2004-2007 at YHZ met station

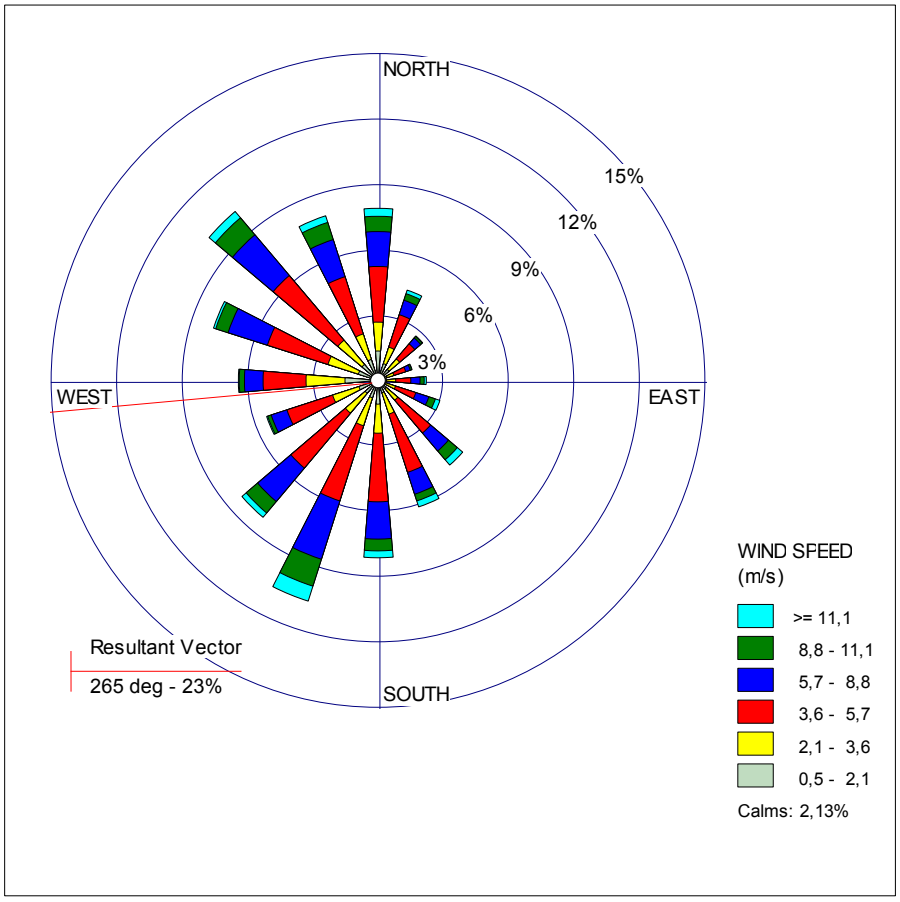

Monthly average values of wind speed, temperature and cloud cover lengths obtained from SYDM MET station during 2004-2007 are given in Table 4.

Table 4 Monthly average values of Surface air parameters at SYD MET station during 2004-2007

	2004			2005			2006			2007		
Month	Wind Speed ($m\ s^{-1}$)	Temp (K)	Cloud cover (m)	Wind Speed ($m\ s^{-1}$)	Temp (K)	Cloud cover (m)	Wind Speed ($m\ s^{-1}$)	Temp (K)	Cloud cover (m)	Wind Speed ($m\ s^{-1}$)	Temp (K)	Cloud cover (m)
Jan	7.45	264.75	8	7.3	270.4	10	8.25	275.05	10	10.05	269	7
Feb	8.35	262.6	9	6.4	268	5	9.25	269.5	4	7.45	264.55	8
Mar	6.25	270	7	9.25	269	8	6.3	269.85	6	7.25	269	10
Apr	7.3	280	6	6.7	278	6	6.7	277.9	4	8	279.75	8
May	6.75	284	10	7.4	281.45	7	4.9	285.3	9	5.9	284.35	5
Jun	6	286.7	5	5.85	288	9	6.25	290.4	7	6.4	284.35	4
Jul	4.4	289.85	7	4.9	291	3	4.9	293.9	5	4.2	291.85	9
Aug	5.4	290.9	8	5.35	292	4	5.4	288.15	9	5.4	290.4	5
Sep	9.5	287	6	5.9	288	6	7.7	286.7	10	5.85	286.85	10
Oct	13.6	282.9	5	6.45	284.9	10	8.25	284.5	3	5.65	282.5	8
Nov	7.55	277	9	7.72	278.45	7	6.6	278.45	6	9.25	277.8	7
Dec	7.8	271.85	8	6.7	274	5	6.4	274.5	8	8	272.35	8
Annual	7.51	274.01	8	8.2	283	6	7.83	280.7	8	9	278	5

With reference to Table 4 it is seen that during 2004-2007 maximum and minimum monthly average wind speeds were recorded in winter and summer respectively. Wind speed ranged between 4.4 m s^{-1} and 10.0 m s^{-1} during the four year period. Maximum and minimum annual average wind speeds were recorded in January 2007 and July 2004 respectively. As expected the maximum and minimum monthly temperature was recorded in summer and winter months. During this period, the ambient temperature ranged between 262.6 K and 293.9 K. Maximum and minimum annual average temperatures were recorded in August 2005 and January 2004 respectively. Monthly maximum cloud-cover lengths were observed during early fall, early and late winter months, whereas the minimum cloud cover lengths were observed at different months in summer.

Wind rose plot in Figure 6 demonstrates the directions of different wind speed categories at SYD MET station during 2004-2007. According to Figure 6, prevailing wind directions were from West and South West. About 12% of the time wind was blowing from South West, nearly 9% of the time wind was from west. Percentage of the time wind blowing from North, North West and South East was comparatively small. Apparently 6% of time wind was from North. The resultant wind vector was found at 248^{o}. Wind speed was nearly zero for 2.45% of the time.

Figure 6 Wind rose plot during 2004-2007 at SYD met station

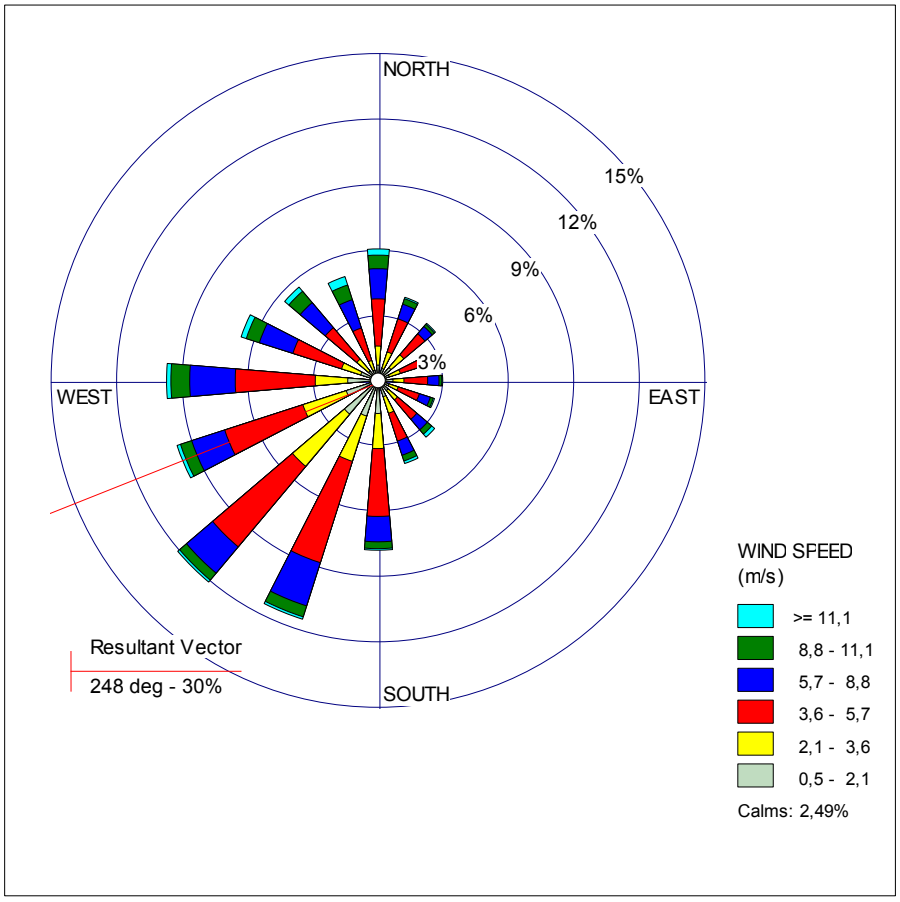

3.5 Base Map

ARCMAP of resolution 1 km×1 km from Arc GIS v9.3 (ESRI, 2008) was used as a base map for understanding the effect of NO_x, SO_2, and $PM_{2.5}$ dispersion on Nova Scotia air shed.

3.6 Receptor Mesh type and spacing

Various types of receptor meshes such as uniform Cartesian, Polar, Discrete, Nested and Plant boundary can be used in AERMOD for modeling purpose. Uniform Cartesian receptor mesh was chosen for this modeling study.

Uniform Cartesian receptor mesh with different spacing was created in the seven different domains to obtained maximum number of receptors. Uniform Cartesian mesh spacing are as follows; 2.48 km × 2.52 km for HFX domain, 2.49 km × 2.48 km for LNN domain, 2.47 km ×

2.51 km for PIC domain, 2.37 km × 2.45 km for PRTHWKS domain, 1.25 km × 1.25 km for PTA domain,1.25 km×1.25 km for SYD domain and 2.5 km×2.5 km for TRR domain. These mesh arrangements can be seen in Figures 3.2a through 3.2g. The number of receptors in seven domains varies between a maximum of 774 to a minimum of 441 including the elevation and hill height of each receptor. Five discrete receptors were assigned at five NAPS stations in HFX, PIC, PRTHWKS and SYD domain to compare the AERMOD simulated GLC values with NAPS observed GLC values.

3.7 Terrain Data

According to Boznar, Lesjak, & Mlakar, 1993, the modeler can have the freedom to input the receptor heights for computing the effects of the terrain below or above the bases of the emission sources. In this case, NS DEM of 1 km resolution was used as AERMAP input to assign the elevation and the hill height of each receptor in each modeling domain. DEM is a digital file consisting of terrain elevations for ground positions at regularly spaced horizontal intervals. DEM files are exported county wide to Geotiff file to make compatible input for AERMAP. Each of the modeling regions uses single or multiple Geotiff datasets at a scale of 1:250,000 depending upon the location of the domain. Elevations were assigned to the linear emission sources and transformed into volume emission sources to import in AERMOD for subsequent analyses. Figure 7 shows the AERMAP processed terrain outputs consisting of elevation and hill height of the receptors.

Figures 7a-g AERMAP processed terrain outputs of seven domains

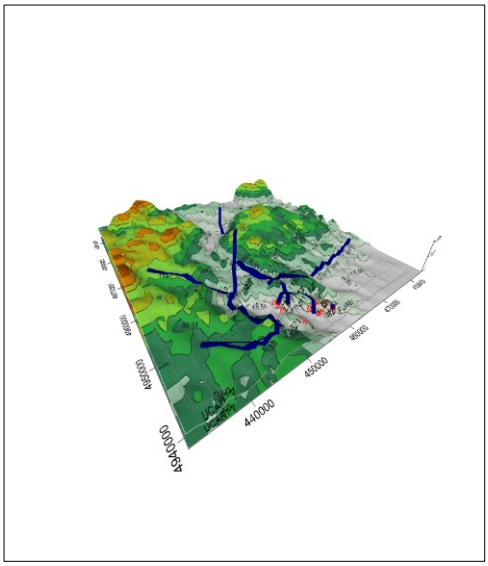

a. HFX domain

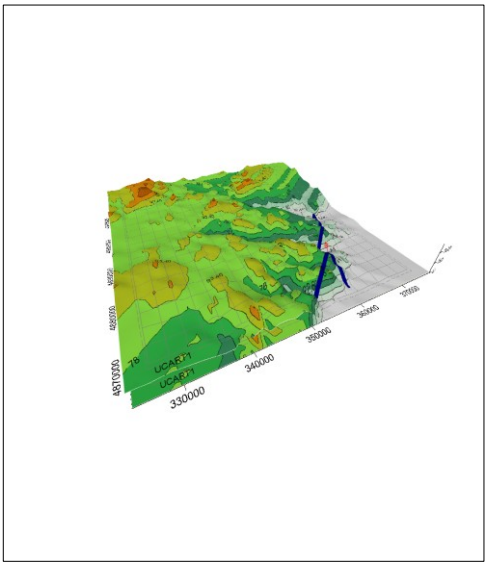

b. LNN domain

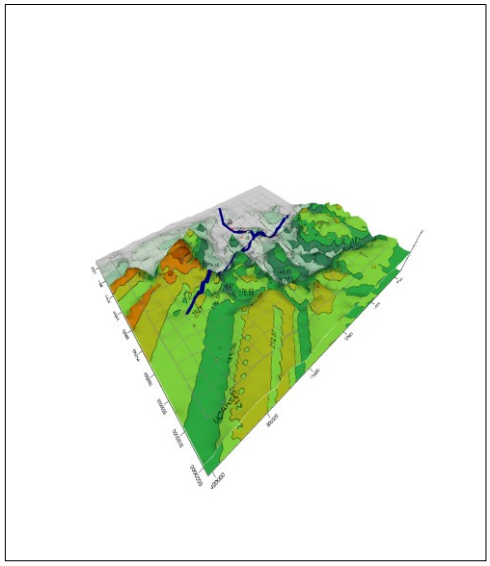

c. PIC domain

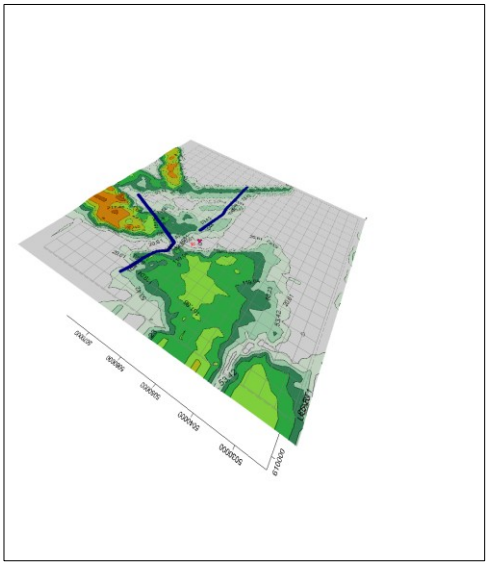

d. PRTHWKS domain

(Figures Cont'd)

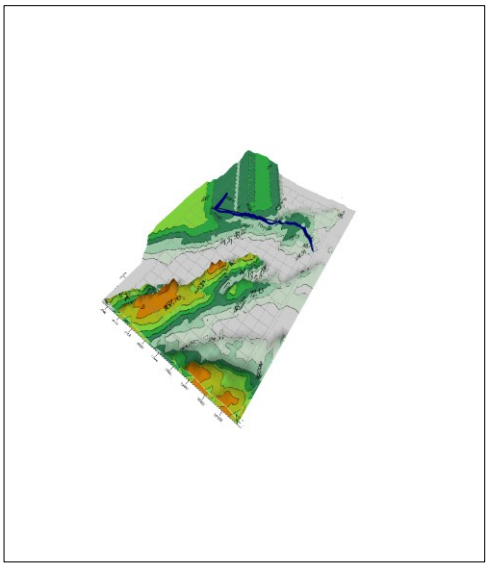

e. PTA domain

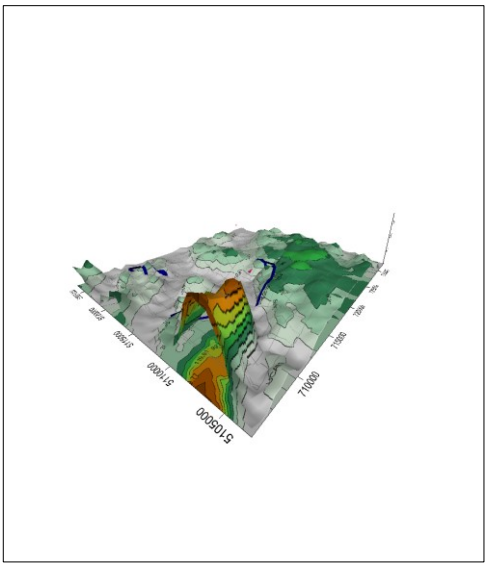

f. SYD domain

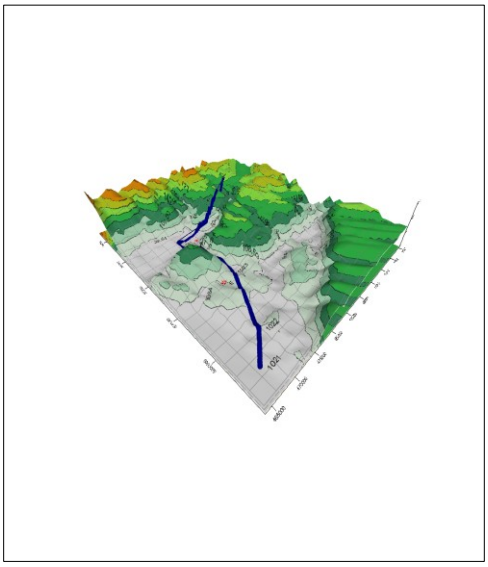

g. TRR domain

3.8 Emission Source Characteristics and Emission Rates

$PM_{2.5}$, SO_2 and NO_x emission sources in NS are categorized in groups such as point, linear and area sources covering industrial, vehicular and domestic sources, respectively. Total amounts of $PM_{2.5}$, SO_2 and NO_x emitted from these sources were estimated using different methods such as continuous monitoring system, predictive emission monitoring and source testing mass balance (Green, 2008). Table 5 shows the summery of total amount of $PM_{2.5}$, SO_2, NO_x emissions per year from 24 point sources in Nova Scotia during 2004-2007, collected from the NPRI database.

Table 5 Point Source Yearly Emission Rate 2004-2007

	2004 ER (t yr^{-1})			2005 ER (t yr^{-1})			2006 ER (t yr^{-1})			2007 ER (t yr^{-1})		
Stack Location	NO_x	SO_2	$PM_{2.5}$	NO_x	SO_2	$PM_{2.5}$	NO_x	SO_2	$PM_{2.5}$	NO_x	SO_2	$PM_{2.5}$
Dartmouth Refinery[a]	602	1112.1	20.1	328.3	NA	NA	293.4	NA	NA	302.8	NA	NA
Dartmouth Refinery[b]	593.2	992.75	61	343	NA	NA	305.1	NA	NA	298.7	NA	NA
Dartmouth Refinery[c]	596.5	1000.5	35	315.8	NA	NA	290.2	NA	NA	292.2	NA	NA
Dartmouth Refinery[d]	565.3	1070.01	9.9	324.5	NA	NA	297.9	NA	NA	304.75	NA	NA
Dartmouth Refinery[e]	558	1045.5	53.6	319.4	NA	NA	300.4	NA	NA	310.5	NA	NA
Dartmouth Refinery[f]	560	1123.98	70.4	340.2	NA	NA	295.4	NA	NA	305.3	NA	NA
Capital Health[a]	35	110.24	4.7	15	NA	NA	32.7	NA	NA	NA	NA	NA
Capital Health[b]	78	267.612	11.4	70.9	NA	NA	68.7	NA	NA	NA	NA	NA
Capital Health[c]	44	150.531	6.4	44.8	NA	NA	43.5	NA	NA	NA	NA	NA
Dalhousie University	85.9	259.923	11.4	88.6	NA	NA	85.1	NA	NA	92.2	NA	NA
Tufts Cove Power Station[a]	1463	5019.87	95.91	1225	NA	NA	425.6	NA	NA	843.3	NA	NA
Tufts Cove Power Station[b]	1422.7	4890.24	155.01	1241	NA	NA	412.8	NA	NA	835.6	NA	NA
Tufts Cove Power Station[c]	1505.6	4758.16	125.21	1256.4	NA	NA	437.7	NA	NA	852.1	NA	NA
Brooklyn Energy Plant	NA	NA	NA	NA	NA	NA	300.5	23.9	60.7	NA	NA	NA
Neenah Paper industry[a]	NA	NA	216.1	NA	NA	NA	NA	NA	NA	146.2	107.1	NA
Neenah Paper industry[b]	NA	NA	210..3	NA	NA	NA	NA	NA	NA	134.4	122.3	NA
Neenah Paper industry[c]	NA	NA	186.4	NA	NA	NA	NA	NA	NA	158.8	98	NA
Neenah Paper industry[d]	NA	NA	230.5	NA	NA	NA	NA	NA	NA	145.9	130.3	NA
New page Paper industry	NA	1164.6	NA	NA	560.5	14.7	NA	NA	NA	NA	NA	NA
ExxonMobil	NA	NA	NA	NA	NA	1.2	NA	NA	NA	NA	NA	NA
Point Aconi	NA	NA	NA	1571	4540	9.6	NA	NA	NA	NA	NA	NA
Lingan Power Station	14882	56755.7	NA	15888	NA	73.7	12814	NA	NA	8941	NA	NA
Brookfield cement plant	NA	NA	NA	NA	NA	NA	NA	NA	NA	587	659	8
Truro Paper Mill	NA	NA	NA	NA	NA	NA	NA	NA	NA	2.5	10.2	0.4

3.8.1 Point Sources

Point emission sources of $PM_{2.5}$, SO_2 and NO_x in NS include the chimney stacks from power generation, cement plants, paper manufacturing industry and oil refineries. These point sources are located in different counties across the province. Twenty four point sources of different emission characteristics' are included in this study. The stack characteristics used in this study is shown in Table 6.

Table 6 Point Emission Source Characteristics

Domain	Stack Location	Stack Characteristics	Latitude (m)	Longitude (m)	Height (m)	Dia (m)	Exit Velocity (m/s)	Exit Temperature (°K)
Halifax	Dartmouth Refinery[a]	Vacuum Furnace Stack	457301.7	4943212.3	51	1.72	10	573
	Dartmouth Refinery[b]	Feed Preheat Furnace Stacks	457799.02	4943127.4	59.5	1.3	1.3	590
	Dartmouth Refinery[c]	Atmospheric Furnace Stack	458045.61	4944442.52	61.9	1.31	8.7	646
	Dartmouth Refinery[d]	Furnace Stacks	459114.14	4943620.57	50.9	1.37	6.4	503
	Dartmouth Refinery[e]	Incinerator Stack	458127.8	4946086	61	0.79	15	788
	Dartmouth Refinery[f]	Flare Stack	4599771.7	4942387.65	56.4	0.61	30.8	1273
	Capital Health[a]	Steel stack	456494	4944584	53.33	1.22	20	563
	Capital Health[b]	Brick stack	447087.29	4951404.04	200	6	5.6	563
	Capital Health[c]	Steel Stack	453561.8	4943704.6	56.08	1.22	20	563
	Dalhousie University	Central Services Building Stack	453380.5	4942761.7	50	1.17	8.5	478
	Tufts Cove Power Station[a]	Tufts Cove Unit 5 Stack	452754.59	4947176.4	24.38	2.9	40.43	727
	Tufts Cove Power Station[b]	Tufts Cove Unit 2 Stack	452538.54	4949045.45	152	2.44	12	448
	Tufts Cove Power Station[c]	Tufts Cove Unit 3 Stack	452620.73	4948141.3	152	3	29	453
Lunenburg	Brooklyn Energy Plant	FBB Stack	364050.1	4879215.3	56.39	2.44	23.2	444
Pictou	Neenah Paper industry[a]	Recovery Boiler/Modo Scrubber	521948.50	5055566.5	80.77	3.05	13.5	342
	Neenah Paper industry[b]	Power Boiler/Venturi Scrubber	522921.77	5051901.82	62.18	1.52	23	341
	Neenah Paper industry[c]	Dissolving Tank vent	520312.25	5049636.13	62.18	1.22	9.3	356
	Neenah Paper industry[d]	High Level Roof Vent	521725.35	5050396.17	76.99	1.83	20.7	321
Port Hawsbury	New page Paper industry	Power Boiler stack	626196.73	5052845.18	51.8	3.02	20.7	460
	ExxonMobil	Fractionation Plant Flare	629646.5	5049116.4	53.6	2.98	0.1	1273
Point Aconi	Point Aconi	Point Aconi Unit 1 Stack	707545.6	5133413.4	100	3.7	29	435
Sydney	Lingan Power Station	Lingan Units Stack	728296.9	5124509.2	152	4.7	30	443
Truro	Brookfield cement plant	Main Stack	473730.6	5009588.6	60.96	3.66	19	558
	Truro Paper mill	Chimney stack	478467.6	5024646.3	50	0.15	15	373

The actual unit operation time of the chimney stacks and flare were unavailable. Therefore it was assumed that the point sources were in operation for 24-hrs a day throughout the year. On this basis, the emission rate of each chimney stack and flare were calculated. An emission factor of 1 was therefore chosen for all point sources in all domains (AERMOD Implementation Workgroup, 2009) under source group emission factor input option. Equation 4 provides the details of chimney stack emission rate calculation. For the flare sources, the effective release height of the plume was calculated as per Equations [5] and [6] due to the high temperature.

Emission rate from point sources are calculated as**,**

$$\boldsymbol{ERch = \frac{Et}{T}} \qquad [4]$$

Where,

ER_{ch} = Emission rate for a point source

Et = Total emission in grams

T = Emission period in sec

Effective release height of the flare plume

$$\boldsymbol{H_{sl} = H_s + 4.56 \times 10^{-3} \left(\frac{H_r}{4.1868}\right)^{0.478}} \qquad [5]$$

Where:

H_{sl} = effective flare height (m)

H_s = stack height above ground (m)

H_r = net heat release rate (Joules per sec, J/s)

The net heat release rate is computed as follows:

$$\boldsymbol{H_r = 44.64 \times V \times \sum_{i=1}^{n} f_i H_i \times (1 - F_r)} \qquad [6]$$

Where:

V= volumetric flow rate to the flare ($m^3\ s^{-1}$)

f_i = volume fraction of each gas component

H_i = net heating value of each component (J/g-mole)

F_r = fraction of radiative heat loss

3.8.2 Automobile Sources

Automobile emissions of $PM_{2.5}$, SO_2 and NO_x from six major highways 101,102,103, 104, 105, 106 and four main roads namely 107, 111, 118 and 125 were used for this modeling study. Lengths of the highways and main roads are given in Table 7. Automobile emission sources include light duty passenger vehicle (LDPV), light duty commercial vehicle (LDCV), medium duty commercial vehicle (MDCV) and bus (Transport Canada, May 2008).

Table 7 Lengths of the highways and main roads

Domain	Highway	Main Road	Length (km)	Total length (km)
Halifax (HFX)	101		56.66	
	102		57.83	
	103		12.81	
		107	36.86	
		111	9.04	
		118	32.65	205.84
Lunenburg (LNN)	103		28.76	28.76
Pictou (PIC)	104		44.54	
	106		19.38	63.92
Point Aconi (PTA)	105		17.45	17.45
Porthawksbury (PRTHWKS)	104		35.54	
	105		17.91	53.45
Sydney (SYD)		125	17.91	
	105		4.36	22.27
Truro (TRR)	102		35.53	
	103		26.07	61.6

Highways were divided into a number of sections by specifying the starting and end point geographical coordinates. These co-ordinates were used by AERMOD to convert section length into a volume source and treat each of these sections as a ‘volume source’ in subsequent analysis. The model also requires a specific value for the width of the highways and the average

pollutant release height. The width of highways and average emission height were chosen as 15m and 4m respectively by referring to Lake's AERMOD guide. Emission rate from each section length of highways was calculated by a total estimate method described Zou, 2010 along with the help of 'User guide for urban transportation emissions calculator' (Transport Canada, May 2008). Emission factors of CACs such as NO_x, SO_2, VOC, TPM, PM_{10}, and $PM_{2.5}$ for conventional vehicles were developed by Environment Canada using MOBILE6.2C. These emission factors were estimated based on national speed profiles of urban and inter-urban vehicles (Environment Canada, 2003). MOBILE6.2C estimates emission factors for CO, NO_x, SO_2, VOC, as well as particulate matter (TPM, PM_{10}, and $PM_{2.5}$) from type of fuel used in the vehicle combustion. CAC emission factors have the units of g per km as they are better estimated by distance travelled than amount of fuel consumed. Emission factors provided by Environment Canada for light duty passenger vehicle (LDPV), light duty commercial vehicle (LDCV), medium duty commercial vehicle (MDCV) and bus were used in this study.

Equations [7]-[9] provide the mathematical details of the above method. In this method average CAC emission factors are calculated for different contaminants based on total number of on road vehicle data available in Nova Scotia Emission inventory guide. Equation [7] is utilized to calculate the average emission factor for any of the major fuel using type vehicles such as Propane, Compressed natural gas and Electric vehicles under each category of LDPV, LDCV, MDCV and bus. Equation [8] is used to calculate the total emission factors from all kinds of vehicles on road. Emission rate of a road segment during a specific time period is calculated using equation [9].

$$\mathbf{EF_{type}} = \frac{\sum_{t=1}^{i} \mathbf{Et}}{\mathbf{n}} \qquad [7]$$

$$\mathbf{EF_{road}} = \frac{\mathbf{EFtype}}{\mathbf{N}} \qquad [8]$$

$$\mathbf{ER_{road}} = \frac{\mathbf{EFroad \times Nv \times L}}{\boldsymbol{T}} \qquad [9]$$

Where,

Ef_{type} = Average emission factor from type of fuel used vehicles under different category of automobile emission sources

Et = Individual CAC emission rate from each type of fuel used in the vehicles under different category of automobile emission sources

n = Total number of vehicles based on type of fuel used under each category of automobile emission sources

EF_{road} = Average emission factor (calculated as average g) from the total number of on road vehicles during a particular period

N = Total number of different category of automobiles emission sources

ER_{road} = On road emission rate (g sec^{-1})

L= Length of the road segment (m)

N_v = Total number of vehicles in a particular segment (no m^{-1})

T= Time period (sec)

Emission rates of the pollutants calculated using the above equations gives minimum and maximum values of 0.002 g s^{-1} and 0.8 g s^{-1} respectively. A source group emission factor of 0.1 was used during 7 p.m. through 7 a.m. and 1 for rest of the time by considering highest traffic density during day time and lowest in the night for purpose of the simulations.

3.9 Simulation Study

AERMOD simulations were performed using the maximum available data for most sensitive parameters in seven domains in different years during 2004-2007. Meteorological data from YHZM and SYDM met stations was processed in AERMET depending upon the nearest location of each domain. For example in HFX, LNN, TRR and PIC hourly surface air data from YHZM is used, whereas in PRTHWKS, SYD and PTA domain the hourly surface data from SYDM station was used. In the initial stage a number of trials were conducted to select the optimum grid size to carry out the entire dispersion study. Selective results are given in Section 4.1. Monitored GLC values of PM2.5 were available only during 2004 from two NAPS stations at Lake major and Pictou. Measured NOx was available only at Halifax downtown NAPS station. Monthly monitored SO2 GLC values were available from Halifax downtown, PortHawksbury and Sydney NAPS stations. These monitored data were compared with the simulated data to study the model performance in NS.

3.10 Canadian Ambient Air Quality Standards (CWS)

Canadian Environment Ministry established CWS in January 1998. CWS, given in Table 8 provides the details on maximum desirable, acceptable and tolerable limits for $PM_{2.5}$, NO_2 and SO_2 at the ground level. These values can be used to compare with AERMOD predicted GLCs to estimate the level of pollution across the province.

Table 8 Canada wide ambient air quality standards

Pollutant	Averaging Time	Maximum Desirable Level	Maximum Acceptable Level	Maximum Tolerable Level
Sulfur dioxide (SO_2)	annual	11 ppb	23 ppb	---
	24 hours	57 ppb	115 ppb	306 ppb
	1 hour	172 ppb	334 ppb	---
Nitrogen Dioxide (NO_2)	annual	32 ppb	53 ppb	---
	24 hours	---	106 ppb	160 ppb
	1 hour	---	213 ppb	532 ppb
$PM_{2.5}$	24 hours			30 µg m^{-3}

3.11 Model Performance Analysis

AERMOD performance is evaluated by comparing the simulated GLC values with observed GLC values from four NAPS stations across the province. The coefficient of determination (R^2) value indicates the strength of relationship between the simulated and observed values. R^2 describes the proportion of the variance in measured data computed by the model (Hoare, Regan, & Wilson, 2008). R^2 ranges from 0 to 1 and calculated using Equation 10,

$$\mathbf{R^2} = \left[\frac{\sum_{i=1}^{n}(Oi-Oavg)(Si-Savg)}{[\sum_{i=1}^{n}(Oi-Oavg)^2 \sum_{i=1}^{n}(si-savg)^2]}\right]^2 \qquad [10]$$

Where, O_i = observed GLC values

S_i = model predicted GLC values

O_{avg} = average of observed GLC values and

S_{avg} = average of simulated GLC values

CHAPTER 4: RESULTS AND DISCUSSION

Selection of receptor mesh spacing, results and discussion on AERMOD predicted GLCs and dispersion patterns of NO_x, SO_2 and $PM_{2.5}$ respectively in seven modeling domains across NS are comprised in this section. Comparison between the predicted and observed GLC values of the above three pollutants in HFX, SYD, PRTHWKS and PIC domain are also discussed.

4.1 Selection of Receptor mesh Spacing

At an early stage of this dispersion modeling study, several simulations were carried out to understand the effect of receptor mesh spacing on AERMOD predicted GLC values. A Cartesian mesh with horizontal and lateral spacing of 1.25 km × 1.25 km in an area of 48 km × 47 km was chosen in HFX domain in the beginning of this study by referring the study of Zou, 2003. The simulations were carried out for 2004 $PM_{2.5}$ data, using a computer with processor speed of 2.4 GH and Random Accessible Memory of 4GB. AERMOD predicted results are shown in Figure 8. Due to selection of above mentioned spacing, 1650 receptor points were generated which included emission sources as well. Each receptor point was assigned with its elevation and hill height by AERMAP. The simulation took fifteen days for the annual averaging of $PM_{2.5}$ in HFX. After conducting several trials with different spacing, another mesh with horizontal and lateral spacing of 2.45 km × 2.45 km was chosen in HFX to reduce the simulation time to four days without affecting the model performance. In this case 824 receptor points were generated including the emission sources. The simulation results of the simulation are shown in Figure 9. In this case simulation time reduced to four days which is reasonable. Four discrete Cartesian receptors (D1, D2, D3 and D4) were assigned in both cases to check the model efficiency in computing the GLCs at those receptor points. Coordinates of the receptors and GLC values in both cases are given in Table 9; $PM_{2.5}$ concentration values at those four receptors remained same in both cases. With reference to Table 9, it is seen that a mesh spacing between the 1.25 km × 1.25 km and 2.45 km × 2.45 km is suitable for conducting the dispersion study. Therefore, depending upon the dimension of each modeling domain, horizontal and lateral spacing between the 1.25 km × 1.25 km and 2.45 km × 2.45 km were chosen to achieve maximum number of receptor points.

Figure 8a-b Annual GLCs of $PM_{2.5}$ due to point and highway emission sources in HFX domain

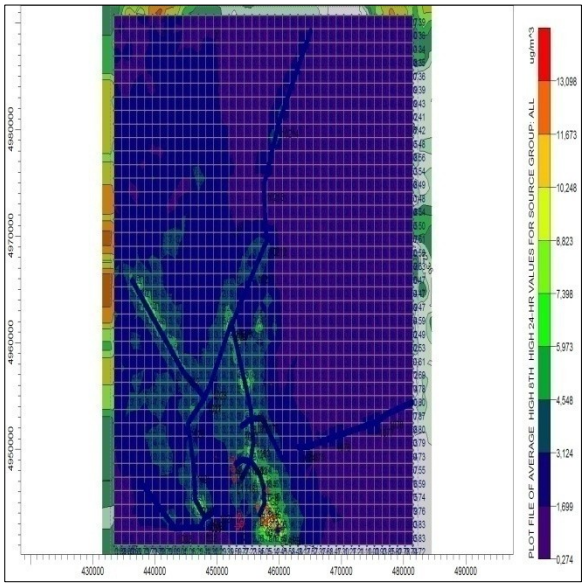

a. $PM_{2.5}$ concentration contours using mesh spacing 1.25 km×1.25 km

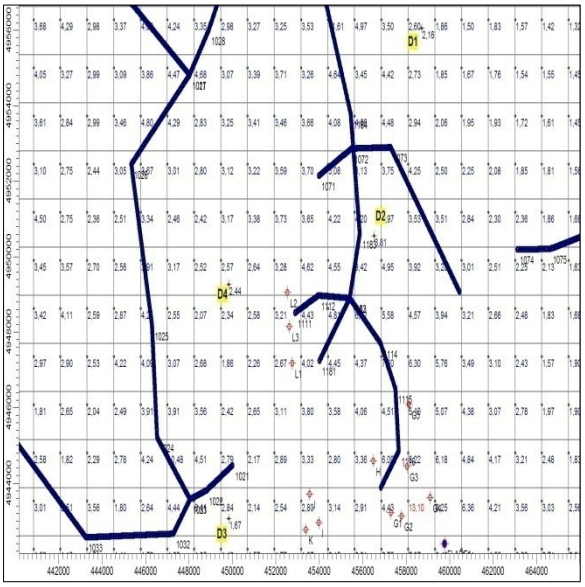

b. Locations and concentrations of $PM_{2.5}$ at four discrete Cartesian receptors

Figures 9a-b Annual GLCs of $PM_{2.5}$ due to point and highway emission sources in HFX domain

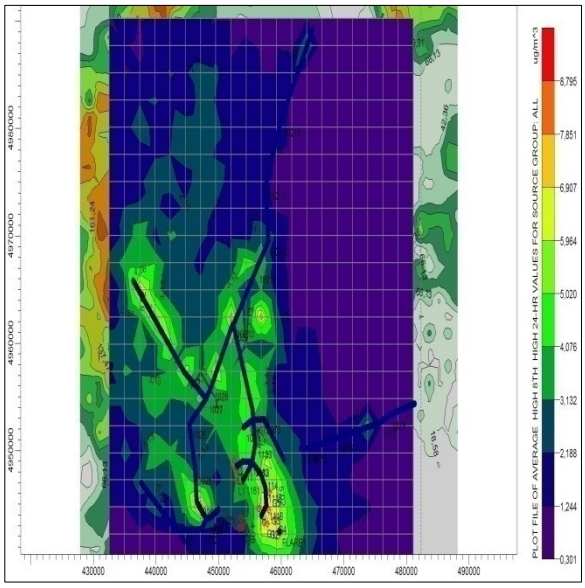

a. $PM_{2.5}$ concentration contours using mesh spacing 2.45 km×2.45 km

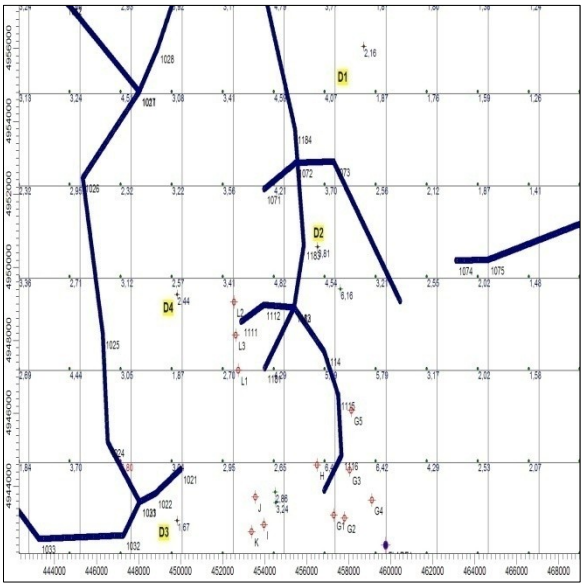

b. Locations and concentrations of $PM_{2.5}$ at four discrete Cartesian receptors

Table 9 $PM_{2.5}$ at four discrete receptors in HFX domain

CASE 1	Discrete Receptor	Latitude (m)	Longitude (m)	$PM_{2.5}$ $[\mu g\ m^{-3}]$
	D1	458691.87	4956093.85	2.16
	D2	456493.64	4950610.9	3.81
	D3	449823.14	4949297.02	1.67
	D4	449848.41	4949271.75	2.44
CASE 2	D1	458691.87	4956093.85	2.16
	D2	456493.64	4950610.9	3.81
	D3	449823.14	4949297.02	1.67
	D4	449848.41	4949271.75	2.44

4.2 Modeling Results for NO_x in HFX and SYD Domain

As discussed in Chapter 3, most of the point and linear emission sources were available from HFX domain. Also the surface air meteorological data was collected from two weather stations in HFX and SYD domain respectively. Based upon above two criterions the dispersion modeling study was initiated from HFX and SYD domain. At preliminarily stages dispersion simulations of NO_x was carried out in above mentioned two domains for four consecutive years from 2004 to 2007. NO_x was chosen in particular due to the availability of more complete emission data than other pollutants such as $PM_{2.5}$ and SO_2. The dispersion pattern and GLC values during each year are discussed here.

4.2.1 Annual Averaging of NO_x in HFX Domain

AERMOD predicted GLC contour maps of NO_x in HFX domain from 2004 to 2007 are shown in the Figure 10. It is indicated that the prevailing wind effect the advection of NO_x towards North East during the four year period. It is also seen from Figures that the dispersion patterns of NO_x were similar during the above period. Capital health and Dalhousie university chimney stacks contributed comparatively lesser amount of ground level NO_x concentration than Tuff's Cove power generation station and Dartmouth refinery during this period. Large release heights of the point sources were affected by the high surface roughness of the urban areas of HFX domain (Grosch & Lee, 1998). Therefore, the high GLCs were found near the emission sources. In case of highways, surface release height did not allow emissions to disperse far from sources. In 2006, the number of vehicles on highway 102 was highest compared to other years, resulting in highest GLC near the intersection of highway 102 and main road 118. Locations and elevations of annual maximum and minimum ground level NO_x concentration receptors are given in Table 10. With reference to the table for HFX domain, it is seen that the annual maximum GLCs are predicted at same location, 2.5 km east of the Dartmouth refinery in 2004, 2005 and 2007. In 2006, the highest GLC was found at 500 m North East of the intersection of highway 102 and main road 118. Minimum GLC receptor (x-479431.09m: y-4991077m) is located at the North East corner of the domain boundary. During the modeling period minimum GLC receptor remained unchanged.

Figures 10a-d Annual GLCs of NO_x due to point and highway emission sources in HFX domain

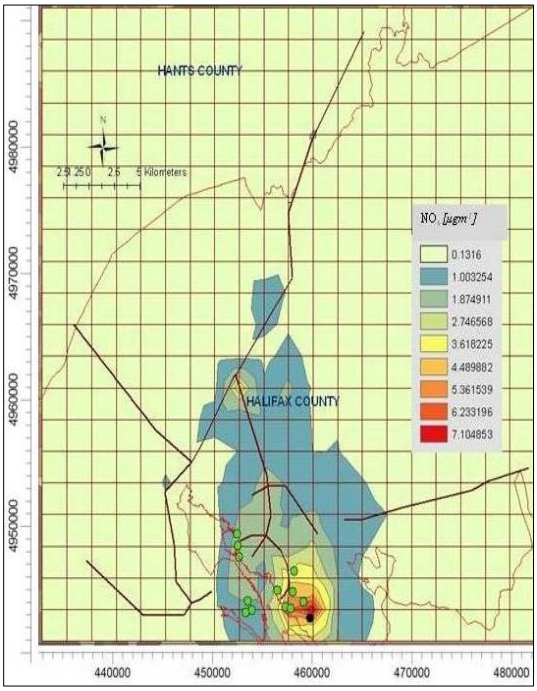

a. 2004

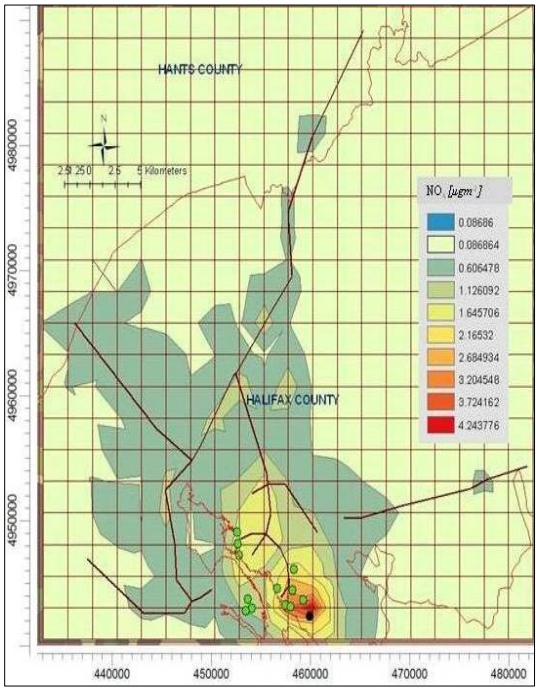

b. 2005

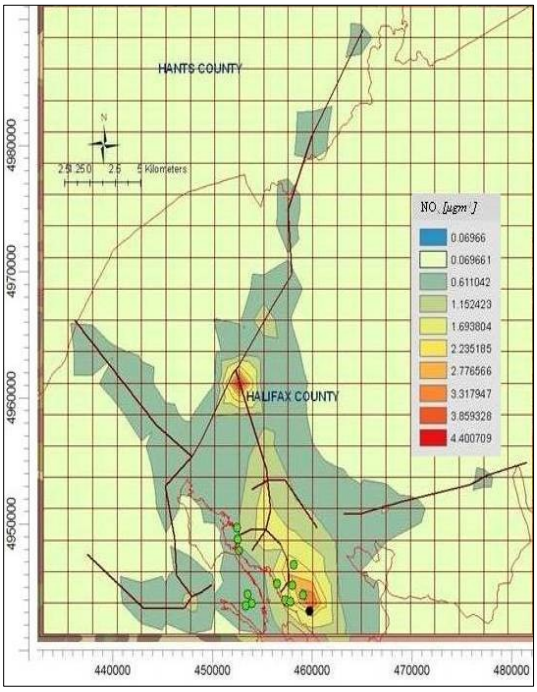

c. 2006

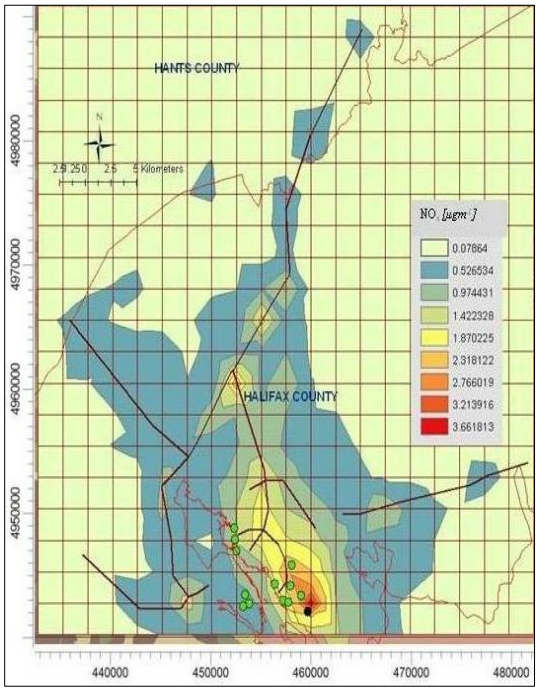

d. 2007

4.2.2 Annual Averaging of NO_x in SYD Domain

AERMOD predicted GLC contour maps of NO_x in SYD domain from 2004 through 2007 are shown in Figure 11. An extremely high (200m) release height of the Lignan power generation station, located at the downwind plume, caused negligible amount of ground level NO_x concentration due to the point release source. With reference to Figure 11, it is seen that the dispersion pattern of NO_x was determined by emissions from highway 105 and main road 125 during the modeling period. Wind direction towards North East dominated the NO_x dispersion in this domain. As seen in case of SYD domain, surface release height and high Bowen ratio due to presence of the water body effected the dispersion of pollutants from vehicle emissions as a result major portion of GLCs were found within 500m radius of highway and main road. Locations and elevations of annual maximum and minimum ground level NO_x concentration receptors are given in the Table 10. With reference to the table, it is seen that the annual maximum GLCs were predicted at the same coordinate which is located at the west end of SYD domain and 2.5 km east of main road 125. Minimum GLC receptor (x-727669m: y-5124407m) was located at 200 m south west of Lignan generation station. Location of minimum GLC receiving receptor remained the same throughout the modeling period. Though the receptor was at downwind direction of highway 105, it was not affected by the emission from highway 105.

Figures 11a-d Annual GLCs of NO_x due to point and highway emission sources in SYD domain

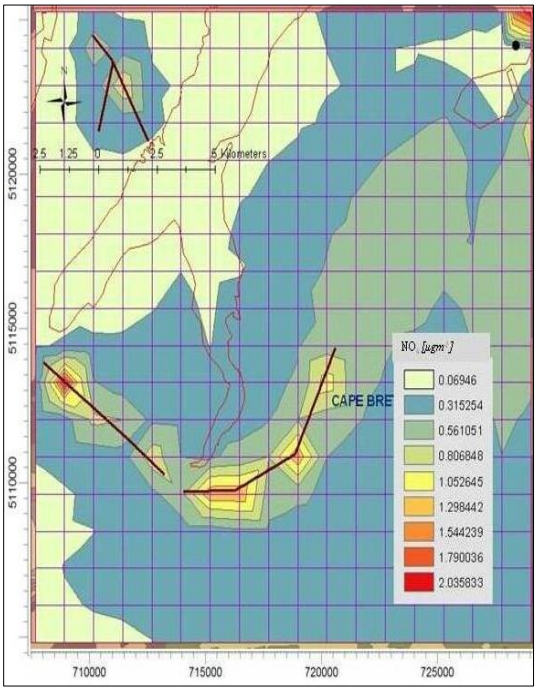

a. 2004

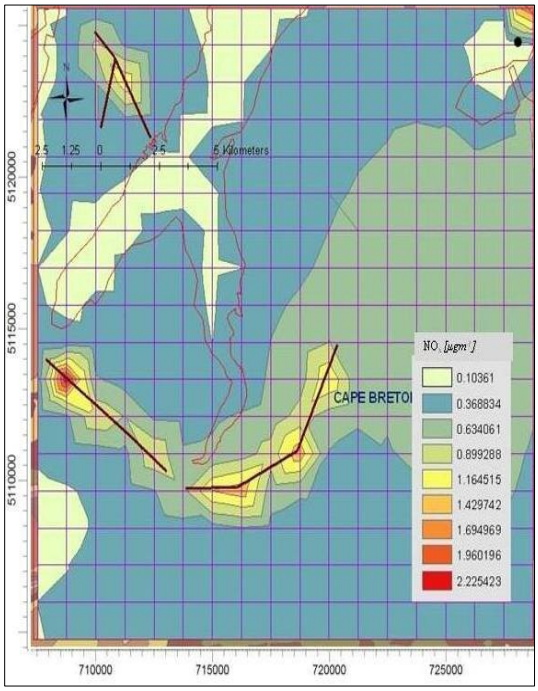

b. 2005

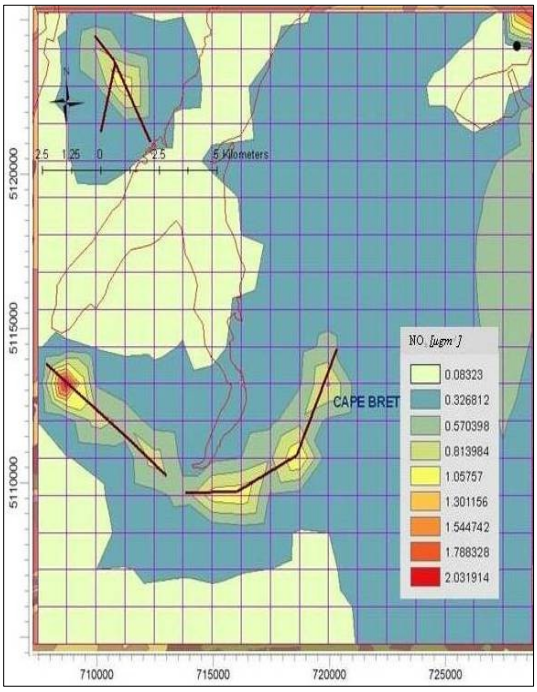

c. 2006

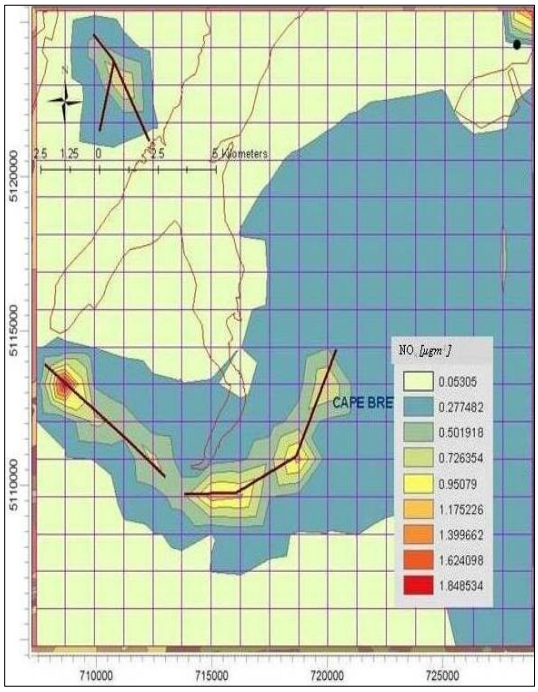

d. 2007

Table 10 Annual MAX and MIN NO_x GLC receptors during 2004-2007

Domain	Year	Annual Min *[μg m^{-3}]* UTM coordinate (m) Elevation (m)	Annual Max *[μg m^{-3}]* UTM coordinate (m) Elevation (m)
HFX	2004	0.136 (479431.09:4991077) NA	8.38 (460010.94:4943021) 41.7
	2005	0.087 (479431.09:4991077) NA	4.763 (460010.94:4943021) 41.7
	2006	0.069 (479431.09:4991077) NA	4.942 (452728.38:4960726) 101.7
	2007	0.078 (479431.09:4991077) NA	4.11 (460010.94:4943021) 41.7
SYD	2004	0.044 (727669:5124407) 28.2	2.048 (708919:5113157) 32.1
	2005	0.1036 (727669:5124407) 28.2	2.491 (708919:5113157) 32.1
	2006	0.083 (727669:5124407) 28.2	2.276 (708919:5113157) 32.1
	2007	0.053 (727669:5124407) 28.2	2.073 (708919:5113157) 32.1

4.3 Modeling of NO_x, SO_2 and $PM_{2.5}$ Dispersion in Seven Domains across Nova Scotia

In the next stage of the dispersion study, an attempt was made to conduct the simulations of NO_x, $PM_{2.5}$ and SO_2 for four year period from 2004 to 2007 in LNN, PTA, TRR, PRTHWKS, SYD, PIC and HFX domain. It was then seen that several mandatory model input information was missing from the Nova Scotia Emission Inventory. One of the important information was the total quantity of NO_x, $PM_{2.5}$ and SO_2 emission from every point source in each domain. Another missing data was traffic counts from the highways and the main roads during every year in each domain. Therefore it was not possible to run the dispersion simulations for four consecutive years in every domain. A decision was then taken to conduct the dispersion study based upon the maximum available data for every domain during the above period. On this basis LNN, PTA, TRR and HFX domain had more complete NO_x, SO_2 and $PM_{2.5}$ emission data for the years 2006, 2005, 2007 and 2004 respectively. PRTHWKS domain had NO_x and $PM_{2.5}$ data for the year 2005 and SO_2 data for the year 2004. SYD domain had NO_x and SO_2 data for the year 2004 and $PM_{2.5}$ data for the year 2005. PIC domain had NO_x and SO_2 data for the year 2005 and $PM_{2.5}$ data for the year 2004. The dispersion study in each domain includes the annual, monthly and hourly averaging of NO_x, SO_2 and $PM_{2.5}$. In the case of annual averaging of NO_x dispersion in HFX and SYD domain are discussed in detail than previous section as the information will be used in the next section for comparison with the monitored GLC at 3 NAPS stations.

4.3.1 Modeling Study in LNN domain

Emission of NO_x, SO_2 and $PM_{2.5}$ from Brooklyn energy plant and 28.76 km section length of highway 103 are included for conducting the dispersion simulation studies in LNN domain during 2006.

4.3.1.1 Annual averaging of NO_x, SO_2 and $PM_{2.5}$

AERMOD predicted GLC contour maps of NO_x, SO_2 and $PM_{2.5}$ during annual averaging period are shown in the Figures 12 through 14. As seen from Figures 12 and 14, highest annual average NO_x and $PM_{2.5}$ concentration gradients were found at 4 km North East of the Brooklyn energy power plant. The highest annual average SO_2 concentration is seen at South end of the domain,

near to highway 103. With reference to above figures, GLCs of the three pollutants were low at far distances from the emission sources during annual averaging period. According to Table 11 the minimum and maximum annual average predicted NO_x concentrations were 0.003 µg m^{-3} located at 326637.18m: 4867589m, elevation NA and 0.679 µg m^{-3} located at 364104.94m: 4880056.5m, elevation 27.1 m respectively. The annual minimum and maximum predicted SO_2 concentration were 0.001 µg m^{-3} found at 326637.18m: 4867589m, elevation NA and 0.127µg m^{-3} at the coordinates 354113.53m: 4870082.5m, elevation 55.5 m respectively. The minimum and maximum annual average $PM_{2.5}$ concentrations were 0.001 µg m^{-3} found at 326637.18m: 4867589m elevation NA and 0.151µgm^{-3} at 364104.94m: 4880056.5m, elevation 27.1 m respectively. High GLCs could be seen far from emission sources due to small surface roughness and flat terrain but the low emission rate and the height of the stack influenced high GLCs of NO_x and $PM_{2.5}$ near the emission source (Grosch & Lee, 1998). With reference to highway emission data, it is seen that the SO_2, emission from highway vehicles was higher than the point source emission. Advection of SO_2 was affected by the lower release height of the vehicles. High GLCs are also seen along the length of the highway within 1 km radius due to poor dispersion of highway emission.

Figure 12 Annual GLCs of NO_x due to point and highway emission sources

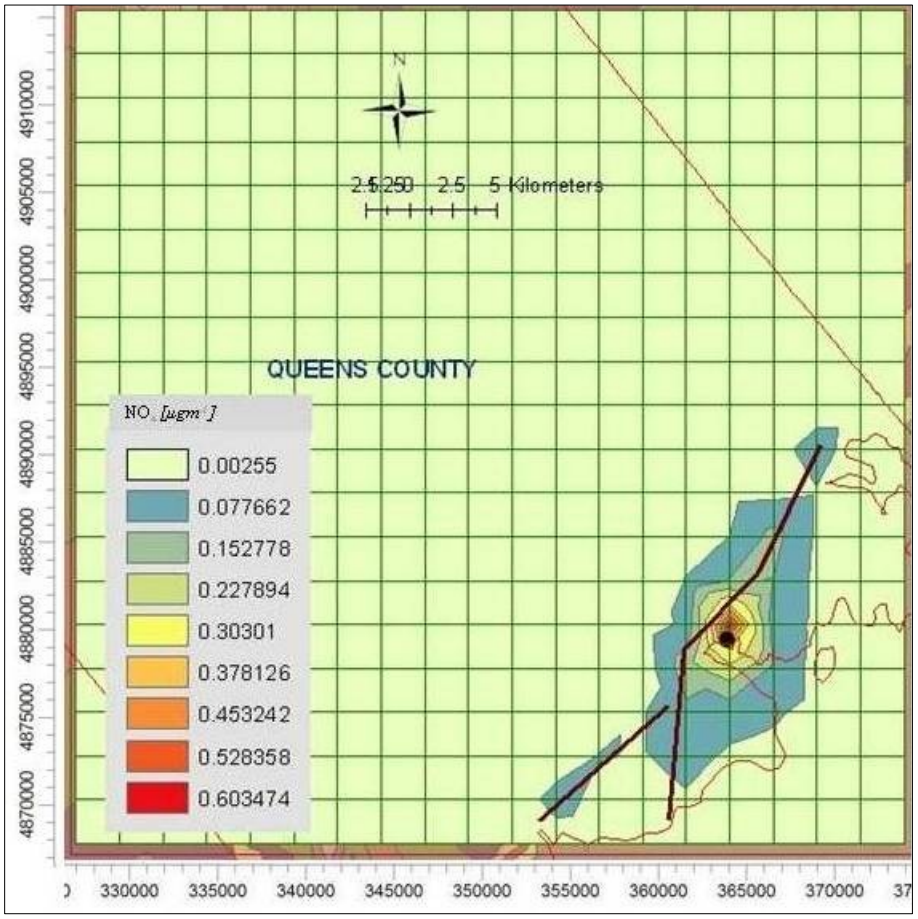

Figure 13 Annual GLCs of SO_2 due to due to point and highway emission sources

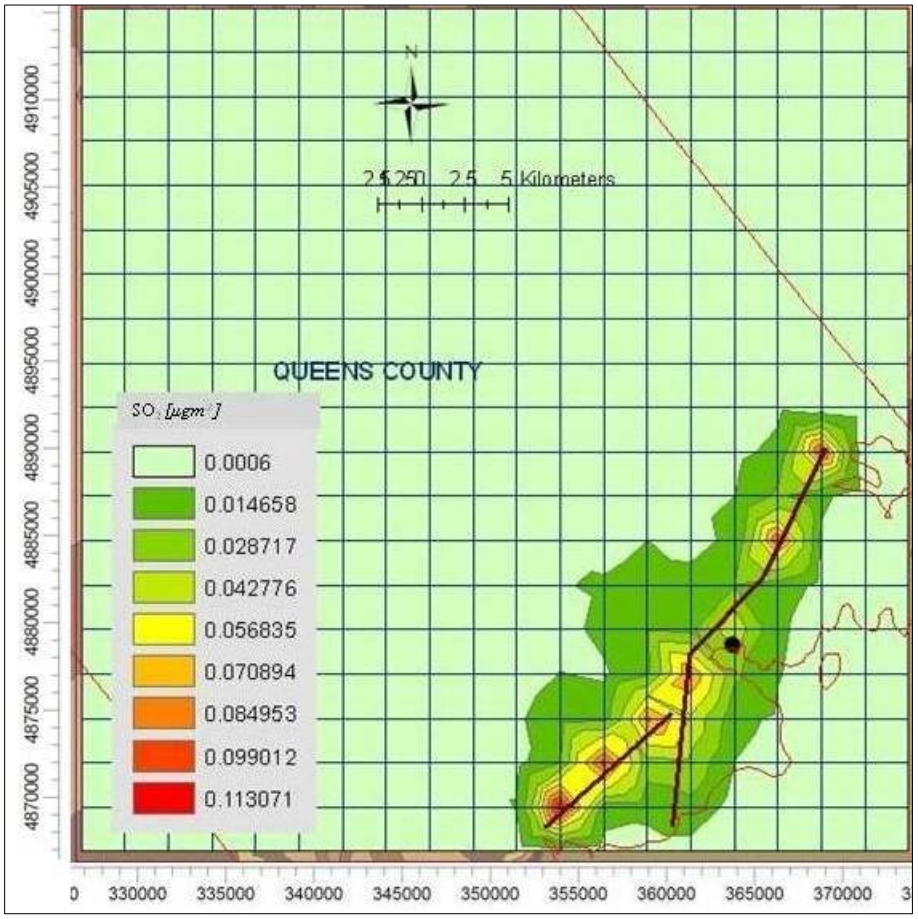

Figure 14 Annual GLCs of $PM_{2.5}$ due to due to point and highway emission sources

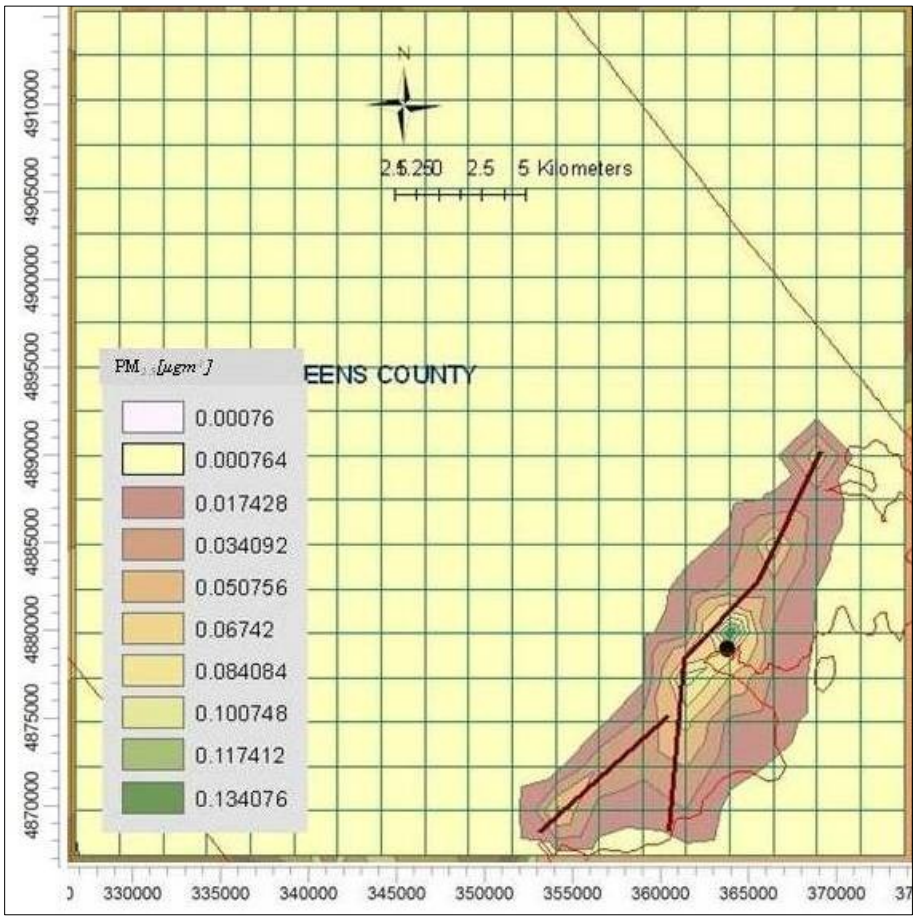

Table 11 Annual MAX and MIN GLCs of NO_x, SO_2 and $PM_{2.5}$

Pollutant	Annual Min *[µg m^{-3}]* UTM Coordinate(m) Elevation (m)	Annual Max *[µg m^{-3}]* UTM Coordinate(m) Elevation (m)
NO_x	0.003 (326637.18: 4867589) NA	0.679 (364104.94: 4880056.5) 27.1
SO_2	0.001 (326637.18: 4867589) NA	0.127 (354113.53:4870082.5) 55.5
$PM_{2.5}$	0.001 (326637.18: 4867589) NA	0.151 (364104.94: 4880056.5) 27.1

4.3.1.2 Monthly Averaging of NO_x, SO_2 and $PM_{2.5}$

Figures 15 through 17 show the monthly maps of predicted NO_x, SO_2 and $PM_{2.5}$ concentration contours in the LNN domain respectively. The chimney stack of the Brooklyn energy plant contributed more NO_x and $PM_{2.5}$ emission than highway 103. With reference to the monthly maps, small amount of NO_x dispersed far from emission sources with significant change in ambient temperature such as in the months of April and October. This phenomenon indicates that the release height of point source had greater impact on NO_x dispersal compared to SO_2 and $PM_{2.5.}$ SO_2 and $PM_{2.5}$ dispersed within 5 km radius of emission sources due to highway being the major emission source of these two pollutants. It can be seen from Table 12, the minimum and maximum monthly predicted NO_x concentrations were 0.294 μg m^{-3}(October) at coordinates 364104.94m: 4877563m, elevation 3.4m and 0.952 μg m^{-3} (July) at coordinates 364104.94m: 4880056.5m, elevation 27.1 m respectively. The minimum and maximum monthly predicted SO_2 concentrations were 0.089 μg m^{-3} (December) at coordinate 354113.53m: 4870082.5m, elevation 55.5 m and 0.184 μg m-3 (May) at the same coordinate as minimum concentration respectively. The minimum and maximum hourly predicted $PM_{2.5}$ concentrations were 0.112 μg m^{-3} (December) at coordinates 361607.09m: 4877563m, elevation 7 m and 0.231μg m^{-3} (May) at coordinates 354113.53m: 4870082.5m, elevation 55.5m. Monthly averaging demonstrates that GLCs increased from winter months to summer months due to ambient temperature rise in summer months. It is also seen from Figure 15 through 17 that the dispersal rate was also higher during summer months compared to winter months. Enhancement of SO_2 and $PM_{2.5}$ GLC during late fall months was influenced by the lower dispersal rate. It can be seen from Table 12 that the minimum GLCs of all three pollutants remained constant throughout the year. This scenario indicates, after occurrence of maximum dispersal, negligible amount of pollutants concentration persisted at ground level.

Figures 15a-l Monthly LCs of NO_x due to point and highway emission sources

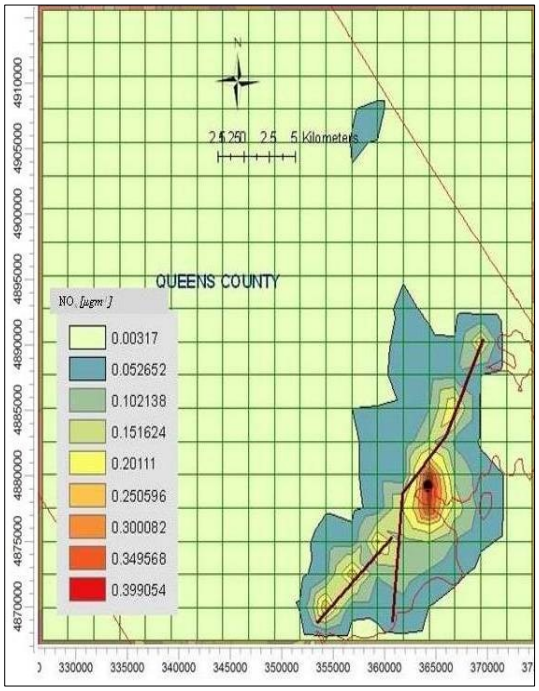

a. January

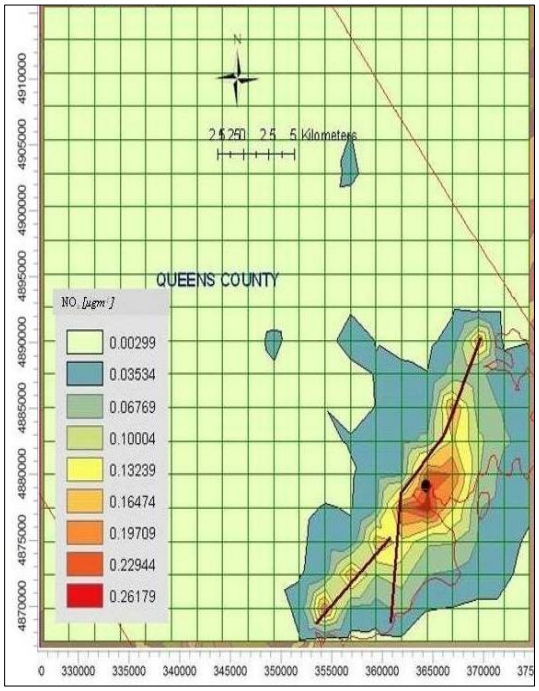

b. February

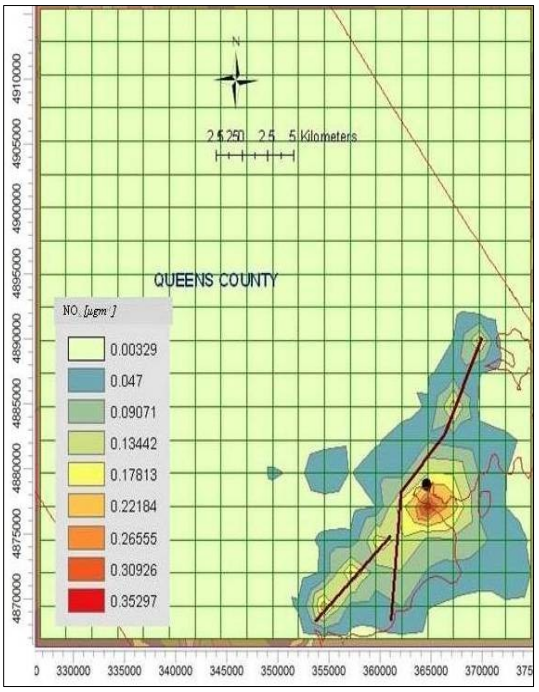

c. March

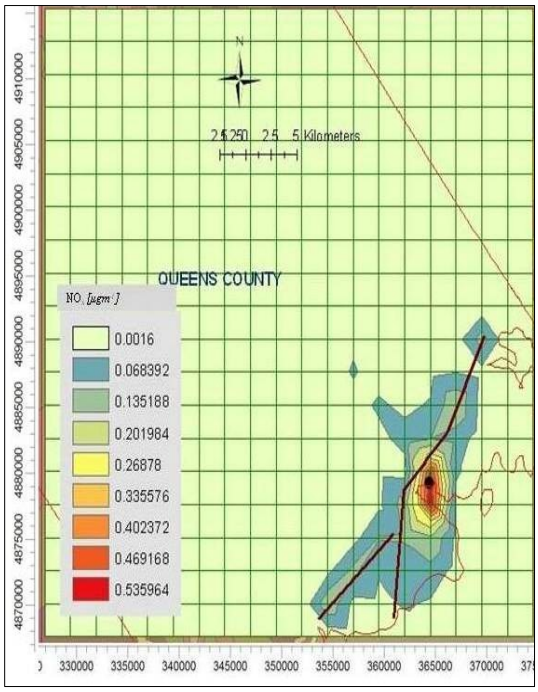

d. April

(Figures Cont'd)

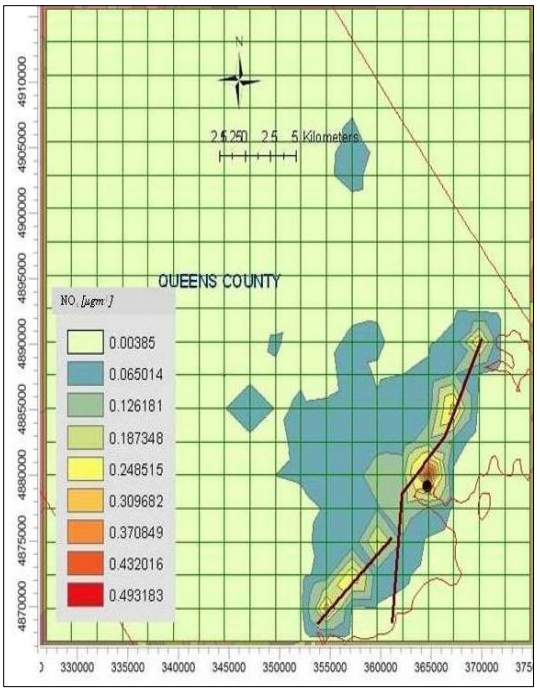

e. May

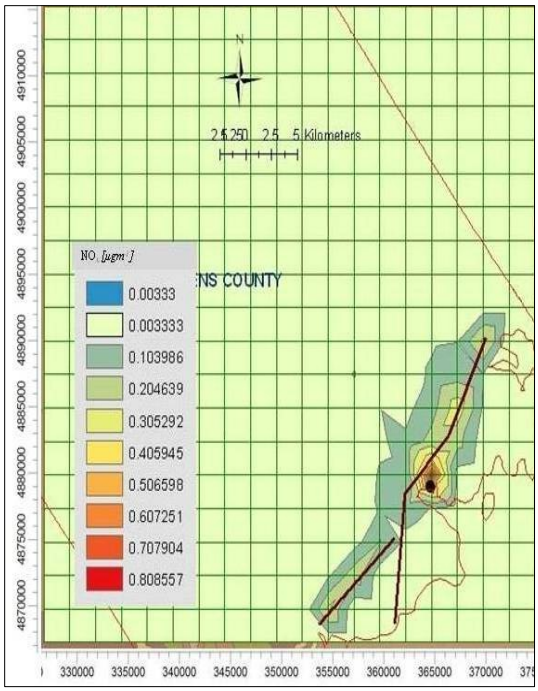

f. June

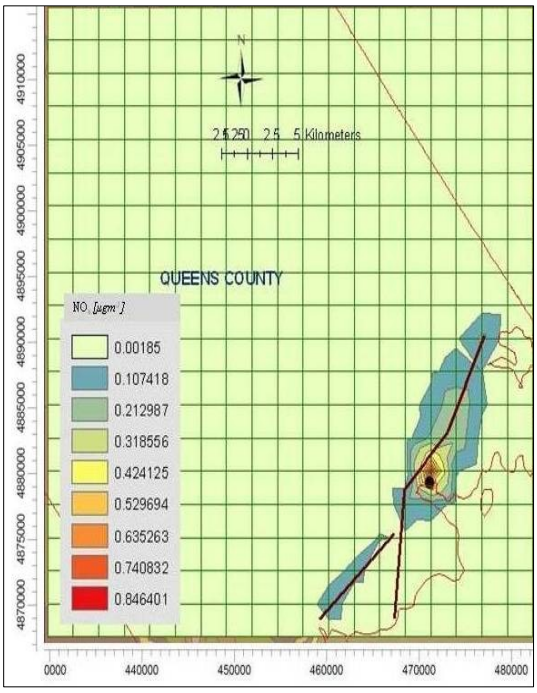

g. July

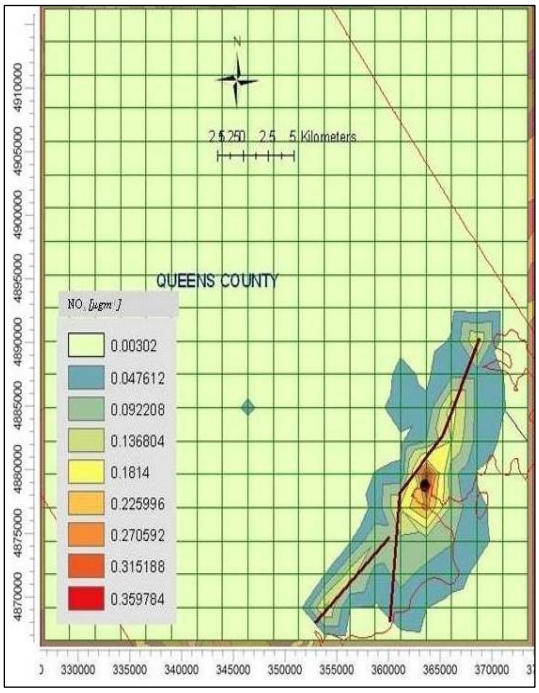

h. August

(Figures Cont'd)

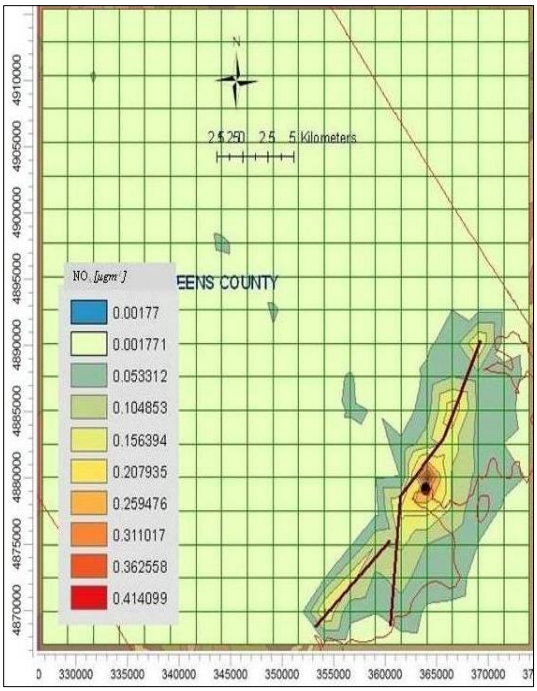

i. September

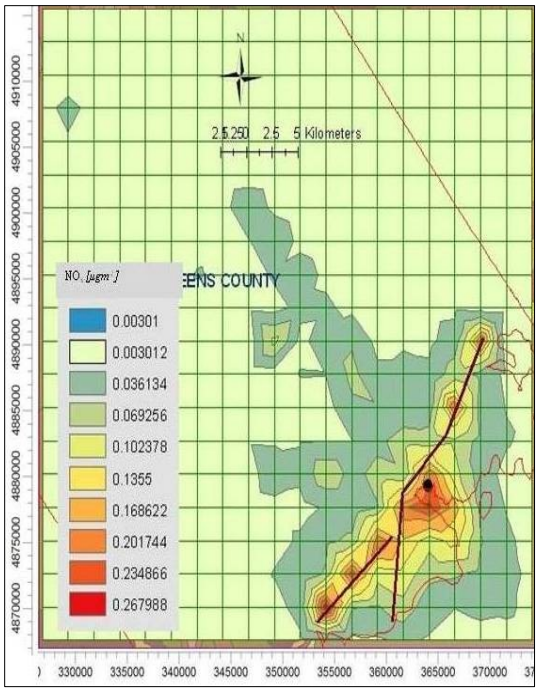

j. October

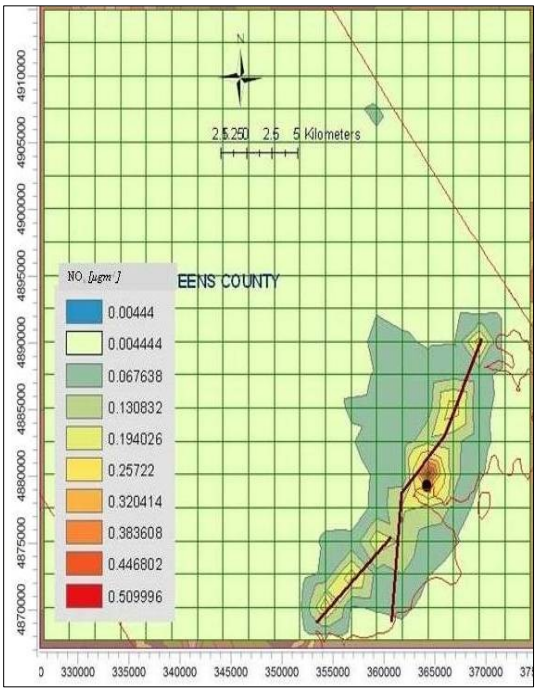

k. November

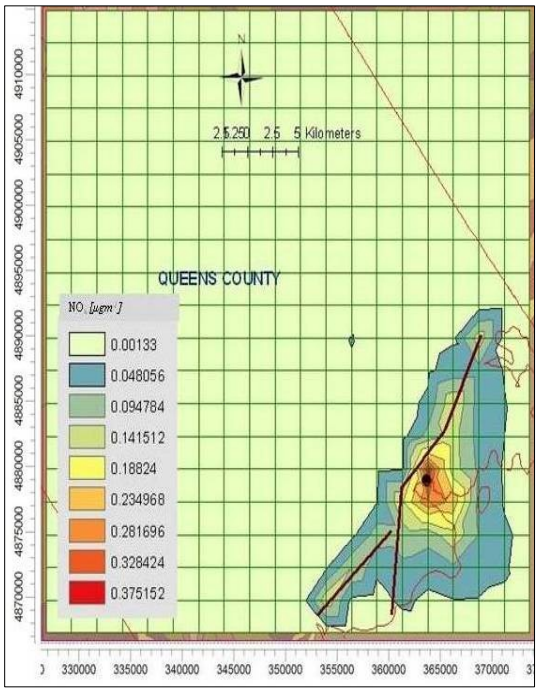

l. December

Figures 16a-l Monthly GLCs of SO_2 due to point and highway emission sources

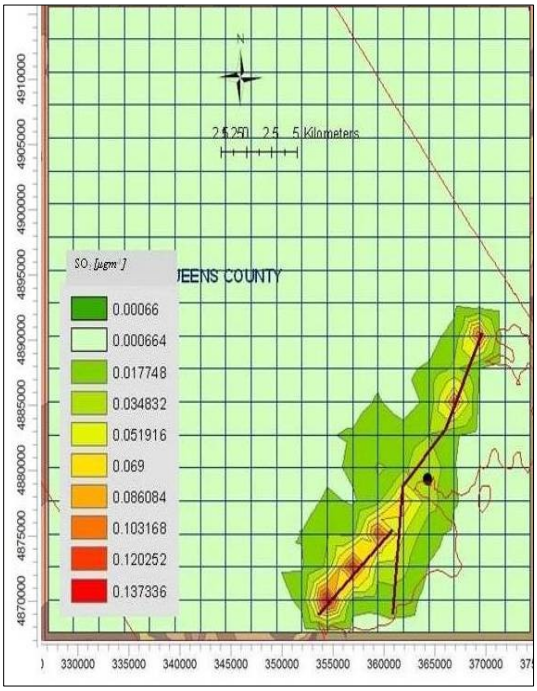

a. January

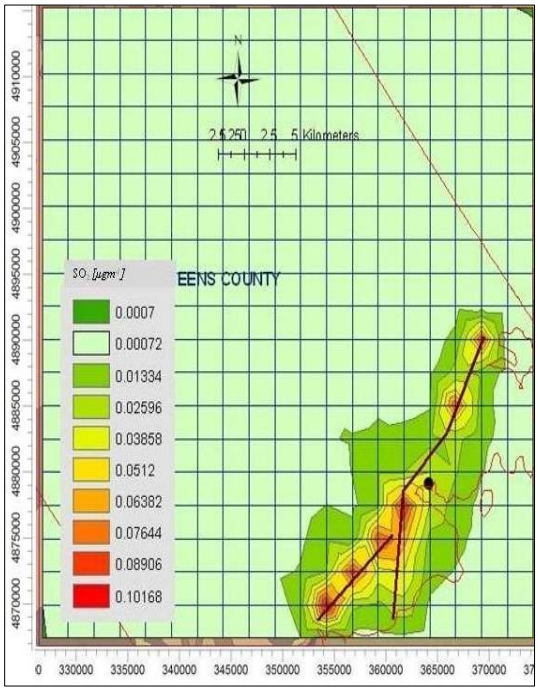

b. February

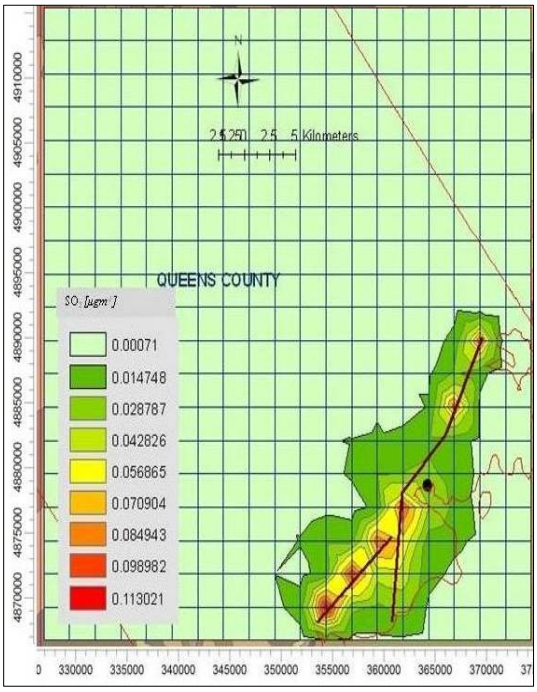

c. March

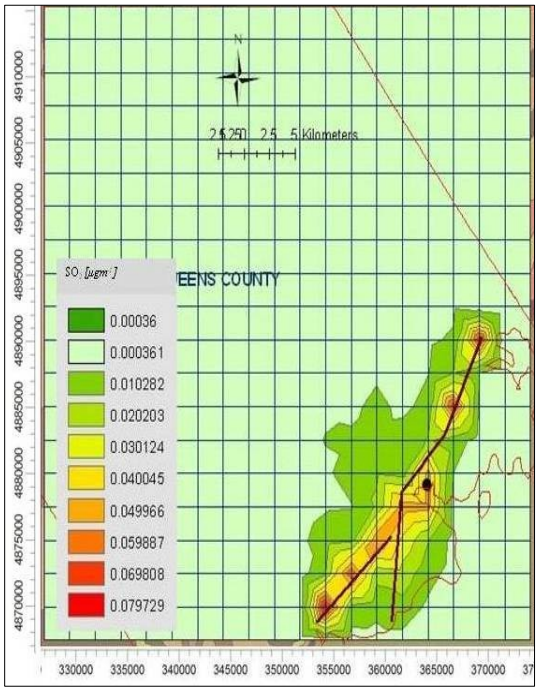

d. April

(Figures Cont'd)

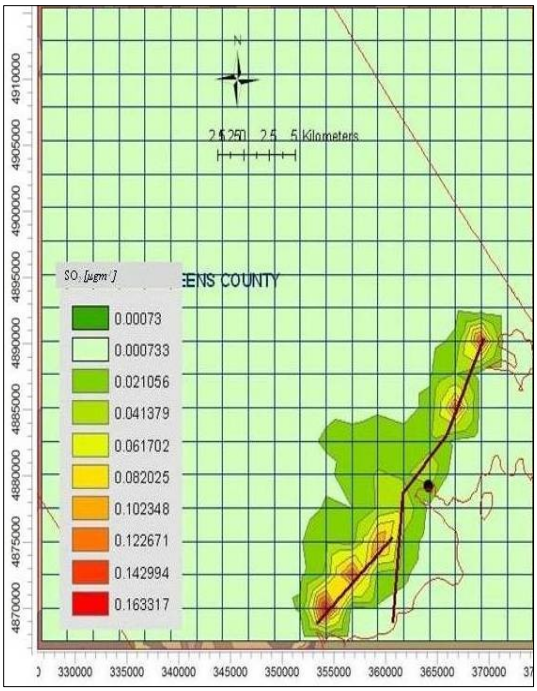

e. May

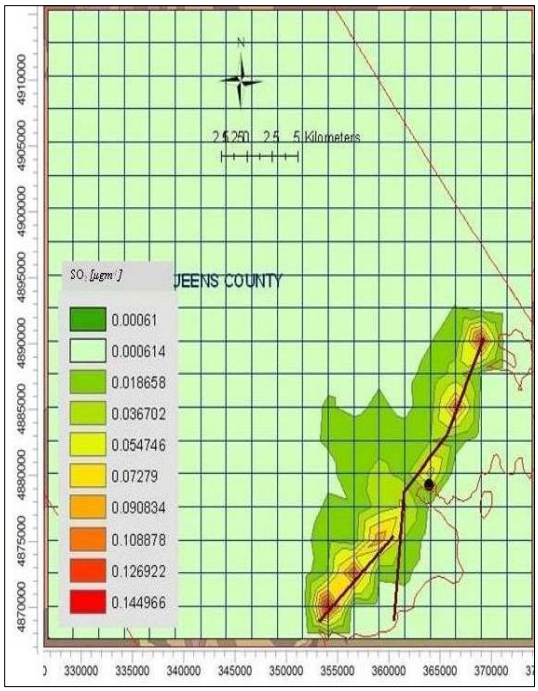

f. June

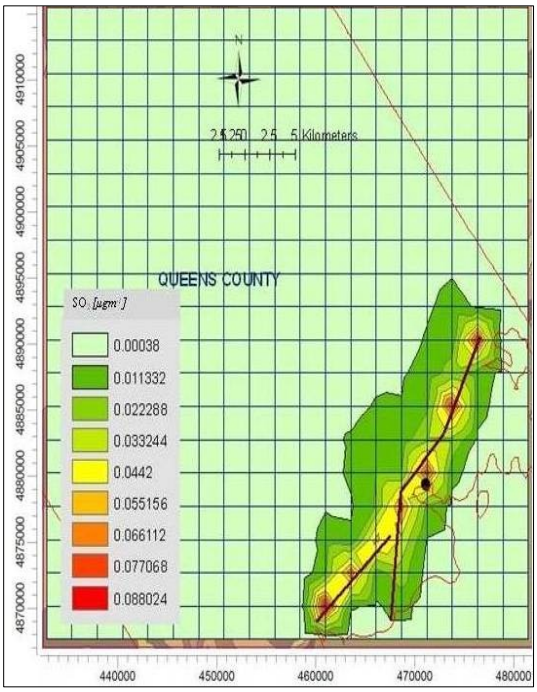

g. July

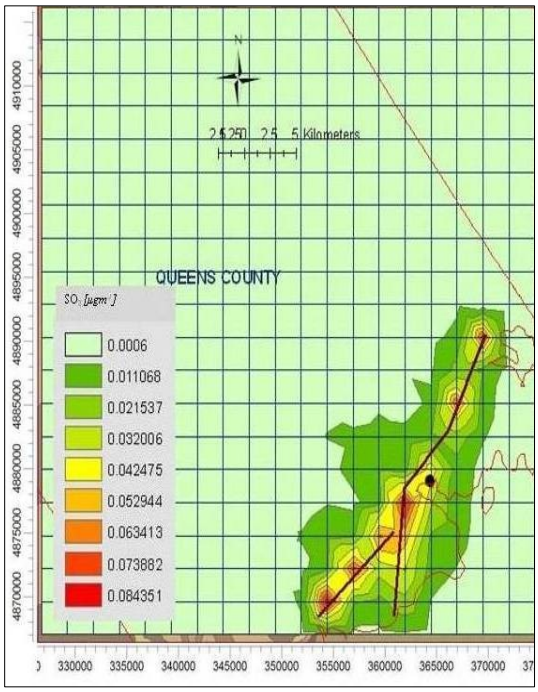

h. August

(Figures Cont'd)

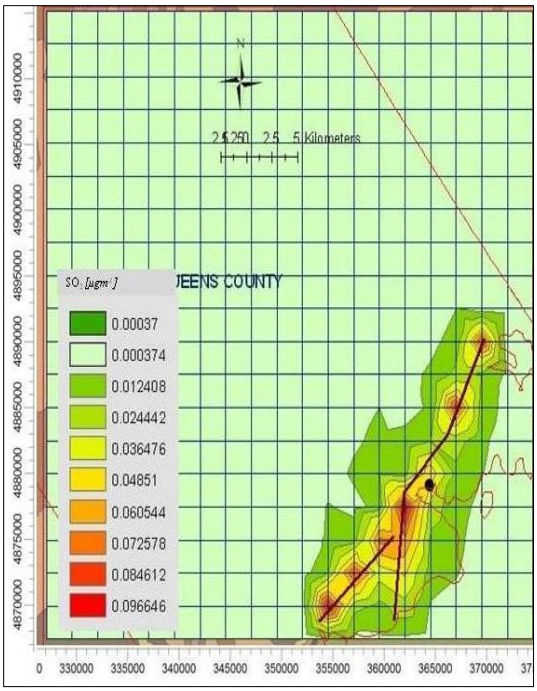

i. September

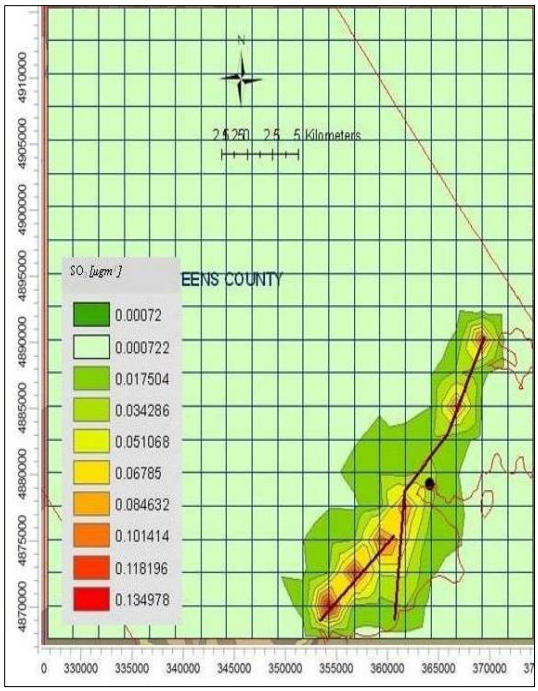

j. October

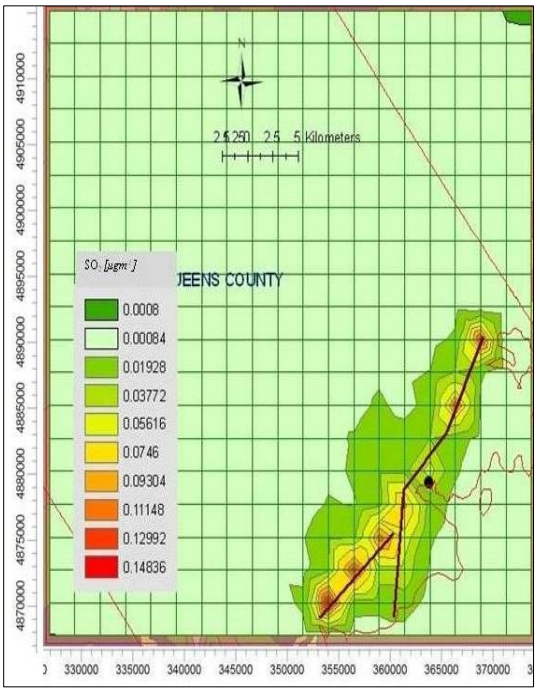

k. November

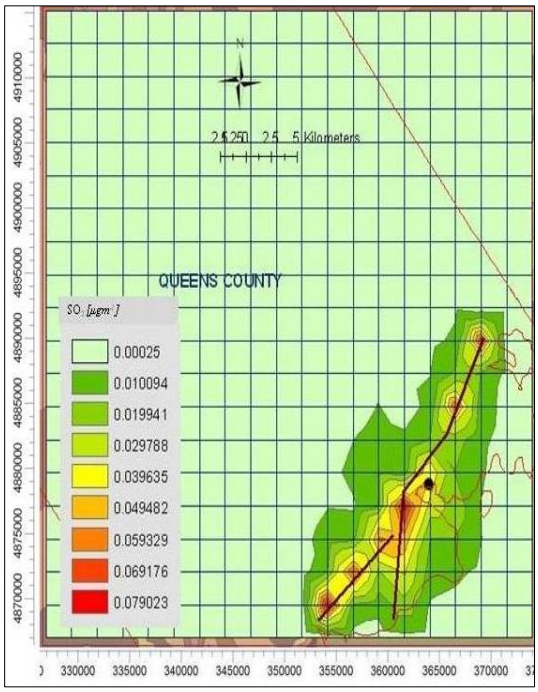

l. December

Figures 17a-l Monthly GLCs of $PM_{2.5}$ due to point and highway emission sources

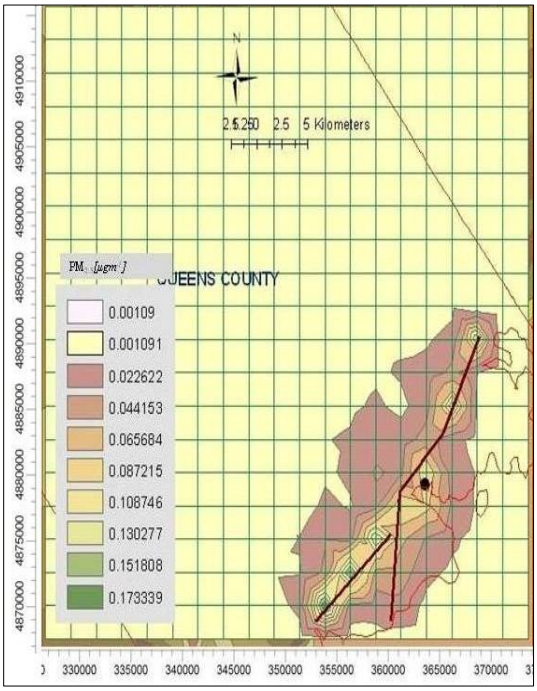

a. January

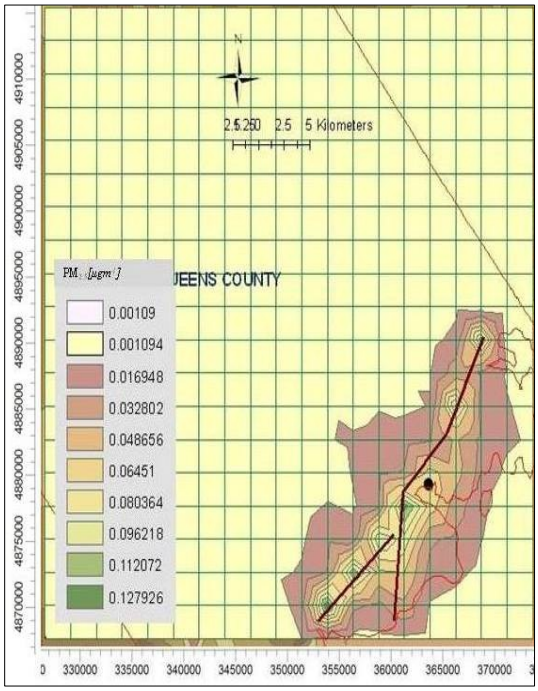

b. February

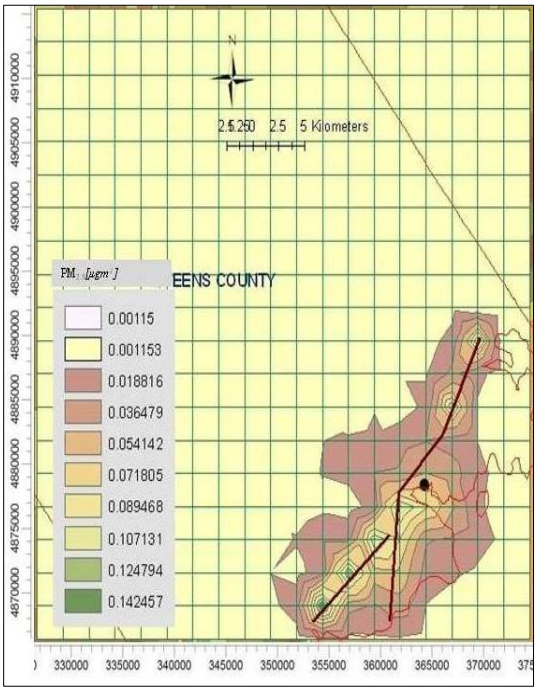

c. March

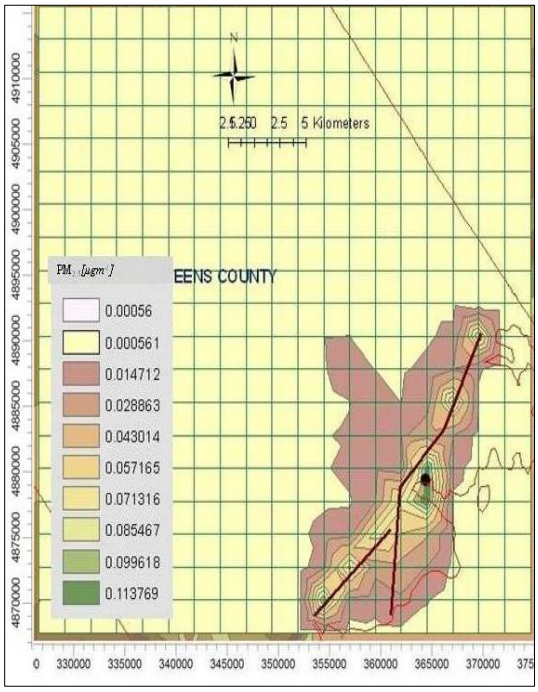

d. April

(Figures Cont'd)

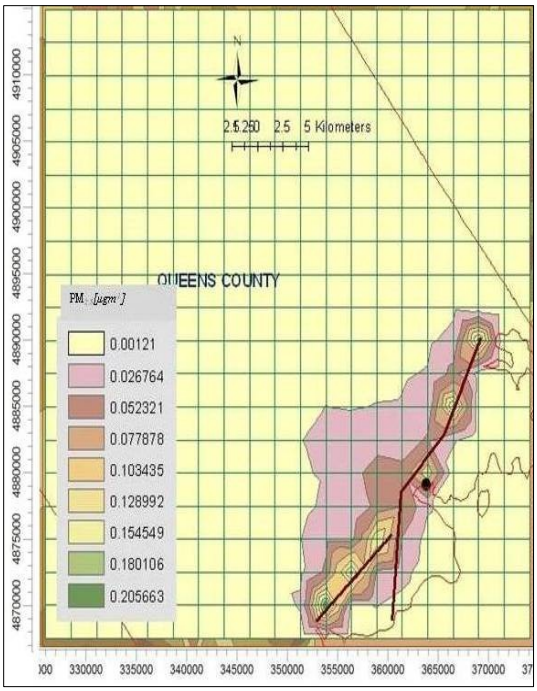

e. May

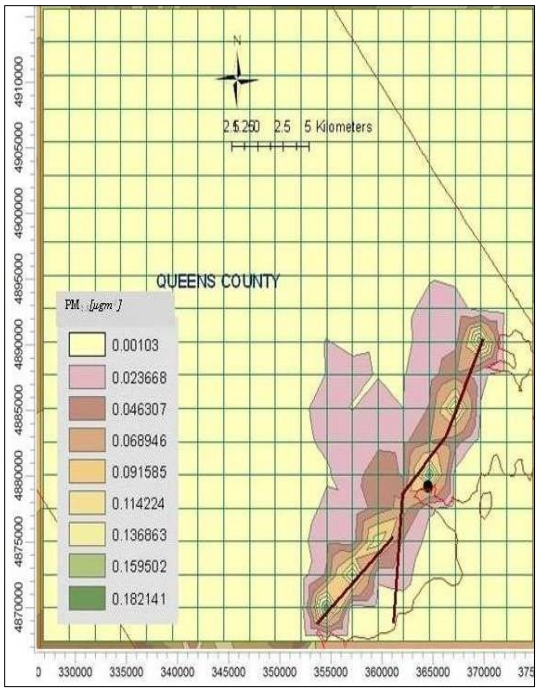

f. June

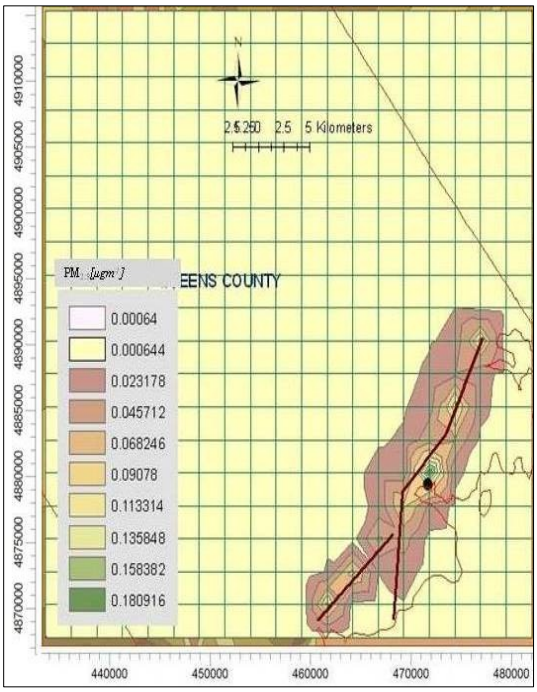

g. July

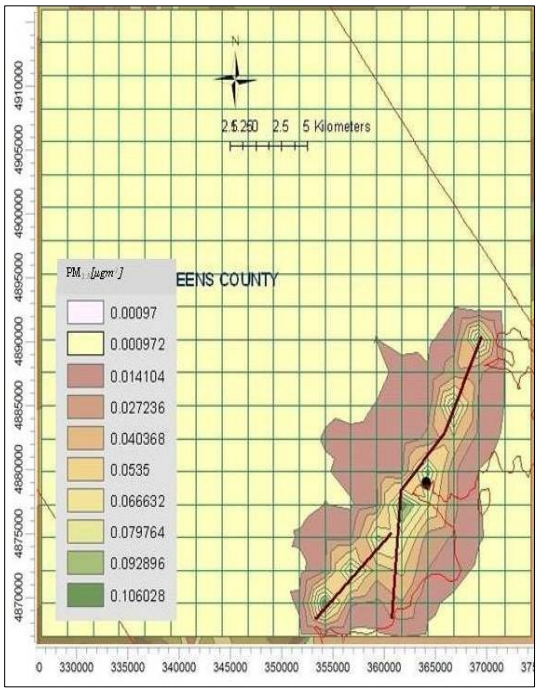

h. August

(Figures Cont'd)

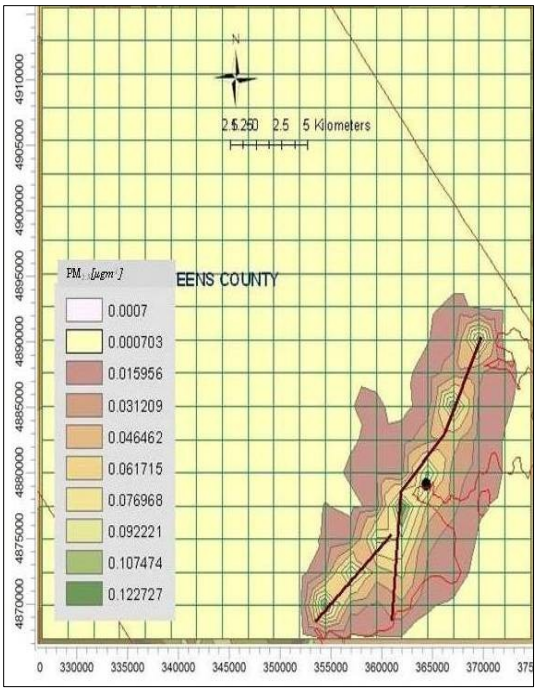

i. September

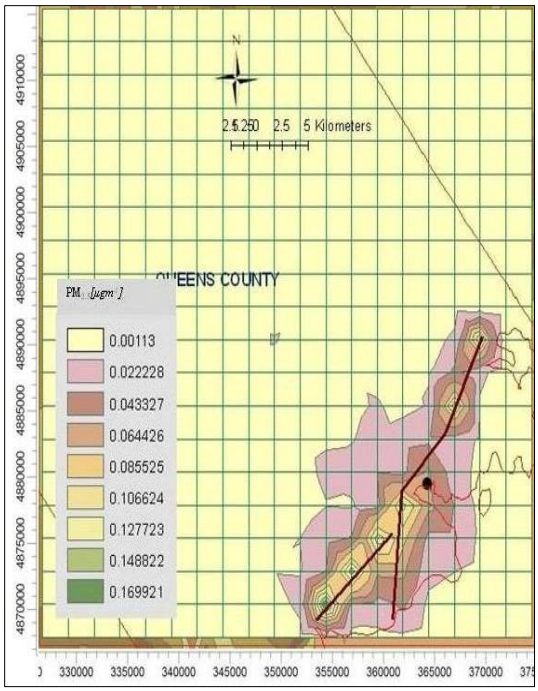

j. October

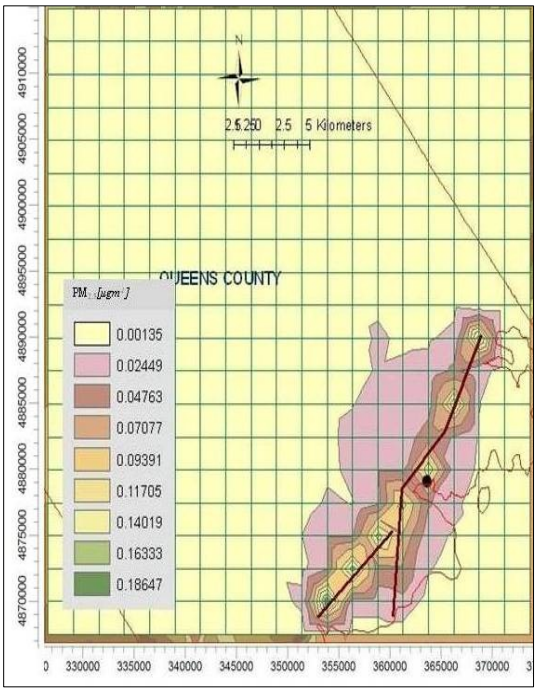

k. November

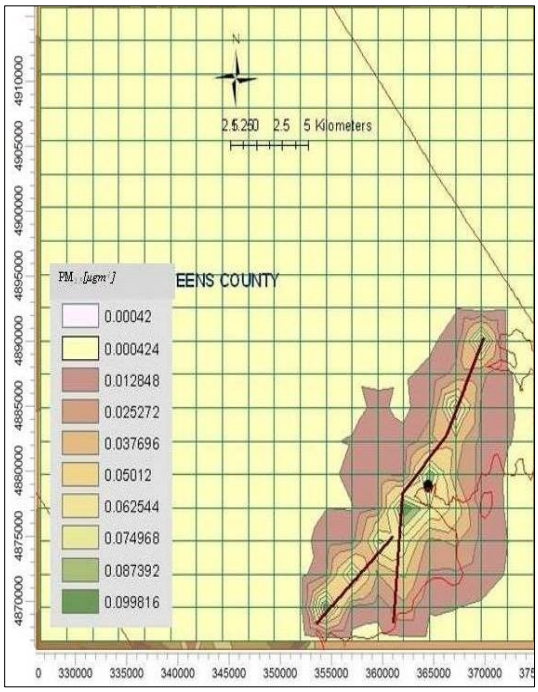

l. December

Table 12 Monthly MAX and MIN GLCs of NO_x, SO_2 and $PM_{2.5}$

Month	NO_x		SO_2		$PM_{2.5}$	
	Monthly Min *[μg m^{-3}]* UTM Coordinate (m) Elevation (m)	Monthly Max *[μg m^{-3}]* UTM Coordinate (m) Elevation (m)	Monthly Min *[μg m^{-3}]* UTM Coordinate (m) Elevation (m)	Monthly Max *[μg m^{-3}]* UTM Coordinate (m) Elevation (m)	Monthly Min *[μg m^{-3}]* UTM Coordinate (m) Elevation (m)	Monthly Max *[μg m^{-3}]* UTM Coordinate (m) Elevation (m)
Jan	0.003 (326637.18: 4867589) NA	0.449 (364104.94:4880056.5) 27.1	0.001 (326637.18: 4867589) NA	0.154 (354113.53:4870082.5) 55.5	0.001 (326637.18: 4867589) NA	0.195 (354113.53:4870082.5) 55.5
Feb	0.003 (326637.18: 4867589) NA	0.294 (364104.94:4877563) 3.4	0.001 (326637.18: 4867589) NA	0.114 (354113.53:4870082.5) 55.5	0.001 (326637.18: 4867589) NA	0.144 (354113.53:4870082.5) 55.5
Mar	0.003 (334130.75:4867589) NA	0.397 (364104.94:4877563) 3.4	0.001 (326637.18: 4867589) NA	0.127 (354113.53:4870082.5) 55.5	0.001 (326637.18: 4867589) NA	0.16 (354113.53:4870082.5) 55.5
Apr	0.002 (326637.18: 4867589) NA	0.603 (364104.94:4877563) 3.4	0.0003 (326637.18: 4867589) NA	0.09 (354113.53:4870082.5) 55.5	0.001 (326637.18: 4867589) NA	0.128 (354113.53:4870082.5) 55.5
May	0.004 (326637.18: 4867589) NA	0.554 (364104.94:4880056.5) 27.1	0.001 (326637.18: 4867589) NA	0.184 (354113.53:4870082.5) 55.5	0.001 (326637.18: 4867589) NA	0.231 (354113.53:4870082.5) 55.5
June	0.003 (326637.18: 4867589) NA	0.909 (364104.94:4880056.5) 27.1	0.001 (326637.18: 4867589) NA	0.163 (354113.53:4870082.5) 55.5	0.001 (326637.18: 4867589) NA	0.205 (354113.53:4870082.5) 55.5
July	0.002 (326637.18: 4867589) NA	0.952 (364104.94:4880056.5) 27.1	0.0003 (326637.18: 4867589) NA	0.099 (354113.53:4870082.5) 55.5	0.001 (326637.18: 4867589) NA	0.203 (364104.94:4880056.5) 27.1
Aug	0.003 (326637.18: 4867589) NA	0.404 (364104.94:4880056.5) 27.1	0.001 (326637.18: 4867589) NA	0.095 (354113.53:4870082.5) 55.5	0.001 (326637.18: 4867589) NA	0.119 (354113.53:4870082.5) 55.5
Sep	0.002 (326637.18: 4867589) NA	0.466 (364104.94:4880056.5) 27.1	0.000 (326637.18: 4867589) NA	0.109 (361607.09:4877563) 7	0.001 (326637.18: 4867589) NA	0.138 (361607.09:4877563) 7
Oct	0.003 (326637.18: 4867589) NA	0.301 (354113.53:4870082.5) 55.5	0.001 (326637.18: 4867589) NA	0.152 (354113.53:4870082.5) 55.5	0.001 (326637.18: 4867589) NA	0.191 (354113.53:4870082.5) 55.5
Nov	0.004 (326637.18: 4867589) NA	0.573 (364104.94:4880056.5) 27.1	0.001 (326637.18: 4867589) NA	0.167 (354113.53:4870082.5) 55.5	0.001 (326637.18: 4867589) NA	0.21 (354113.53:4870082.5) 55.5
Dec	0.001 (331632.88:4867589) NA	0.422 (364104.94:4880056.5) 27.1	0.001 (326637.18: 4867589) NA	0.089 (354113.53:4870082.5) 55.5	0.001 (326637.18: 4867589) NA	0.112 (361607.09:4877563) 7

4.3.1.3 Hourly Averaging of NO_x, SO_2 and $PM_{2.5}$

Figures 18 through 20 show hourly predicted GLC contour maps of NO_x, SO_2 and $PM_{2.5}$ respectively in the LNN domain. As seen from Figures 18 through 20, NO_x dispersed far distances from emission sources only during 1-hr averaging period whereas in the case of SO_2 and $PM_{2.5,}$ pollutants dispersed far distances from the highway 103 throughout the day. GLCs of the pollutants reduced with longer averaging time. Emission rate and stack height of Brooklyn Energy plant interfered with GLC during different averaging periods and contributed larger amount of ground level NO_x concentrations compared to vehicles. GLC reduction rate of the pollutants during 1-hr, 3-hr and 8-hr averaging periods were low compared to 12-hr and 24-hr period. As seen in Table 13, highest and lowest GLC receptors remained same throughout the day. With reference to the table, large amount of GLC reduction took place during 12-hr period Highest GLC receptor was located at North East of the emission sources as it is seen during annual averaging period. Highway 103 contributed larger amount of SO_2 and $PM_{2.5}$ and GLC reduction rate was higher compared to NO_x during hourly averaging period. This phenomenon was expected due to advection of SO_2 and $PM_{2.5}$ across small surface roughness value of this domain. With reference to the figures, it is also seen that the differences between maximum and minimum concentrations were greater when the pollutants were released from an elevated emission source.

Figures 18a-e Hourly GLCs of NO_x due to point and highway emission sources

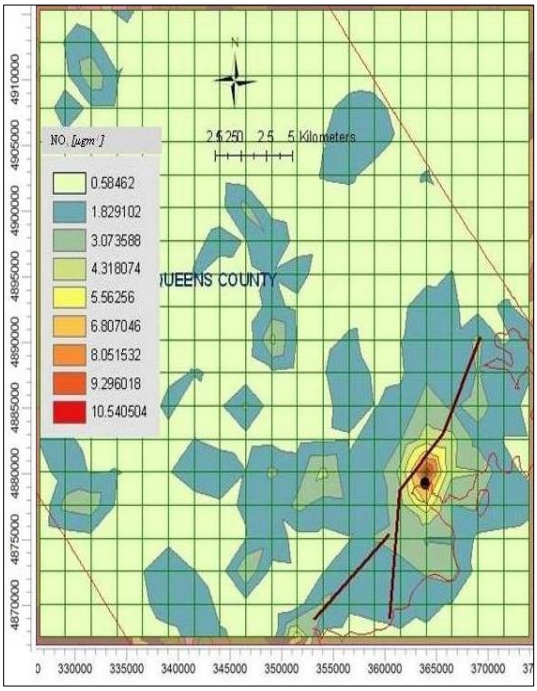

a. 1 hour

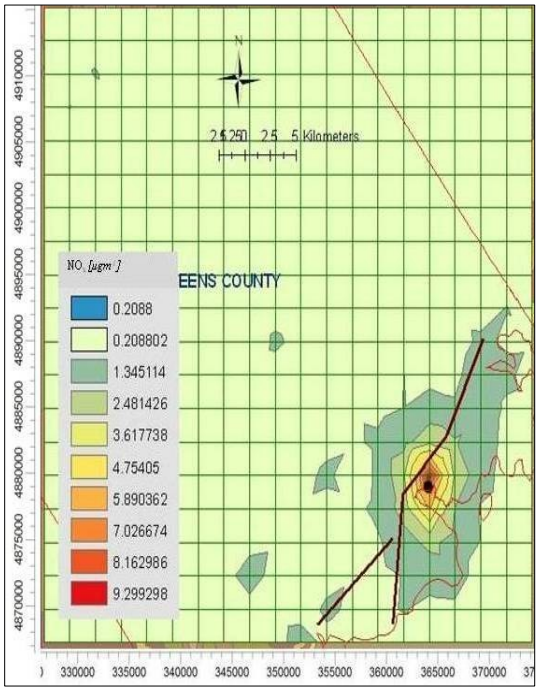

b. 3 hour

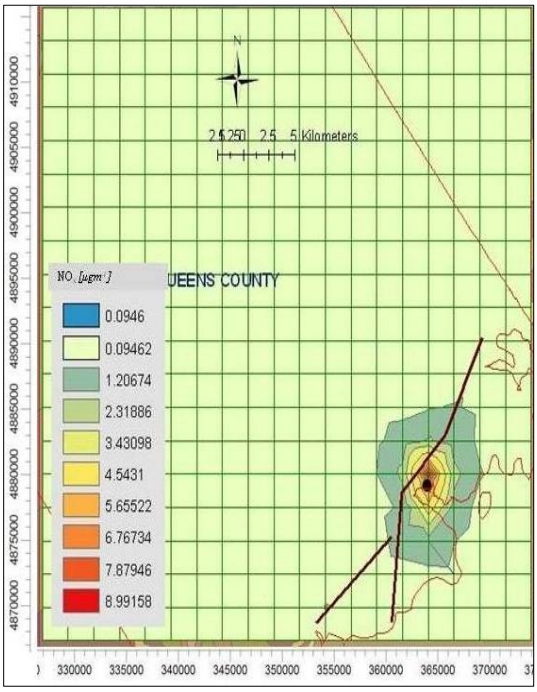

c. 8 hour

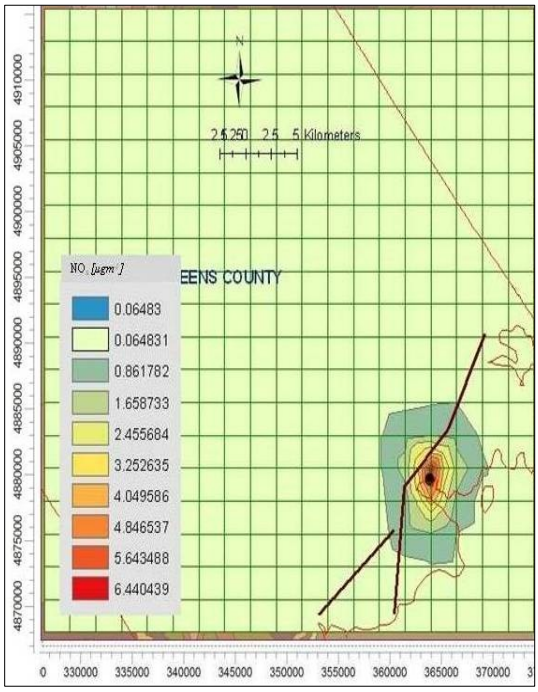

d. 12 hour

(Figure Cont'd)

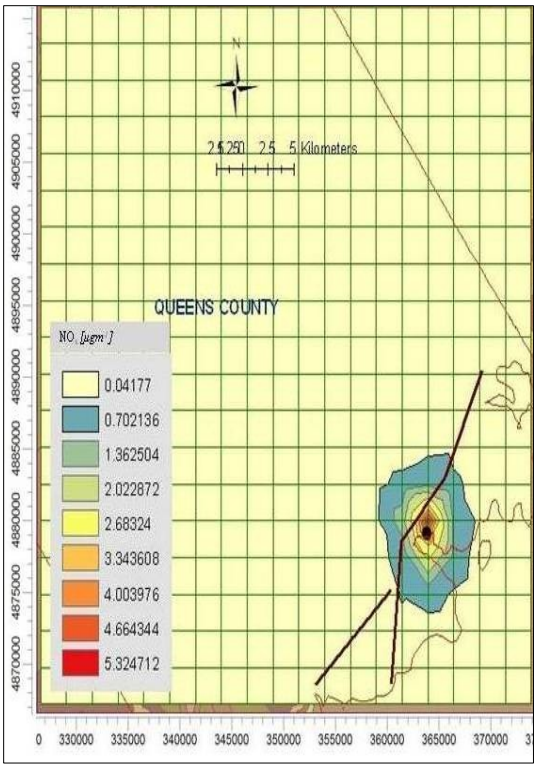
N
2.5 0 2.5 5 Kilometers
QUEENS COUNTY
NO [µgm³]
0.04177
0.702136
1.362504
2.022872
2.68324
3.343608
4.003976
4.664344
5.324712
4910000
4905000
4900000
4895000
4890000
4885000
4880000
4875000
4870000
0
330000
335000
340000
345000
350000
355000
360000
365000
370000

e. 24 hour

Figures 19a-e Hourly GLCs of SO_2 due to point and highway emission sources

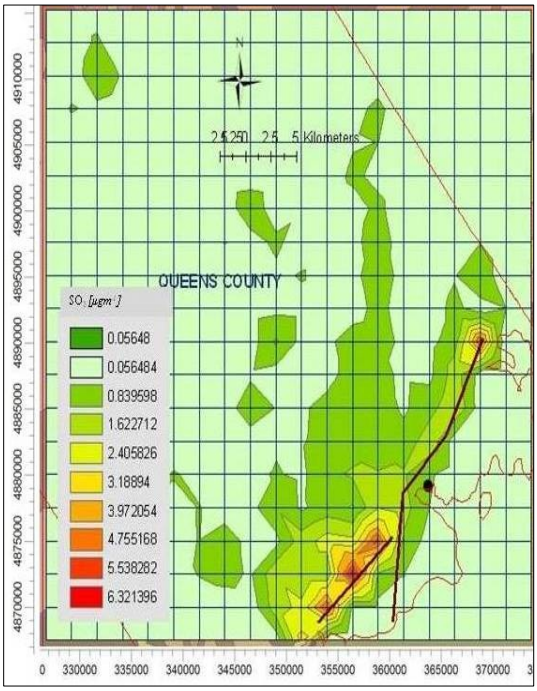

a. 1 hour

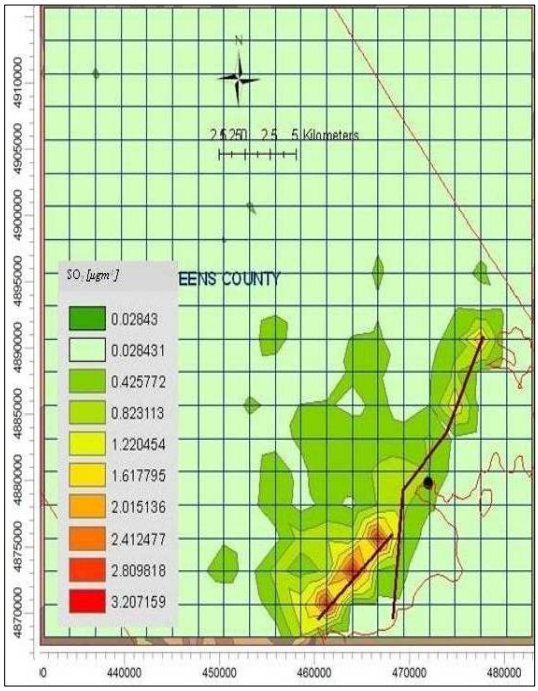

b. 3 hour

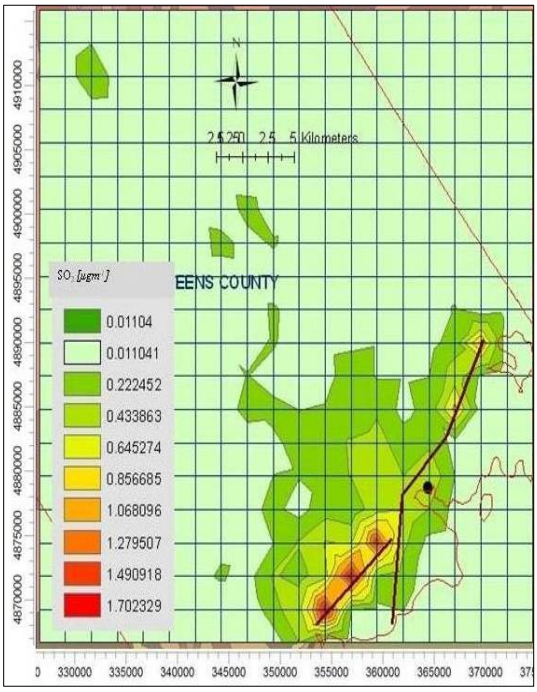

c. 8 hour

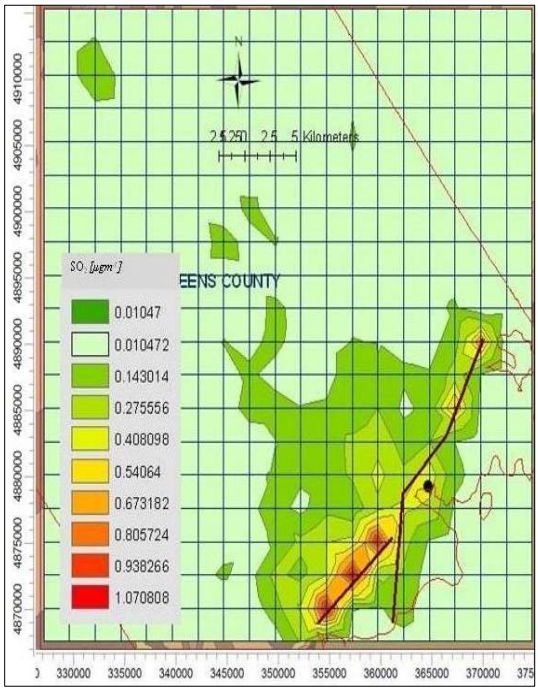

d. 12 hour

(Figure Cont'd)

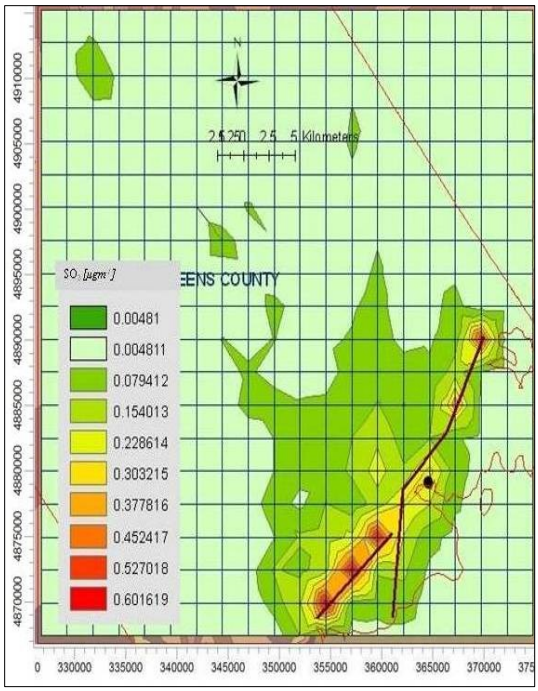
N
2.5 0 2.5 5 Kilometers
SO2 [µgm-3]
0.00481
0.004811
0.079412
0.154013
0.228614
0.303215
0.377816
0.452417
0.527018
0.601619
4910000
4905000
4900000
4895000
4890000
4885000
4880000
4875000
4870000
0
330000
335000
340000
345000
350000
355000
360000
365000
370000

e. 24 hour

Figures 20a-e Hourly GLCs of $PM_{2.5}$ due to point and highway emission sources

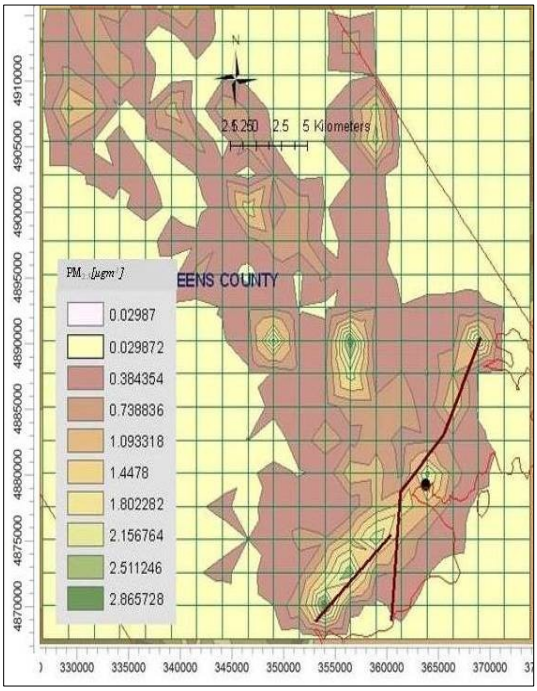

a. 1 hour

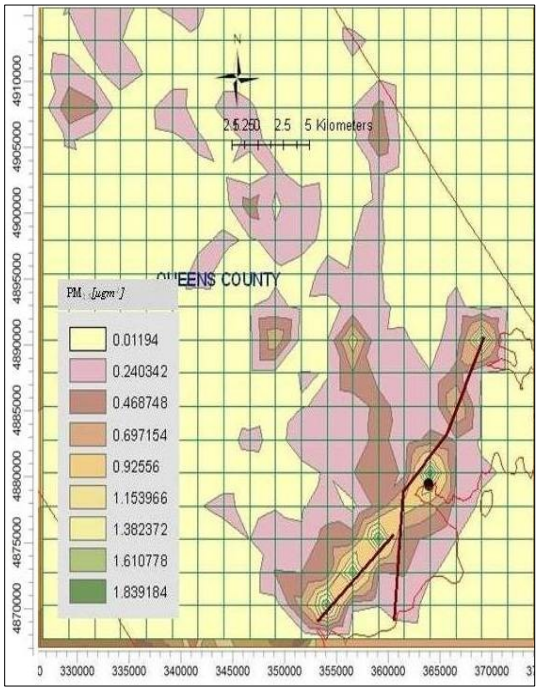

b. 3 hour

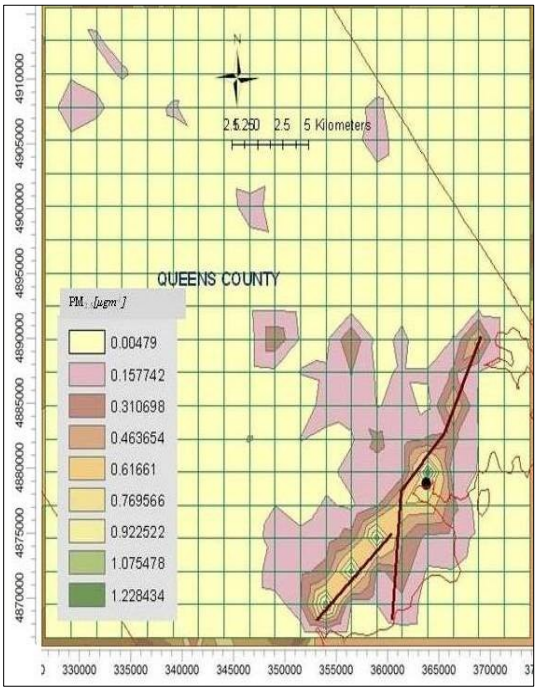

c. 8 hour

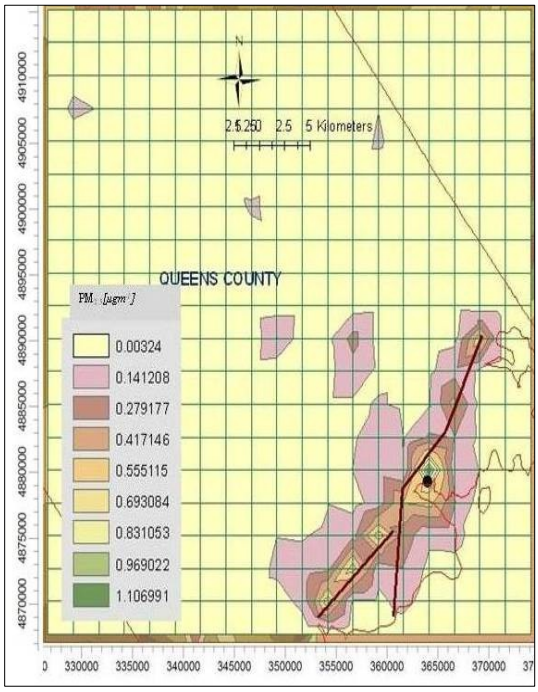

d. 12 hour

(Figure Cont'd)

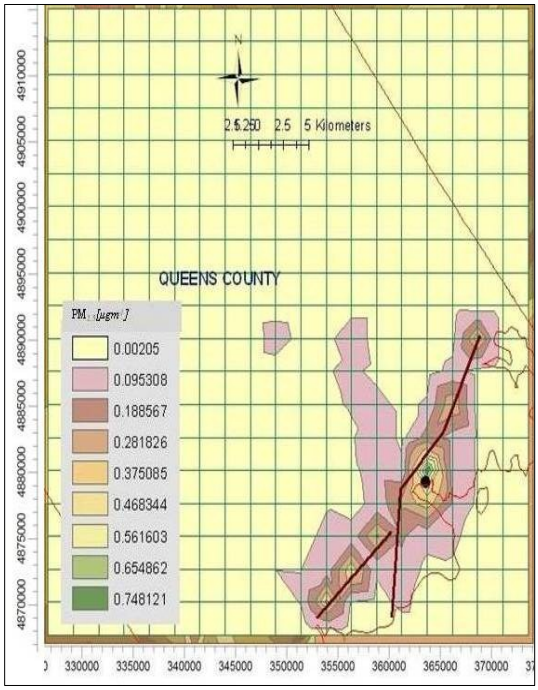

e. 24 hour

Table 13 Hourly MAX and MIN GLCs of NO_x, SO_2 and $PM_{2.5}$

Hour	NO_x		SO_2		$PM_{2.5}$	
	Hourly Min *[µg m^{-3}]* UTM Coordinate (m) Elevation (m)	Hourly Max *[µg m^{-3}]* UTM Coordinate (m) Elevation (m)	Hourly Min *[µg m^{-3}]* UTM Coordinate (m) Elevation (m)	Hourly Max *[µg m^{-3}]* UTM Coordinate (m) Elevation (m)	Hourly Min *[µg m^{-3}]* UTM Coordinate (m) Elevation (m)	Hourly Max *[µg m^{-3}]* (UTM Coordinate (m) Elevation (m)
1	0.585 (329135.03: 4872576) NA	11.785 (364104.94:4880056.5) 27.1	0.056 (326637.18: 4867589) NA	7.105 (356611.38:4872576) 38.7	0.03 (334130.75:4867589) NA	3.22 (354113.53:4870082.5) 55.5
3	0.209 (329135.03:4867589) NA	10.435 (364104.94:4880056.5) 27.1	0.028 (326637.18: 4867589) NA	3.604 (356611.38:4872576) 38.7	0.012 (334130.75:4867589) NA	2.07 (364104.94:4880056.5) 27.1
8	0.095 (326637.18: 4870082.5) NA	10.104 (364104.94:4880056.5) 27.1	0.011 (326637.18: 4867589) NA	1.914 (356611.38:4872576) 38.7	0.005 (331632,88:4867589) NA	1.38 (364104.94:4880056.5) 27.1
12	0.065 (326637.18: 4870082.5) NA	7.237 (364104.94:4880056.5) 27.1	0.01 (326637.18: 4867589) NA	1.203 (356611.38:4872576) 38.7	0.003 (334130.75:4867589) NA	1.245 (364104.94:4880056.5) 27.1
24	0.042 (326637.18: 4867589) NA	5.985 (364104.94:4880056.5) 27.1	0.005 (326637.18: 4867589) NA	0.676 (356611.38:4872576) 38.7	0.002 (334130.75:4867589) NA	0.841 (364104.94:4880056.5) 27.1

4.3.2 Modeling Study in PTA domain

Emission of NO_x, SO_2 and $PM_{2.5}$ from Point Aconi energy plant and 17.45 km section length of highway 105 were used for conducting the simulation studies in PTA domain during 2005.

4.3.2.1 Annual Averaging of NO_x, SO_2 and $PM_{2.5}$

AERMOD predicted GLC contour maps of NO_x, SO_2 and $PM_{2.5}$ during annual averaging period are shown Figures 21 through 23. As seen in Figures 21 through 23, the highest annual averaged NO_x concentration gradient was found at 2.5 km south of Point Aconi plant. Highest annual averaged SO_2 and $PM_{2.5}$ concentration were seen at western part of the domain, by east side of the highway 105. High NO_x, SO_2 and $PM_{2.5}$ concentration gradients were also seen within 1 km radius of the highway 105. The results demonstrated that the highway emission contributed larger amount of $PM_{2.5}$ compared to the point source emission. Prevailing wind at 248^o influenced the advection of pollutants. Most of the pollutants released from Point Aconi plant had advected towards east due to wind direction and large release height (100m from the ground surface). With reference to Table 14, minimum and maximum annual predicted NO_x concentrations were 0.016 $\mu g\ m^{-3}$ located at 692740.68m: 51086245m, elevation NA and 0.76 $\mu g\ m^{-3}$ located at 707730.9m: 5132381m, elevation 21 m respectively. Annual minimum and maximum predicted SO_2 concentration were 0.087 $\mu g\ m^{-3}$ found at 692740.68m: 5108624.5m, elevation NA and 1.075 $\mu g\ m^{-3}$ at 693989.9m: 5124879m, elevation NA respectively. The minimum and maximum annual average $PM_{2.5}$ concentrations in PTA domain were 0.001$\mu g\ m^{-3}$ found at 698986.56m: 5108624.5m elevation 184.6 m and 0.492$\mu g\ m^{-3}$ at 693989.9m: 5124879m, elevation NA respectively.

Figure 21 Annual GLCs of NO_x due to point and highway emission sources

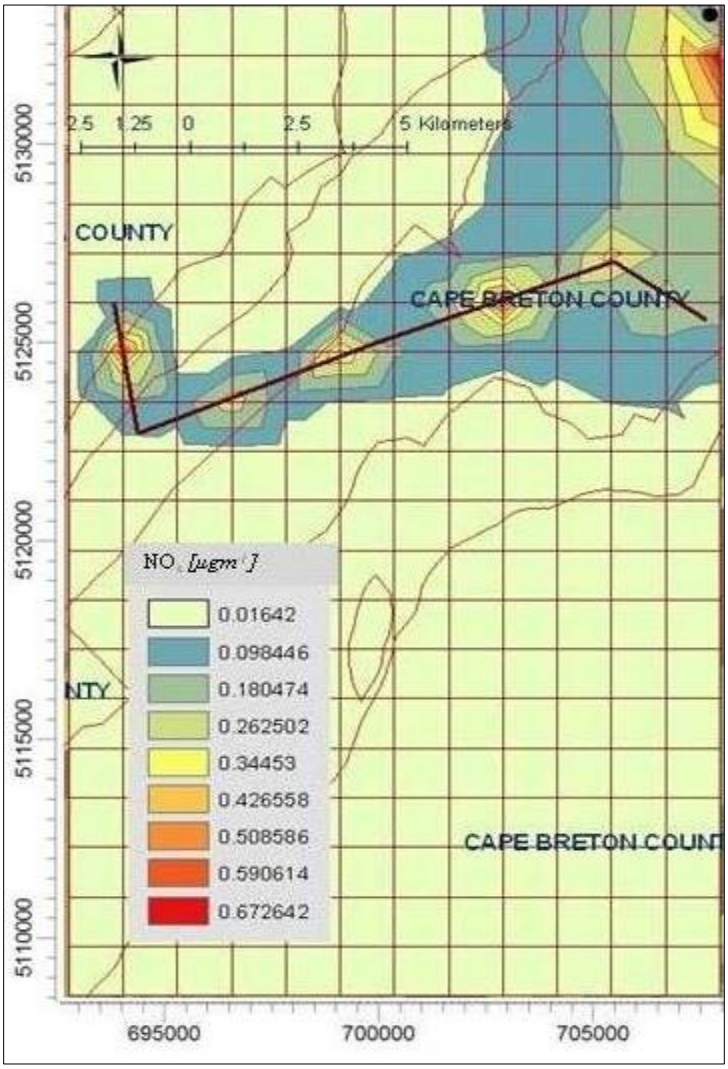

Figure 22 Annual GLCs of SO_2 due to due to point and highway emission sources

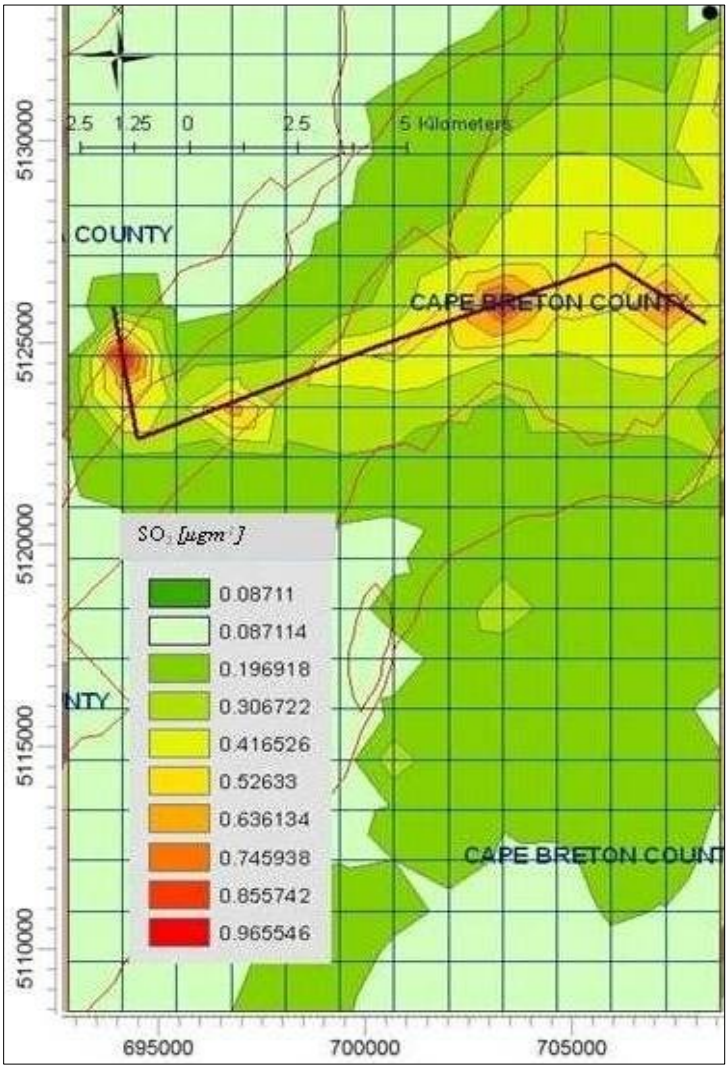

Figure 23 Annual GLCs of $PM_{2.5}$ due to due to point and highway emission sources

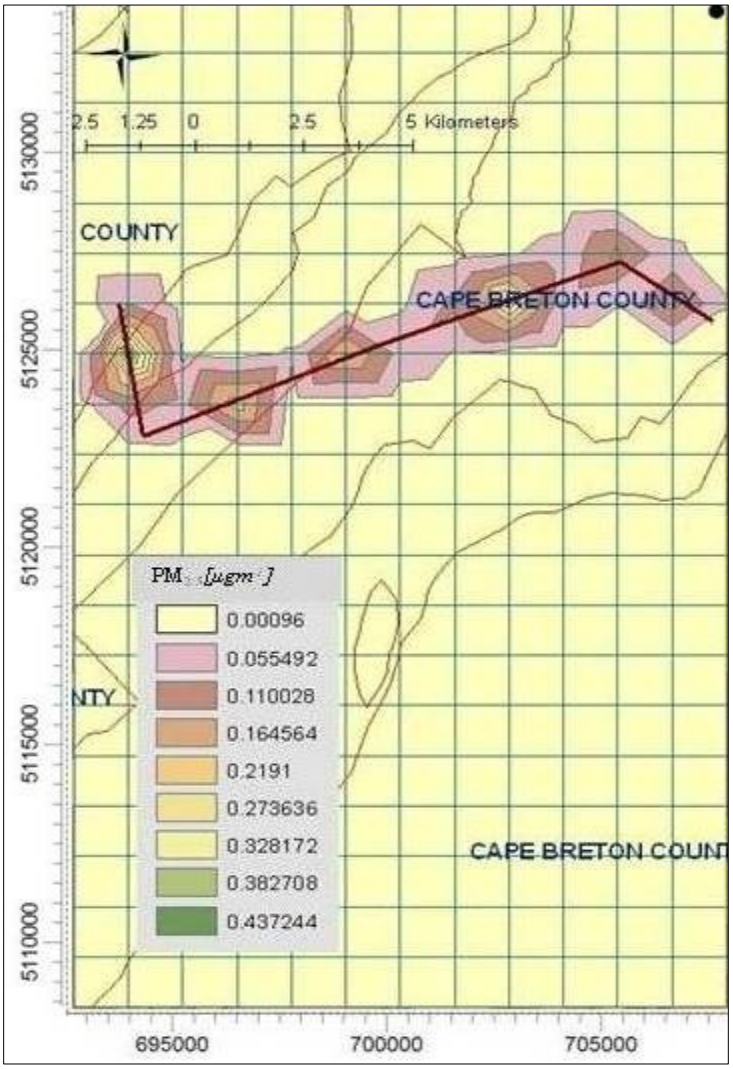

Table 14 Annual MAX and MIN GLCs of NO_x, SO_2 and $PM_{2.5}$

Pollutant	Annual Min *[µg m^{-3}]* UTM Coordinate (m) Elevation (m)	Annual Max *[µg m^{-3}]* UTM Coordinate (m) Elevation (m)
NO_x	0.016 (692740.68:5108624.5) NA	0.76 (707730.9:5132381) 21
SO_2	0.087 (692740.68:5108624.5) NA	1.075 (693989.9:5124879) NA
$PM_{2.5}$	0.001 (698986.56:5108624.5) 184.6	0.492 (693989.9:5124879) NA

4.3.2.2 Monthly Averaging of NO_x, SO_2 and $PM_{2.5}$

Figures 24 through 26 show the predicted monthly GLC contour maps of NO_x, SO_2 and $PM_{2.5}$ in PTA domain. As seen from the figures, dispersion pattern of NO_x and $PM_{2.5}$ were similar. It is seen from the meteorological observations that GLC of NO_x increased with the decrease in wind speed. High GLC of NO_x existed near highway 105. Both the Point Aconi generation station chimney stack and highway 105 contributed large amount of SO_2 in this domain. Therefore SO_2 dispersed far distances from the emission sources during February through October. This phenomenon indicates that the SO_2 dispersal was influenced by the lower ambient temperature during January, November and December. SO_2 was advected towards the prevailing wind at 248^o. High release height was interfered by the atmospheric stability during winter months with low ambient temperature. Released pollutants were carried out of the domain during summer. According to Table 15 the minimum and maximum monthly predicted NO_x concentrations were 1.13 $\mu g\ m^{-3}$ (September) at coordinates 693989.9m: 5124879m, elevation NA and 2.344 $\mu g\ m^{-3}$ (February) at coordinates 702734.1m: 5126129m, elevation 64.2 m respectively. The minimum and maximum monthly predicted SO_2 concentrations were 0.799 $\mu g\ m^{-3}$ (September) at coordinates 693989.9m: 5124879m, elevation NA and 1.967$\mu g\ m^{-3}$ (May) at coordinates 702734.1m: 5126129m, elevation 64.2 m respectively. The minimum and maximum monthly predicted $PM_{2.5}$ concentrations were 0.002 $\mu g\ m^{-3}$ (September) at coordinates 707730.9m: 5132381m, elevation 21 and 1.93$\mu g\ m^{-3}$ (November) at coordinates 693989.9m: 5124879m, elevation NA respectively. From Table 15 it is seen that GLCs of pollutants were high in winter months. This is due to high release height and prevailing wind direction. Variation in minimum predicted GLCs of pollutants was significant throughout the year.

Figures 24a-l Monthly GLCs of NO_x due to point and highway emission sources

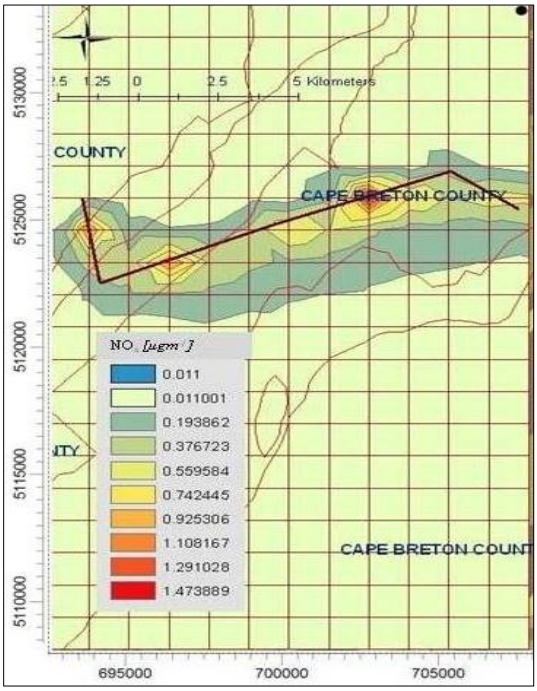

a. January

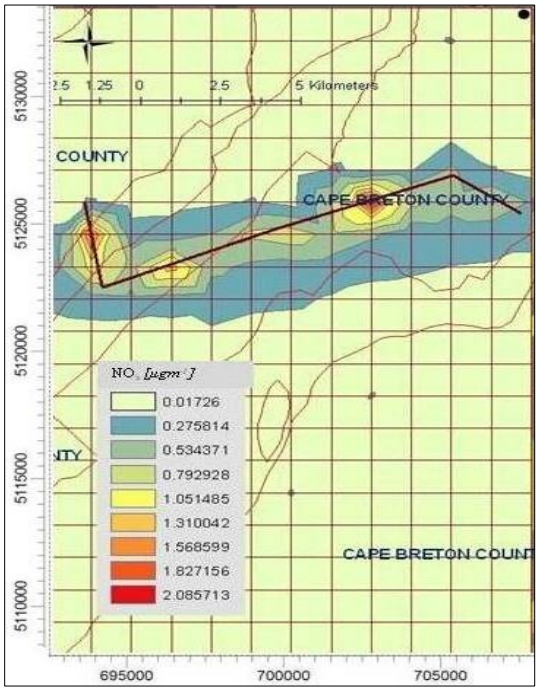

b. February

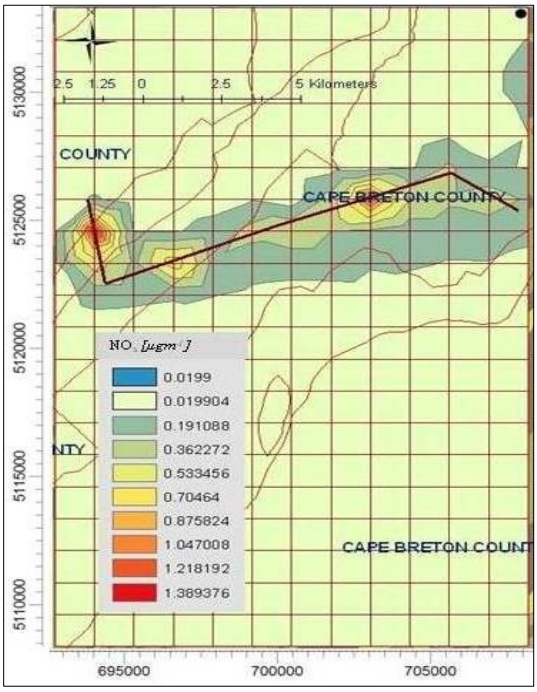

c. March

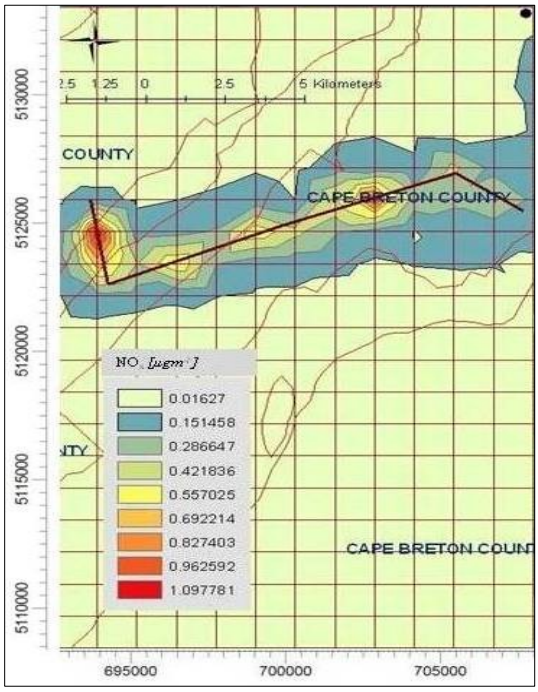

d. April

(Figures Cont'd)

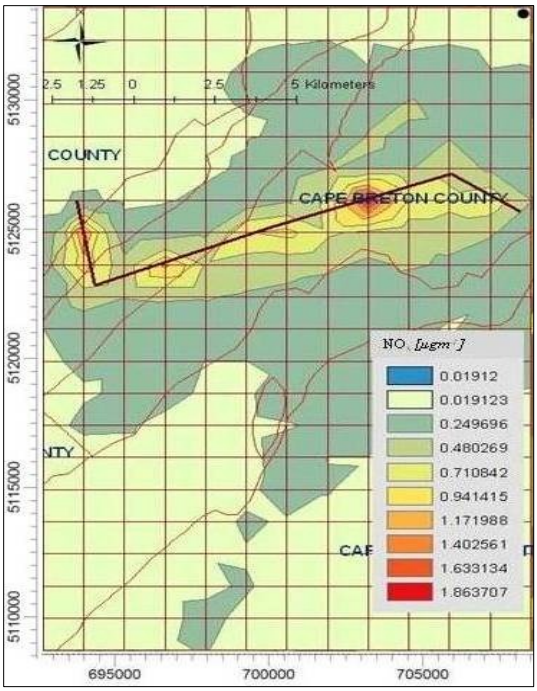

e. May

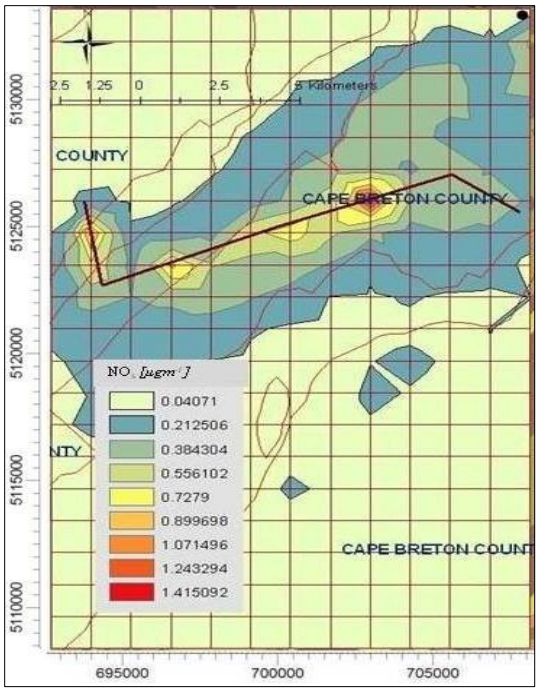

f. June

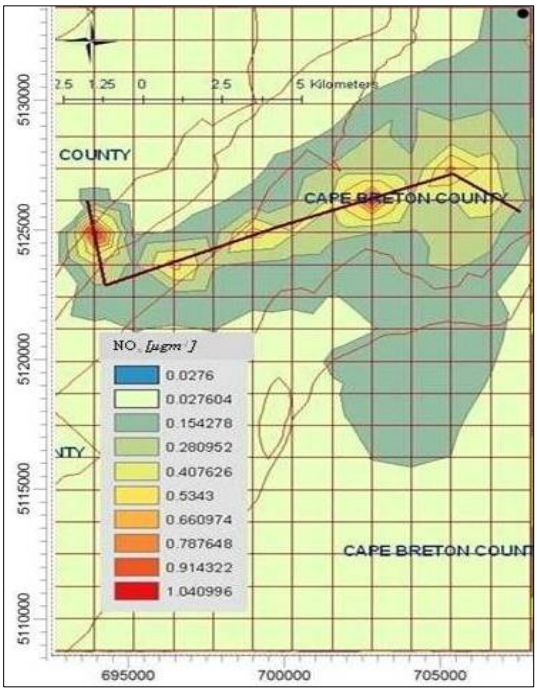

g. July

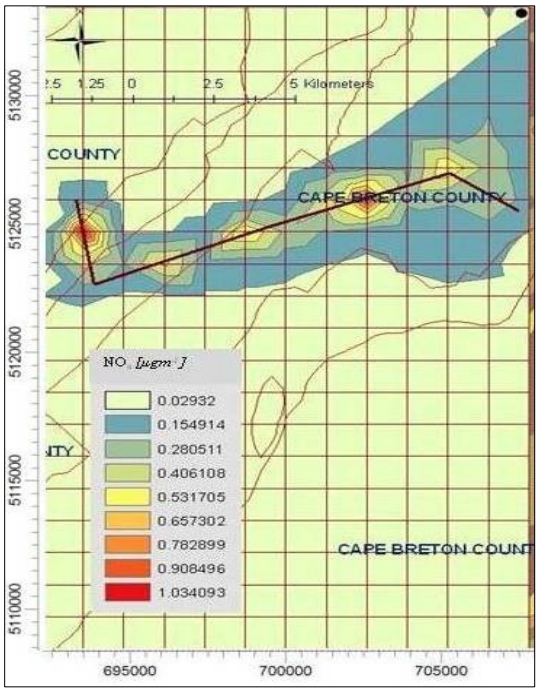

h. August

(Figures Cont'd)

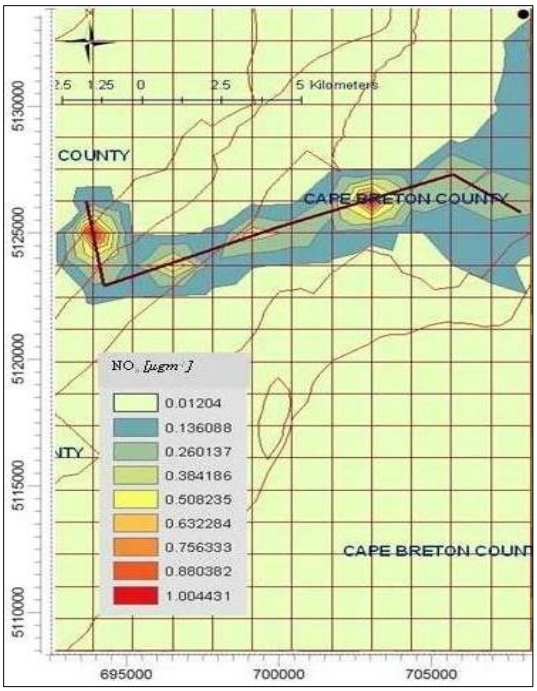

i. September

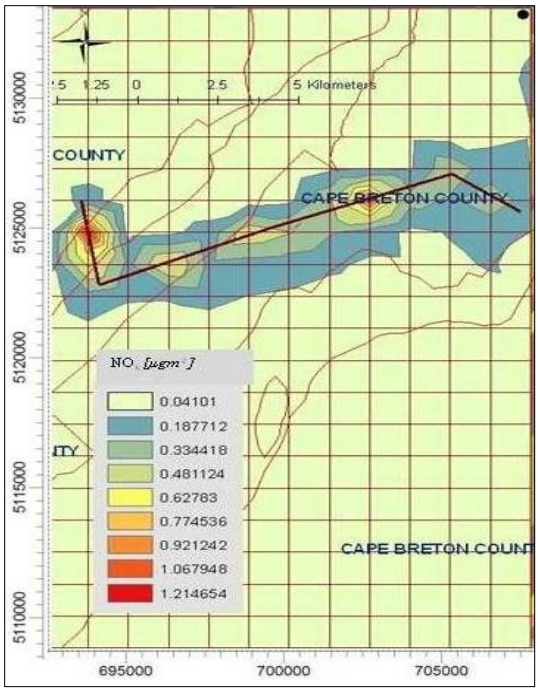

j. October

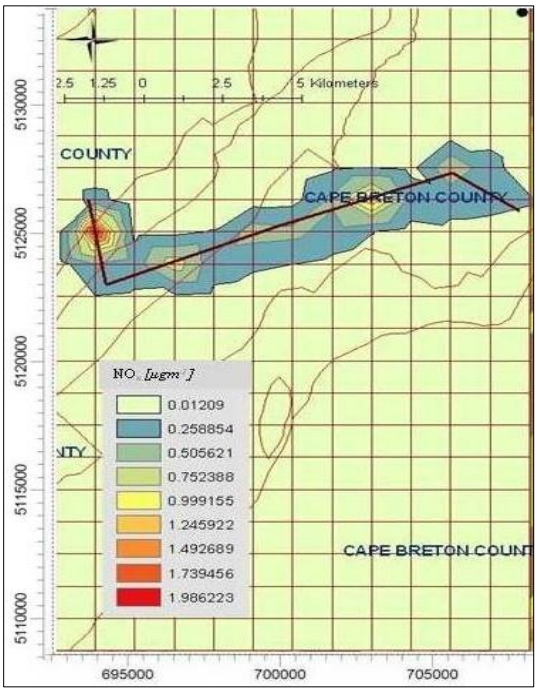

k. November

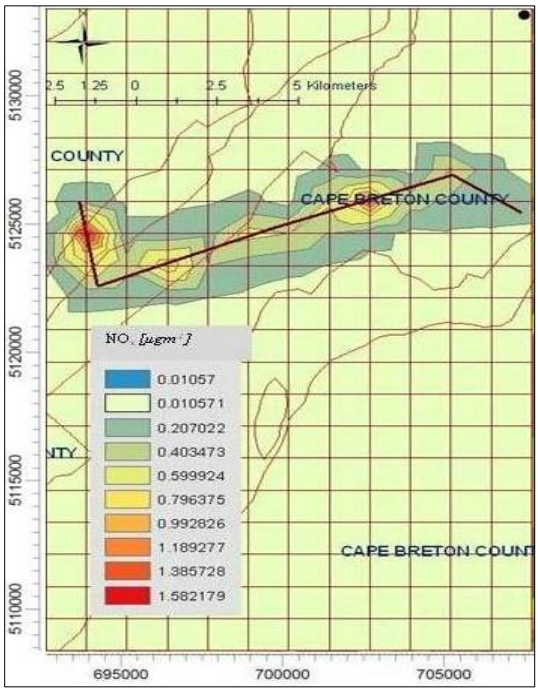

l. December

Figures 25a-l Monthly GLCs of SO_2 due to point and highway emission sources

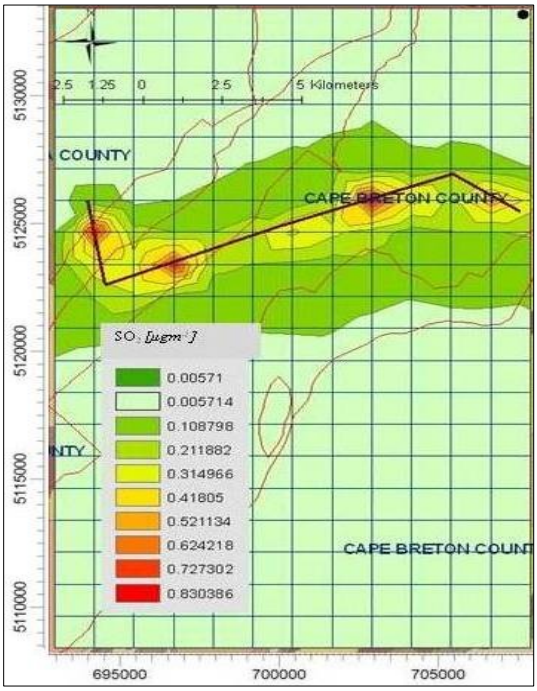

a. January

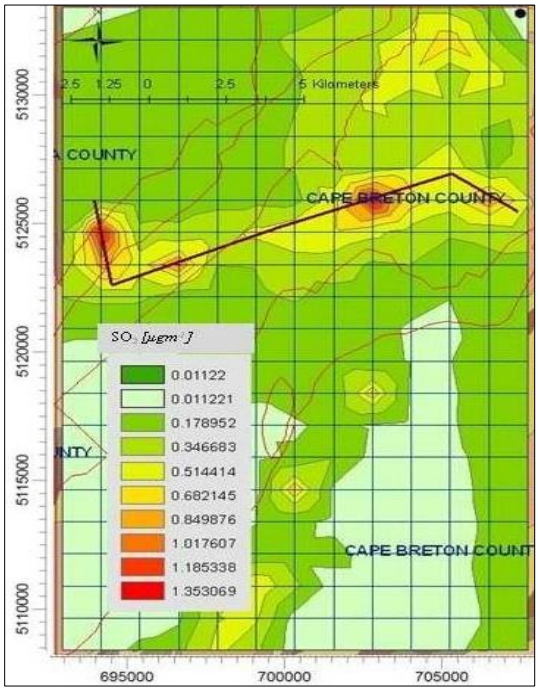

b. February

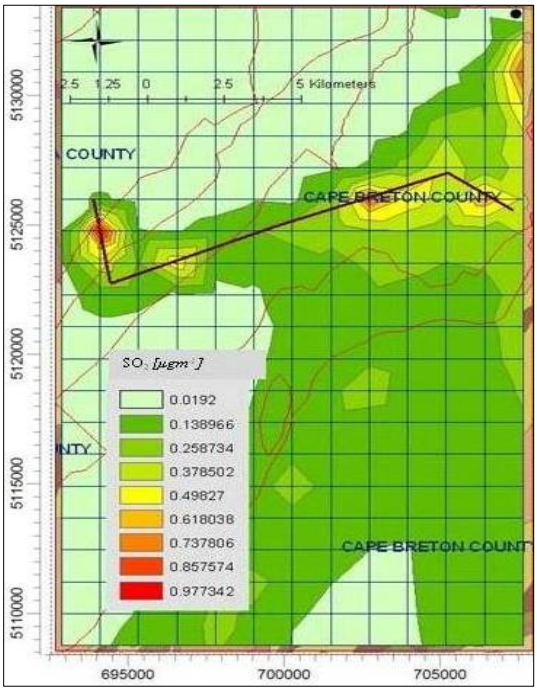

c. March

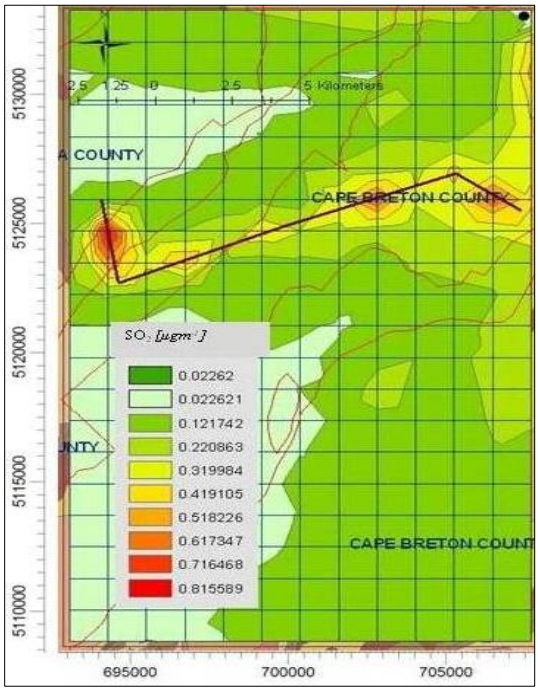

d. April

(Figures Cont'd)

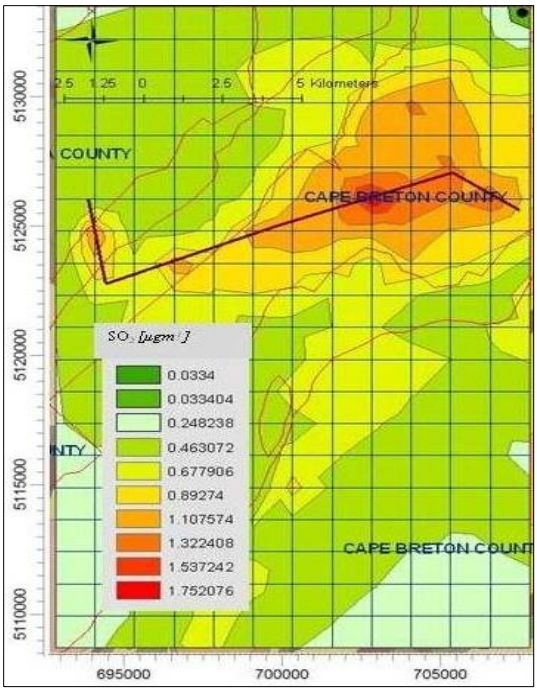

e. May

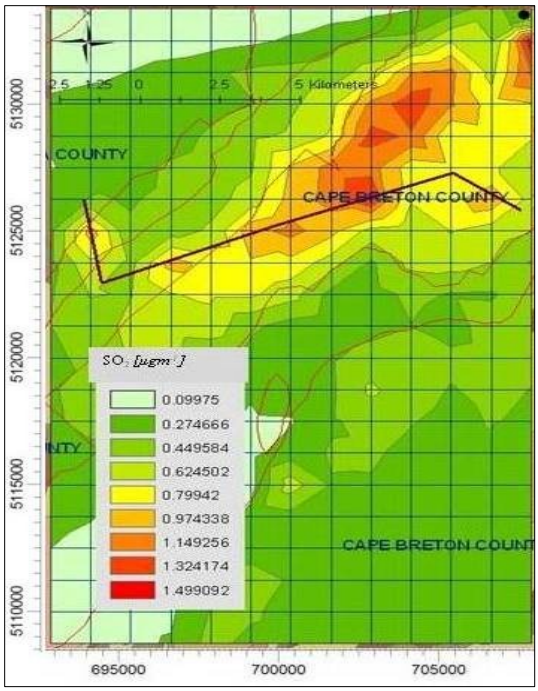

f. June

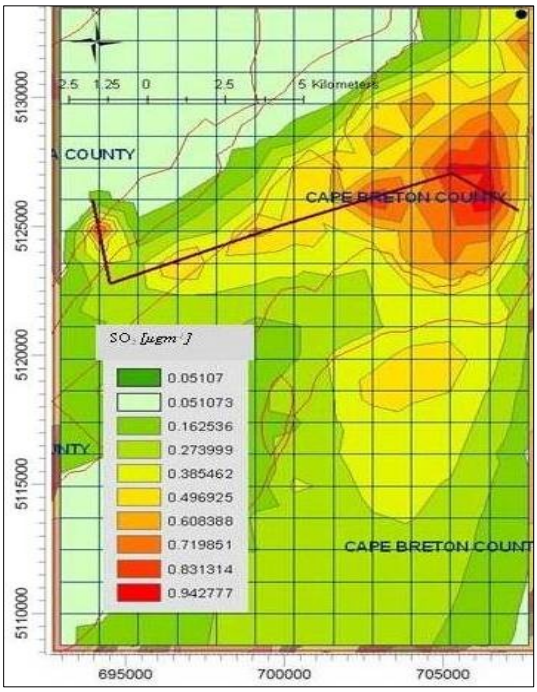

g. July

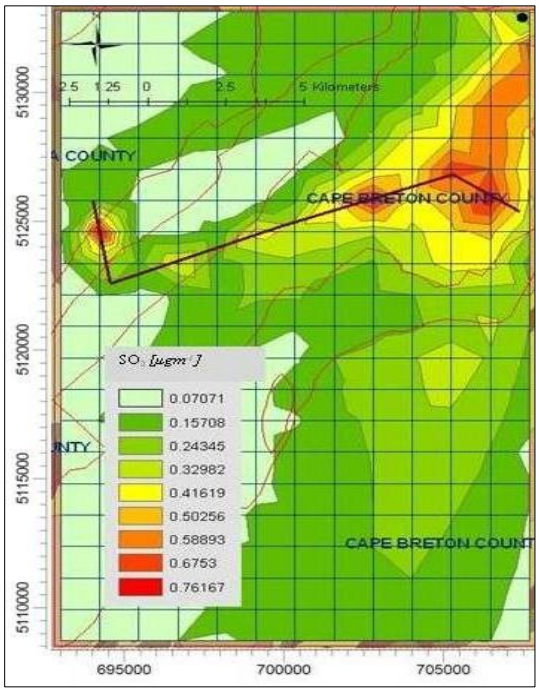

h. August

(Figures Cont'd)

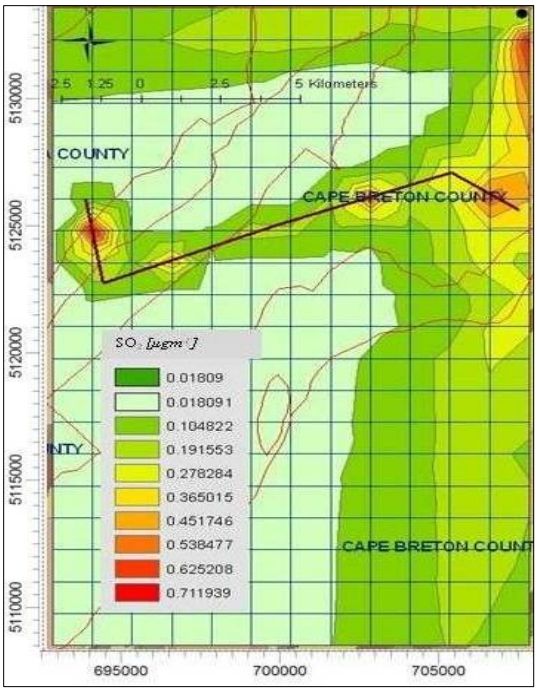

i. September

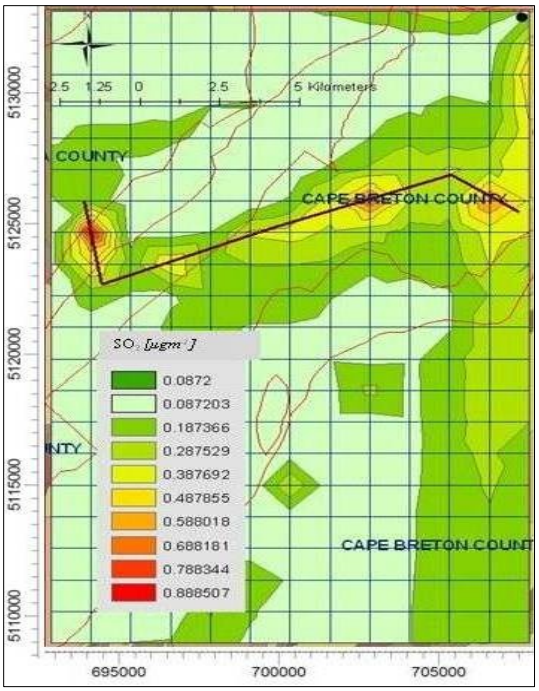

j. October

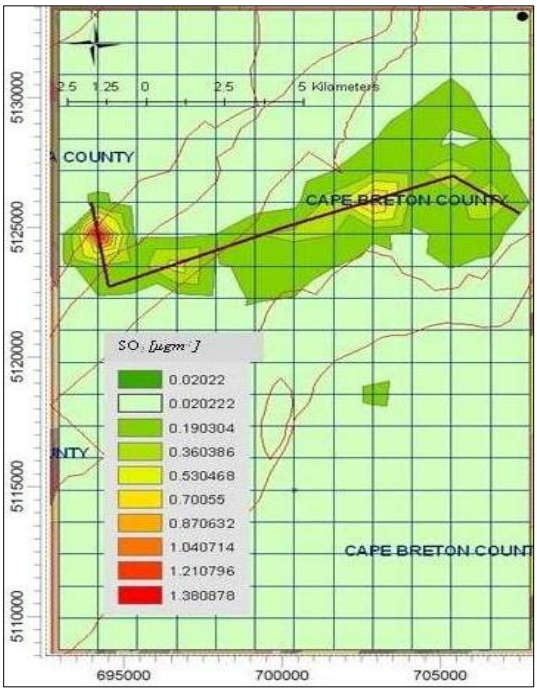

k. November

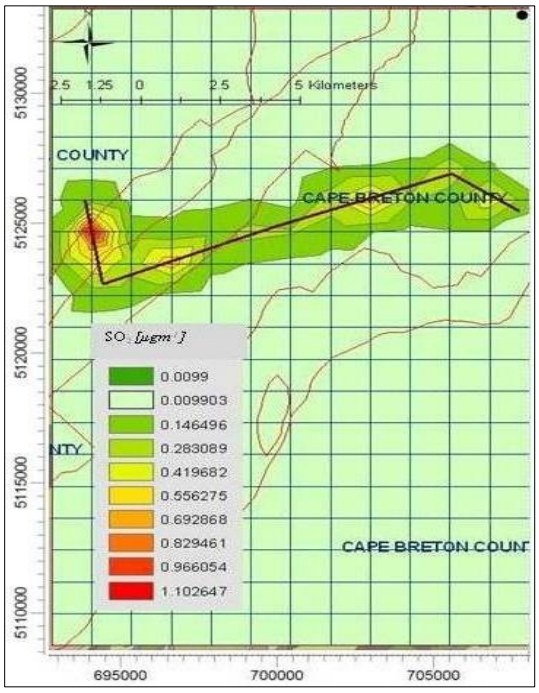

l. December

Figures 26a-l Monthly GLCs of $PM_{2.5}$ due to point and highway emission sources

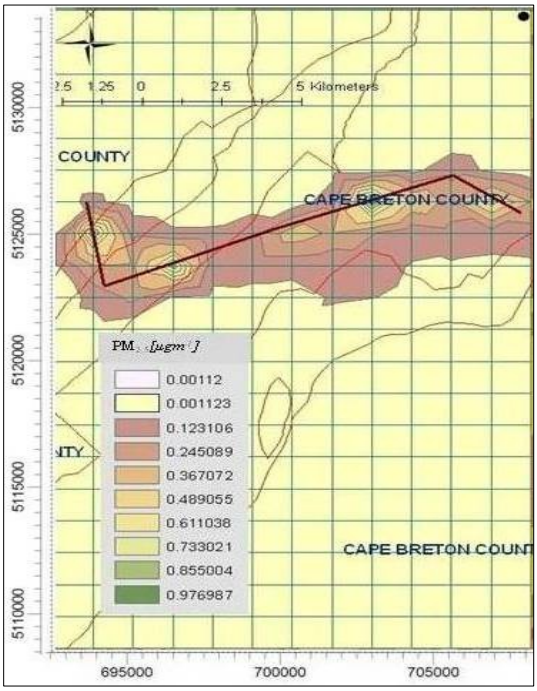

a. January

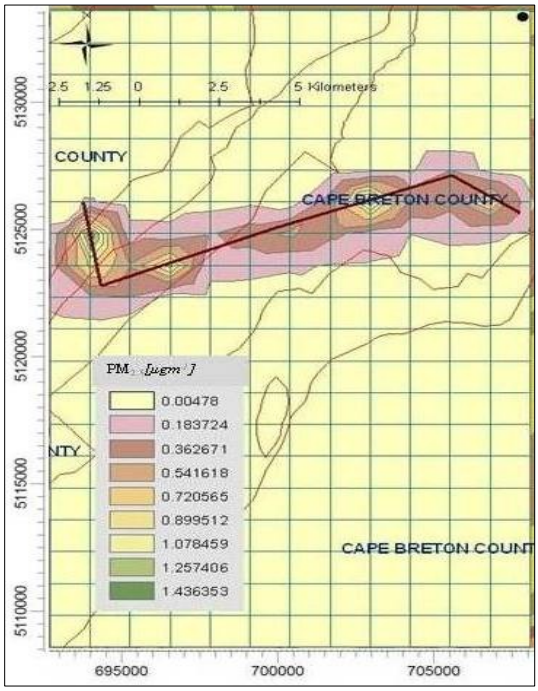

b. February

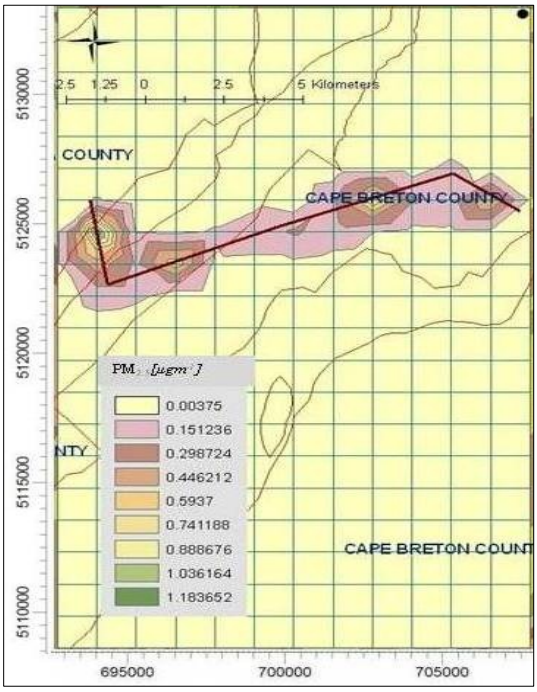

c. March

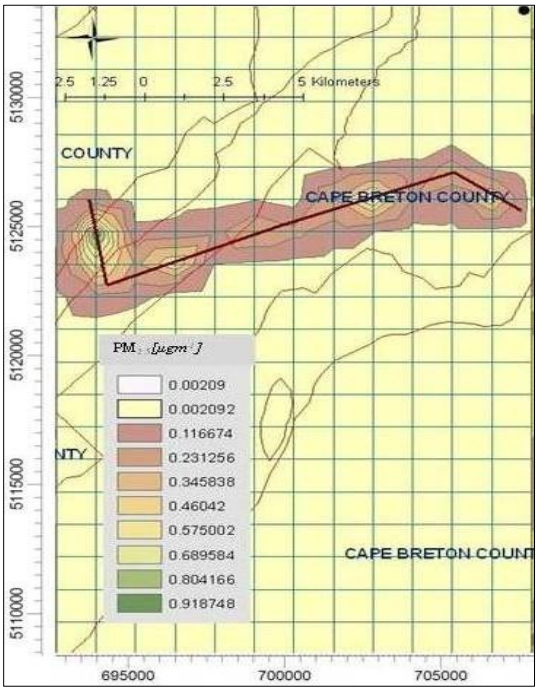

d. April

(Figures Cont'd)

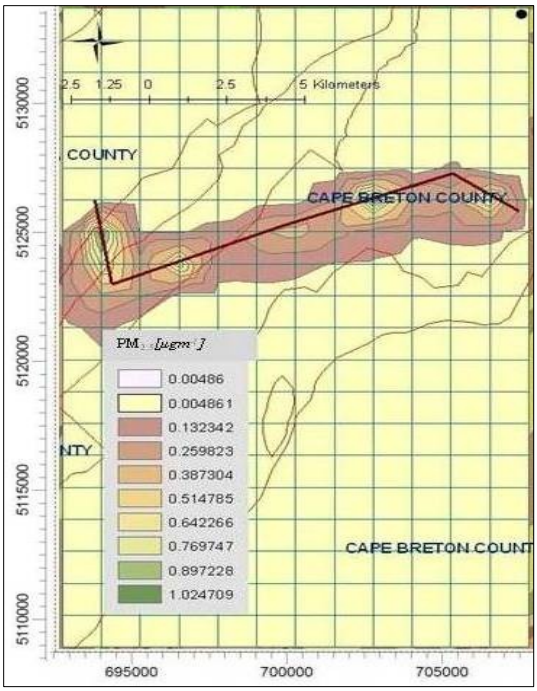

e. May

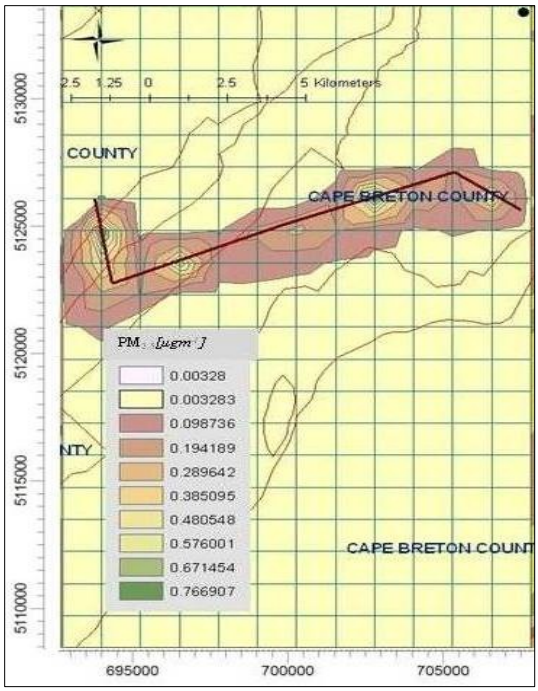

f. June

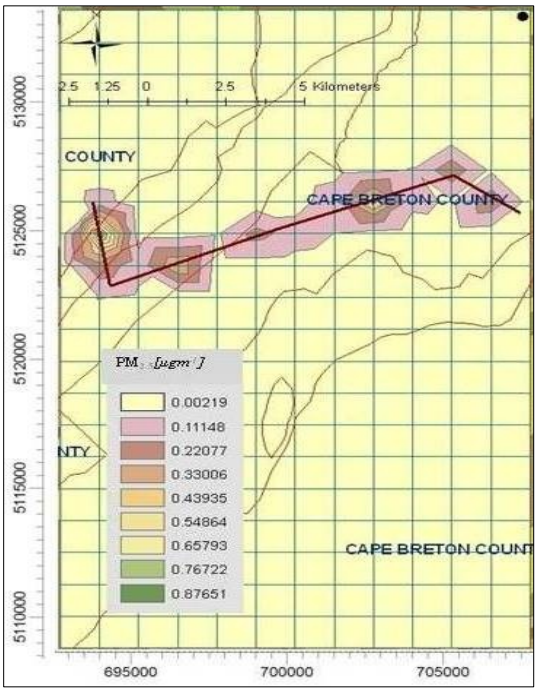

g. July

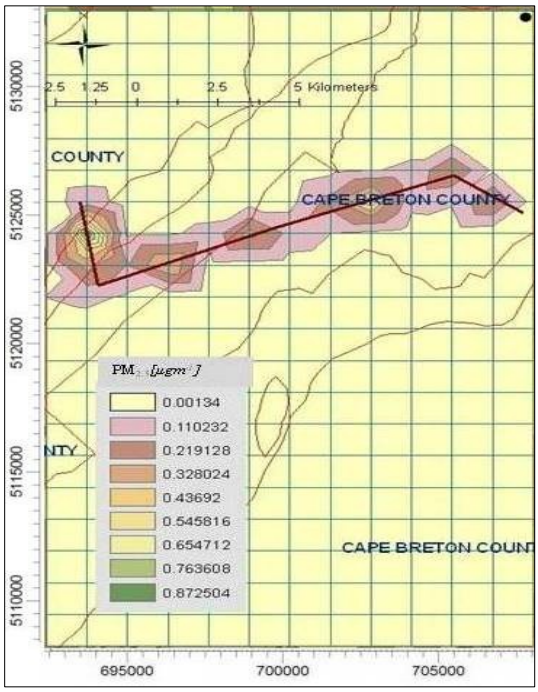

h. August

(Figures Cont'd)

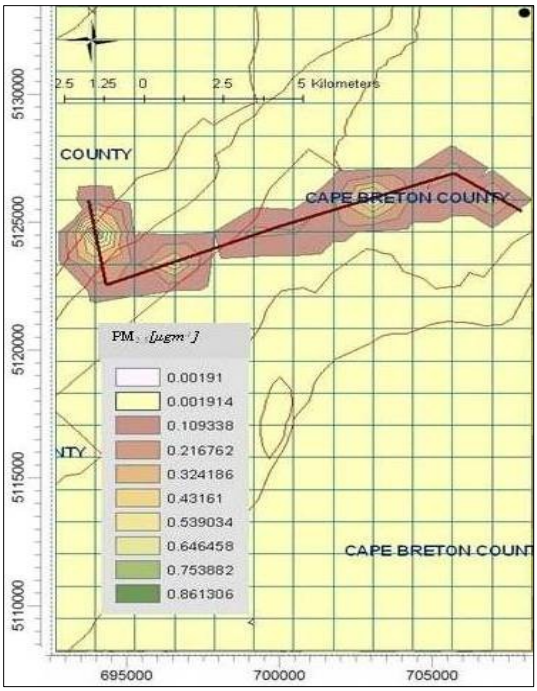

i. September

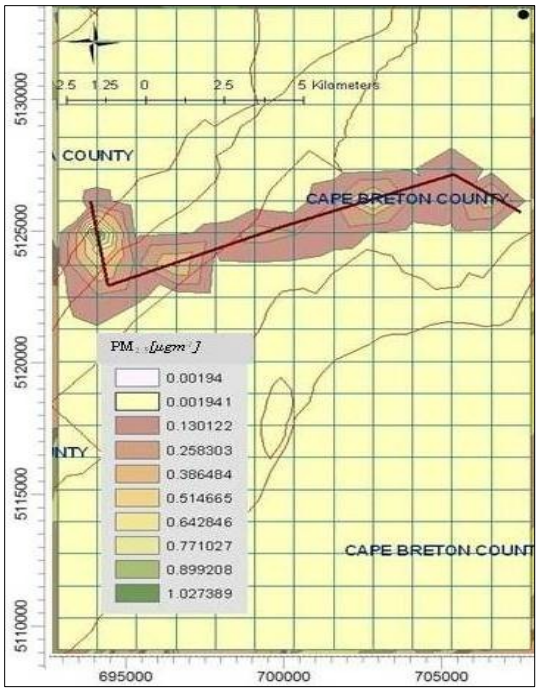

j. October

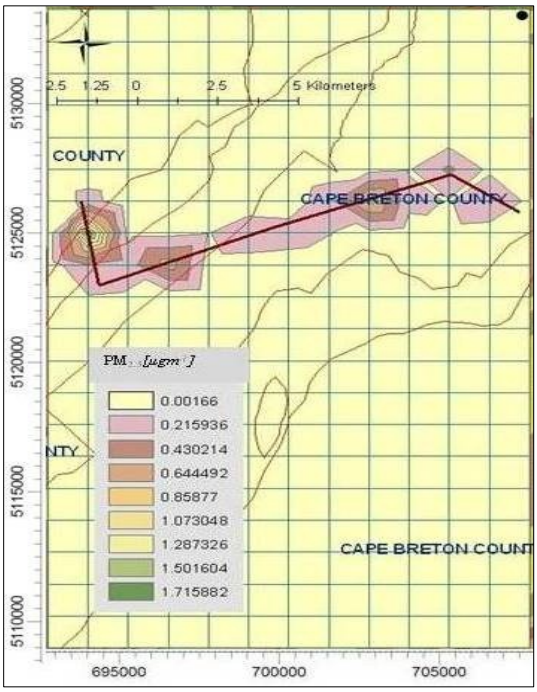

k. November

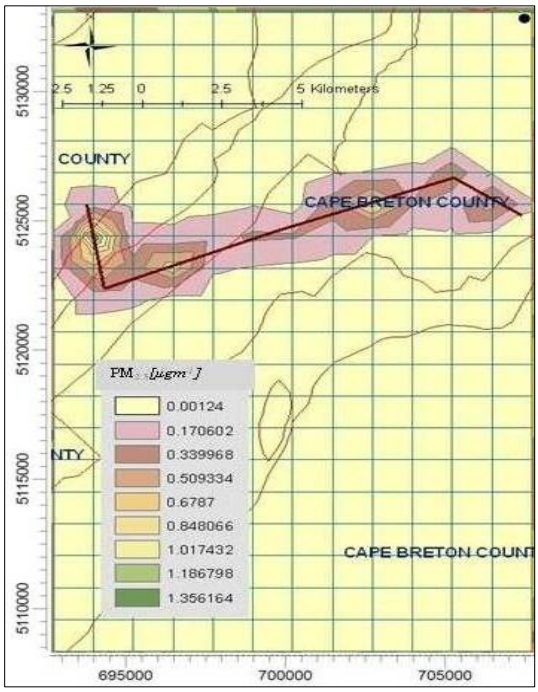

l. December

Table 15 Monthly MAX and MIN GLCs of NO_x, SO_2 and $PM_{2.5}$

	NO_x		SO_2		$PM_{2.5}$	
Month	Monthly Min *[μg m^{-3}]* UTM Coordinate (m) Elevation (m)	Monthly Max *[μg m^{-3}]* UTM Coordinate (m) Elevation (m)	Monthly Min *[μg m^{-3}]* UTM Coordinate (m) Elevation (m)	Monthly Max *[μg m^{-3}]* UTM Coordinate (m) Elevation (m)	Monthly Min *[μg m^{-3}]* UTM Coordinate (m) Elevation (m)	Monthly Max *[μg m^{-3}]* UTM Coordinate (m) Elevation (m)
Jan	0.011 (707730.9:5133631) 21.3	1.657 (702734.1:5126129) 64.2	0.006 (707730.9:5133631) 21.3	0.93 (702734.1:5126129) 64.2	0.001 (698986.6:5108624) 184.6	1.009 (702734.1:5126129) 64.2
Feb	0.017 (707730.9:5133631) 21.3	2.344 (702734.1:5126129) 64.2	0.011 (707730.9:5133631) 21.3	1.52 (702734.1:5126129) 64.2	0.005 (695239.1:5108624.5) 153.3	1.615 (693989.9:5124879) NA
Mar	0.2 (692470.7:5133631) NA	1.56 (693989.9:5124879) NA	0.019 (695239.1:5131130.5) NA	1.1 (693989.9:5124879) NA	0.004 (695239.1:5108624.5) 153.3	1.33 (693989.9:5124879) NA
Apr	0.016 (707730.9:5133631) 21.3	1.233 (693989.9:5124879) NA	0.023 (707730.9:5133631) 21.3	0.92 (693989.9:5124879) NA	0.002 (698986.6:5109875) 229.8	1.003 (693989.9:5124879) NA
May	0.019 (707730.9:5133631) 21.3	2.094 (702734.1:5126129) 64.2	0.033 (707730.9:5133631) 21.3	1.967 (702734.1:5126129) 64.2	0.005 (707730.9:5108624.5) 137.4	1.152 (702734.1:5126129) 64.2
June	0.041 (692470.7:5133631) NA	1.58 (702734.1:5126129) 64.2	0.1 (692740.7:5133631) NA	1.67 (707730.9:5132381) 21	0.003 (696488.3:5108624.5) 169.7	0.862 (693989.9:5124879) NA
July	0.028 (692470.7:5133631) NA	1.17 (693989.9:5124879) NA	0.051 (692740.7:5133631) NA	1.054 (706481.7:5126129) 61.9	0.002 (706481.7:5108624.5) 170.2	0.986 (693989.9:5124879) NA
Aug	0.029 (692470.7:5133631) NA	1.16 (693989.9:5124879) NA	0.071 (692740.7:5108624.5) NA	0.85 (693989.9:5124879) NA	0.001 (707730.9:5108624.5) 137.4	0.981 (693989.9:5124879) NA
Sep	0.012 (692470.7:5133631) NA	1.13 (693989.9:5124879) NA	0.018 (692740.7:5108624.5) NA	0.799 (693989.9:5124879) NA	0 (692740.7:5108624.5) NA	0.002 (707730.9:5132381) 21
Oct	0.041 (700235.8:5109875) 186.8	1.4 (693989.9:5124879) NA	0.087 (692741.7:5119877.5) NA	0.989 (693989.9:5124879) NA	0.002 (707730.9:5108624.5) 137.4	1.156 (693989.9:5124879) NA
Nov	0.012 (695239.1:5108624.5) 153.3	2.23 (693989.9:5124879) NA	0.02 (707730.9:5133631) 21.3	1.55 (693989.9:5124879) NA	0.002 (695239.1:5108624.5) 153.3	1.93 (693989.9:5124879) NA
Dec	0.011 (700235.8:5113626) 140.3	1.78 (693989.9:5124879) NA	0.01 (707730.9:5133631) 21.3	1.24 (693989.9:5124879) NA	0.001 (698986.6:5108624) 184.6	1.526 (693989.9:5124879) NA

4.3.2.3 Hourly averaging of NO_x, SO_2 and $PM_{2.5}$

Figures 27 through 29 shows hourly predicted GLC contour maps of NO_x, SO_2 and $PM_{2.5}$ respectively in PTA domain. With reference to the figures it is seen that the GLCs of pollutants decreased with longer averaging period. Point Aconi plant contributed a greater amount of ground level NO_x compared to highway vehicles, whereas highway 105 contributed larger amounts of SO_2 and $PM_{2.5}$ compared to Point Aconi Plant. Hourly dispersion patterns of NO_x indicated that there was temperature inversion during early morning and afternoon hours therefore, highest NO_x concentration gradients were bisected. The minimum and maximum hourly predicted NO_x, SO_2 and $PM_{2.5}$ concentrations at a specific receptor location with elevation are given in Table 16. From Table 16 it is seen that 1-hr highest SO_2 concentration receptor has an elevation of 191.4 m which demonstrates that the highest concentration are found at higher elevations during the advection process (U.S. EPA., 1998). As the emission rate of $PM_{2.5}$ was significantly low, high concentration values are seen within 2 km radius of the highway 105, Figure 29.

Figures 27a-e Hourly GLCs of NO_x due to point and highway emission sources

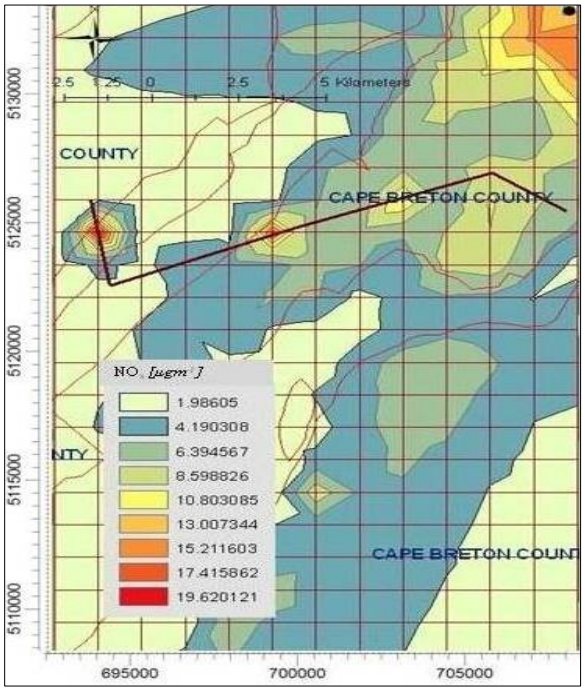

a. 1 hour

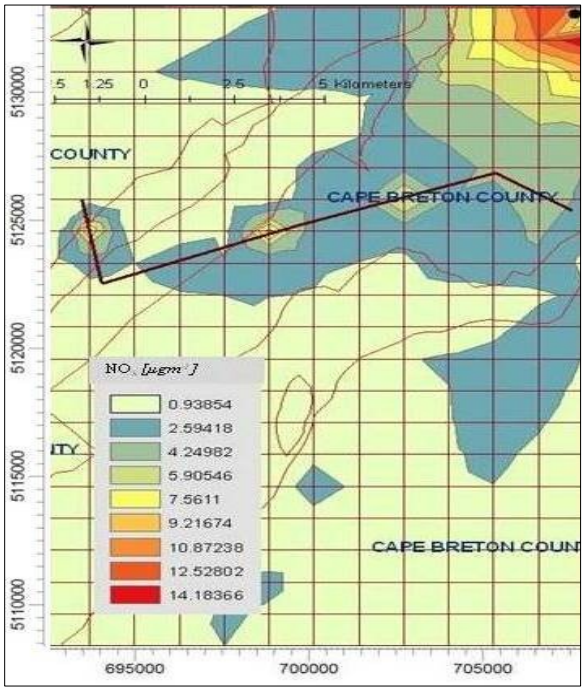

b. 3 hour

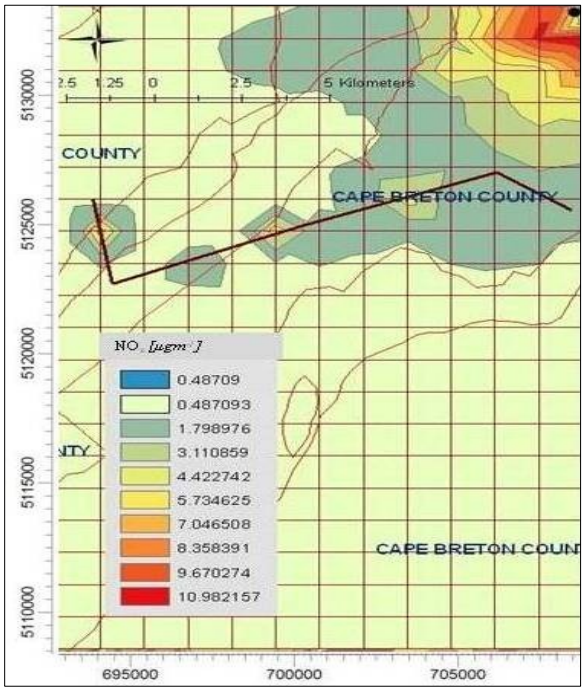

c. 8 hour

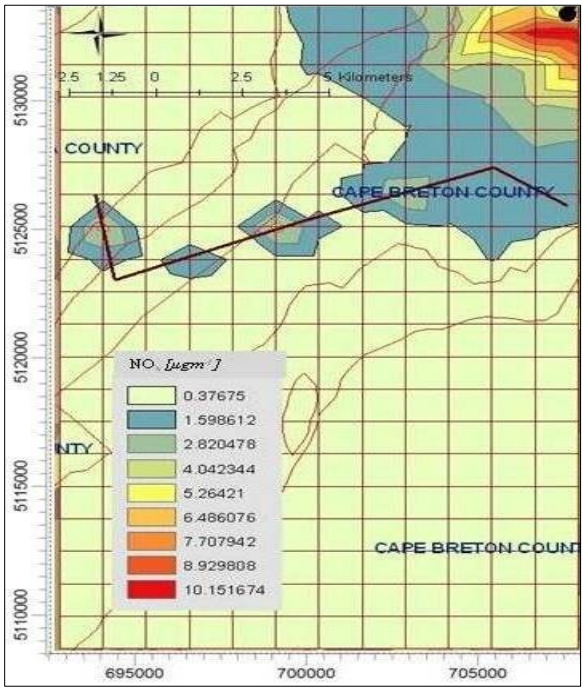

d. 12 hour

(Figure Cont'd)

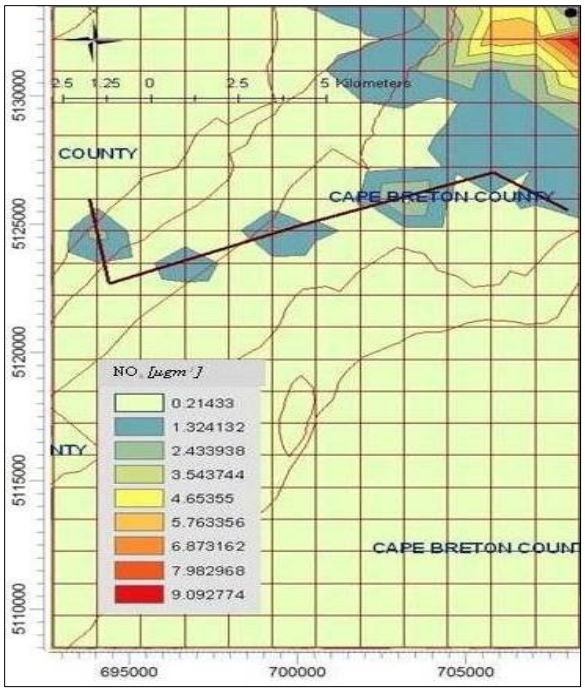
2.5 1.25 0 2.5 5 Kilometers
COUNTY
CAPE BRETON COUNTY
NO2 [µgm-3]
0.21433
1.324132
2.433938
3.543744
4.65355
5.763356
6.873162
7.982968
9.092774
NTY
CAPE BRETON COUNT
5130000
5125000
5120000
5115000
5110000
695000
700000
705000

e. 24 hour

Figures 28a-e Hourly GLCs of SO_2 due to point and highway emission sources

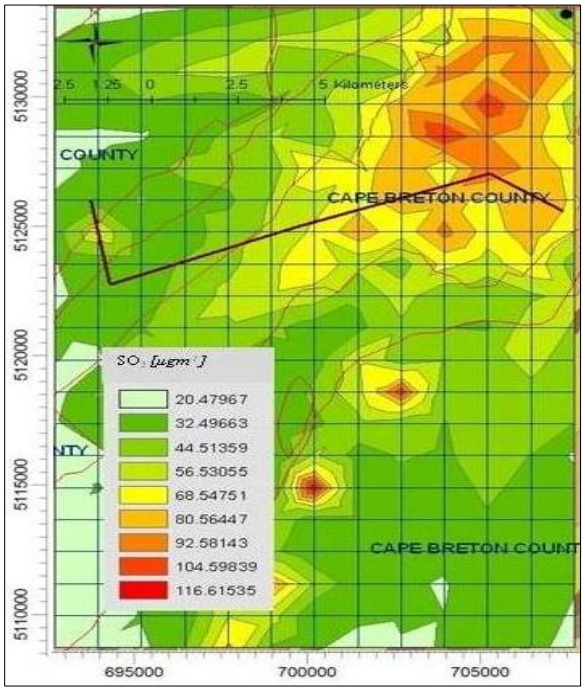

a. 1 hour

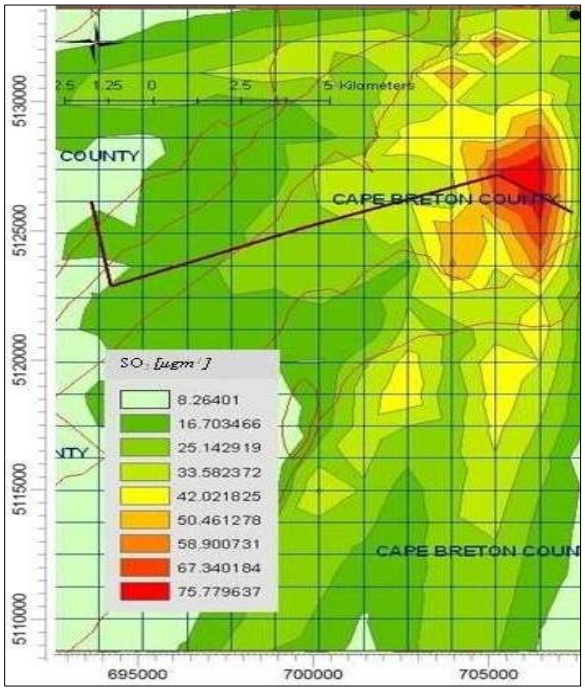

b. 3 hour

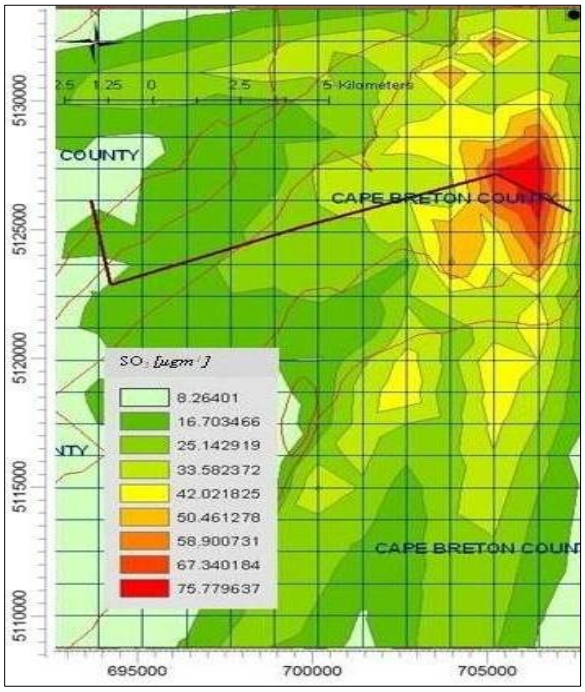

c. 8 hour

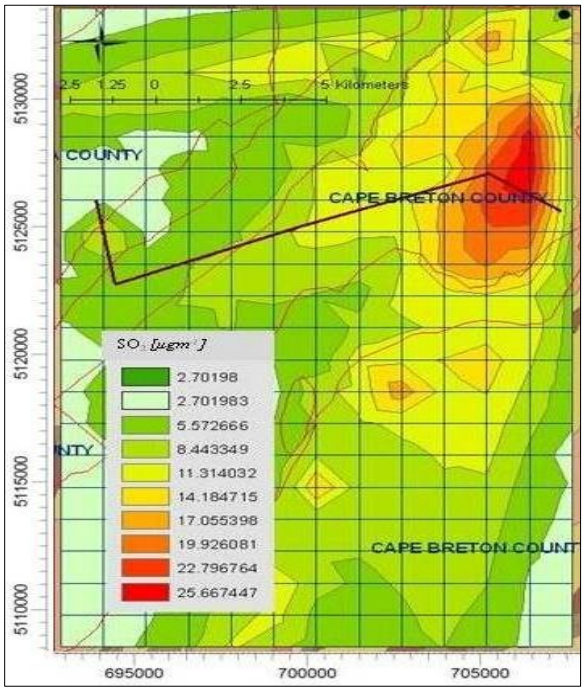

d. 12 hour

(Figure Cont'd)

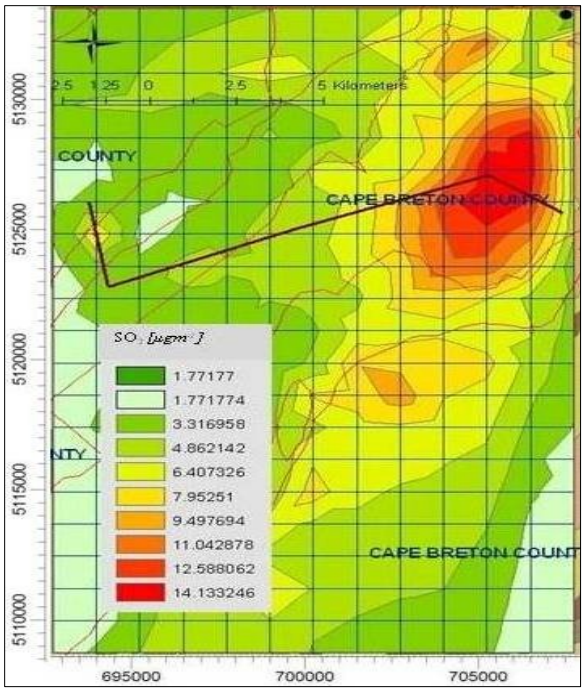
2.5 1.25 0 2.5 5 Kilometers
COUNTY
CAPE BRETON COUNTY
SO2 [µgm-3]
1.77177
1.771774
3.316958
4.862142
6.407326
7.95251
9.497694
11.042878
12.588062
14.133246
CAPE BRETON COUNT
5130000
5125000
5120000
5115000
5110000
695000
700000
705000

e. 24 hour

Figures 29a-e Hourly GLCs of $PM_{2.5}$ due to point and highway emission sources

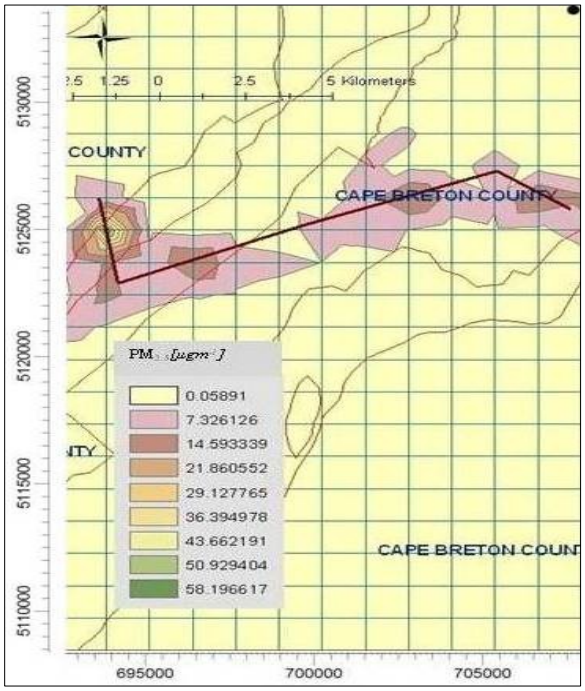

a. 1 hour

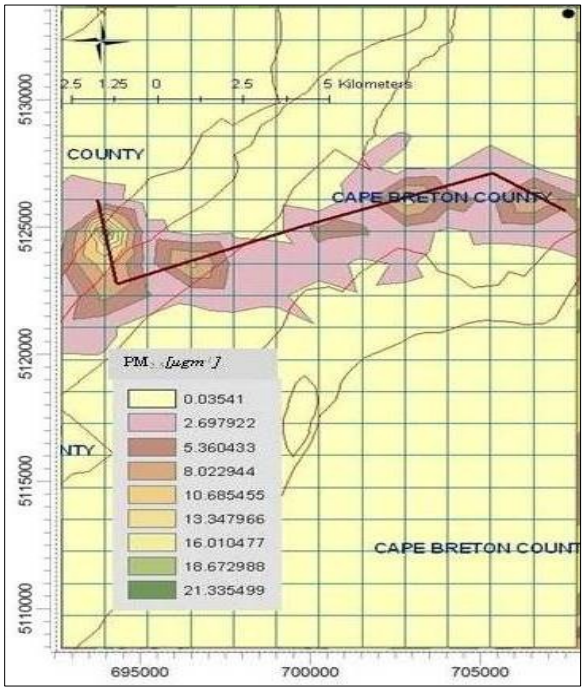

b. 3 hour

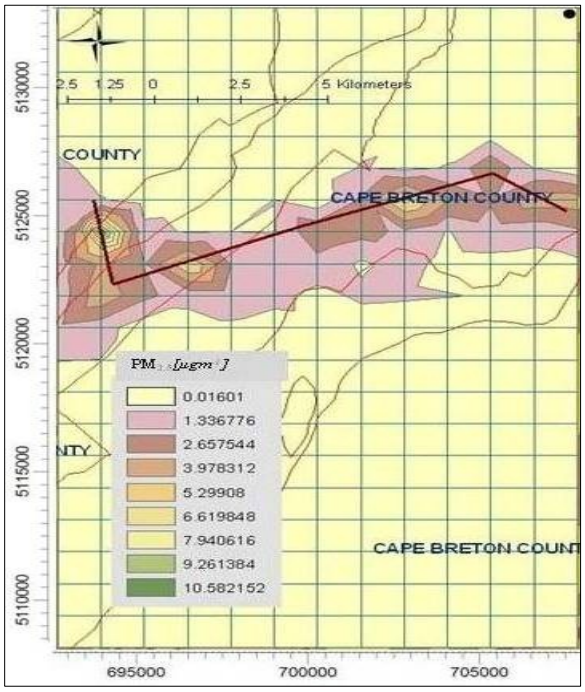

c. 8 hour

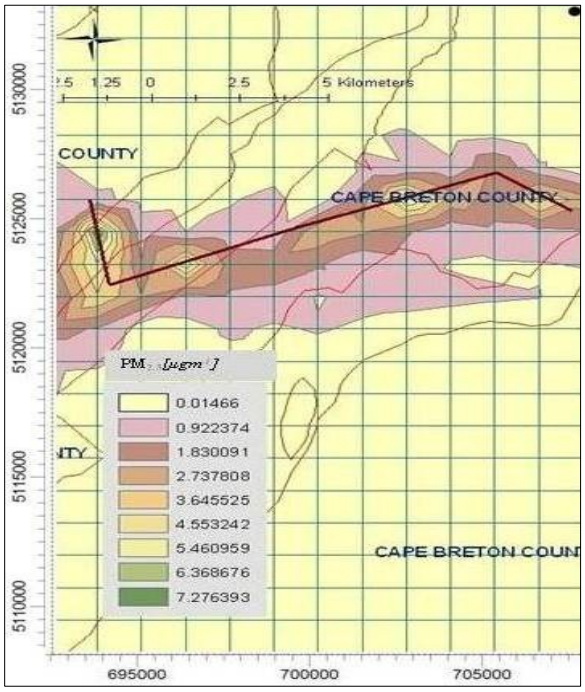

d. 12 hour

(Figure Cont'd)

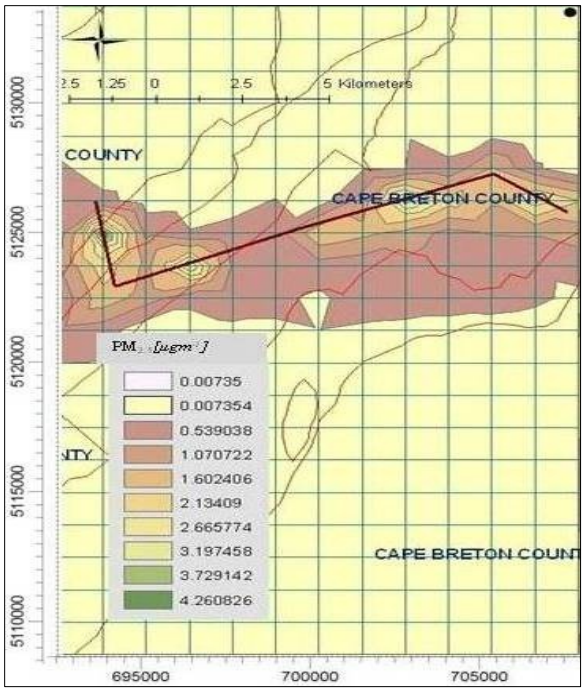

e. 24 hour

Table 16 Hourly MAX and MIN GLCs of NO_x, SO_2 and $PM_{2.5}$

	NO_x		SO_2		$PM_{2.5}$	
Hour	Hourly Min *[µg m^{-3}]* UTM Coordinate (m) Elevation (m)	Hourly Max *[µg m^{-3}]* UTM Coordinate (m) Elevation (m)	Hourly Min *[µg m^{-3}]* UTM Coordinate (m) Elevation (m)	Hourly Max *[µg m^{-3}]* UTM Coordinate (m) Elevation (m)	Hourly Min *[µg m^{-3}]* UTM Coordinate (m) Elevation (m)	Hourly Max *[µg m^{-3}]* UTM Coordinate (m) Elevation (m)
1	1.986 (697737.44:5113626) NA	21.824 (693989.9:5124879) NA	20.48 (692740.68:5108624.5) NA	128.63 (700235.8:5114876) 191.4	0.059 (695239.06:510862 4.5) 153.3	65.464 (693989.9:5124879) NA
3	0.939 (692740.68: 5113626) NA	15.839 (707730.9:5132381) 21	8.264 (692740.68:5108624.5) NA	84.2 (706481.7:5127379.5) 60.5	0.035 (695239.06:510862 4.5) 153.3	23.988 (693989.9:5124879) NA
8	0.487 (692740.68:5108624. 5) NA	12.294 (707730.9:5132381) 21	3.521 (692740.68:5109875) NA	41.94 (706481.7:5127379.5) 60.5	0.016 (695239.06:510862 4.5) 153.3	11.9 (693989.9:5124879) NA
12	0.377 (692740.68:5111125) NA	11.374 (46°18'47.38":60°18' 7.03") 21	2.702 (693989.87:5109875) NA	28.53 (706481.7:5127379.5) 60.5	0.015 (695239.06:510862 4.5) 153.3	8.184 (693989.9:5124879) NA
24	0.214 (692740.68:5108624. 5) NA	10.203 (707730.9:5132381) 21	1.772 (692740.68:5111125) NA	15.68 (705232.5:5127379.5) 27.8	0.007 (695239.06:510862 4.5) 153.3	4.793 (693989.9:5124879) NA

4.3.3 Modeling Study in TRR domain

Emission of NO_x, SO_2 and $PM_{2.5}$ from Brookfield Cement plant, Truro paper mill and 35.53 km and 26.07 km section lengths of highways 102 and 104 respectively were used for conducting the simulation studies in TRR domain during 2007.

4.3.3.1 Annual averaging of NO_x, SO_2 and $PM_{2.5}$

Model predicted GLC contour maps of NO_x, SO_2 and $PM_{2.5}$ during annual averaging period are shown in Figures 30 through 32. As seen from the figures, the highest annual average NO_x, SO_2 and $PM_{2.5}$ concentration gradients were found at 6.8 km north east of the Brookfield cement plant and by the side of highway 102. It is seen from Table 17, the minimum and maximum annual average predicted NO_x concentrations were 0.033 μg m^{-3} located at 509016.8m: 5043268m, elevation NA and 9.688 μg m^{-3} located at 476621.9m: 5015953m, elevation 53.4 m respectively. The annual minimum and maximum predicted SO_2 concentrations were 0.024 μg m^{-3} found at 476621.9m: 5008503m, elevation 63.5 and 1.075 μg m^{-3} at the coordinates 476621.9m: 5015953m, elevation 53.4 respectively. The minimum and maximum annual average $PM_{2.5}$ concentrations in TRR were 0.002 μg m^{-3} found at 464162.3m: 5040785m, elevation 290 m and 2.282 μg m^{-3} at 476621.9m: 5015953m, elevation 53.4 respectively. Brookfield cement plant and the Truro paper mill contributed small amount of total emission compared to the vehicles on highway 102. Therefore the dispersion phenomenon in this domain was dominated by highway emission sources. Air pollutants were advected by the prevailing wind towards east of highway 102. Most of the areas in this domain were not affected by the emission from above mentioned sources.

Figure 30 Annual GLCs of NO_x due to point and highway emission sources

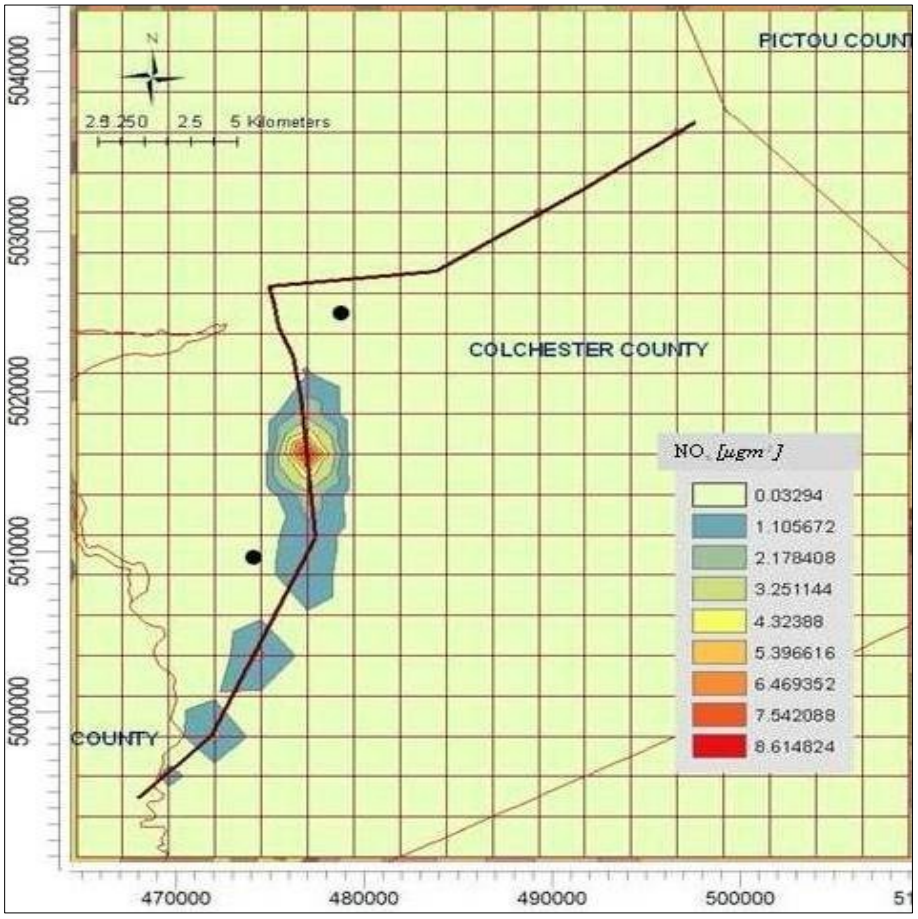

Figure 31 Annual GLCs of SO_2 due to due to point and highway emission sources

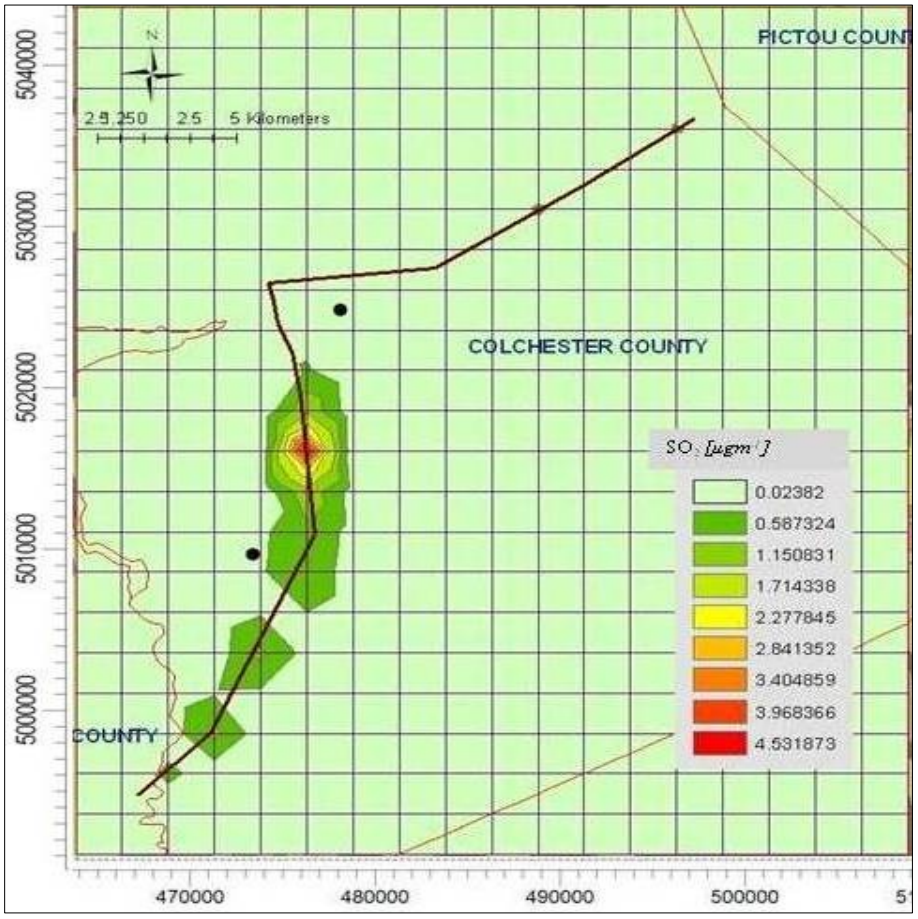

Figure 32 Annual GLCs of $PM_{2.5}$ due to due to point and highway emission sources

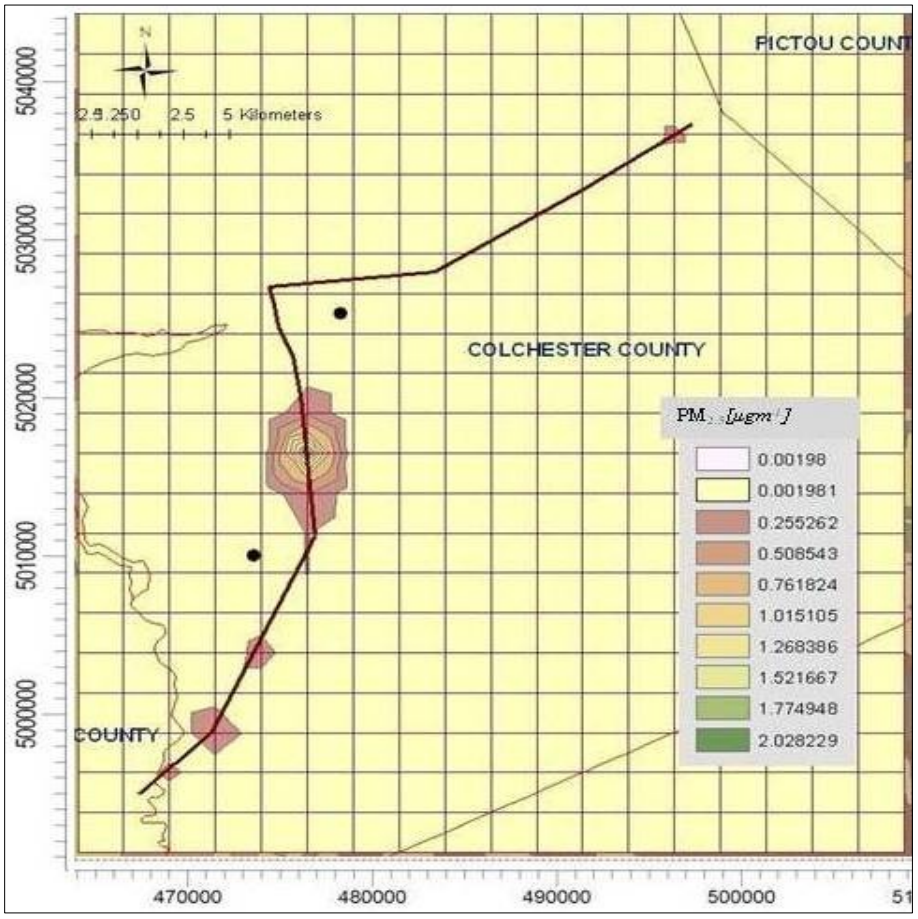

Table 17 Annual MAX and MIN GLCs of NO_x, SO_2 and $PM_{2.5}$

Pollutant	Annual Min *[µg m^{-3}]* UTM coordinate (m) Elevation (m)	Annual Max *[µg m^{-3}]* UTM coordinate (m) Elevation (m)
NO_x	0.033 (509016.8:5043268) NA	9.688 (476621.9:5015953) 53.4
SO_2	0.024 (476621.9:5008503) 63.5	5.095 (476621.9:5015953) 53.4
$PM_{2.5}$	0.002 (464162.3:5040785) 290	2.282 (476621.9:5015953) 53.4

4.3.3.2 Monthly averaging of NO_x, SO_2 and $PM_{2.5}$

Figures 33 through 35 show the monthly predictions of NO_x, SO_2 and $PM_{2.5}$ concentration contour maps in the TRR domain. As seen from the figures, dispersion patterns of the pollutants were similar. Highest GLC receptor remained unchanged throughout the year for all three pollutants. It is seen from Table 18, the minimum and maximum monthly predicted NO_x concentrations were 6.349 µg m^{-3} (April) at coordinates 476621.9m: 5015953m, elevation 53.4m and 12.5µg m^{-3} (January) at coordinates 476621.9m: 5015953m, elevation 53.4m respectively. The minimum and maximum monthly predicted SO_2 concentrations were 3.53 µg m^{-3} (April) at coordinates 476621.9m: 5015953m, elevation 53.4 m and 6.99 µg m^{-3} (December) at coordinates 476621.9m: 5015953m, elevation 53.4m respectively. The minimum and maximum monthly predicted $PM_{2.5}$ concentrations were 4.083 µg m^{-3} (April) at coordinates 476621.9m: 5015953m, elevation 53.4 m and 8.727 µg m^{-3} (November) at coordinates 476621.9m: 5015953m, elevation 53.4 m respectively. Monthly averaging shows that the highest GLCs were found during winter months. This phenomenon might be the result of stable atmospheric condition during winter. No significant change in GLCs was found during summer months. Low surface roughness length of grass land caused low GLC during warm conditions. Also no significant change in minimum GLCs was found throughout the year.

Figures 33a-l Monthly GLCs of NO_x due to point and highway emission sources

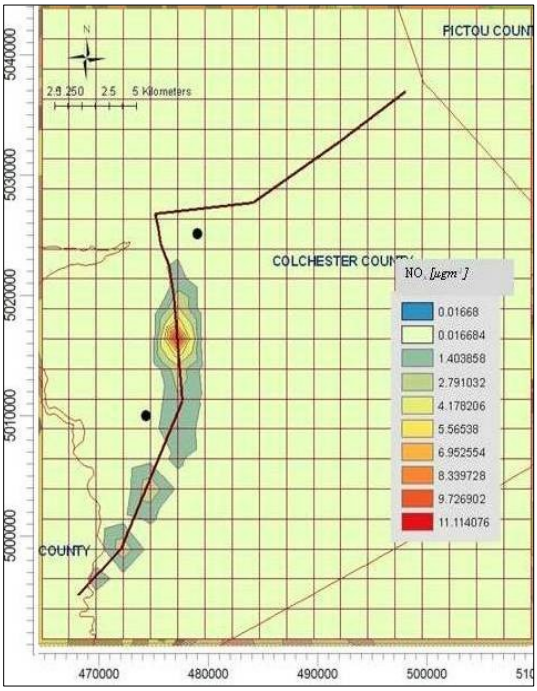

a. January

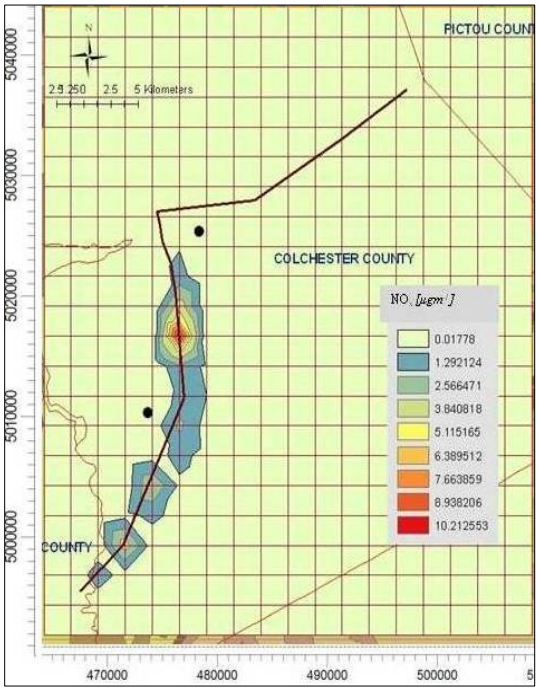

b. February

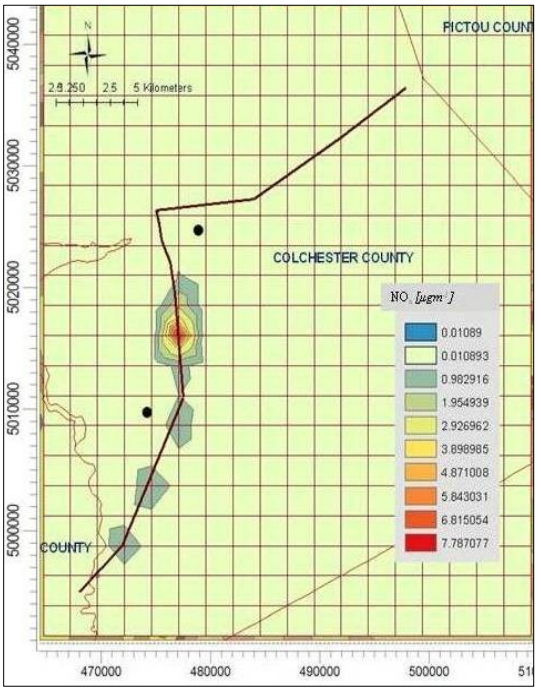

c. March

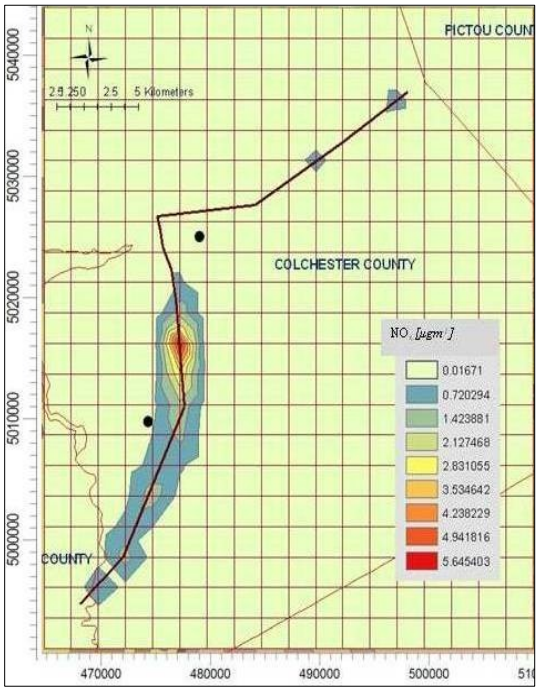

d. April

(Figures Cont'd)

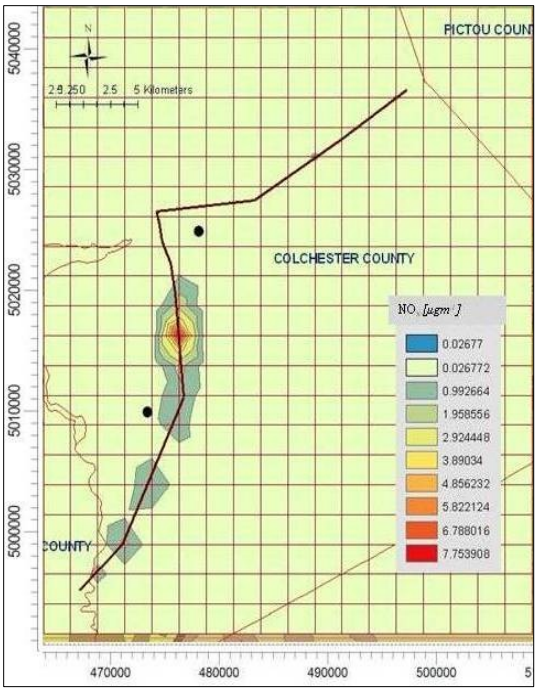

e. May

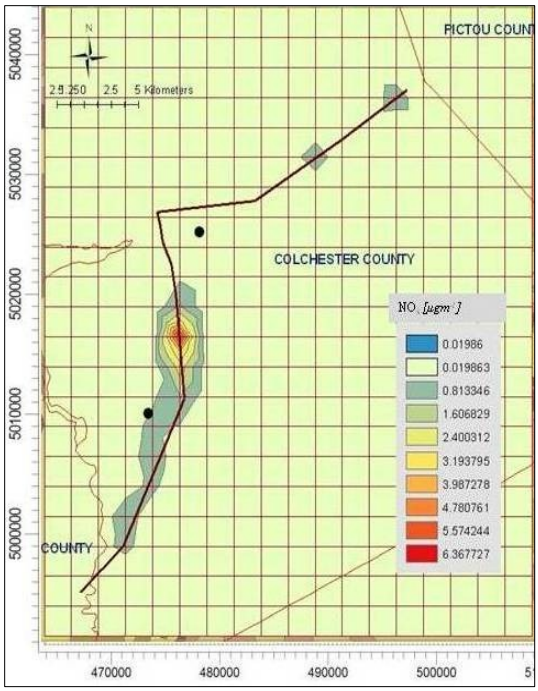

f. June

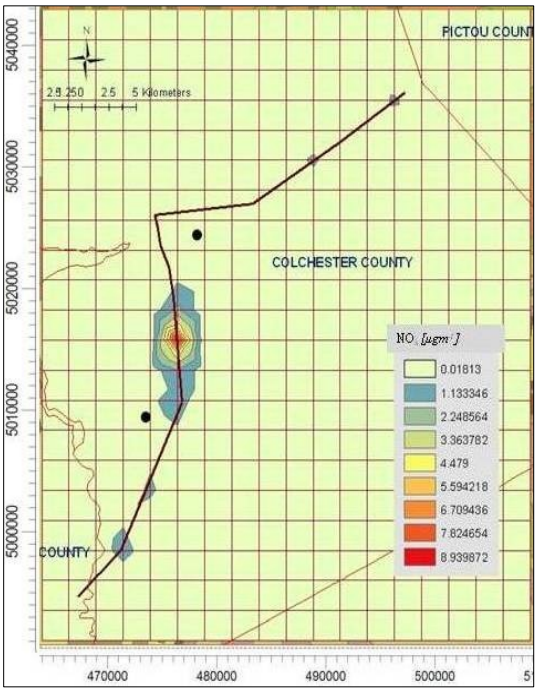

g. July

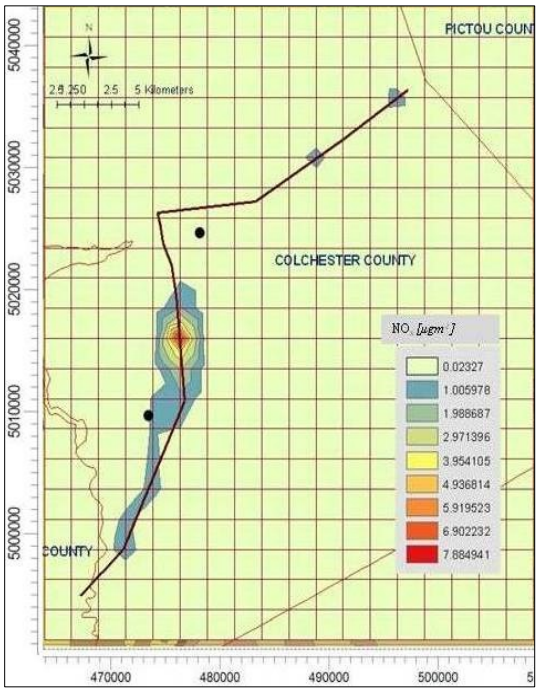

h. August

(Figures Cont'd)

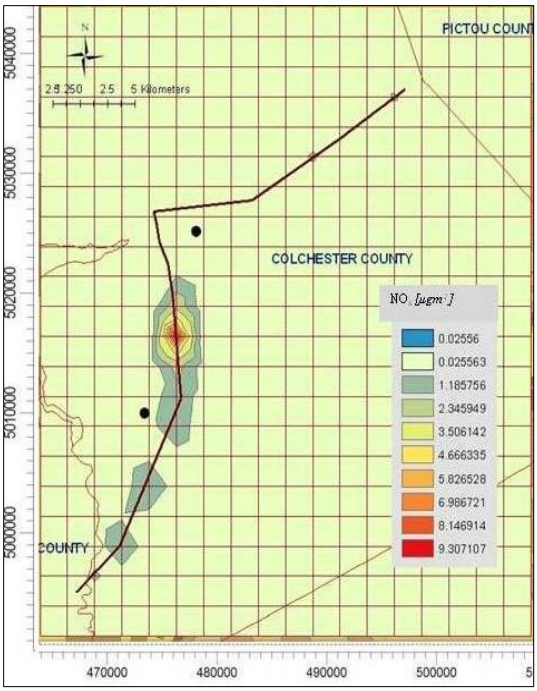

i. September

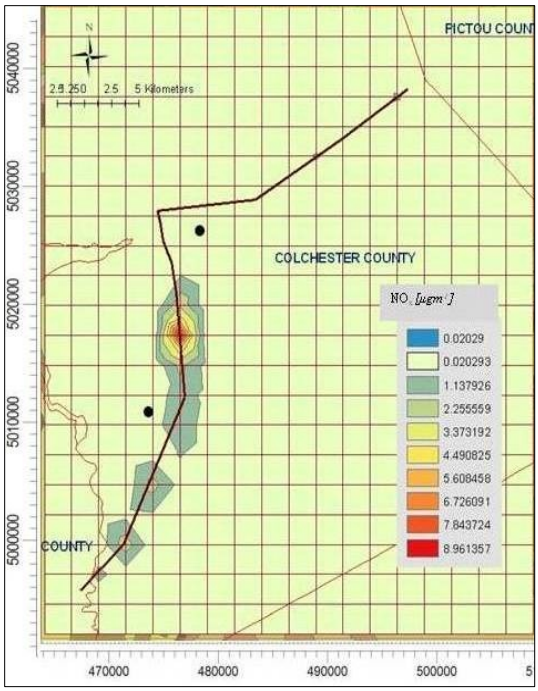

j. October

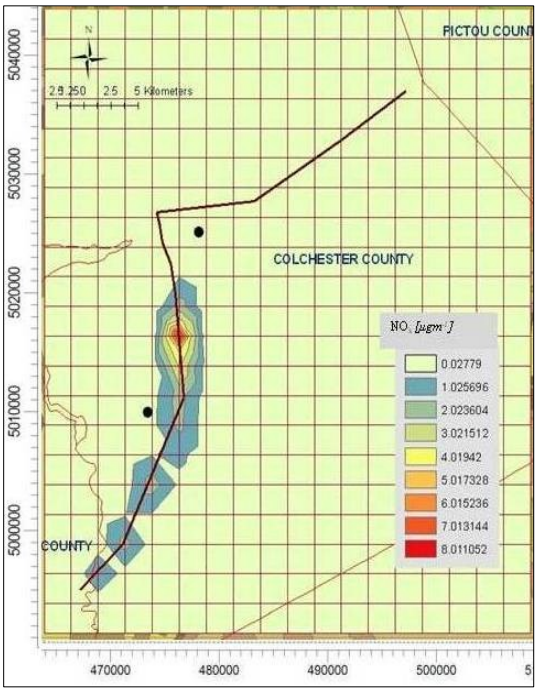

k. November

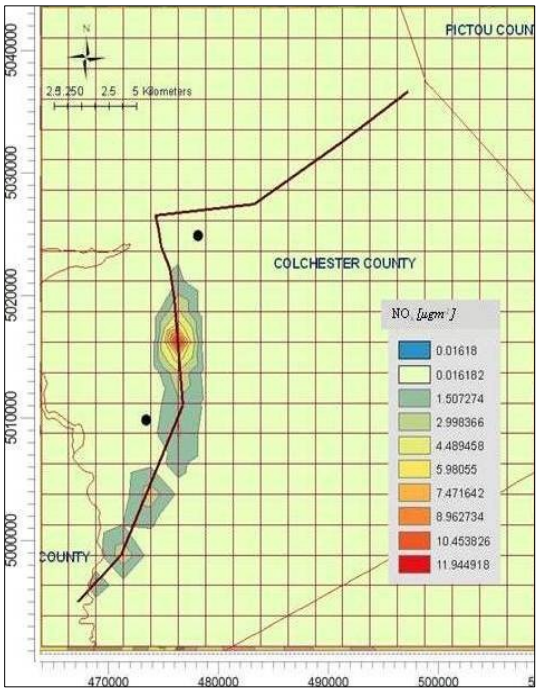

l. December

Figures 34a-l Monthly GLCs of SO_2 due to point and highway emission sources

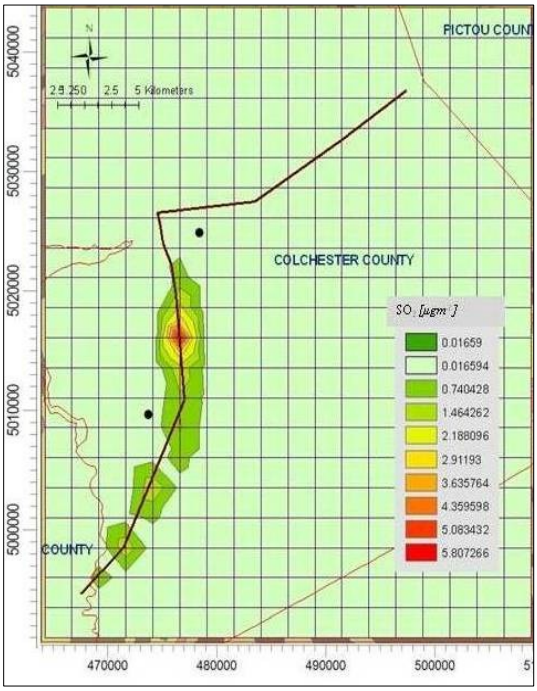

a. January

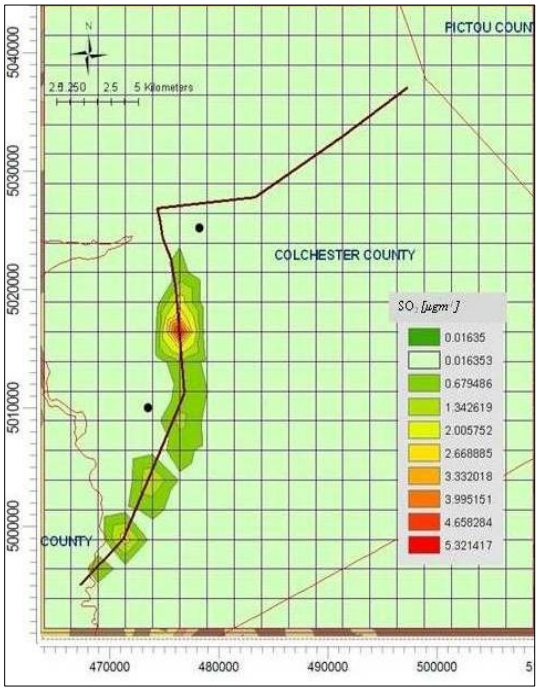

b. February

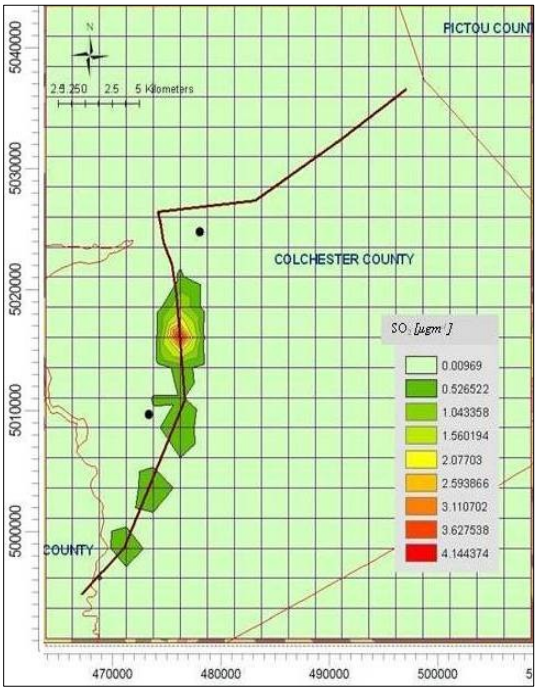

c. March

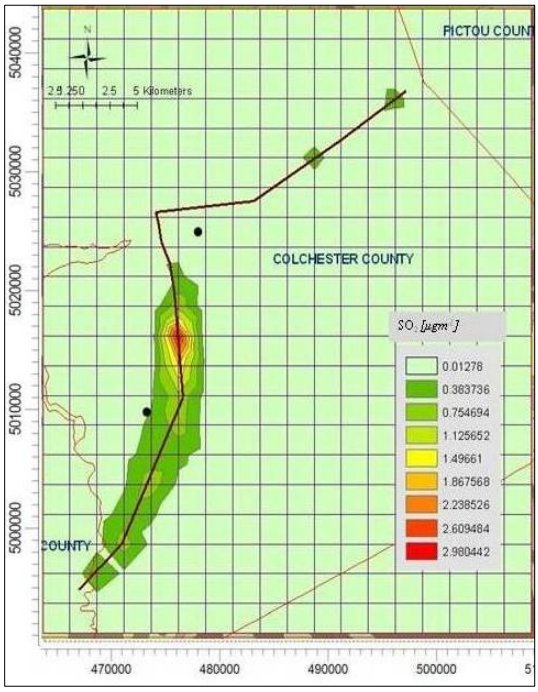

d. April

(Figures Cont'd)

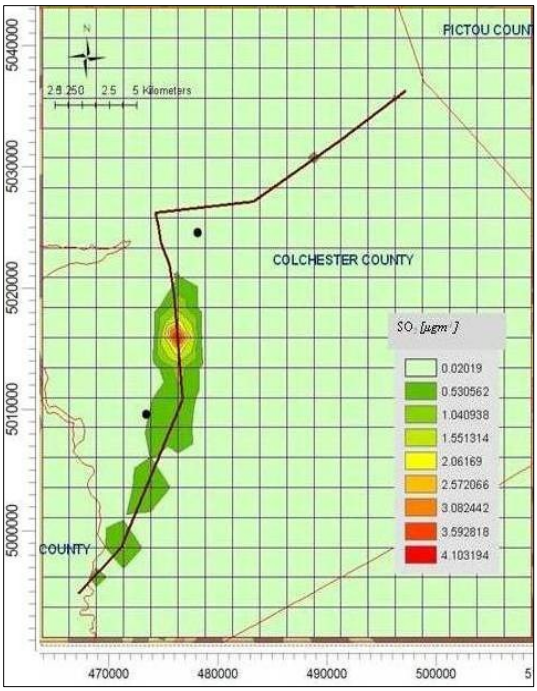

e. May

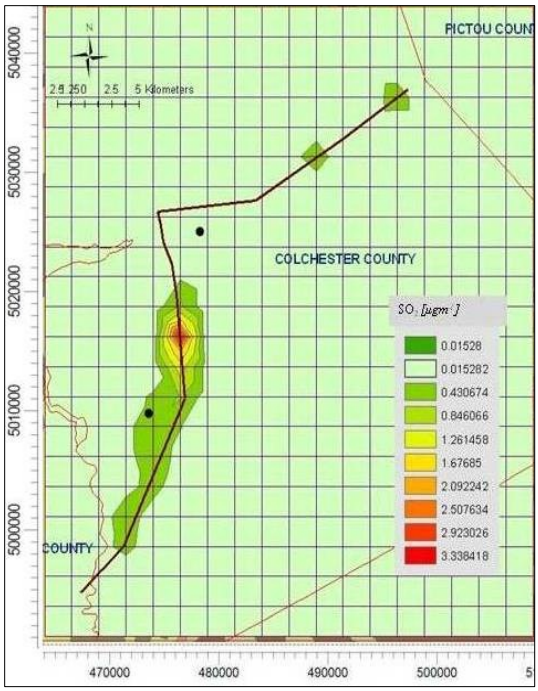

f. June

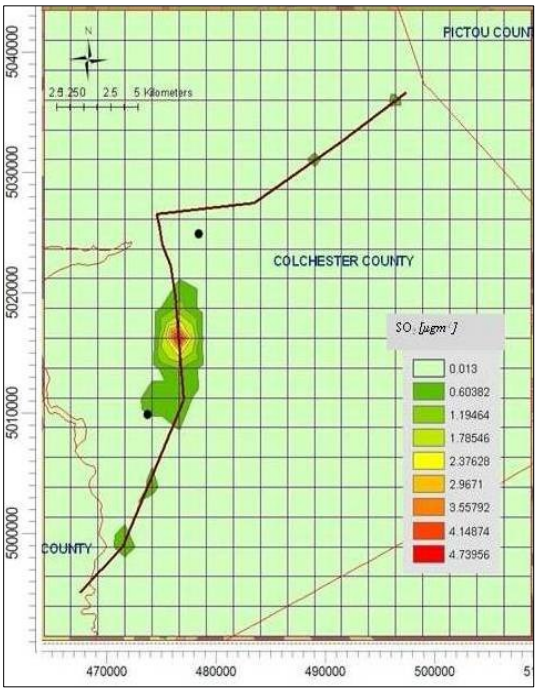

g. July

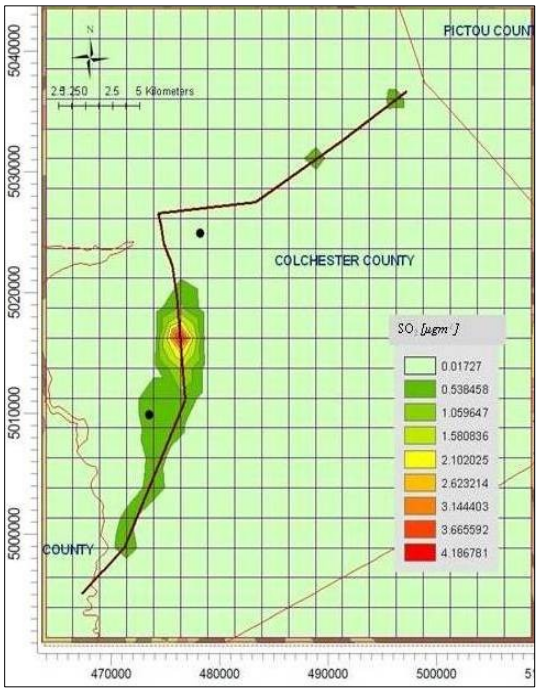

h. August

(Figures Cont'd)

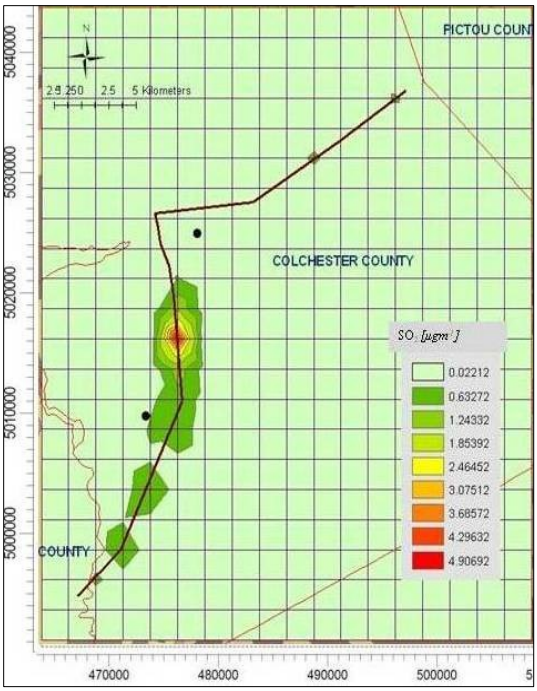

i. September

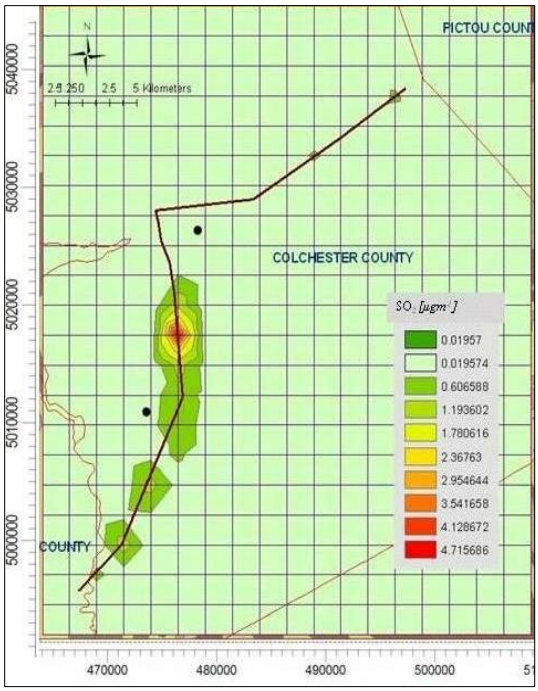

j. October

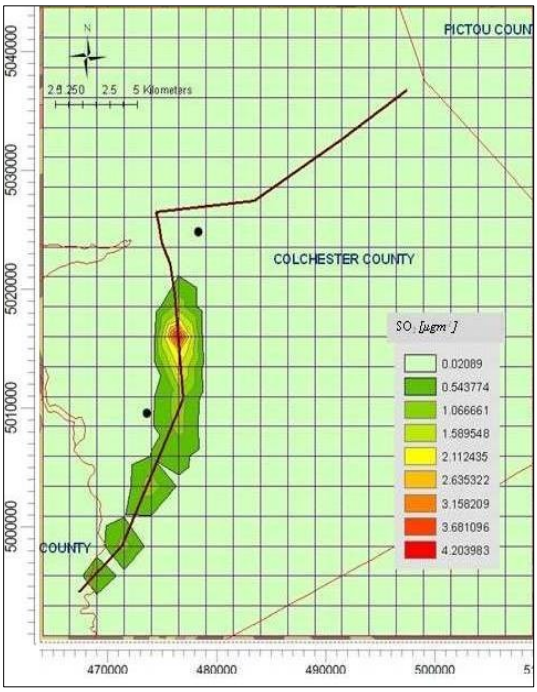

k. November

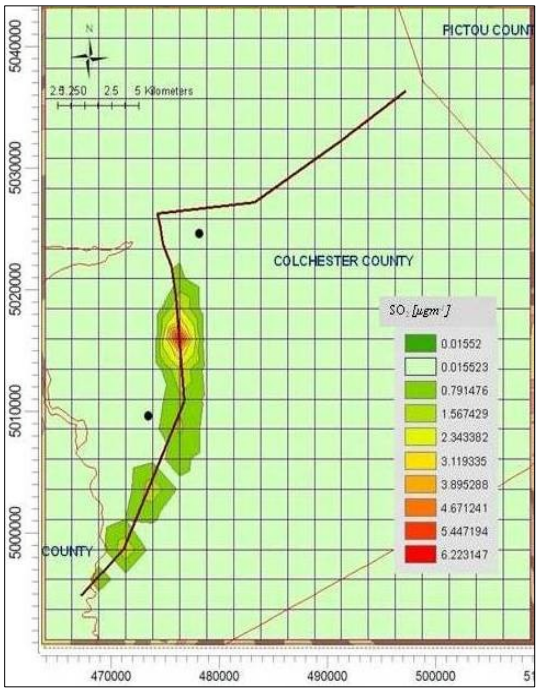

l. December

Figures 35a-l Monthly GLCs of $PM_{2.5}$ due to point and highway emission sources

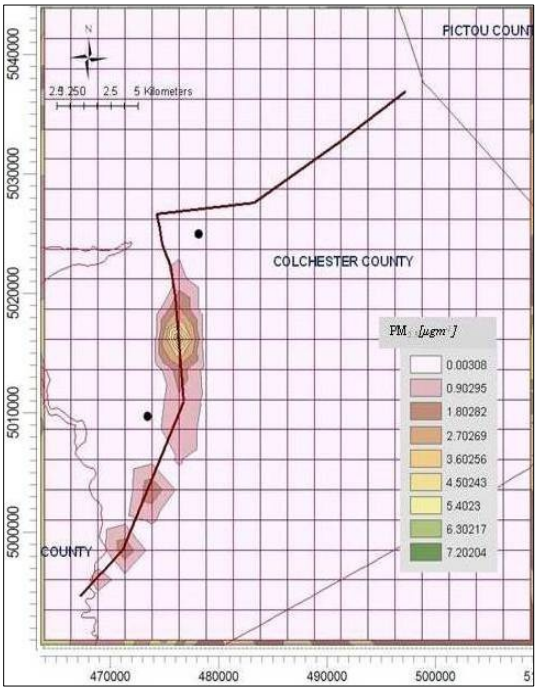

a. January

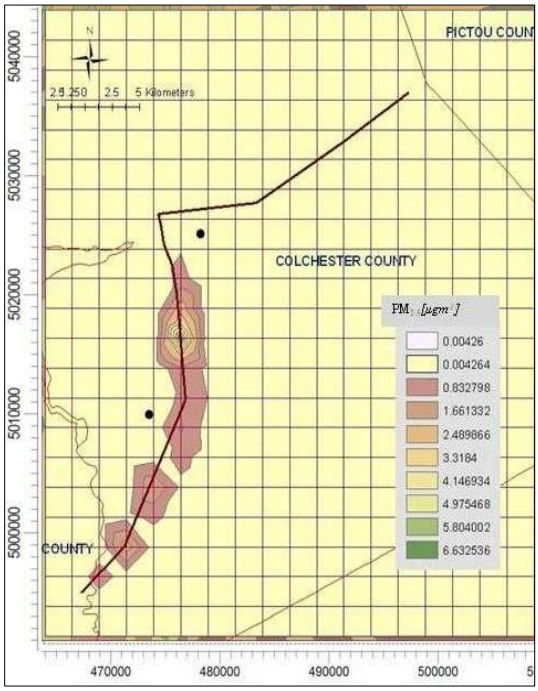

b.February

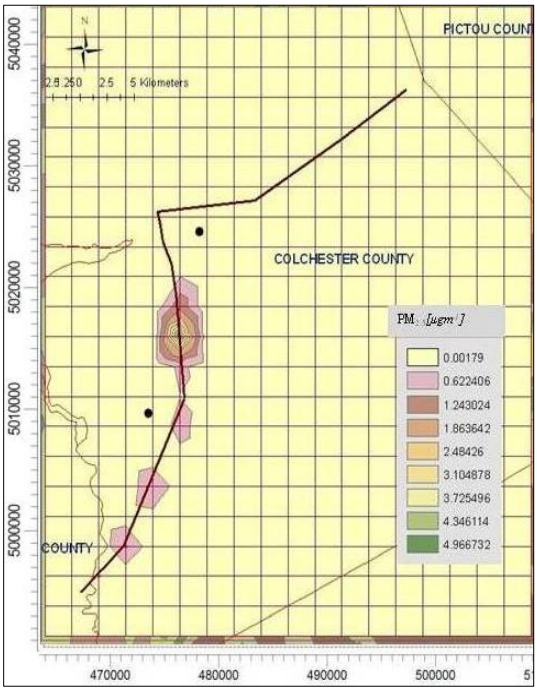

c. March

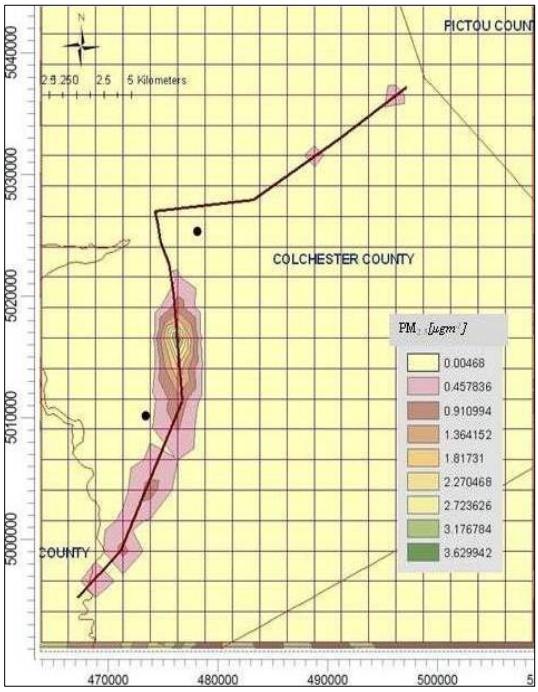

d. April

(Figures Cont'd)

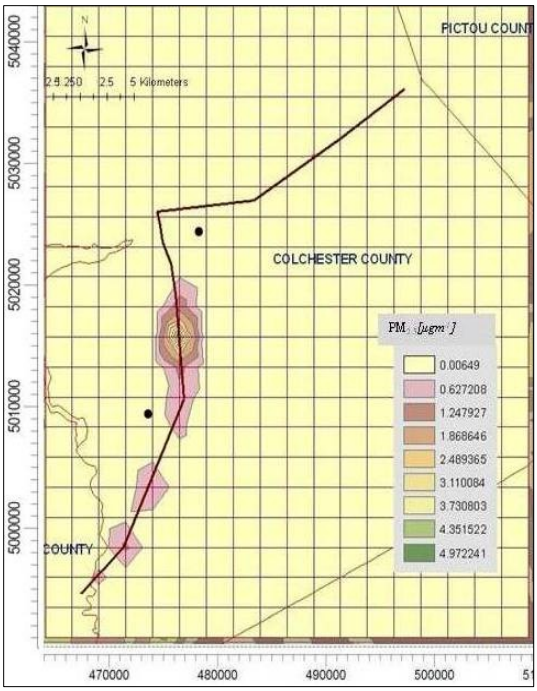

e. May

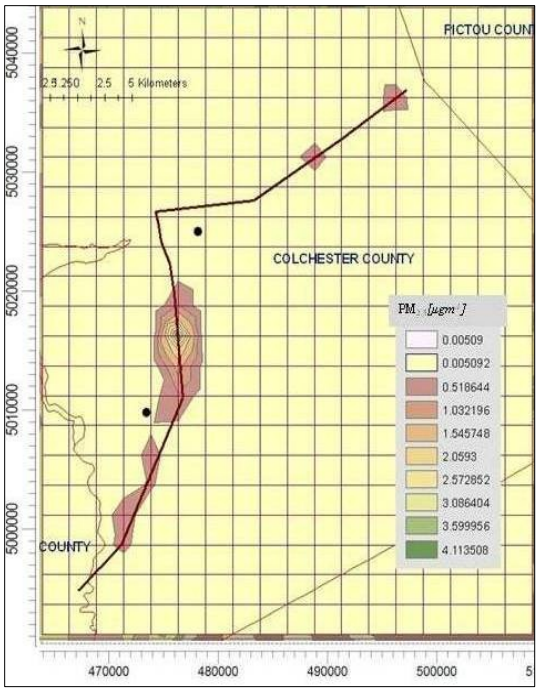

f. June

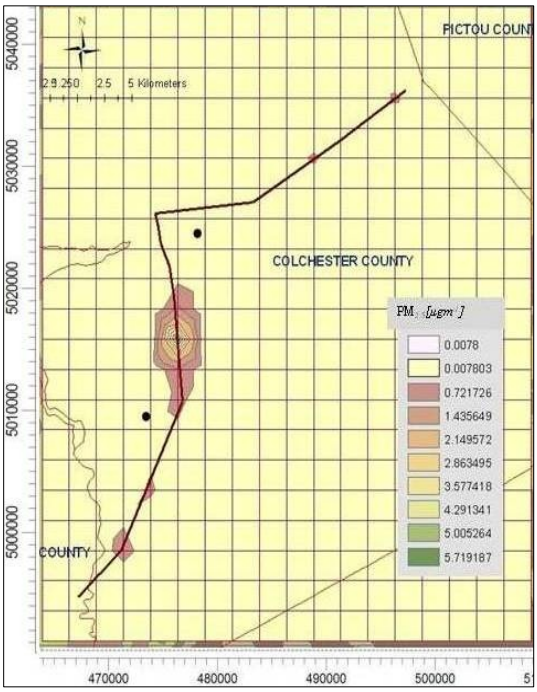

g. July

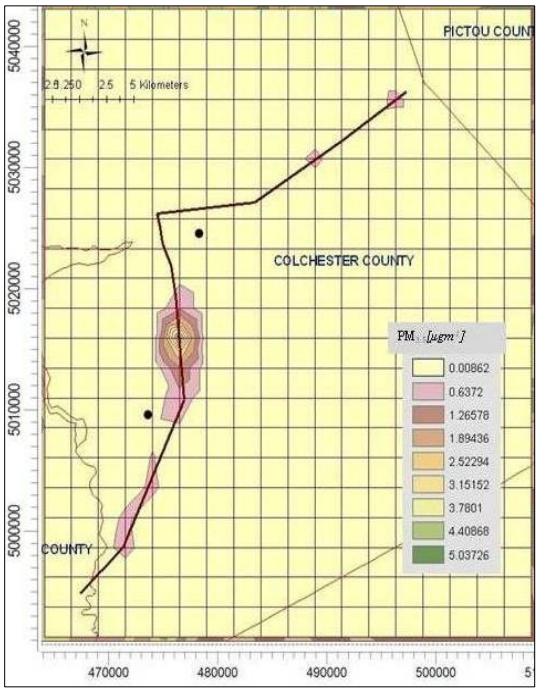

h. August

(Figures Cont'd)

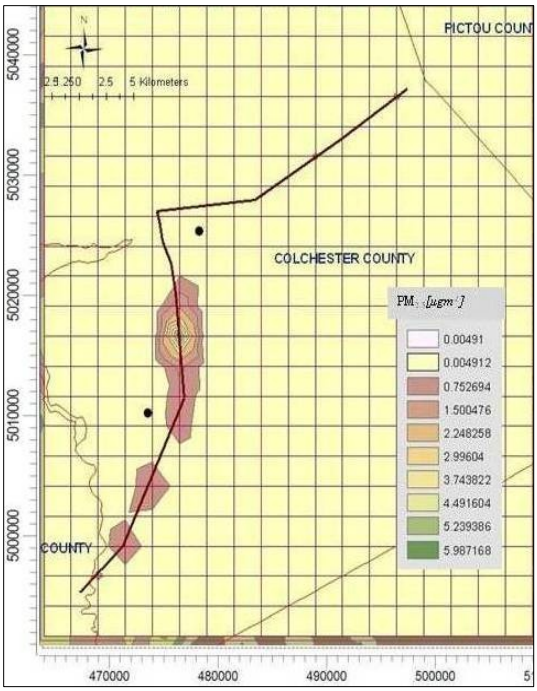

i. September

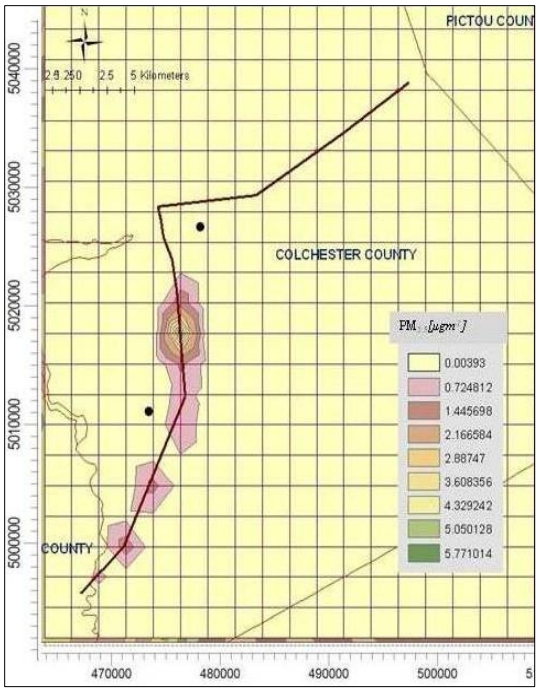

j. October

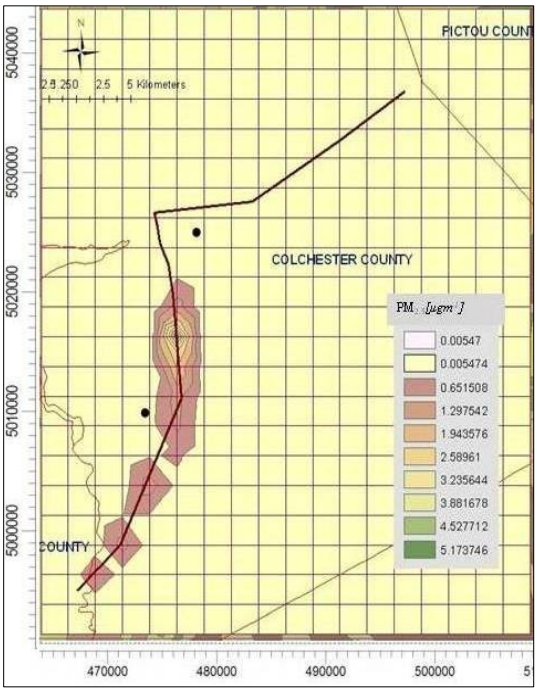

k. November

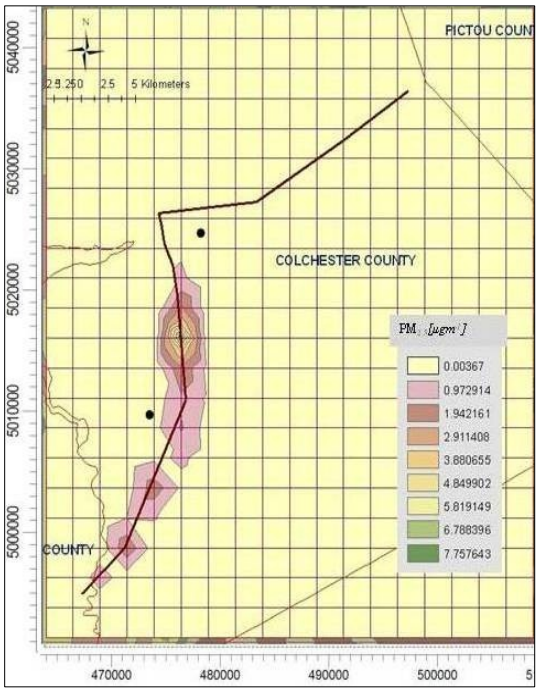

l. December

Table 18 Monthly MAX and MIN GLCs of NO_x, SO_2 and $PM_{2.5}$

Month	NO_x		SO_2		$PM_{2.5}$	
	Monthly Min *[$\mu g\ m^{-3}$]* UTM coordinate (m) Elevation (m)	Monthly Max *[$\mu g\ m^{-3}$]* UTM coordinate (m) Elevation (m)	Monthly Min *[$\mu g\ m^{-3}$]* UTM coordinate (m) Elevation (m)	Monthly Max *[$\mu g\ m^{-3}$]* UTM coordinate (m) Elevation (m)	Monthly Min *[$\mu g\ m^{-3}$]* UTM coordinate (m) Elevation (m)	Monthly Max *[$\mu g\ m^{-3}$]* UTM coordinate (m) Elevation (m)
Jan	0.017 (464162.3:5043268) 297.1	12.5 (476621.9:5015953) 53.4	0.017 (464162.3:5043268) 297.1	6.53 (476621.9:5015953) 53.4	0.003 (464162.3:5043268) 297.1	8.102 (476621.9:5015953) 53.4
Feb	0.018 (464162.3:5043268) 297.1	11.49 (476621.9:5015953) 53.4	0.016 (464162.3:5043268) 297.1	5.985 (476621.9:5015953) 53.4	0.004 (509016.8:5040785) NA	7.461 (476621.9:5015953) 53.4
Mar	0.011 (469146.1:5043268) 275	8.76 (476621.9:5015953) 53.4	0.01 (484097.6:4998570) 69.5	4.66 (476621.9:5015953) 53.4	0.002 (464162.3:5040785) 290	5.587 (476621.9:5015953) 53.4
Apr	0.017 (509016.8:5043268) NA	6.349 (476621.9:5015953) 53.4	0.013 (509016.8:5043268) NA	3.53 (476621.9:5015953) 53.4	0.005 (464162.3:5043268) 297.1	4.083 (476621.9:5015953) 53.4
May	0.027 (509016.8:5043268) NA	8.72 (476621.9:5015953) 53.4	0.02 (509016.8:5043268) NA	4.61 (476621.9:5015953) 53.4	0.006 (464162.3:5043268) 297.1	5.593 (476621.9:5015953) 53.4
June	0.2 (506524.9:5043268) NA	7.161 (476621.9:5015953) 53.4	0.015 (509016.8:5040785) NA	3.754 (476621.9:5015953) 53.4	0.005 (496557.3:5043268) 260.1	4.627 (476621.9:5015953) 53.4
July	0.018 (509016.8:4991121) NA	10.055 (476621.9:5015953) 53.4	0.013 (509016.8:4991121) NA	5.33 (476621.9:5015953) 53.4	0.008 (509016.8:4993604) NA	6.433 (476621.9:5015953) 53.4
Aug	0.023 (509016.8:4991121) NA	8.868 (476621.9:5015953) 53.4	0.017 (509016.8:4991121) NA	4.708 (476621.9:5015953) 53.4	0.009 (504033:5020919) 234.2	5.666 (476621.9:5015953) 53.4
Sep	0.026 (464162.3:5043268) 297.1	10.467 (476621.9:5015953) 53.4	0.022 (509016.8:5043268) NA	5.518 (476621.9:5015953) 53.4	0.005 (464162.3:5040785) 290	6.735 (476621.9:5015953) 53.4
Oct	0.02 (464162.3:5043268) 297.1	10.079 (476621.9:5015953) 53.4	0.02 (464162.3:5040785) 290	5.3 (476621.9:5015953) 53.4	0.004 (464162.3:5043268) 297.1	6.492 (476621.9:5015953) 53.4
Nov	0.028 (509016.8:5040785) NA	9.01 (476621.9:5015953) 53.4	0.021 (509016.8:5043268) NA	4.727 (476621.9:5015953) 53.4	0.005 (464162.3:5043268) 297.1	5.82 (476621.9:5015953) 53.4
Dec	0.016 (464162.3:5043268) 297.1	13.44 (476621.9:5015953) 53.4	0.016 (464162.3:5043268) 297.1	6.99 (476621.9:5015953) 53.4	0.004 (464162.3:5043268) 297.1	8.727 (476621.9:5015953) 53.4

4.3.3.3 Hourly Averaging of NO_x, SO_2 and $PM_{2.5}$

Figures 36 through 38 show the hourly predicted NO_x, SO_2 and $PM_{2.5}$ concentration contours respectively in TRR domain. As seen from Figures 36 through 38 the dispersion patterns of NO_x and $PM_{2.5}$ were similar with the monthly and annual patterns, whereas SO_2 dispersion pattern show an existence of high surface concentrations towards North East of the domain. This could be the result of high amount of SO_2 being released from the Truro paper mill. The minimum and maximum hourly predicted NO_x, SO_2 and $PM_{2.5}$ concentrations at a specific receptor location with elevation are given in Table 19. It is seen from the Table 19 that the highest concentration receptor remained same as annual and monthly averaging for all three pollutants.

Figures 36a-e Hourly GLCs of NO_x due to point and highway emission sources

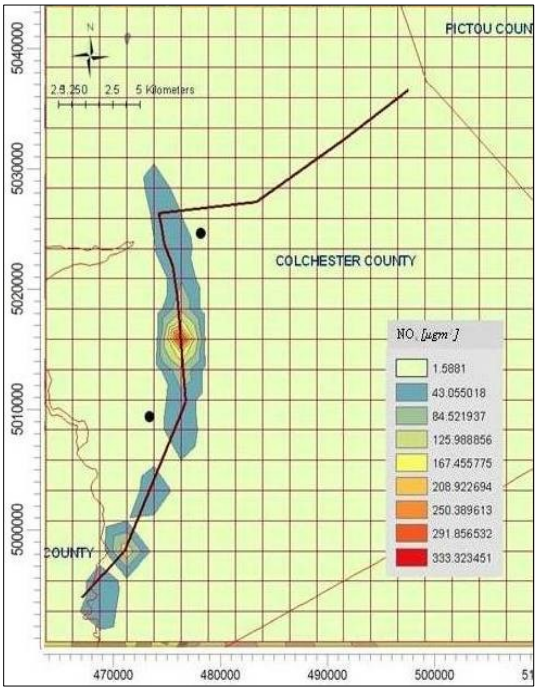

a. 1 hour

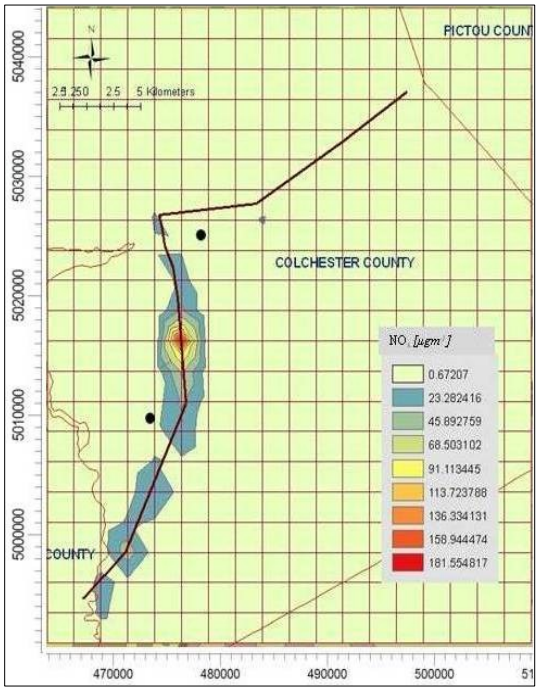

b. 3 hour

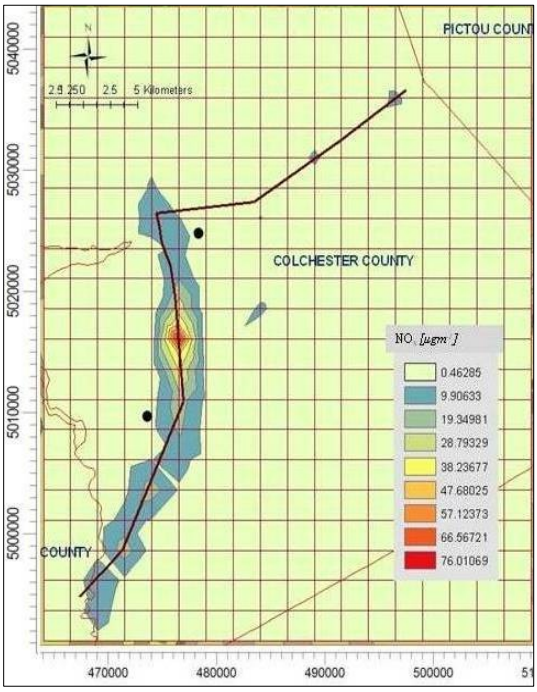

c. 8 hour

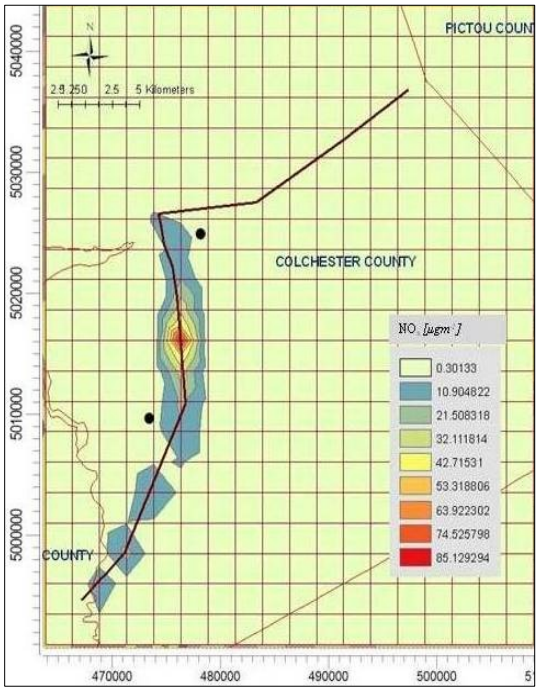

d. 12 hour

(Figure Cont'd)

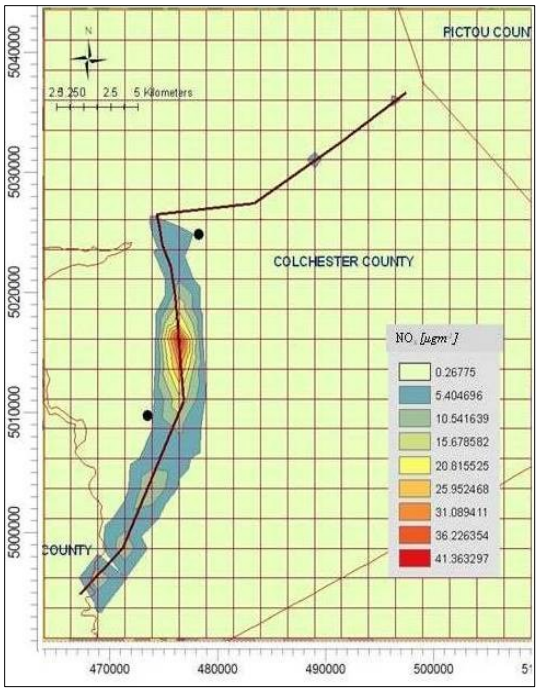
PICTOU COUN
COLCHESTER COUNTY
COUNTY
2.5 0 2.5 5 Kilometers
NO2 [µgm-3]
0.26775
5.404696
10.541639
15.678582
20.815525
25.952468
31.089411
36.226354
41.363297
5040000
5030000
5020000
5010000
5000000
470000
480000
490000
500000

e. 24 hour

Figures 37a-e Hourly GLCs of SO_2 due to point and highway emission sources

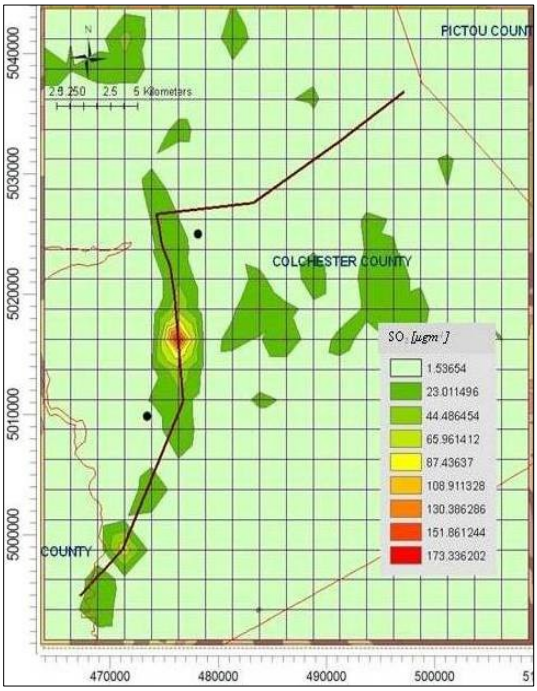

a. 1 hour

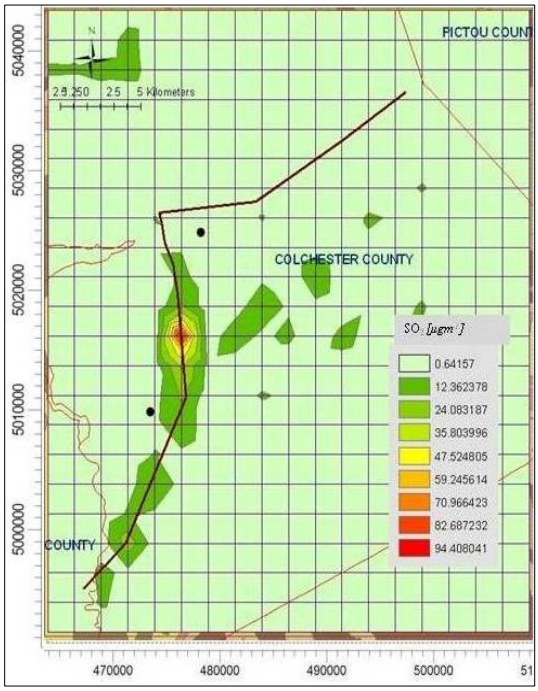

b. 3 hour

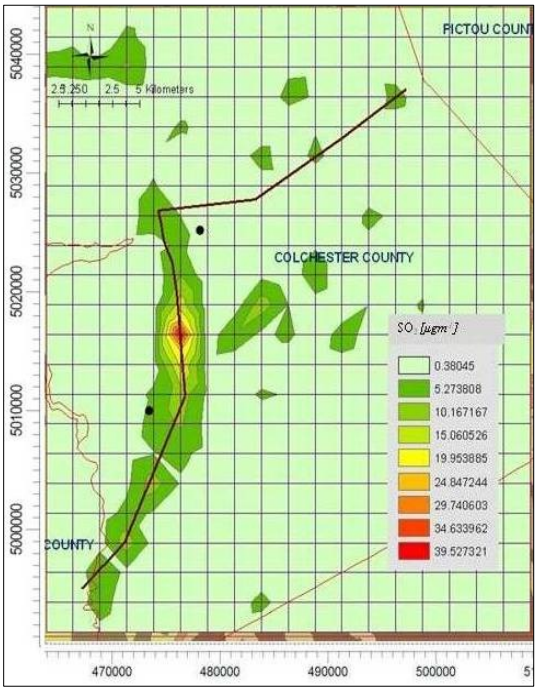

c. 8 hour

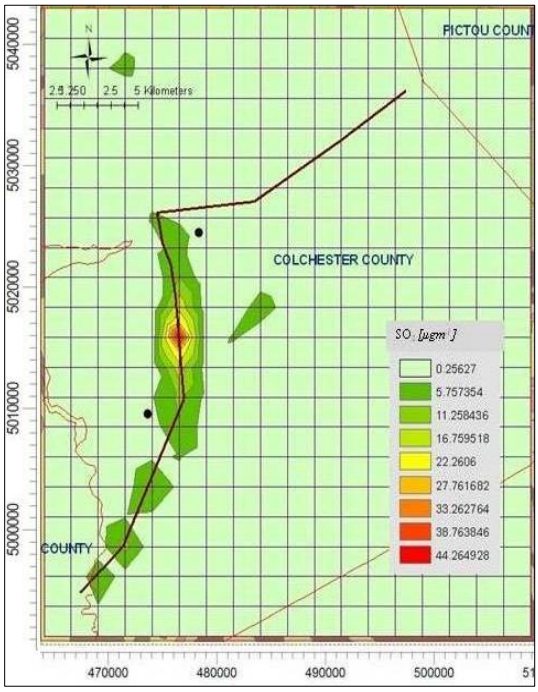

d. 12 hour

(Figure Cont'd)

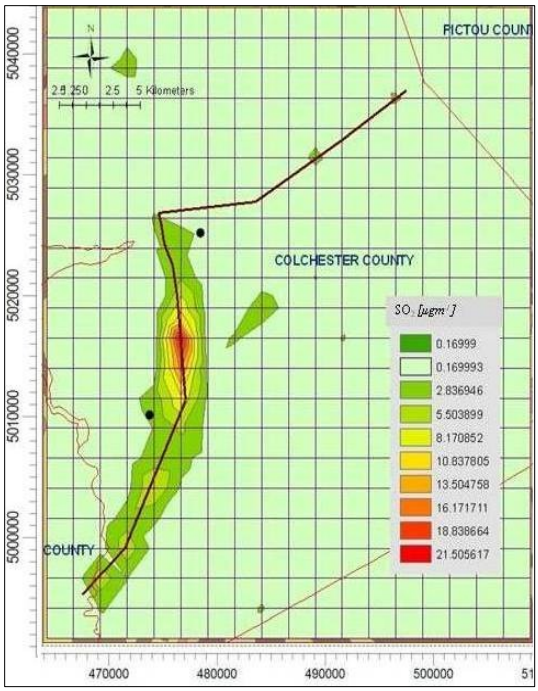
N
2.5 2.5 0 2.5 5 Kilometers
PICTOU COUNTY
COLCHESTER COUNTY
COUNTY
SO2 [µgm-3]
0.16999
0.169993
2.836946
5.503899
8.170852
10.837805
13.504758
16.171711
18.838664
21.505617
5040000
5030000
5020000
5010000
5000000
470000
480000
490000
500000

e. 24 hour

Figures 38a-l Hourly GLCs of $PM_{2.5}$ due to point and highway emission sources

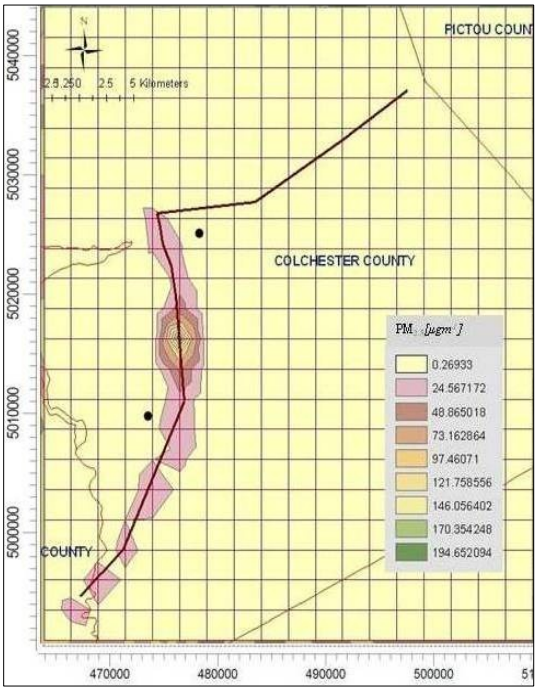

a. 1 hour

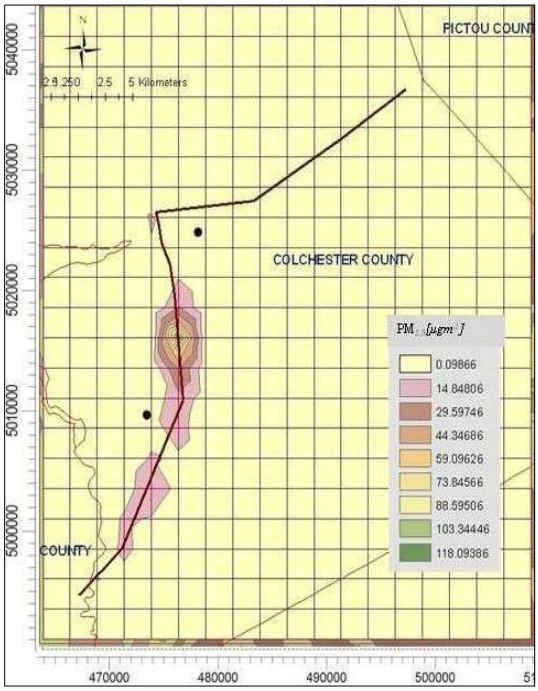

b. 3 hour

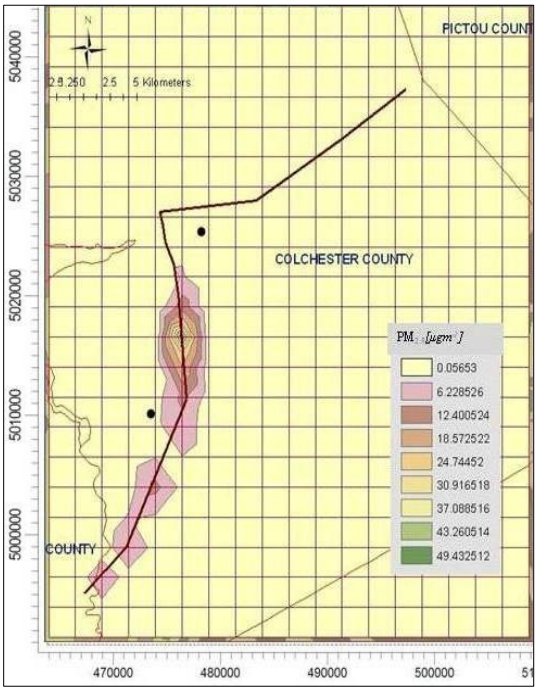

c. 8 hour

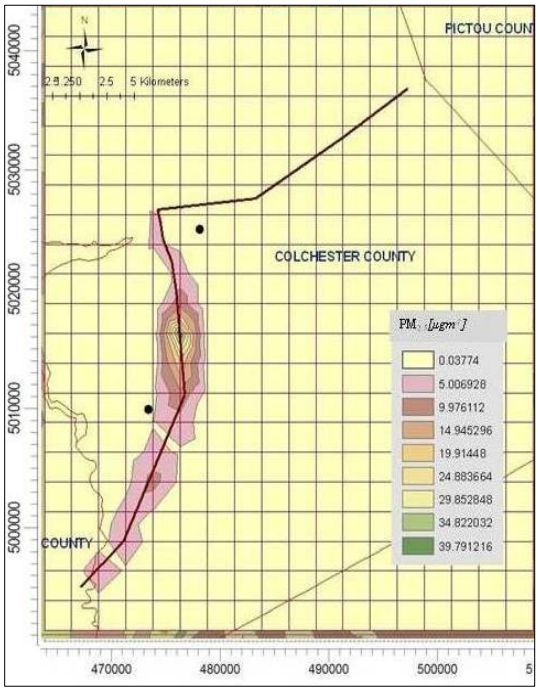

d. 12 hour

(Figure Cont'd)

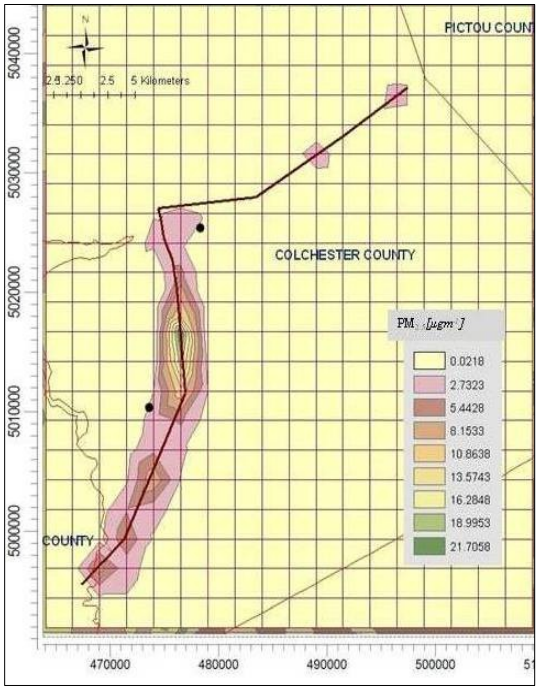

e. 24 hour

Table 19 Hourly MAX and MIN GLCs of NO_x, SO_2 and $PM_{2.5}$

	NO_x		SO_2		$PM_{2.5}$	
Hour	Hourly Min *[µg m^{-3}]* UTM coordinate(m) Elevation(m)	Hourly Max *[µg m^{-3}]* UTM coordinate(m) Elevation(m)	Hourly Min *[µg m^{-3}]* UTM coordinate(m) Elevation(m)	Hourly Max *[µg m^{-3}]* UTM coordinate(m) Elevation(m)	Hourly Min *[µg m^{-3}]* UTM coordinate(m) Elevation(m)	Hourly Max *[µg m^{-3}]* UTM coordinate(m) Elevation(m)
1	1.588 (509016.8:4993604) NA	374.79 (476621.9:5015953) 53.4	1.537 (509016.8:5035818) NA	194.81 (476621.9:5015953) 53.4	0.269 (464162.3:5043268) 297.1	218.94 (476621.9:5015953) 53.4
3	0.672 (509016.8:4993604) NA	204.165 (476621.9:5015953) 53.4	0.642 (509016.8:4993604) NA	106.13 (476621.9:5015953) 53.4	0.099 (464162.3:5043268) 297.1	132.843 (476621.9:5015953) 53.4
8	0.463 (509016.8:5030852) NA	85.454 (476621.9:5015953) 53.4	0.38 (509016.8:5030852) NA	44.42 (476621.9:5015953) 53.4	0.057 (464162.3:5043268) 297.1	55.605 (476621.9:5015953) 53.4
12	0.301 (509017.8:4991121) NA	95.73 (476621.9:5015953) 53.4	0.256 (509016.8:4993604) NA	49.76 (476621.9:5015953) 53.4	0.038 (464162.3:5043268) 297.1	44.76 (476621.9:5015953) 53.4
24	0.268 (509016.8:4993604) NA	46.5 (476621.9:5015953) 53.4	0.17 (509016.8:4993604) NA	24.17 (476621.9:5015953) 53.4	0.022 (464162.3:5043268) 297.1	24.416 (476621.9:5015953) 53.4

4.3.4 Modeling Study in PRTHWKS domain

Emission of NO_x and $PM_{2.5}$ from New Page paper industry, 35.54 km and 17.91 km section length of highways 104 and 105 respectively were used for conducting the dispersion simulation studies in PRTHWKS domain during 2005.

4.3.4.1 Annual averaging of NO_x and $PM_{2.5}$

AERMOD predicted GLC contour maps of NO_x and $PM_{2.5}$ in PRTHWKS domain during annual averaging period are shown in Figures 39 and 40. As seen from the Figures 39 and 40, the highest annual average NO_x and $PM_{2.5}$ concentration gradients were found at 13.5 km North West of the New Page paper industry by the east side of highway 104. With reference to the above figures, highways contributed lager amount of total $PM_{2.5}$ compared to the point sources and the dispersion of pollutants were dominated by the resultant wind vector at 248^o. High GLC gradients were observed at north east of the New Page Paper Mill, situated at downwind of the plant. From Table 20 it is seen that the highest GLC receptor was same for both pollutants. The minimum and maximum annual average predicted NO_x concentrations were 0.003 $\mu g\ m^{-3}$ located at 609908.3m: 5024716m elevation 124 m and 0.748 $\mu g\ m^{-3}$ located at 614638.56m: 5059019.5m, elevation 66.6m respectively. The minimum and maximum annual average $PM_{2.5}$ concentrations in PRTHWKS domain were 0.002 $\mu g\ m^{-3}$ found at 609908.3m: 5027166m elevation 162.1 m and 0.594 $\mu g\ m^{-3}$ at 614638.56m: 5059019.5m, elevation 66.6 m respectively.

Figure 39 Annual GLCs of NO_x due to point and highway emission sources

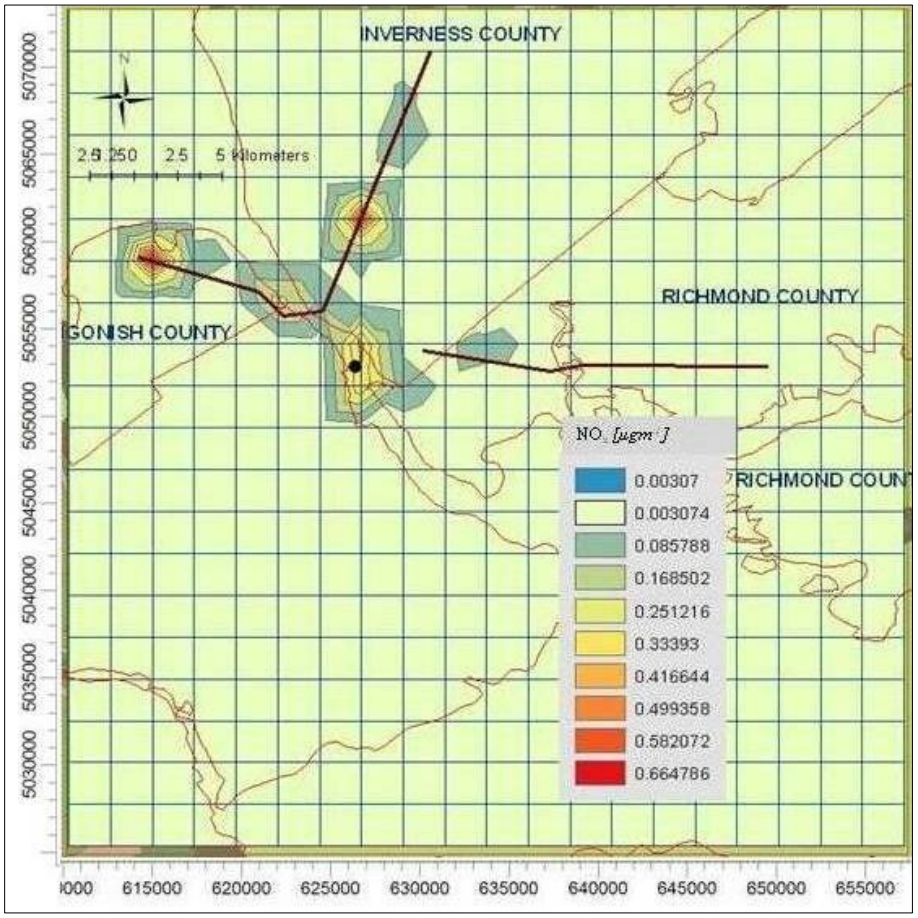

Figure 40 Annual GLCs of $PM_{2.5}$ due to due to point and highway emission sources

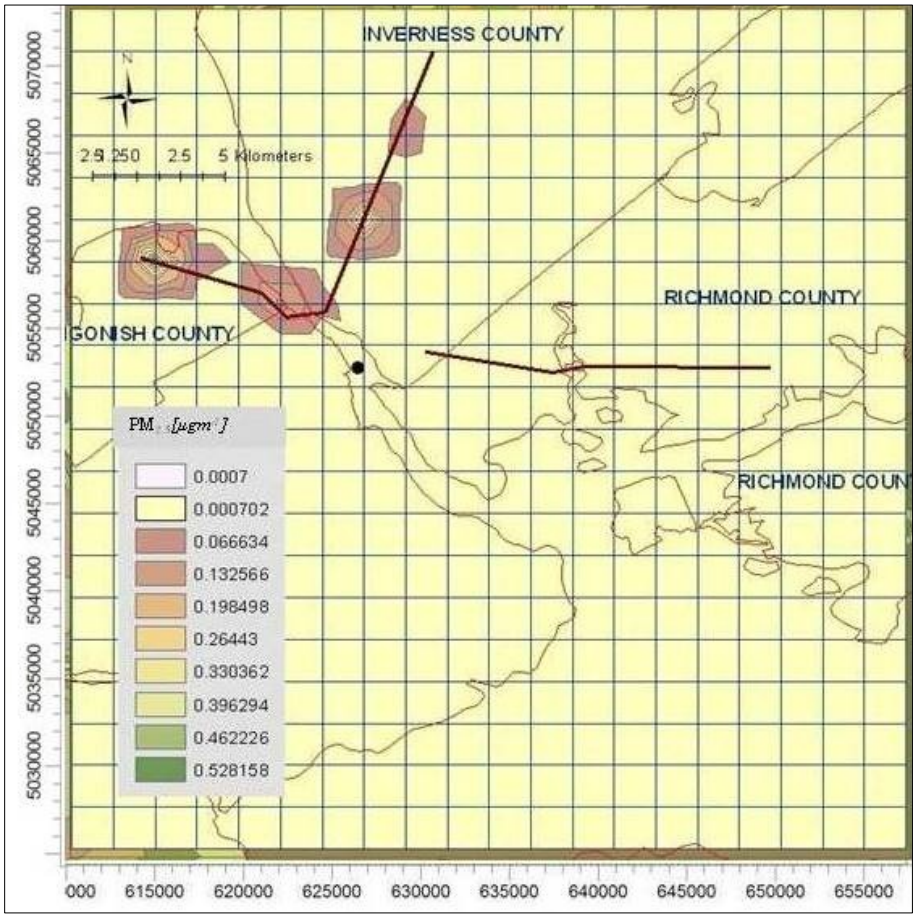

Table 20 Annual MAX and MIN GLCs of NO_x, and $PM_{2.5}$

Pollutant	Annual Min *[µg m^{-3}]* UTM coordinate(m) Elevation(m)	Annual Max *[µg m^{-3}]* UTM coordinate(m) Elevation(m)
NO_x	0.003 (609908.3:5024716) 124	0.748 (614638.56:5059019.5) 66.6
$PM_{2.5}$	0.001 (609908.3:5027166) 162.1	0.594 (614638.56:5059019.5) 66.6

4.3.4.2 Monthly averaging of NO_x and $PM_{2.5}$

Figures 41 and 42 show the monthly GLC gradient maps of NO_x and $PM_{2.5}$ in PRTHWKS domain. As seen from the figures, dispersion patterns of both the pollutants were similar throughout the year. Monthly averaging shows GLCs of pollutants were high in both winter and summer months. As seen from Table 21, the highest GLC receptor remained unchanged throughout the year for both pollutants. This was expected as the highways contributed more amount of total emission than the chimney stacks. The minimum and maximum monthly predicted NO_x concentrations were 0.973µg m^{-3} (May) at coordinates 614638.56m: 5059019.5m, elevation 66.6m and 2.166 µg m^{-3} (November) at coordinates 614638.56m: 5059019.5m, elevation 66.6m respectively. The minimum and maximum monthly predicted $PM_{2.5}$ concentrations were 0.862 µg m^{-3} (May) at coordinates 614638.56m: 5059019.5m, elevation 66.6 m and 1.938 µg m^{-3} (November) at coordinates 614638.56m: 5059019.5m, elevation 66.6m respectively. Dispersion patterns also indicated an existence of stable atmospheric condition in the domain.

Figures 41a-l Monthly GLCs of NO_x due to point and highway emission sources

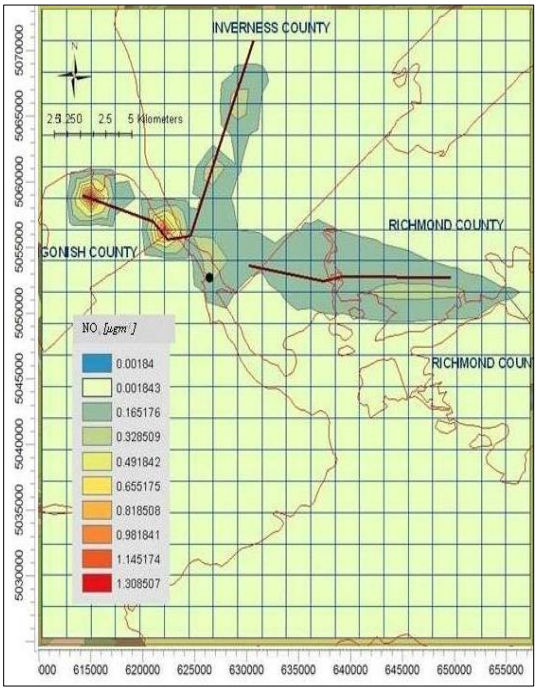

a. January

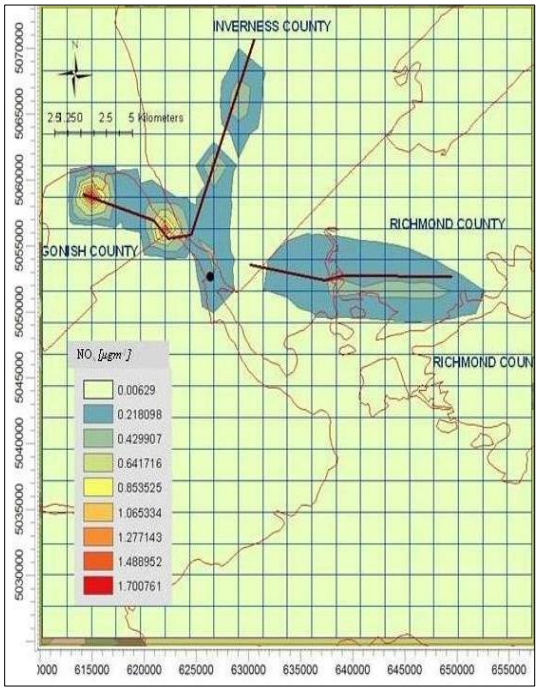

b. February

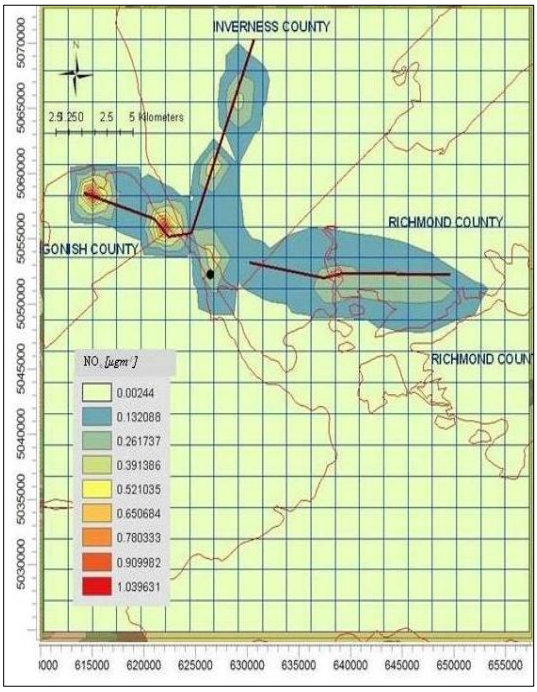

c. March

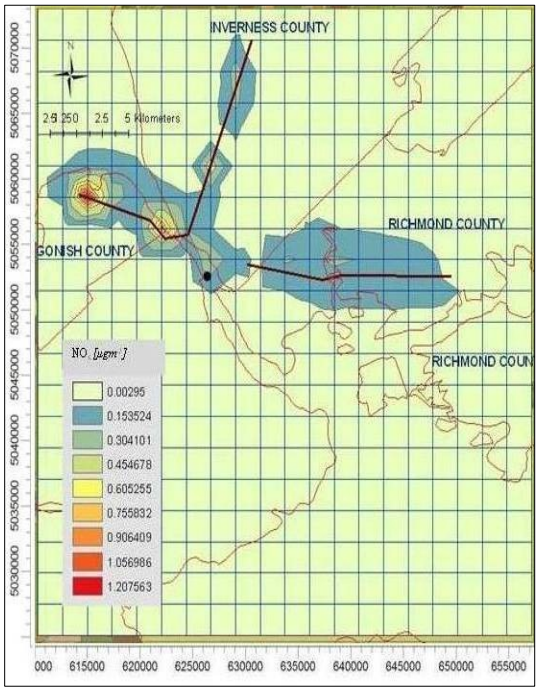

d. April

(Figures Cont'd)

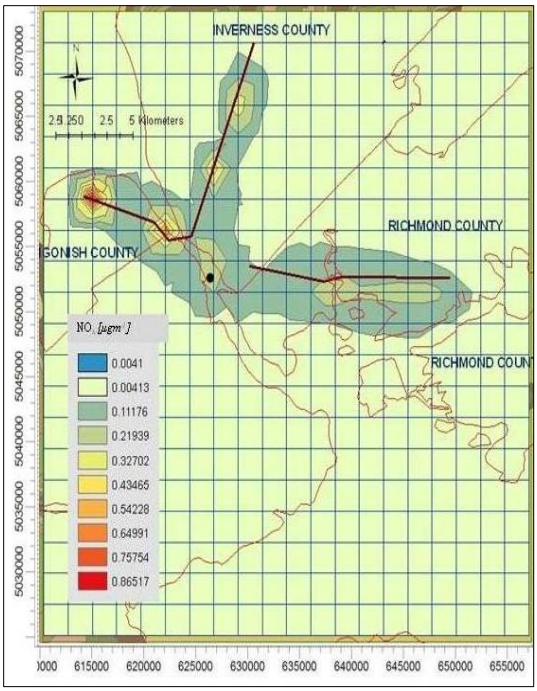

e. May

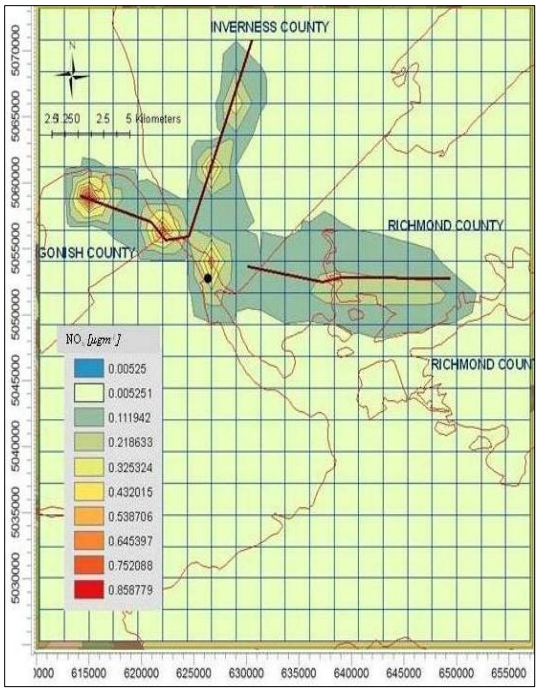

f. June

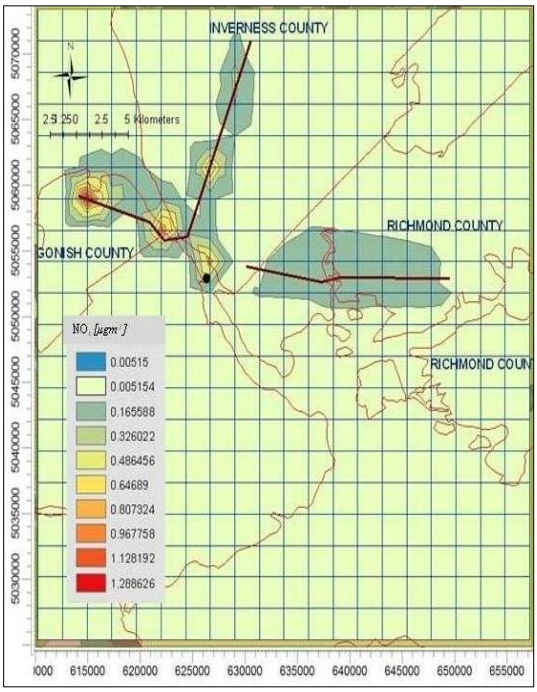

g. July

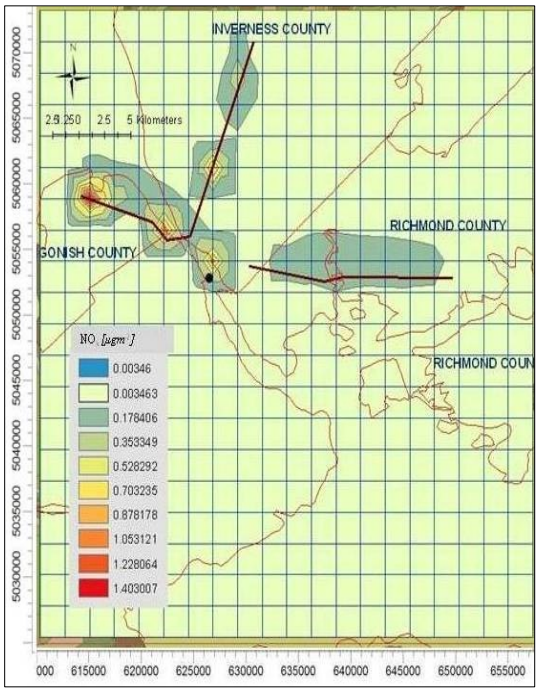

h. August

(Figures Cont'd)

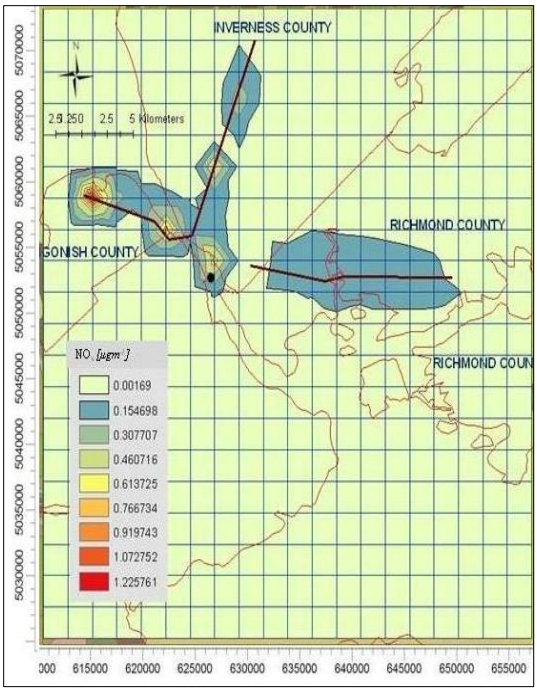

i. September

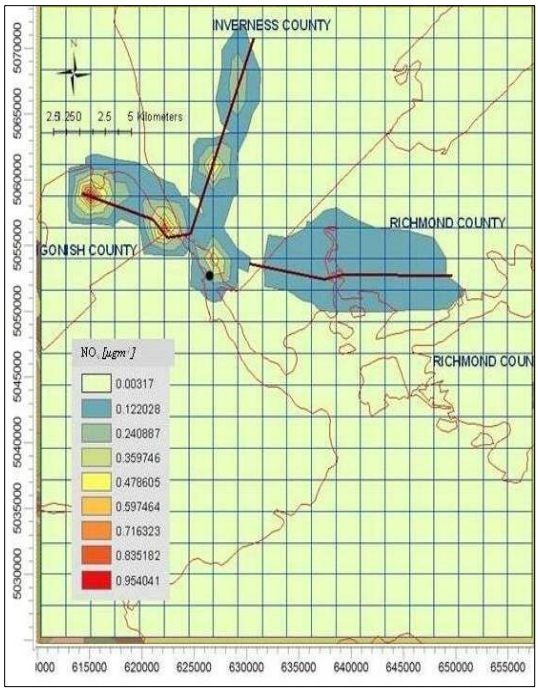

j. October

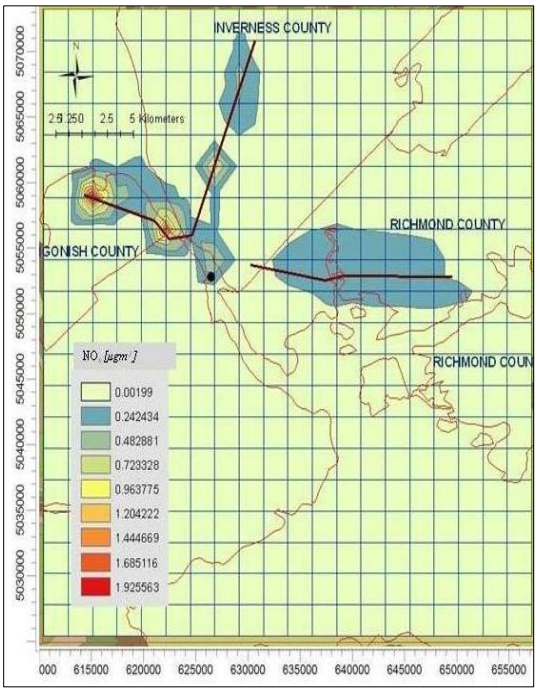

k. November

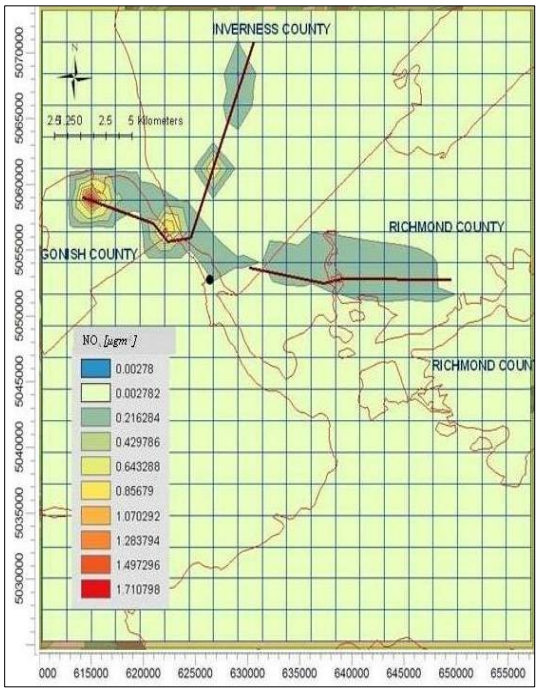

l. December

Figures 42a-l Monthly GLCs of $PM_{2.5}$ due to point and highway emission sources

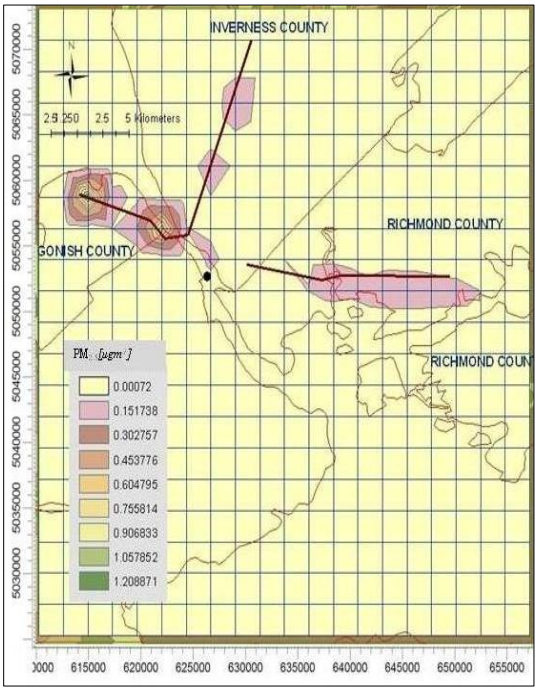

a. January

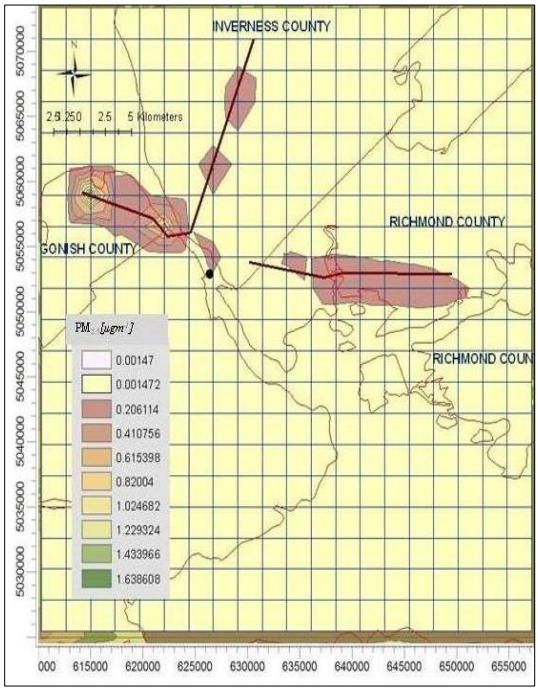

b. February

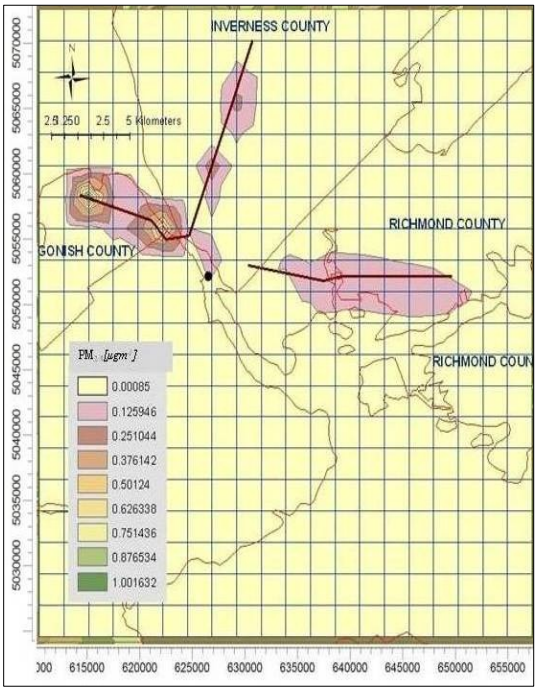

c. March

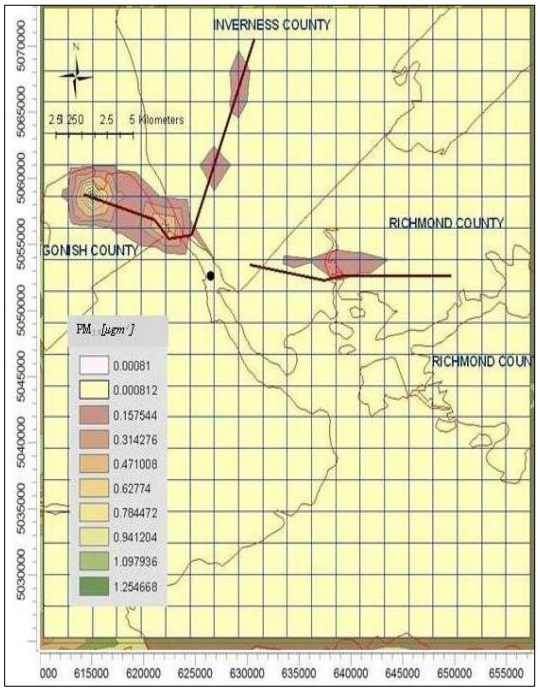

d. April

(Figures Cont'd)

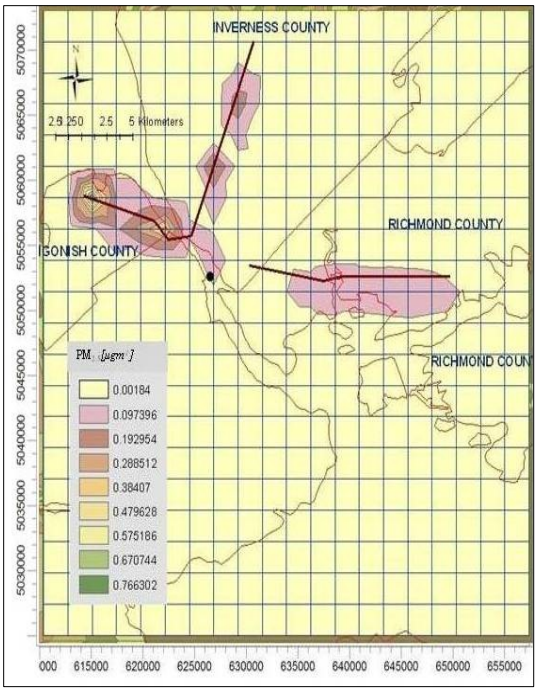

e. May

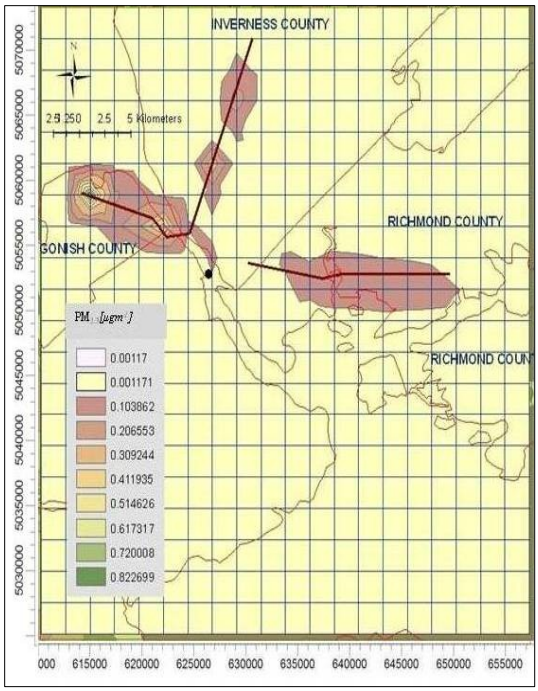

f. June

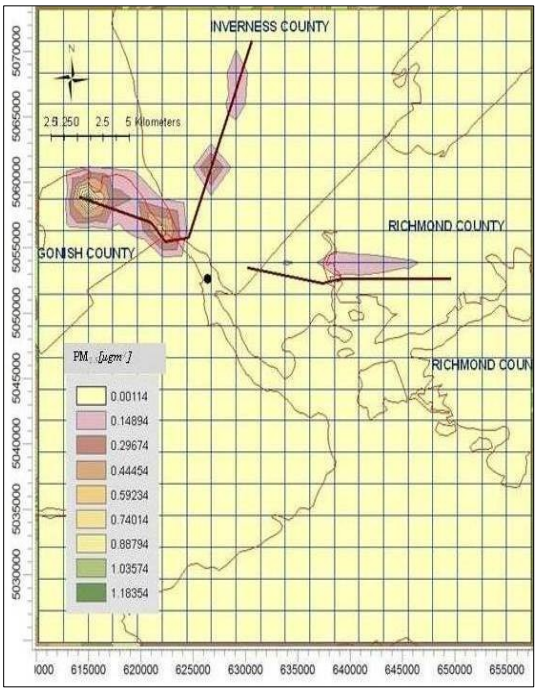

g. July

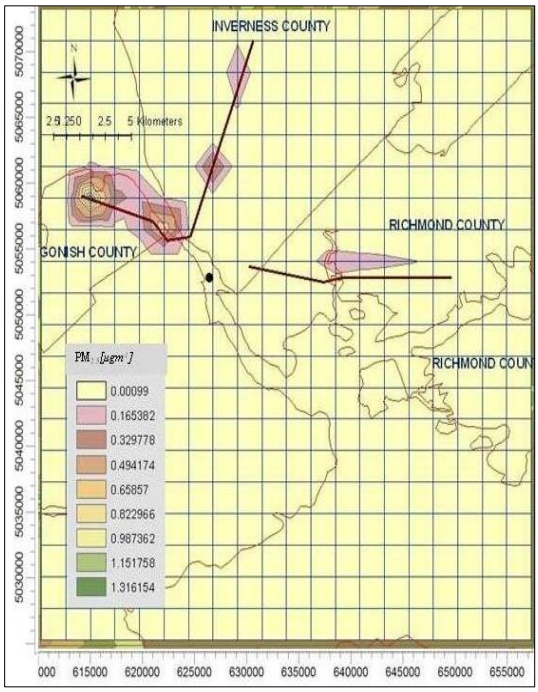

h. August

(Figures Cont'd)

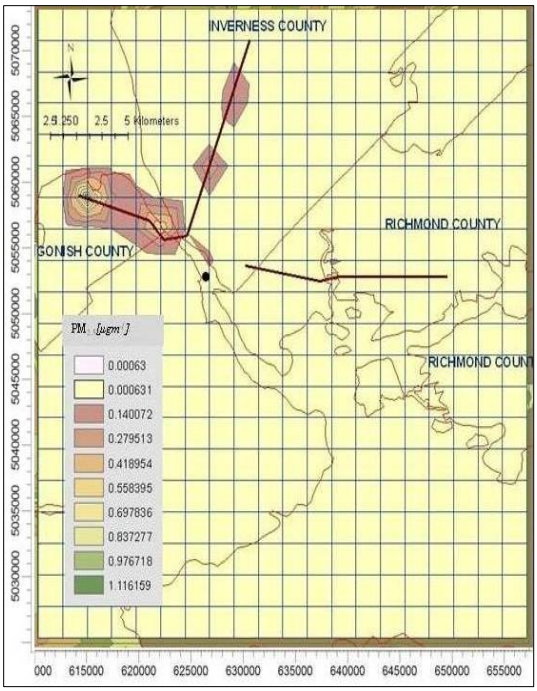

i. September

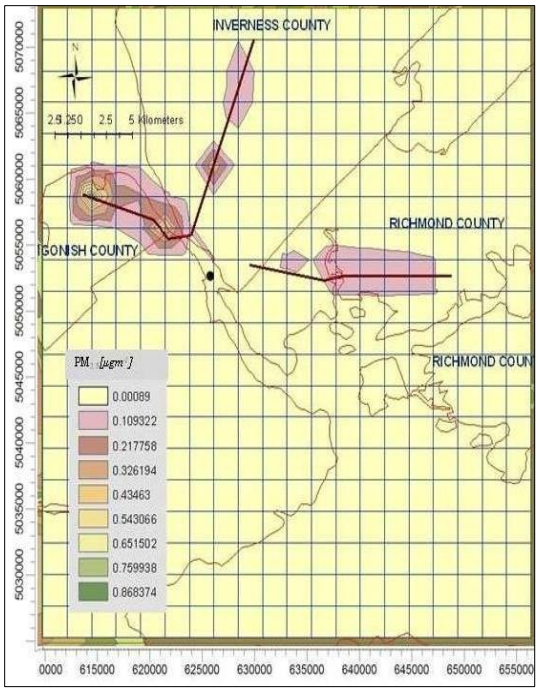

j. October

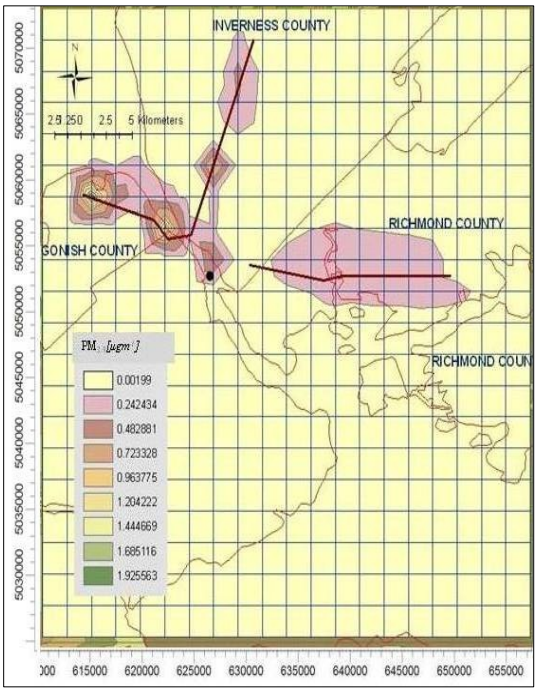

k. November

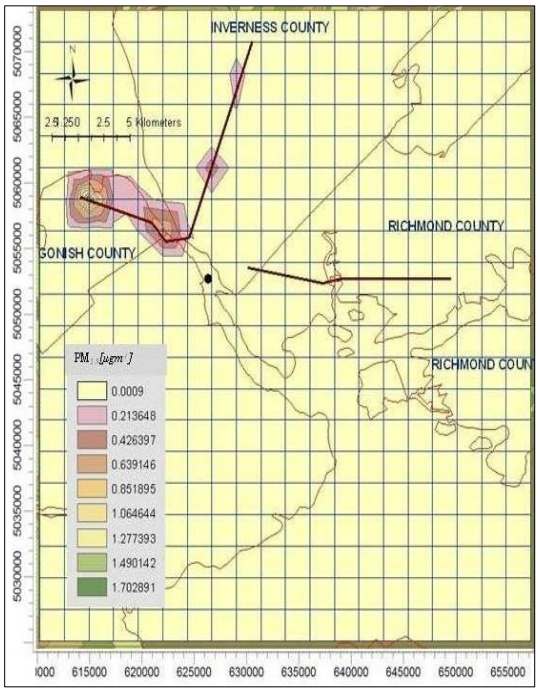

l. December

Table 21 Monthly MAX and MIN GLCs of NO_x and $PM_{2.5}$

	NO_x		$PM_{2.5}$	
Month	Monthly Min *[$\mu g\ m^{-3}$]* UTM coordinate (m) Elevation (m)	Monthly Max *[$\mu g\ m^{-3}$]* UTM coordinate (m) Elevation (m)	Monthly Min *[$\mu g\ m^{-3}$]* UTM coordinate (m) Elevation (m)	Monthly Max *[$\mu g\ m^{-3}$]* UTM coordinate (m) Elevation (m)
Jan	0.002 (609908.3:5029617) 172.8	1.472 (614638.56:5059019.5) 66.6	0.001 (609908.3:5032067) 167.4	1.36 (614638.56:5059019.5) 66.6
Feb	0.006 (609908.3:5029617) 172.8	1.913 (614638.56:5059019.5) 66.6	0.001 (609083.1:5027166) 162.1	1.843 (614638.56:5059019.5) 66.6
Mar	0.002 (609908.3:5032067) 167.4	1.169 (614638.56:5059019.5) 66.6	0.001 (609908.3:5039418) 169.7	1.127 (614638.56:5059019.5) 66.6
Apr	0.003 (612273.4:5032067) 170.7	1.358 (614638.56:5059019.5) 66.6	0.001 (609083.1:5027166) 162.1	1.411 (614638.56:5059019.5) 66.6
May	0.004 (643020.3:5071271) 221.1	0.973 (614638.56:5059019.5) 66.6	0.002 (609908.3:5029617) 172.8	0.862 (614638.56:5059019.5) 66.6
June	0.005 (612273.4:5024716) 109	0.965 (614638.56:5059019.5) 66.6	0.001 (609908.3:5029617) 172.8	0.925 (614638.56:5059019.5) 66.6
July	0.005 (612273.4:5024716) 109	1.449 (614638.56:5059019.5) 66.6	0.001 (609908.3:5029617) 172.8	1.331 (614638.56:5059019.5) 66.6
Aug	0.003 (609083.1:5027166) 162.1	1.578 (614638.56:5059019.5) 66.6	0.001 (609083.1:5027166) 162.1	1.481 (614638.56:5059019.5) 66.6
Sep	0.002 (609908.3:5024716) 124	1.379 (614638.56:5059019.5) 66.6	0.001 (609908.3:5032067) 167.4	1.256 (614638.56:5059019.5) 66.6
Oct	0.003 (609083.1:5027166) 162.1	1.073 (614638.56:5059019.5) 66.6	0.001 (609908.3:5029617) 172.8	0.977 (614638.56:5059019.5) 66.6
Nov	0.002 (612273.4:5027166) 160.7	2.166 (614638.56:5059019.5) 66.6	0.001 (612273.4:5032067) 170.7	1.938 (614638.56:5059019.5) 66.6
Dec	0.003 (609083.1:5027166) 162.1	1.924 (614638.56:5059019.5) 66.6	0.001 (612273.4:5027166) 160.7	1.916 (614638.56:5059019.5) 66.6

4.3.4.3 Hourly Averaging of NO_x and $PM_{2.5}$

Figures 43 and 44 show hourly predicted GLCs of NO_x and $PM_{2.5}$ respectively in PRTHWKS domain. With reference to the Figures it is seen that the point sources contributed larger amount of ground level NO_x concentrations. Highest ground level NO_x concentration receptor during 1-hr and 3hr averaging period was within 5 km radius of the release point. Also it is observed that the highest GLC was found at an elevation of 116.7 m which is expected as per the USEPA AERMOD guide. The highways were the larger contributor of $PM_{2.5}$ than the point emission source therefore; the dispersion pattern was similar throughout the day. The minimum and maximum hourly predicted NO_x and $PM_{2.5}$ concentrations at specific receptor locations with elevations are given in Table 22. With reference to the table it is seen that the highest GLC of NO_x receptor remained unchanged throughout the day.

Figures 43a-e Hourly GLCs of NO_x due to point and highway emission sources

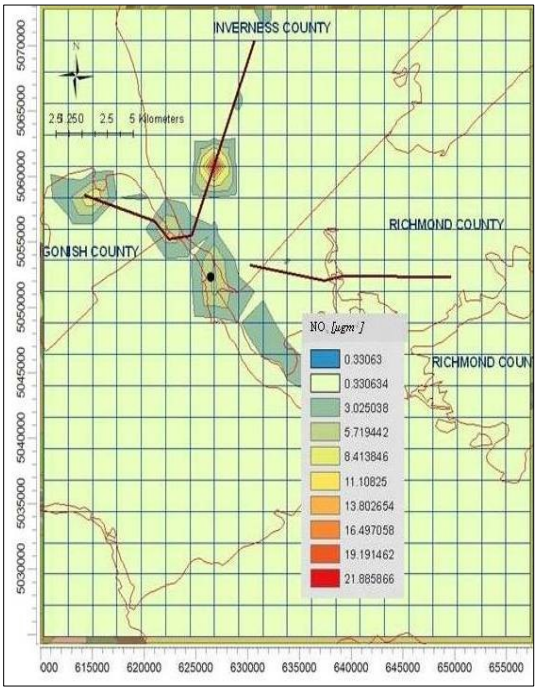

a. 1 hour

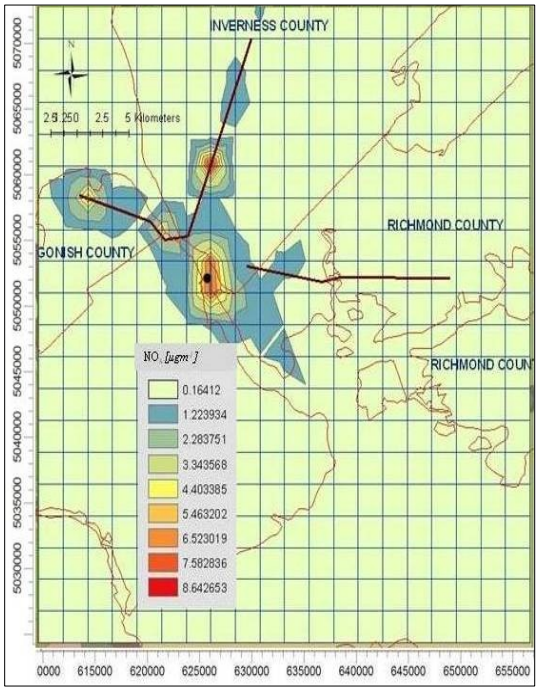

b. 3 hour

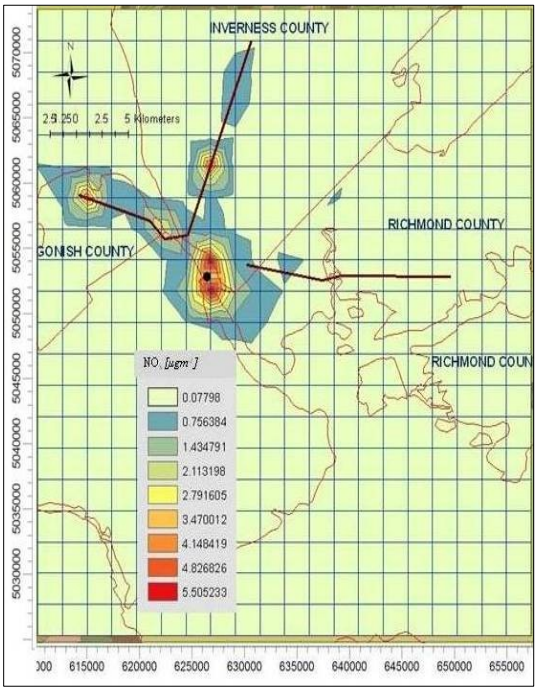

c. 8 hour

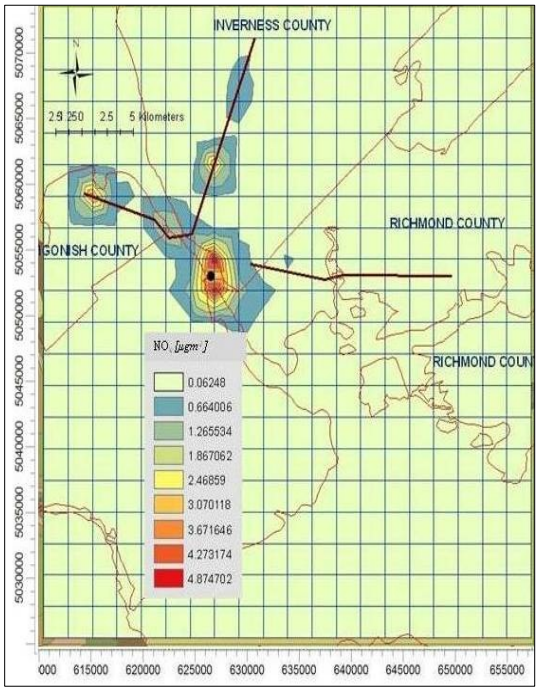

d. 12 hour

(Figure Cont'd)

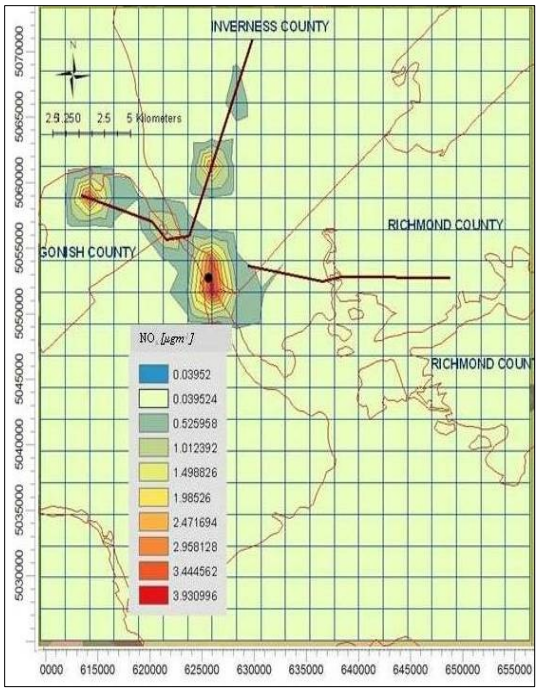
INVERNESS COUNTY
RICHMOND COUNTY
GONISH COUNTY
RICHMOND COUNT
N
2.5 0 2.5 5 Kilometers
NO, [µgm³]
0.03952
0.039524
0.525958
1.012392
1.498826
1.98526
2.471694
2.958128
3.444562
3.930996
5070000
5065000
5060000
5055000
5050000
5045000
5040000
5035000
5030000
0000
615000
620000
625000
630000
635000
640000
645000
650000
655000

e. 24 hour

Figures 44a-e Hourly GLCs of $PM_{2.5}$ due to point and highway emission sources

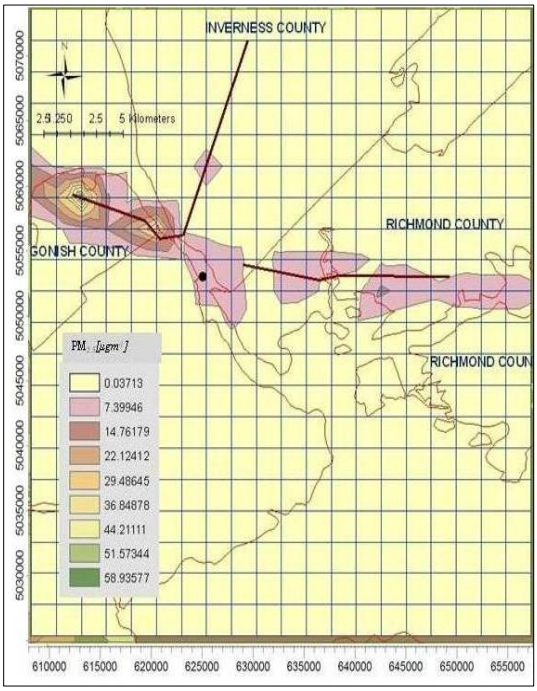

a. 1 hour

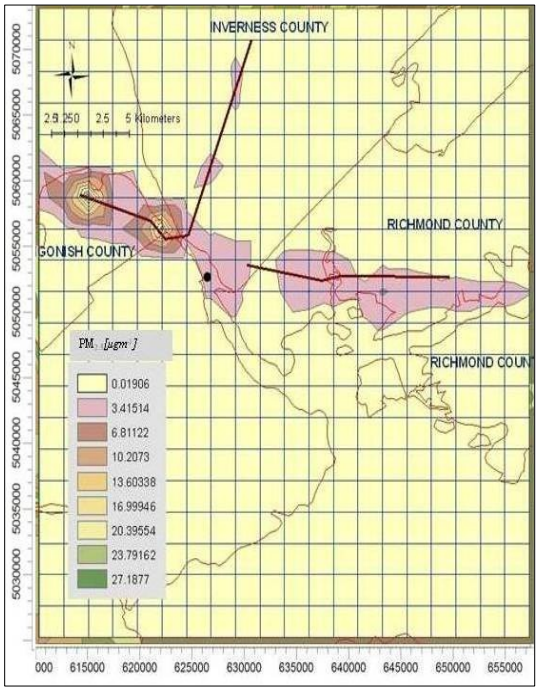

b. 3 hour

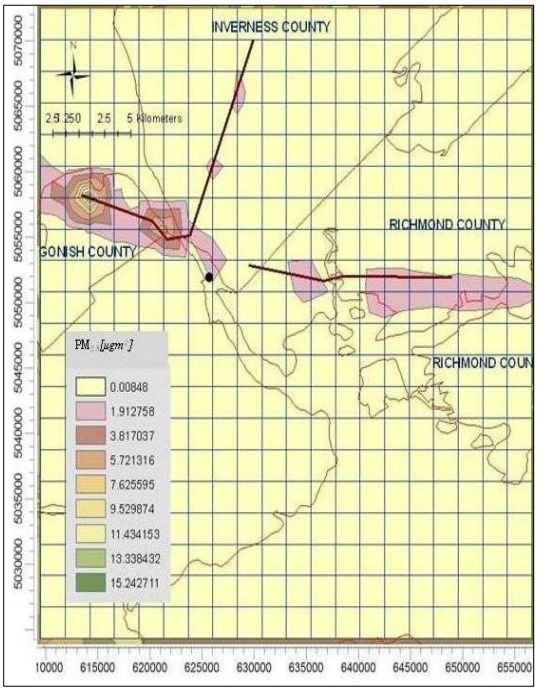

c. 8 hour

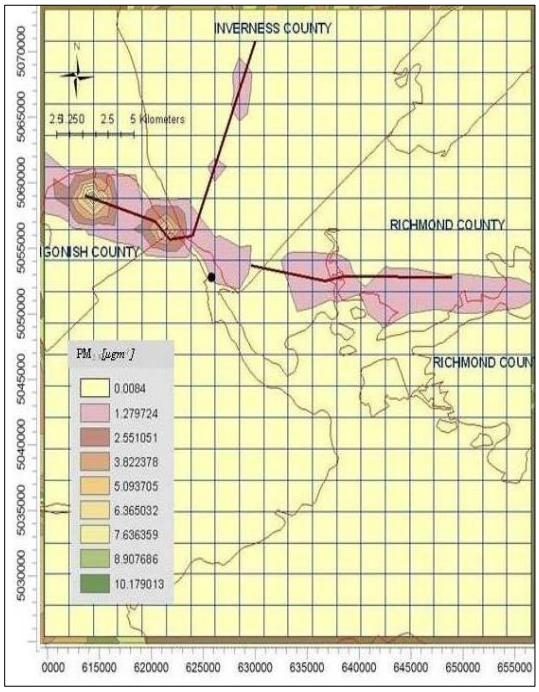

d. 12 hour

(Figure Cont'd)

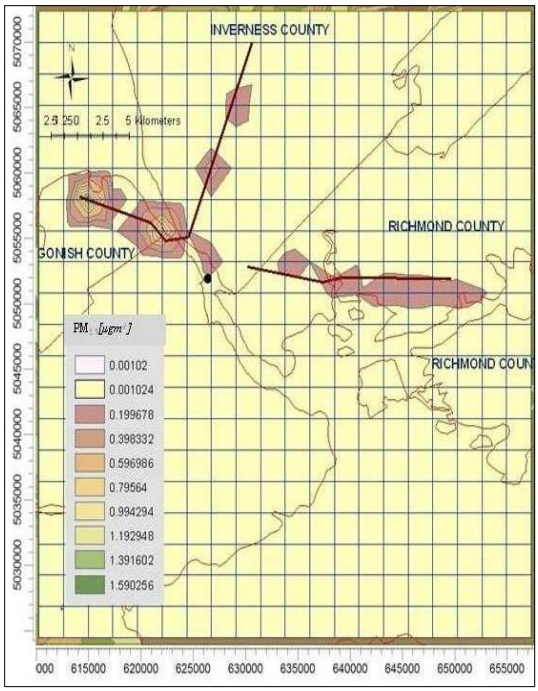

e. 24 hour

Table 22 Hourly MAX and MIN GLCs of NO_x and $PM_{2.5}$

	NO_x		$PM_{2.5}$	
Hour	Hourly Min $[\mu g\ m^{-3}]$ UTM coordinate (m) Elevation (m)	Hourly Max $[\mu g\ m^{-3}]$ UTM coordinate (m) Elevation (m)	Hourly Min $[\mu g\ m^{-3}]$ UTM coordinate (m) Elevation (m)	Hourly Max $[\mu g\ m^{-3}]$ UTM coordinate (m) Elevation (m)
1	0.331 (609908.3:5024716) 124	24.58 (626464.31:5061470) 116.7	0.037 (619368.9:5024716) 36	66.298 (614638.56:5059019.5) 66.6
3	0.164 (609908.3:5024716) 124	9.702 (626464.31:5061470) 116.7	0.019 (614638.6:5041868) 154.2	30.584 (614638.56:5059019.5) 66.6
8	0.078 (609908.3:5024716) 124	6.184 (626464.31:5051669) NA	0.008 (614638.6:5041868) 154.2	17.147 (614638.56:5059019.5) 66.6
12	0.062 (633559.7:5034517) 10.8	5.476 (626464.31:5054119) NA	0.008 (619368.9:5024716) 36	11.45 (614638.56:5059019.5) 66.6
24	0.04 (633559.7:5034517) 10.8	4.417 (626464.31:5051669) NA	0.001 (612273.4:5027166) 160.7	1.798 (614638.56:5059019.5) 66.6

4.3.4.5 SO_2 modeling study in PRTHWKS domain

Emission of SO_2 from New Page paper industry, 35.54 km and 17.91 km section length of highways 104 and 105 respectively were used for conducting the simulation studies in PRTHWKS domain during 2004.

4.3.4.5.1 Annual averaging of SO_2

Dispersion map of surface SO_2 concentration contours in the PRTHWKS domain is presented in Figure 45. It can be seen from the figure that, enhanced SO_2 concentration gradients were found at the North East of the New Page Paper Mill, situated downwind of the plant. The minimum and maximum SO_2 concentration values are seen at 609908.3m: 5024716m, elevation 124m and 626464.31m: 5054119m, elevation NA respectively.

Figure 45 Annual GLCs of SO_2 due to due to point and highway emission sources

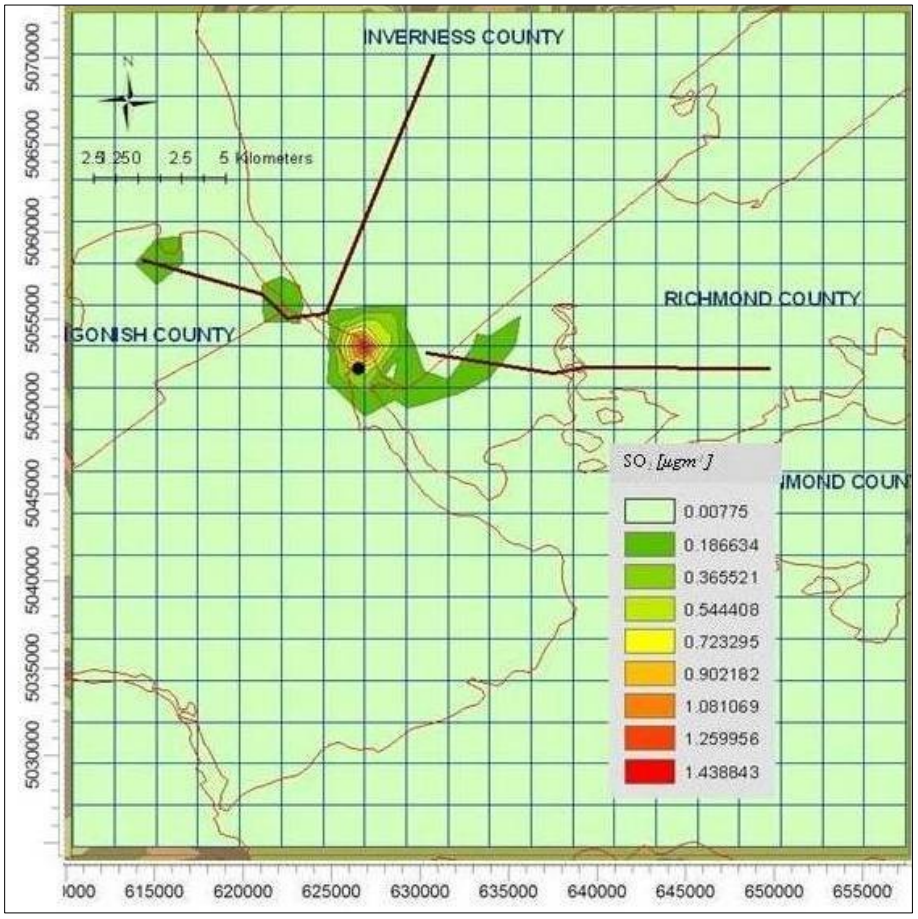

4.3.4.5.2 Monthly averaging of SO_2

Figure 46 shows monthly GLC contour maps of SO_2 in PRTHWKS. Monthly averaging shows GLCs of SO_2 were high in the summer. This phenomenon could be a result of ambient temperature rise during summer months. The GLC was found at downwind of the point emission source. As seen from Table 23, the highest GLC receptor remained same throughout the year. The minimum and maximum monthly predicted NO_x concentrations were 0.442 µg m^{-3} (February) at coordinates 626464.31m: 5054119m, elevation NA and 3.265 µg m^{-3} (August) at coordinates 626464.31m: 5054119m, elevation NA respectively. High GLCs of SO_2 persisted far East from the point emission source in the months of January and February. High GLCs are seen within 10 km radius from the emission sources for rest of the year.

Figures 46a-l Monthly GLCs of SO_2 due to point and highway emission sources

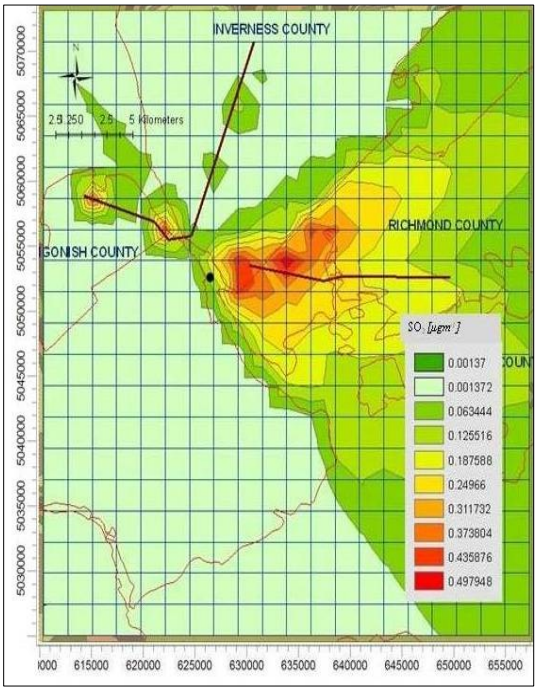

a. January

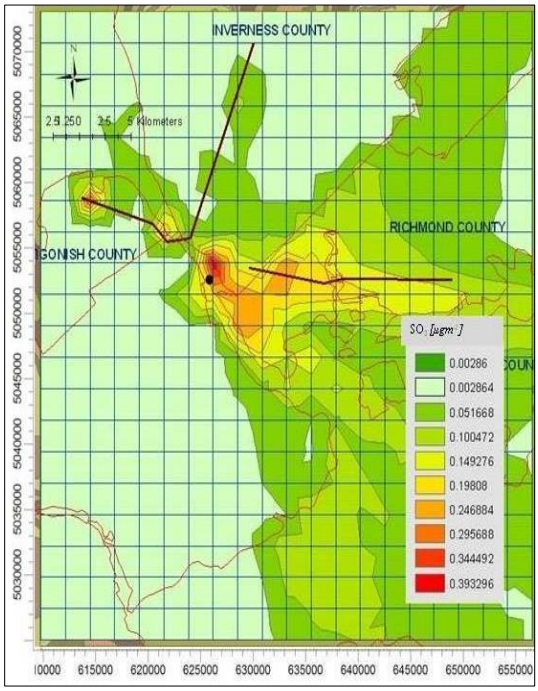

b. February

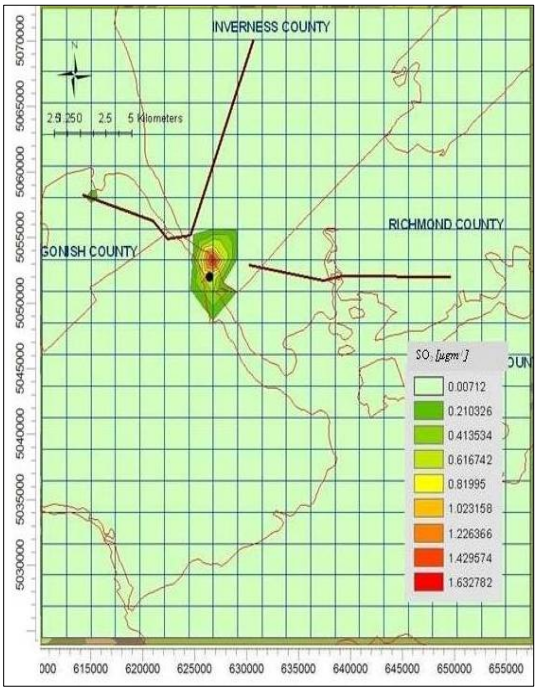

c. March

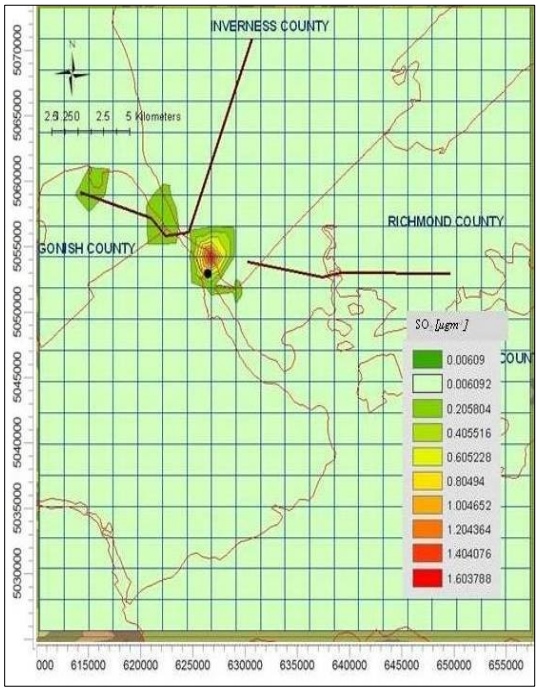

d. April

(Figures Cont'd)

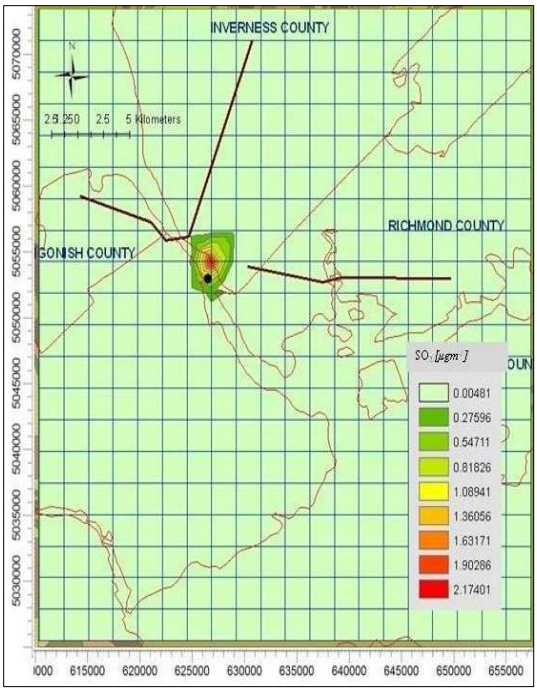

c. May

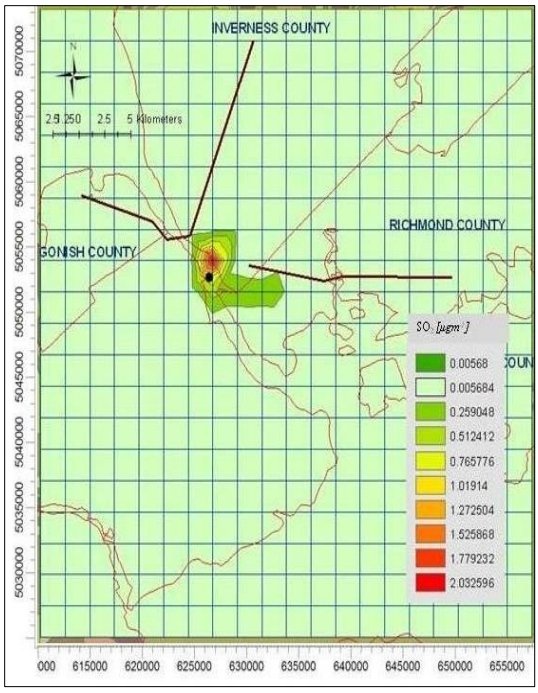

d. June

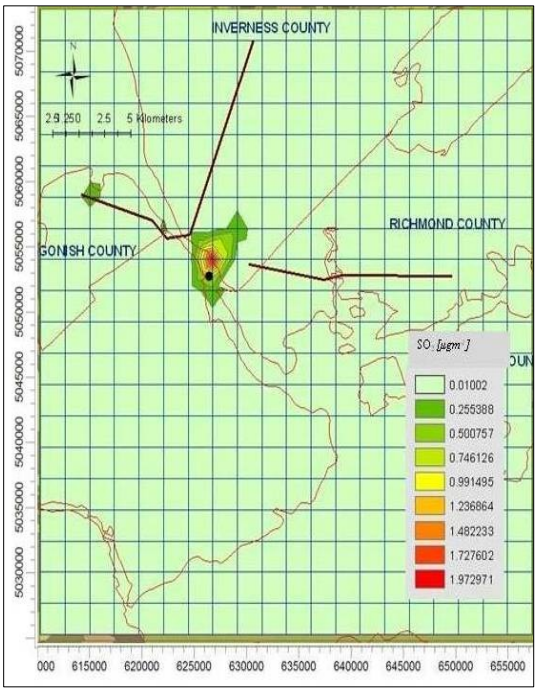

g. July

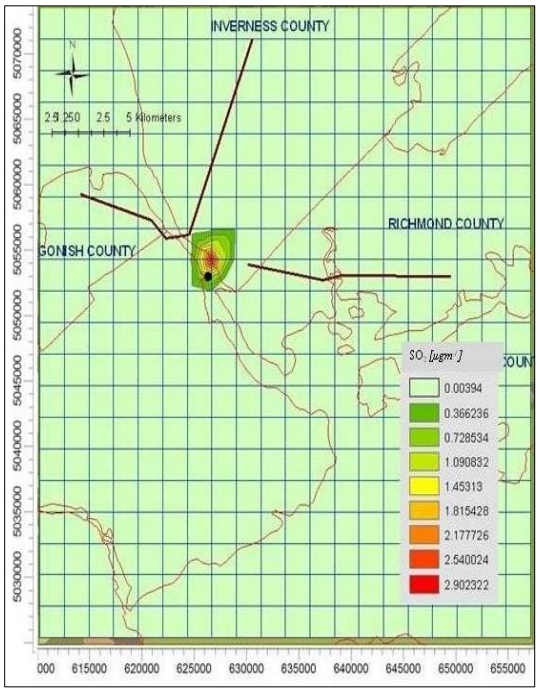

h. August

(Figures Cont'd)

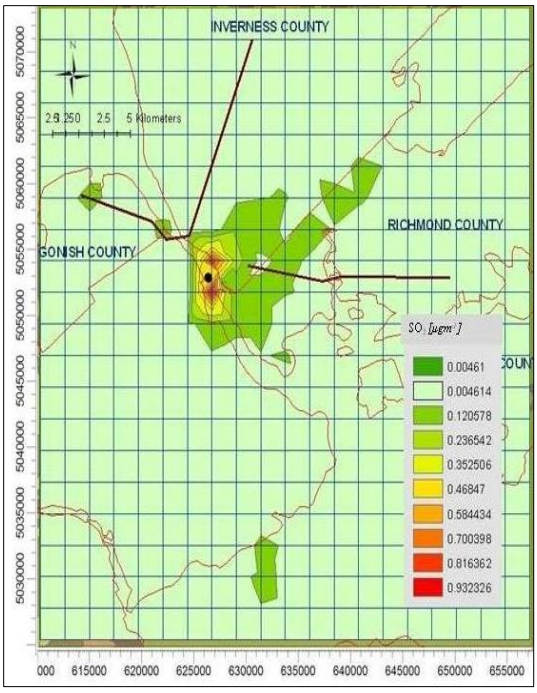

i. September

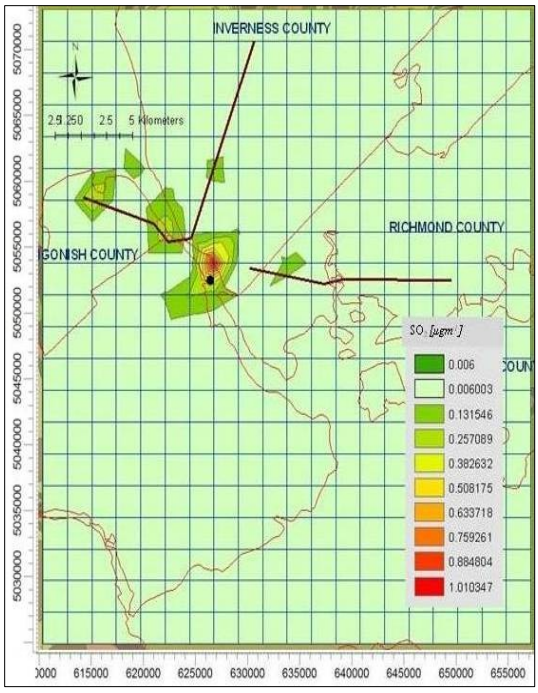

j. October

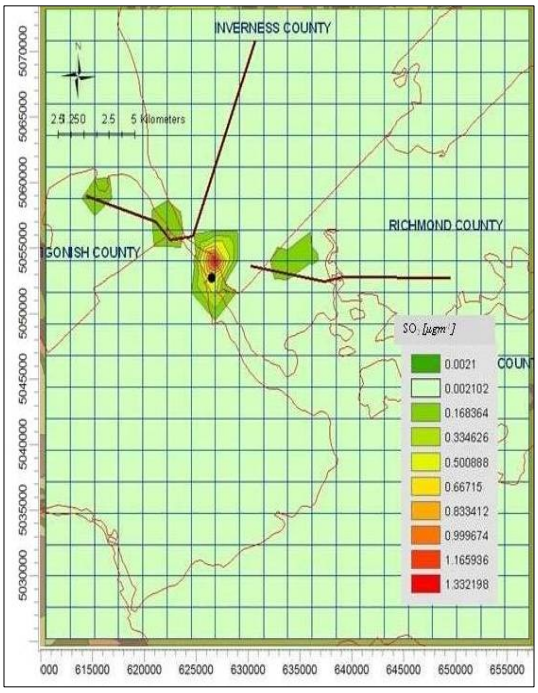

k. November

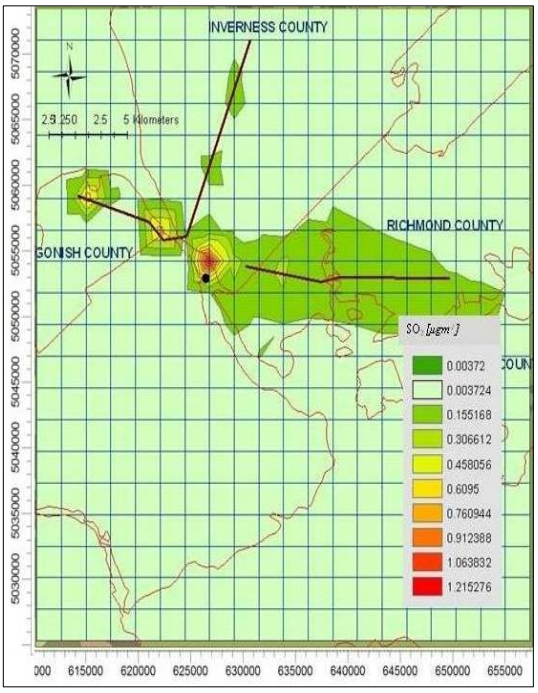

l. December

Table 23 Monthly MAX and MIN GLCs of SO_2

	SO_2	
Month	Monthly Min *[$\mu g\ m^{-3}$]* UTM coordinate (m) Elevation (m)	Monthly Max *[$\mu g\ m^{-3}$]* UTM coordinate (m) Elevation (m)
	0.001	0.56
Jan	(612273.4:5027166)	(633559.69:5054119)
	160.7	NA
	0.003	0.442
Feb	(609908.3:5029617)	(626464.31:5054119)
	172.8	NA
	0.007	1.836
Mar	(609908.3:5054119)	(626464.31:5054119)
	30.5	NA
	0.006	1.804
Apr	(609908.3:5024716)	(626464.31:5054119)
	124	NA
	0.005	2.445
May	(609908.3:5029617)	(626464.31:5054119)
	172.8	NA
	0.006	2.286
June	(612273.4:5024716)	(626464.31:5054119)
	109	NA
	0.01	2.218
July	(657211.1:5027166)	(626464.31:5054119)
	NA	NA
	0.004	3.265
Aug	(619688.8:5024716)	(626464.31:5054119)
	36	NA
	0.005	1.048
Sep	(609908.3:5039418)	(626464.31:5051669)
	169.7	NA
	0.006	1.136
Oct	(626464.3:5032067)	(626464.31:5054119)
	64.6	NA
	0.002	1.498
Nov	(609908.3:5054119)	(626464.31:5054119)
	30.5	NA
	0.004	1.367
Dec	(624099.1:5034517)	(626464.31:5054119)
	87.9	NA

4.3.4.5.3 Hourly averaging of SO_2

Figure 47 show hourly predicted ground level SO_2 concentration contours in PRTHWKS. With reference to above Figure it is seen that the point source contributed larger amount of SO_2. Highest ground level SO_2 concentration receptor during 1-hr averaging period was located at 2 km east the release point due to prevailing wind towards this direction. From 3-hr to 24-hr period, the highest concentration receptor remained the same as monthly averaging. The minimum and maximum hourly predicted SO_2 concentrations at specific receptors with elevations are given in Table 24. With reference to the table, it is seen that minimum GLC receptor changed with averaging periods throughout the day.

Figures 47a-e Hourly GLCs of SO_2 due to point and highway emission sources

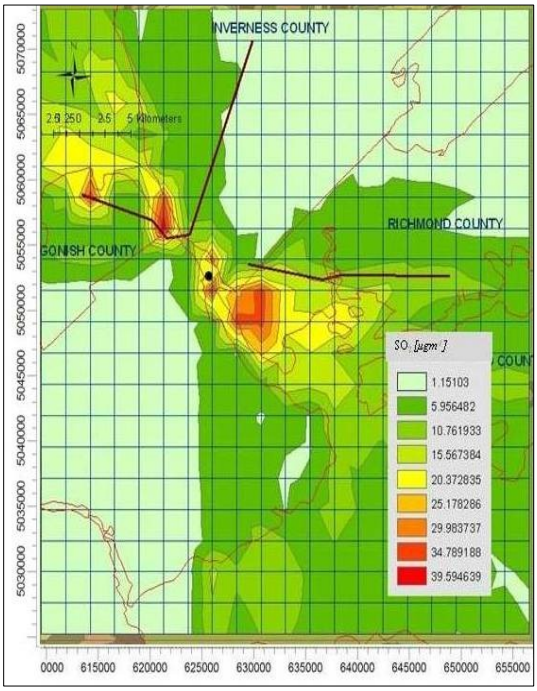

a. 1 hour

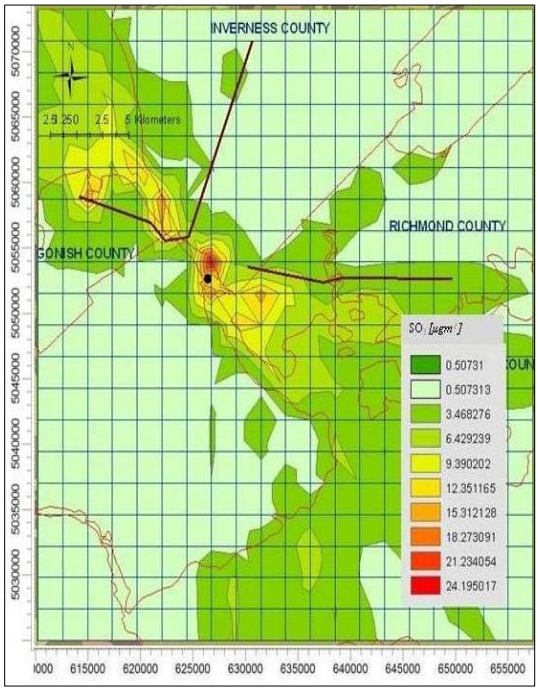

b. 3 hour

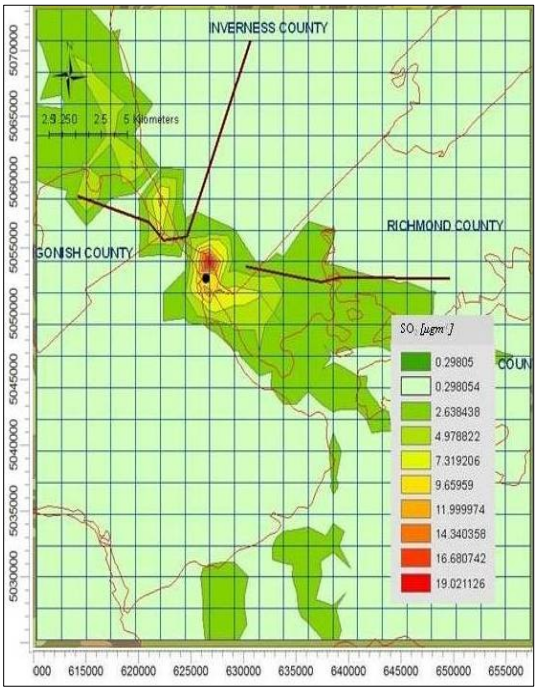

c. 8 hour

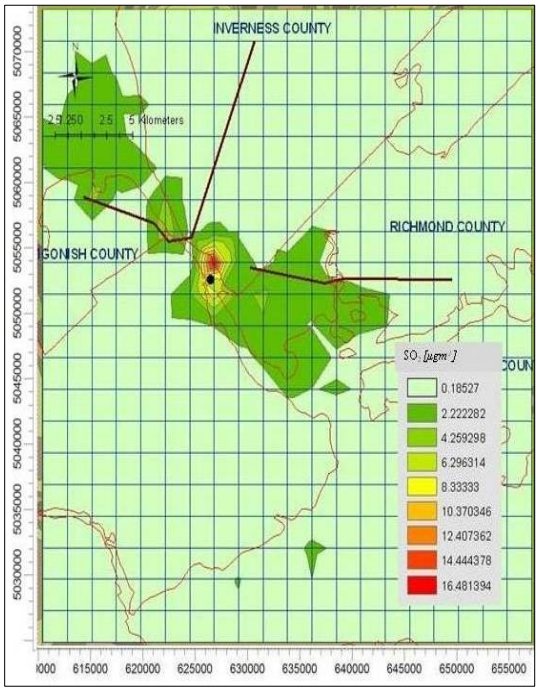

d. 12 hour

(Figure Cont'd)

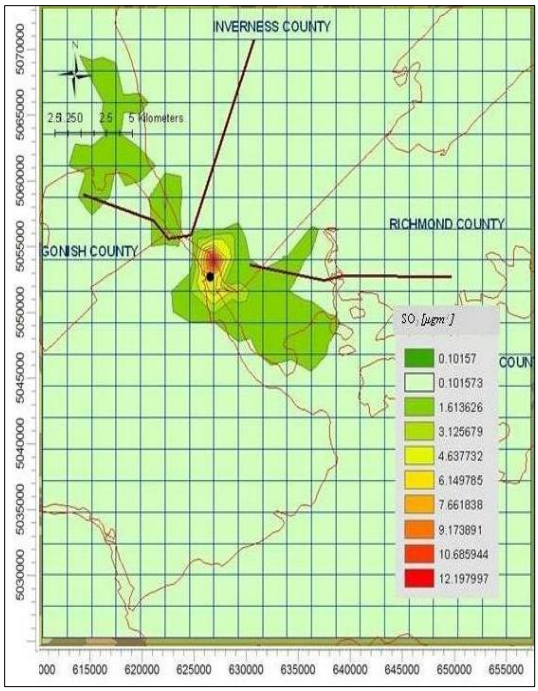

e. 24 hour

Table 24 Hourly MAX and MIN GLCs of SO_2

	SO_2	
Hour	Hourly Min *[µg m^{-3}]* UTM coordinate (m) Elevation (m)	Hourly Max *[µg m^{-3}]* UTM coordinate (m) Elevation (m)
1	1.151 (609908.3:5032067) 167.4	44.4 (621734:5056569) NA
3	0.507 (609908.3:5029617) 172.8	27.156 (626464.31:5054119) NA
8	0.298 (612273.4:5024716) 109	21.362 (626464.31:5054119) NA
12	0.185 (609908.3:5024716) 124	18.518 (626464.31:5054119) NA
24	0.102 (612273.4:5024716) 109	13.71 (626464.31:5054119) NA

4.3.6 Modeling study in SYD domain

Emission of NO_x and SO_2 during 2004 from Lignan generation station and 4.36 km and 17.91 km section length of highway 105 and main road 125 respectively were used for conducting the dispersion simulation study in SYD domain.

4.3.6.1 Annual averaging of NO_x and SO_2

GLC contour maps of NO_x and SO_2 for annual averaging period are shown in Figures 48 and 49. Lignan power generation station contributes the major amount of NO_x and SO_2 compared to the highway and the main road. As seen in the figures, the highest annual average NO_x concentration contour is at 1.2 km North East of the Lignan generation station. With reference to Table 25 the minimum and maximum predicted NO_x concentrations were 0.069µg m^{-3} located at 727669m: 5124407m, elevation 28.2 m and 2.28 µg m^{-3} located at 728919m: 5125657m, elevation NA respectively. The minimum and maximum annual average predicted SO_2 concentrations were 0.241 µg m^{-3} located at 727669m: 5124407m, elevation 28.2m and 8.696 µg m^{-3} located at 728919m: 5125657m, elevation NA respectively. In both cases the highest concentration receptor remained the same and it was located directly downwind of the point emission source. Therefore it is understood that the dispersion of both pollutants were influenced by the prevailing wind direction. High NO_x concentration due to emission from highway 125 is seen within 1 km radius of the source due to low release height as discussed for LNN and TRR domain.

Figure 48 Annual GLCs of NO_x due to point and highway emission sources

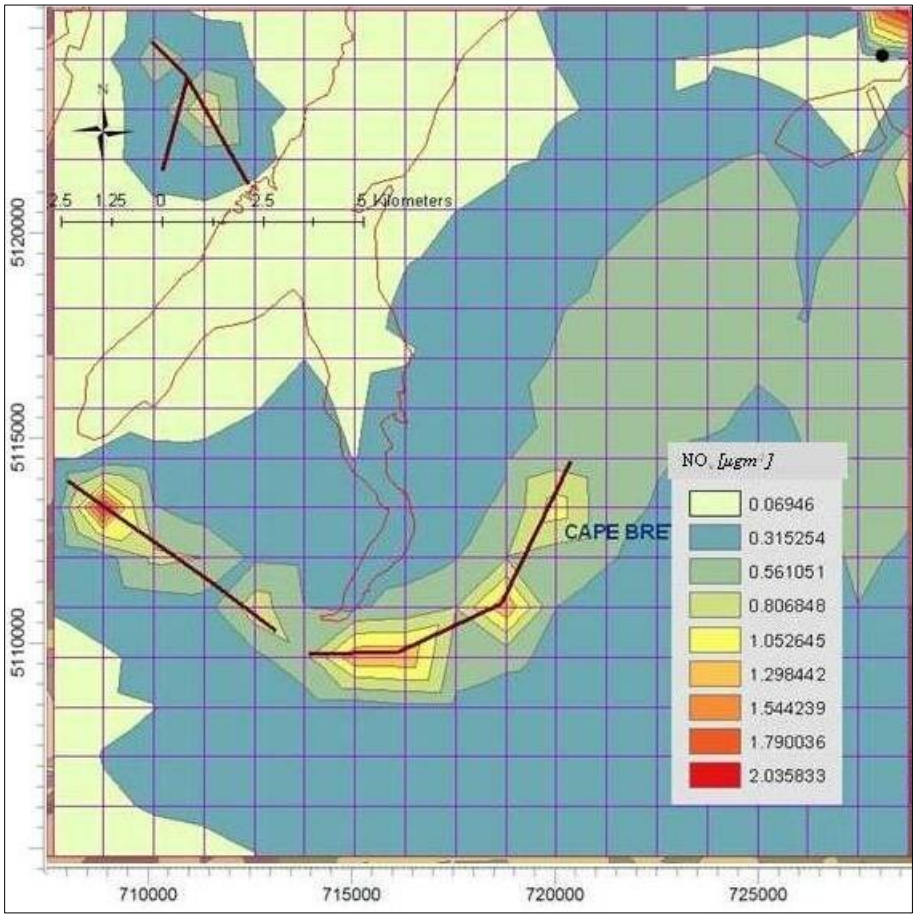

Figure 49 Annual GLCs of SO_2 due to due to point and highway emission sources

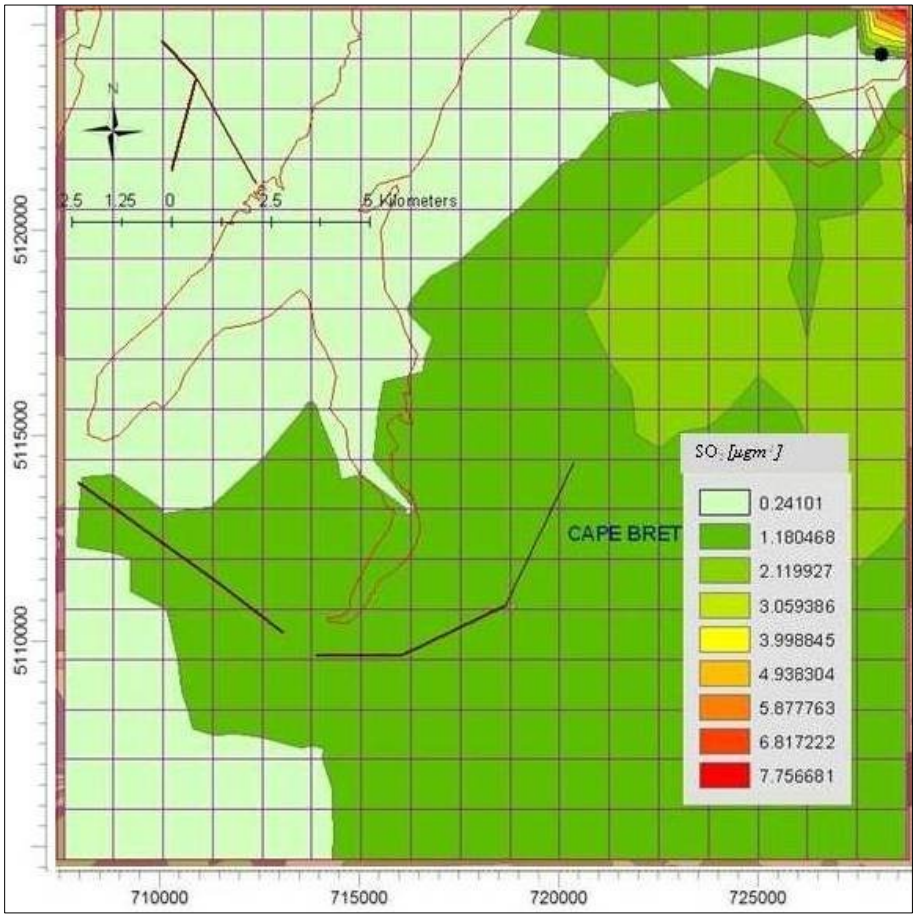

Table 25 Annual MAX and MIN GLCs of NO_x and SO_2

Pollutant	Annual Min *[µg m^{-3}]* UTM coordinate (m) Elevation (m)	Annual Max *[µg m^{-3}]* UTM coordinate (m) Elevation (m)
NO_x	0.069 (727669:5124407) 28.2	2.282 (728919:5125657) NA
SO_2	0.241 (727669:5124407) 28.2	8.696 (728919:5125657) NA

4.3.6.2 Monthly averaging of NO_x and SO_2

Figures 50 and 51 show the maps of monthly predicted NO_x and SO_2 concentration contours in SYD domain. Monthly averaging demonstrates that GLCs increased in summer months due to ambient temperature increase. Emission from the vehicles on the main road had greater impact than point emission during summer and beginning of winter. As seen from Table 26, the minimum and maximum monthly predicted NO_x concentrations were 1.96 µg m^{-3} (November) at coordinates 708919m: 5113157m, elevation 32.1 m and 6.53 µg m^{-3} (July) at coordinates 728919m: 5125657m, elevation NA respectively. The minimum and maximum monthly predicted SO_2 concentrations were 1.689 µg m^{-3} (January) at coordinates 708919m: 5113157m, elevation 32.1m and 24.89 µg m^{-3} (July) at coordinates 708919m: 5113157m, elevation 32.1 m respectively. It is observed that the highest NO_x and SO_2 concentration receptor remained same for both pollutants. This phenomenon indicates that NO_x and SO_2 shared the same point source and impacted more on maximum GLC at a receptor located at the north east end of the domain and directly downwind of the emission source.

Figure 50a-l Monthly GLCs of NO_x due to point and highway emission sources

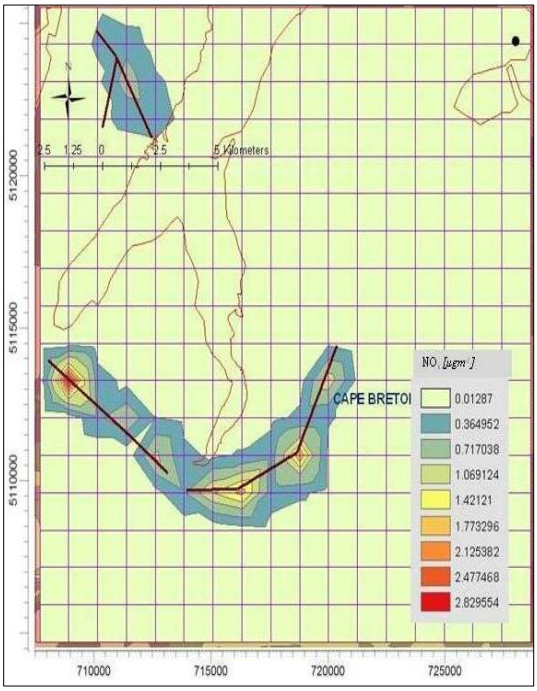

a. January

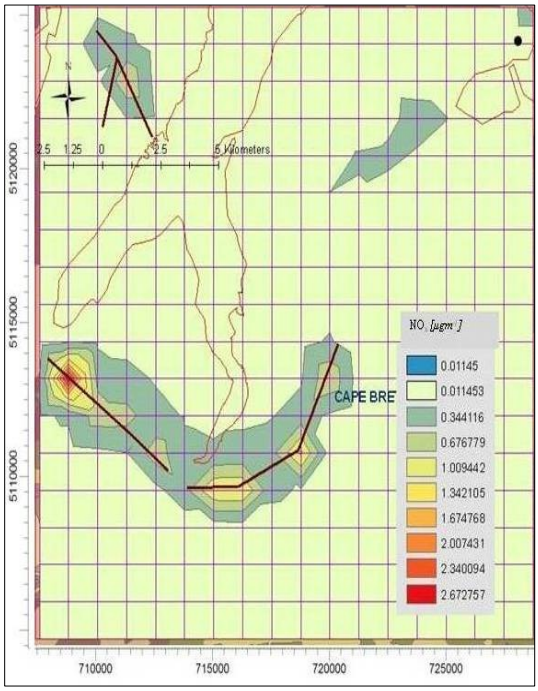

b. February

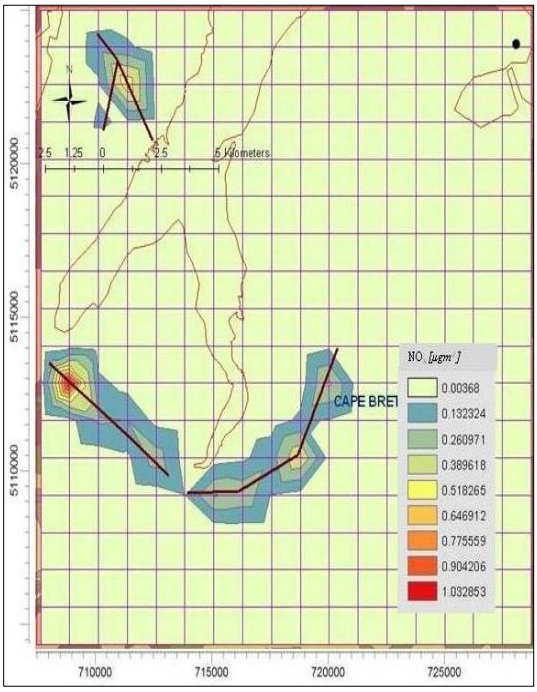

c. March

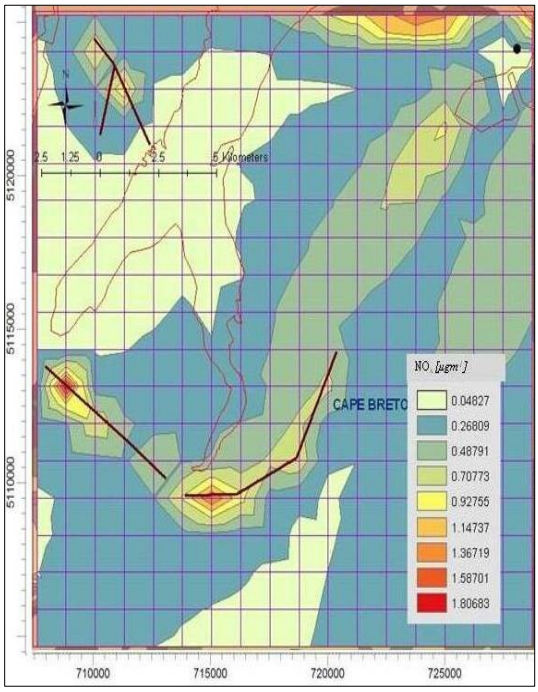

d. April

(Figures Cont'd)

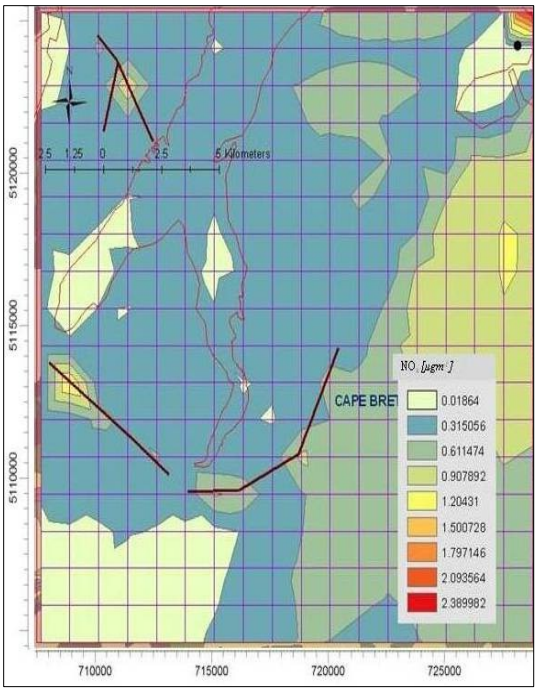

e. May

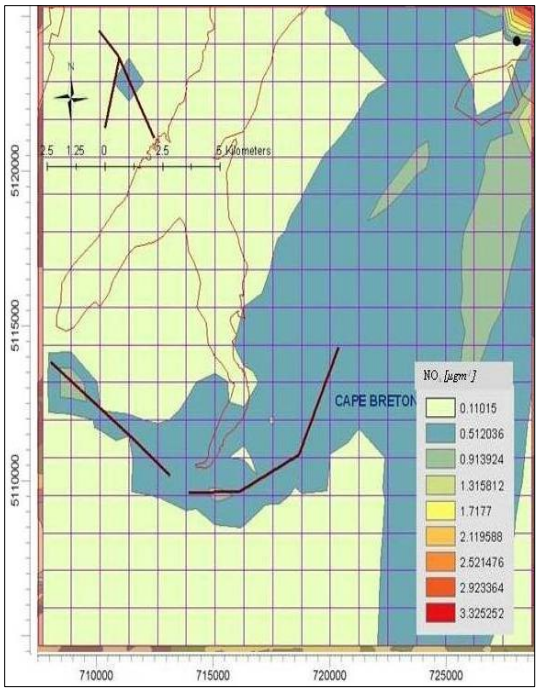

f. June

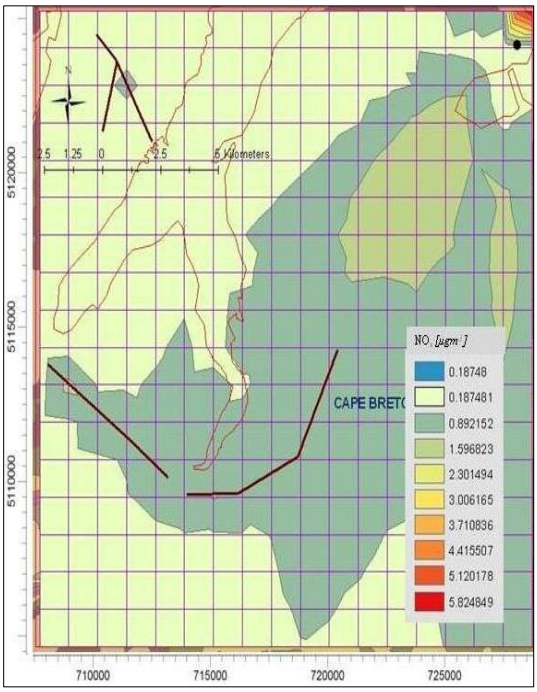

g. July

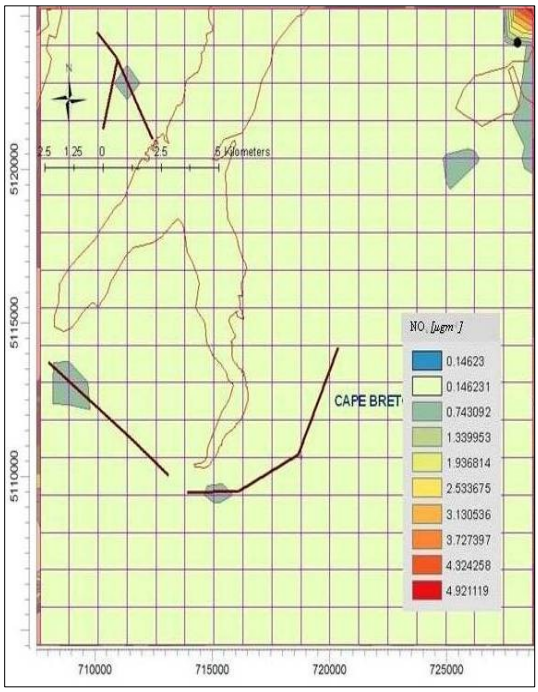

h. August

(Figures Cont'd)

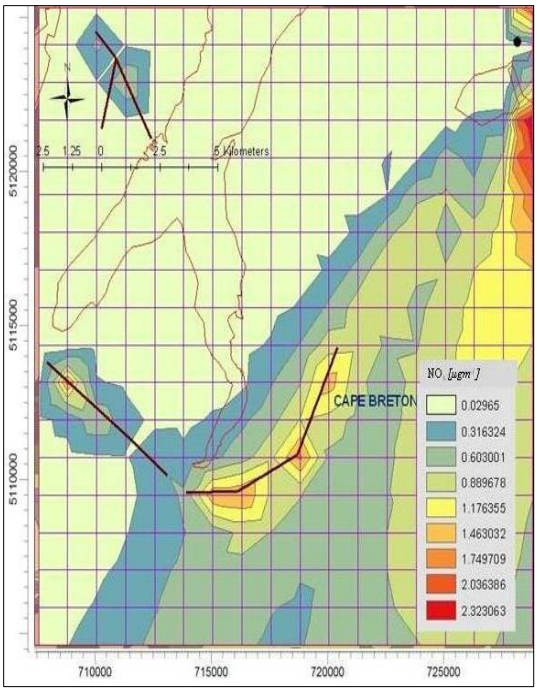

i. September

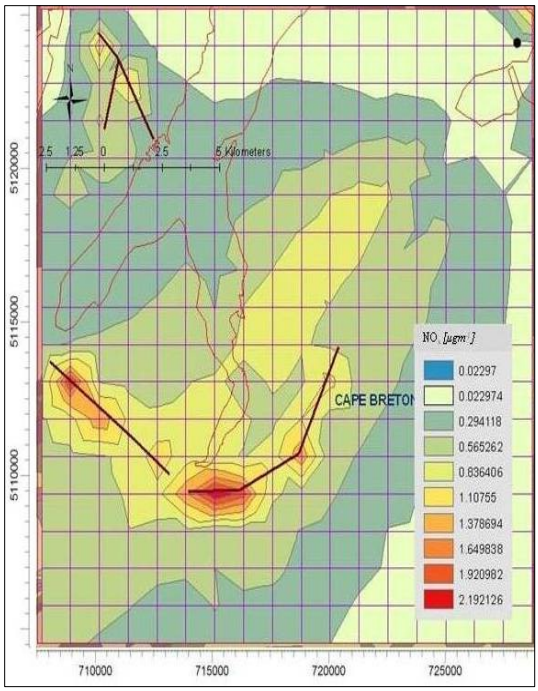

j. October

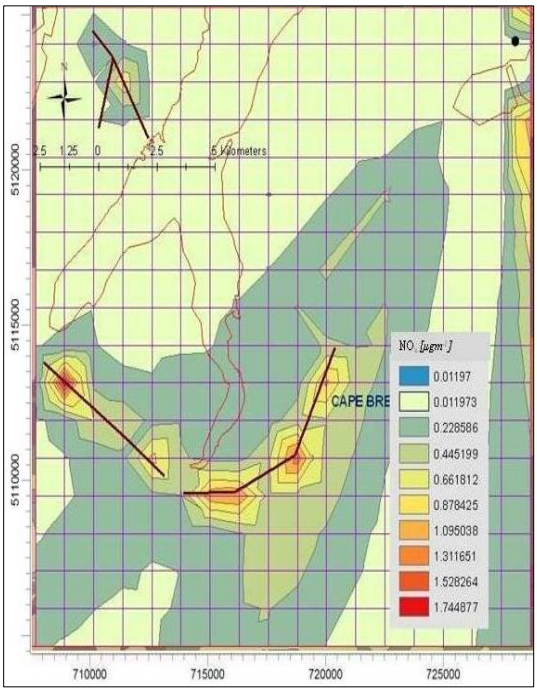

k. November

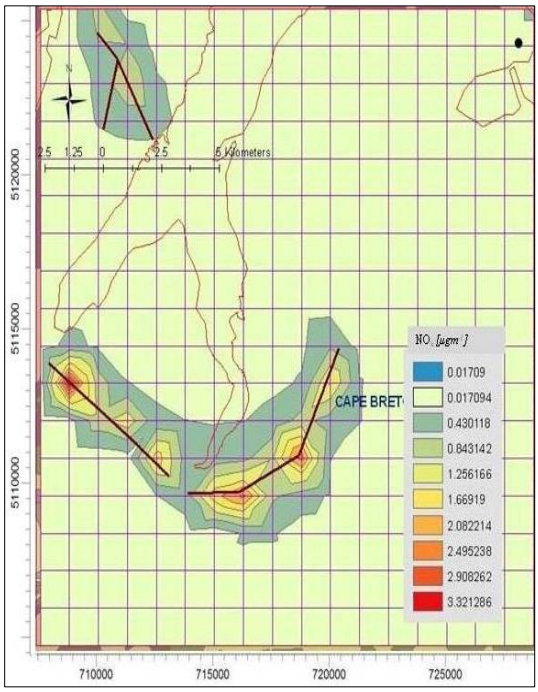

l. December

Figures 51a-l Monthly GLCs of SO_2 due to point and highway emission sources

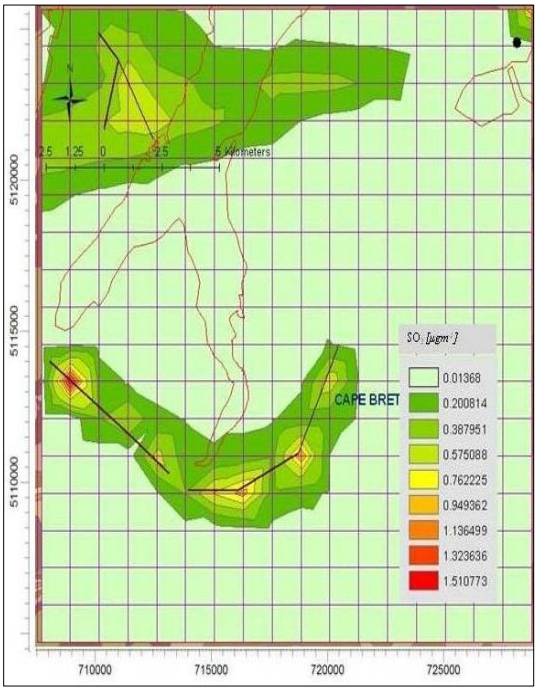

a. January

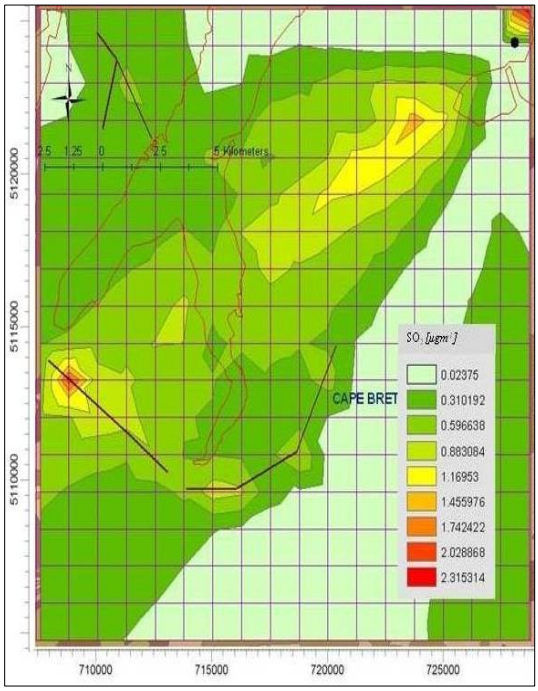

b. February

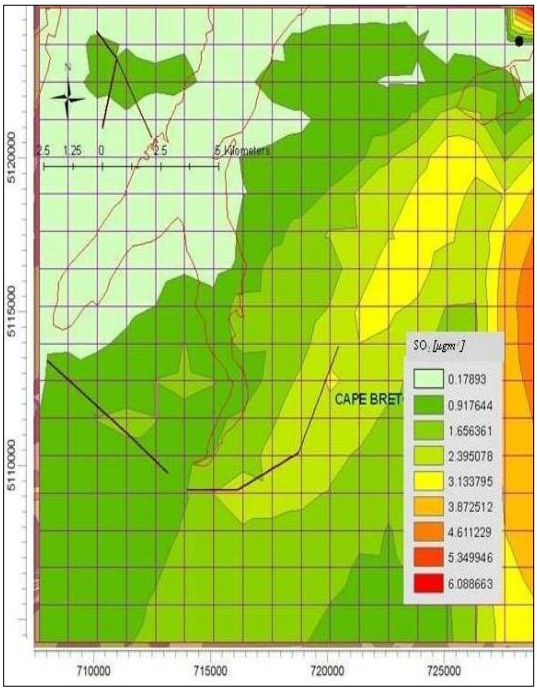

c. March

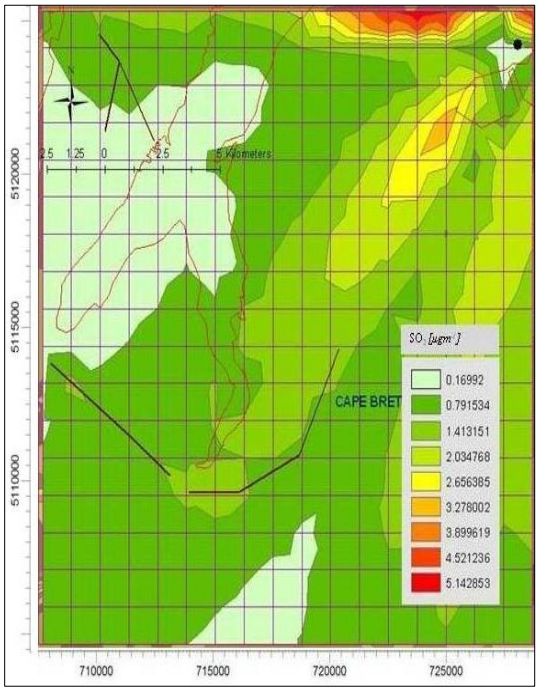

d. April

(Figures Cont'd)

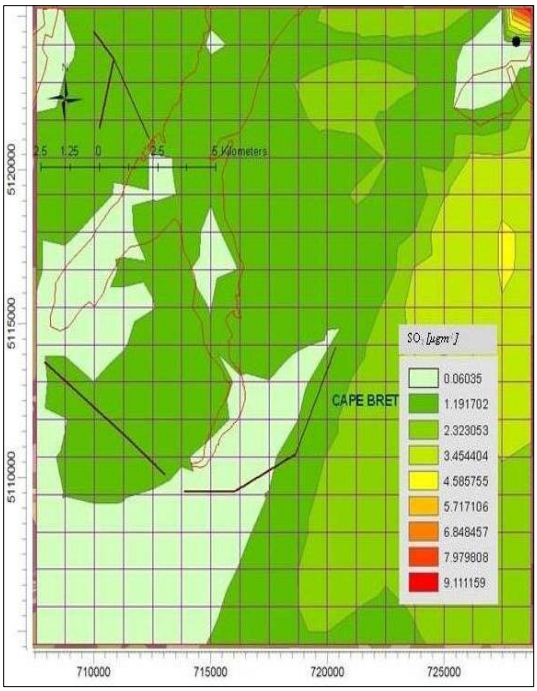

e. May

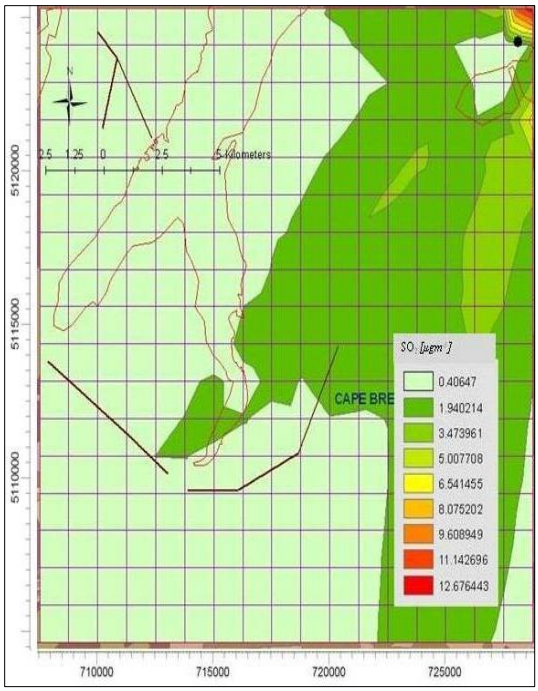

f. June

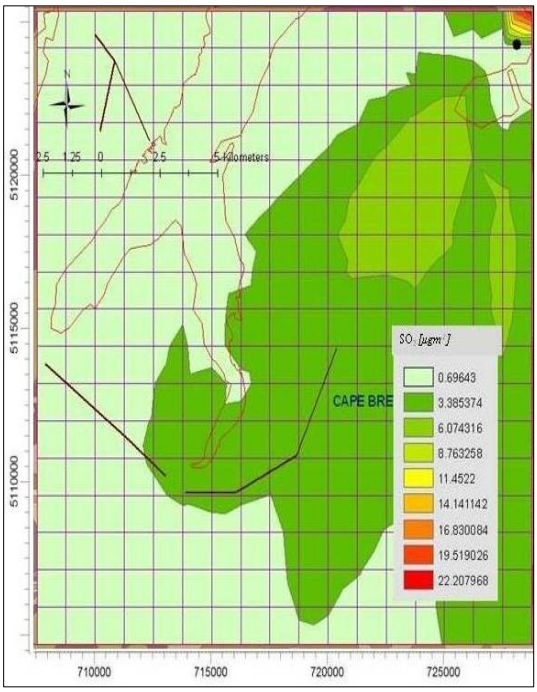

g. July

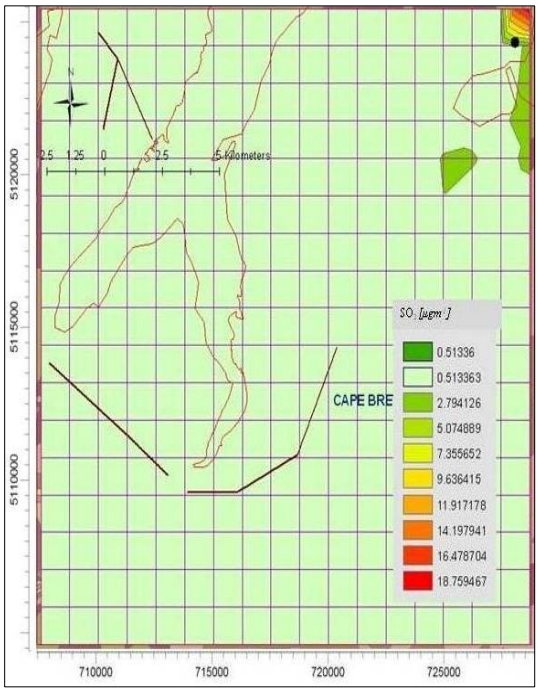

h. August

(Figures Cont'd)

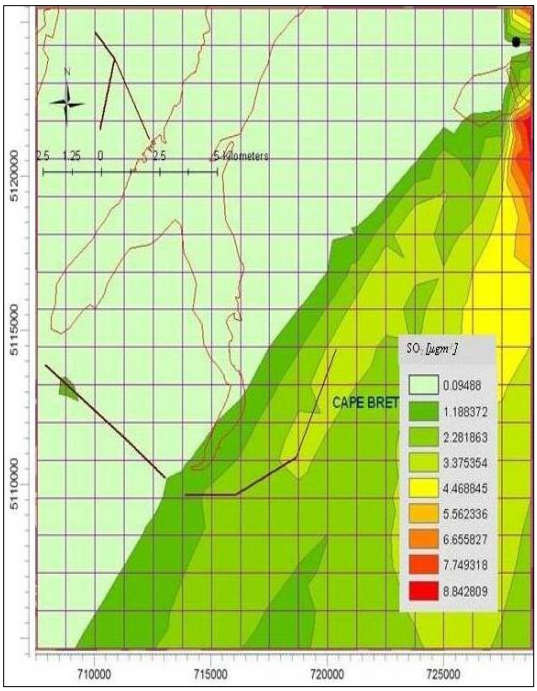

i. September

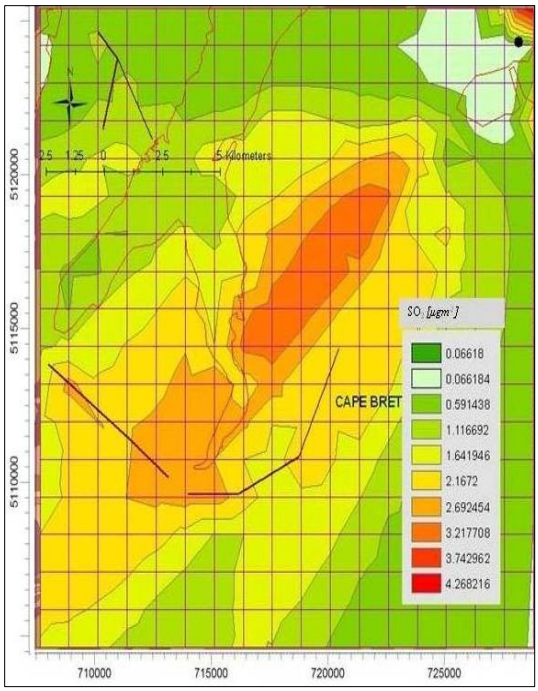

j. October

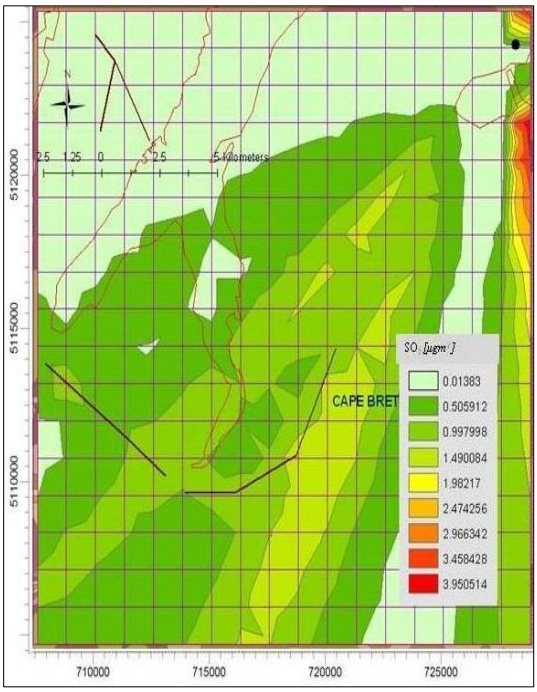

k. November

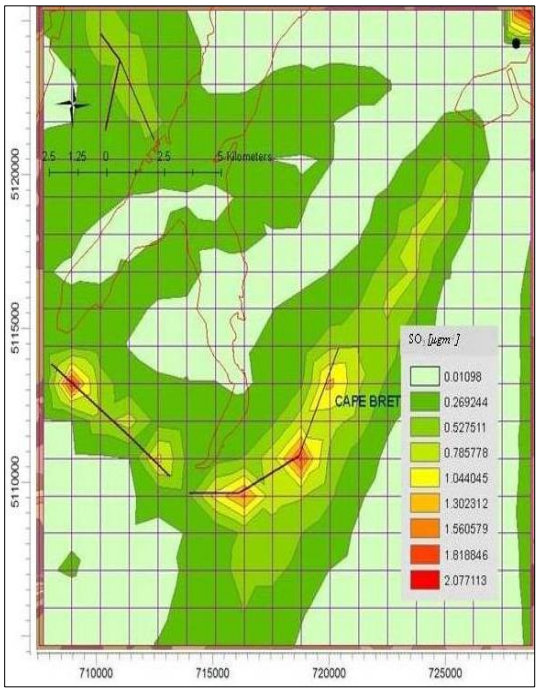

l. December

Table 26 Monthly MAX and MIN GLCs of NO_x and SO_2

Month	NO_x		SO_2	
	Monthly Min *[μg m^{-3}]* UTM coordinate (m) Elevation (m)	Monthly Max *[μg m^{-3}]* UTM coordinate (m) Elevation (m)	Monthly Min *[μg m^{-3}]* UTM coordinate (m) Elevation (m)	Monthly Max *[μg m^{-3}]* UTM coordinate (m) Elevation (m)
Jan	0.013 (716419:5113157) NA	3.182 (708919:5113157) 32.1	0.014 (727669:5124407) 28.2	1.698 (708919:5113157) 32.1
Feb	0.011 (728919:5124407) NA	3 (708919:5113157) 32.1	0.024 (727669:5124407) 28.2	2.602 (708919:5113157) 32.1
Mar	0.053 (727669:5124407) 28.2	1.819 (716419:5109407) 62.1	0.179 (727669:5124407) 28.2	6.827 (708919:5113157) 32.1
Apr	0.048 (727669:5124407) 28.2	2.027 (708919:5113157) 32.1	0.17 (727669:5124407) 28.2	5.764 (708919:5113157) 32.1
May	0.019 (727669:5124407) 28.2	2.686 (728919:5125657) NA	0.06 (727669:5124407) 28.2	10.24 (708919:5113157) 32.1
June	0.11 (727669:5124407) 28.2	3.727 (728919:5125657) NA	0.406 (727669:5124407) 28.2	14.21 (708919:5113157) 32.1
July	0.187 (727669:5124407) 28.2	6.53 (728919:5125657) NA	0.696 (727669:5124407) 28.2	24.89 (708919:5113157) 32.1
Aug	0.146 (725169:5104407) 60.9	5.518 (728919:5125657) NA	0.513 (708919:5115657) NA	21.04 (708919:5113157) 32.1
Sep	0.03 (727669:5124407) 28.2	2.61 (728919:5121907) 5.2	0.095 (727669:5124407) 28.2	9.94 (728919:5121907) 5.2
Oct	0.023 (727669:5124407) 28.2	2.463 (715169:5109407) 54.8	0.066 (727669:5124407) 28.2	4.793 (728919:5125657) NA
Nov	0.012 (727669:5124407) 28.2	1.96 (708919:5113157) 32.1	0.014 (727669:5124407) 28.2	4.44 (728919:5121907) 5.2
Dec	0.017 (727669:5124407) 28.2	3.734 (708919:5113157) 32.1	0.011 (727669:5124407) 28.2	2.33 (728919:5125657) NA

4.3.6.3 Hourly Averaging of NO_x and SO_2

Figures 52 and 53 show the hourly GLC contour maps of NO_x and SO_2 respectively in SYD domain. Dispersion patterns of both pollutants were similar during 1-hr to 24-hr averaging period. Prevailing wind carried pollutants towards North East of the domain and point source emission did not contribute major amount of GLCs inside the domain. As seen in Table 27, the maximum hourly predicted NOx and SO2 concentrations receptors were located directly downwind of the Lignan generation station. With reference to AERMET outputs, the highest GLC receptor changed with time from 1-hr till 24-hr averaging period due to change in prevailing wind direction.

Figures 52a-e Hourly GLCs of NO_x due to point and highway emission sources

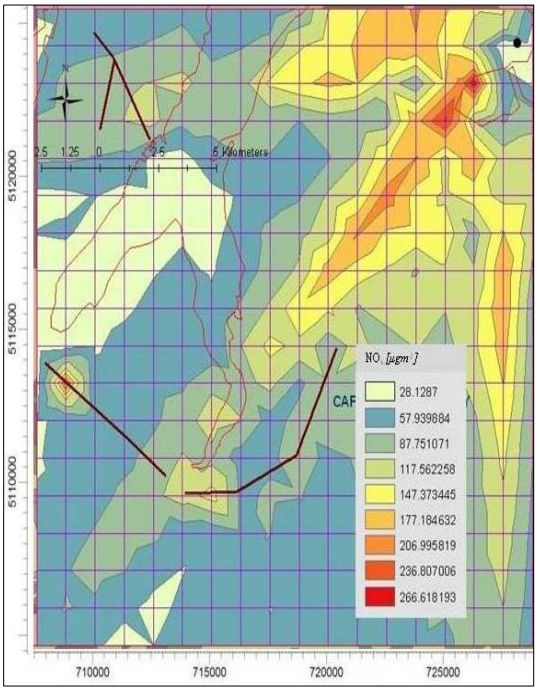

a. 1 hour

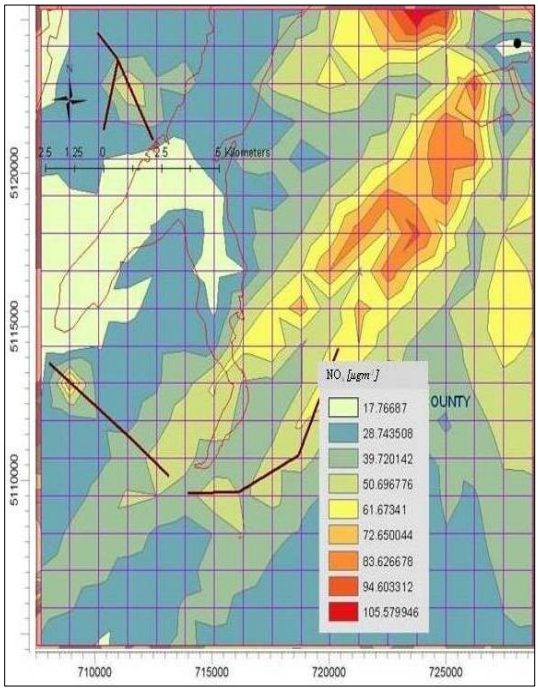

b. 3 hour

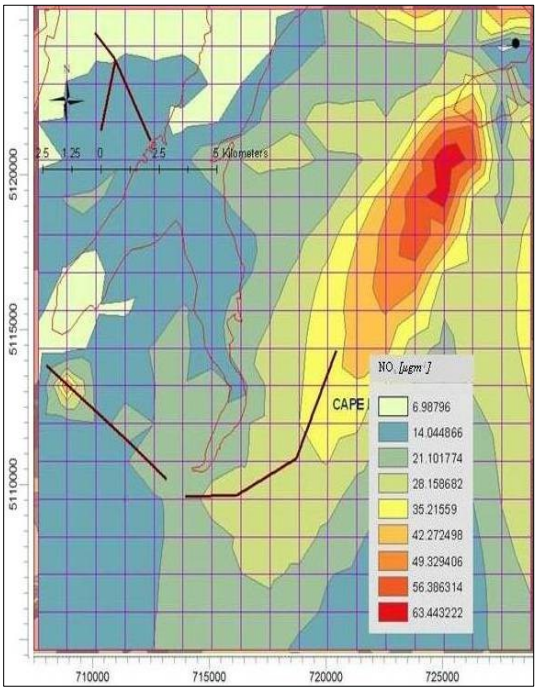

c. 8 hour

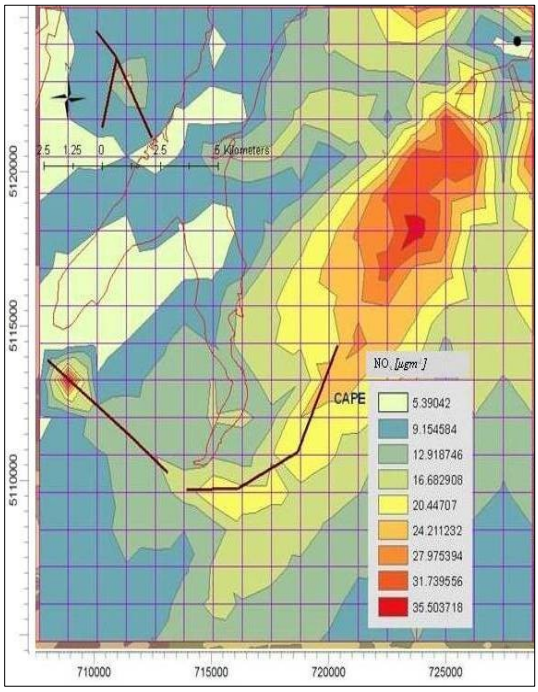

d. 12 hour

(Figure Cont'd)

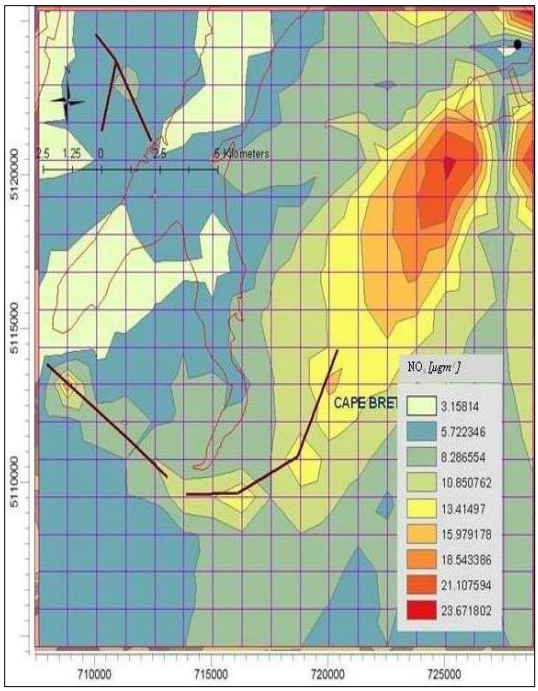
2.5 1.25 0 2.5 5 Kilometers
5120000
5115000
5110000
710000
715000
720000
725000
NO, [µgm⁻³]
3.15814
5.722346
8.286554
10.850762
13.41497
15.979178
18.543386
21.107594
23.671802

e. 24 hour

Figures 53a-e Hourly GLCs of SO_2 due to point and highway emission sources

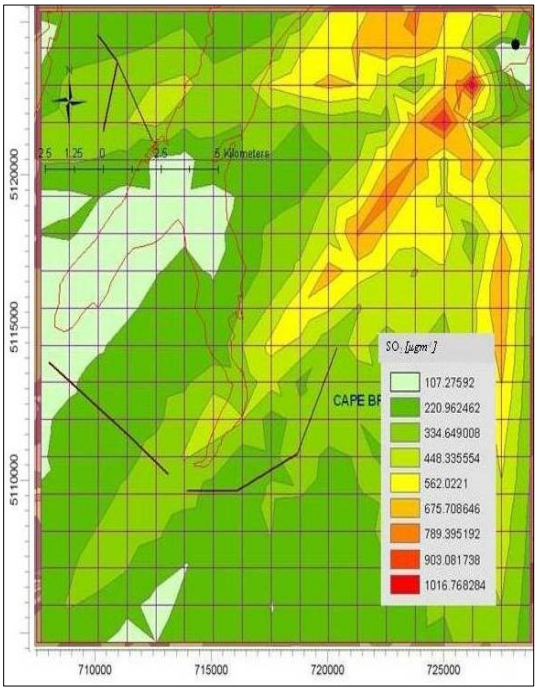

a. 1 hour

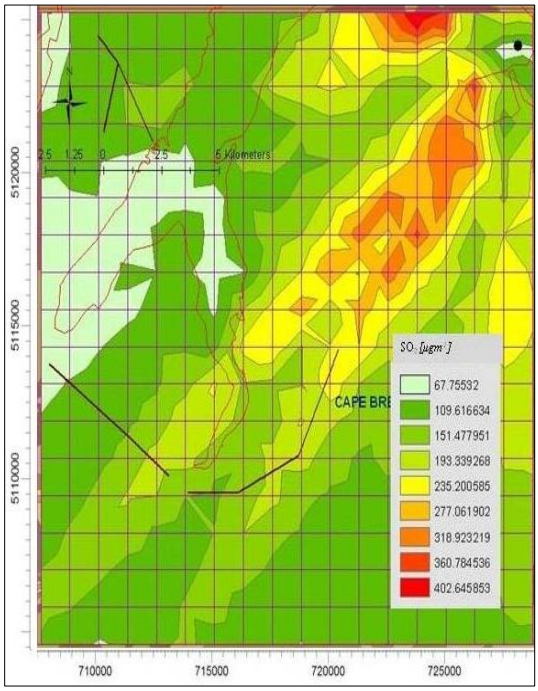

b. 3 hour

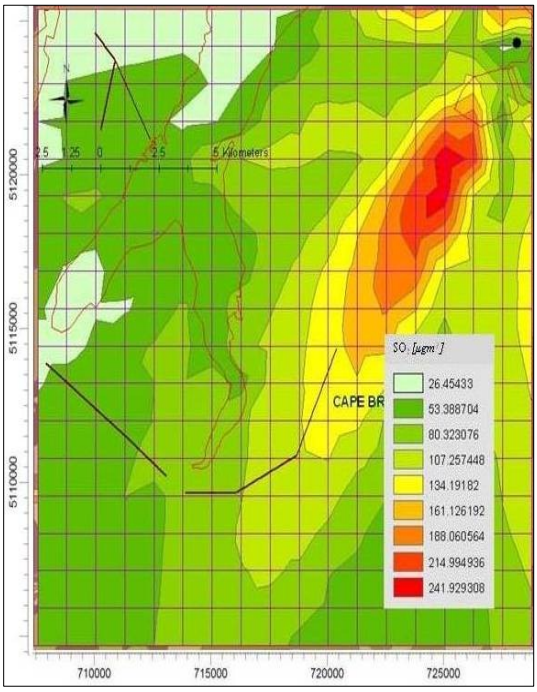

c. 8 hour

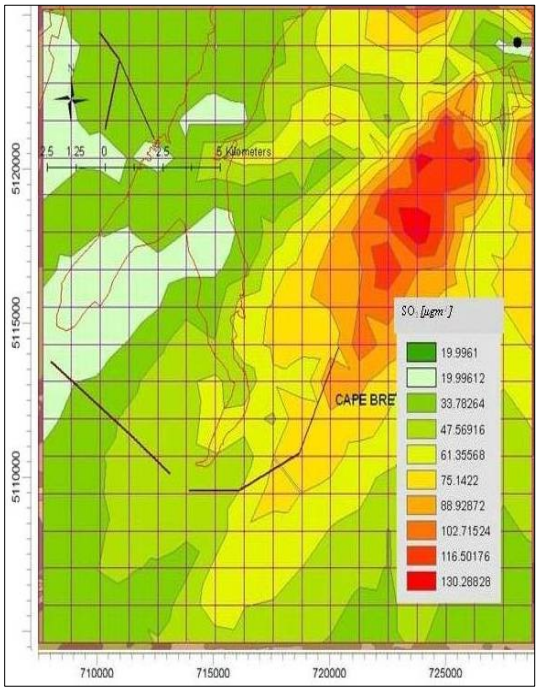

d. 12 hour

(Figure Cont'd)

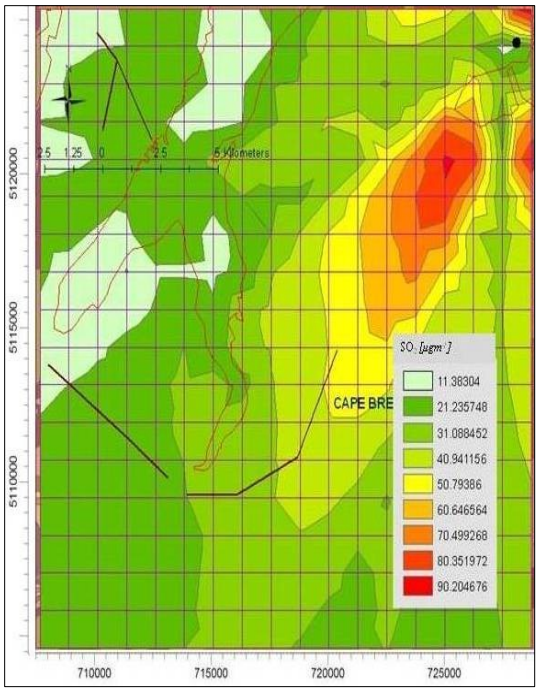

e. 24 hour

Table 27 Hourly MAX and MIN GLCs of NO_x and SO_2

	NO_x		SO_2	
Hour	Hourly Min *[µg m^{-3}]* UTM coordinate (m) Elevation (m)	Hourly Max *[µg m^{-3}]* UTM coordinate (m) Elevation (m)	Hourly Min *[µg m^{-3}]* UTM coordinate (m) Elevation (m)	Hourly Max *[µg m^{-3}]* UTM coordinate (m) Elevation (m)
1	28.129 (727669:5124407) 28.2	296.429 (726419:5123157) NA	107.276 (727669:5124407) 28.2	1130.45 (726419:5123157) NA
3	17.767 (708919:5116907) NA	116.557 (723919:5125657) 23.3	67.75 (708919:5115657) NA	444.51 (723919:5125657) 23.3
8	6.988 (707669:5124407) NA	70.5 (725169:5120657) 10.6	26.454 (707669:5124407) NA	268.86 (725169:5120657) 10.6
12	5.39 (708919:5115657) NA	39.27 (708919:5113157) 32.1	19.996 (708919:5115657) NA	144.08 (723919:5125657) 23.3
24	3.158 (707669:5124407) NA	26.236 (728919:5125657) NA	11.383 (707669:5124407) NA	100.06 (723919:5125657) 23.3

4.3.7 $PM_{2.5}$ Dispersion Study in SYD Domain

Emission of $PM_{2.5}$ during 2005 from Lignan generation station and 4.36 km and 17.91 km section length of highway 105 and main road125 were used for conducting the simulation study in SYD domain.

4.3.7.1 Annual Averaging of $PM_{2.5}$

GLC contour map of $PM_{2.5}$ during annual averaging period is shown in the Figure 54. As seen from Figure 54, both highway and main road appeared to have larger amount of $PM_{2.5}$ contribution. Highest annual average $PM_{2.5}$ concentrations were seen at 1km North East of the main road 125. $PM_{2.5}$ contribution of Lignan generation station was negligible compared to highway 105 in 2005. The minimum and maximum annual average predicted $PM_{2.5}$ concentrations were 0.005 μg m^{-3} located at 708919m: 5106907m, elevation 184.1 m and 1.191μg m^{-3} located at 708919m: 5113157m, elevation 32.1 m respectively. Most of the areas of the domain received low GLCs of $PM_{2.5}$.

Figure 54 Annual GLCs of $PM_{2.5}$ due to due to point and highway emission sources

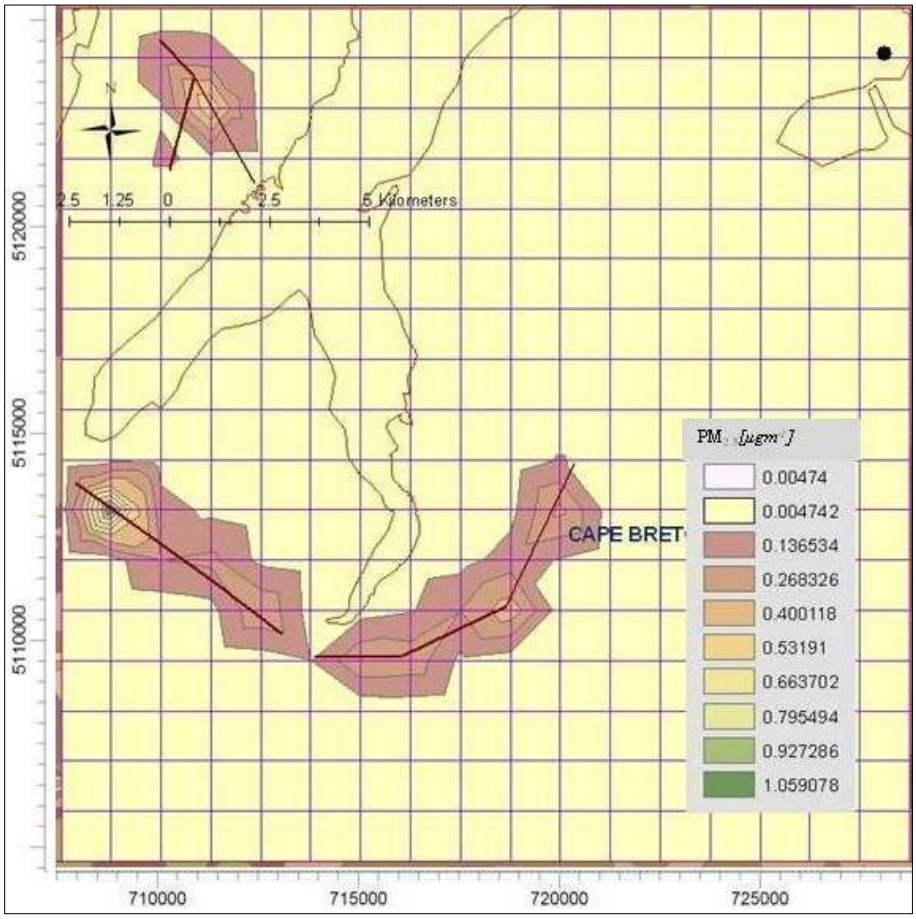

4.3.7.2 Monthly Averaging of $PM_{2.5}$

Figure 55 shows monthly maps of $PM_{2.5}$ concentration contours in 2005. As seen from the Figure, dispersion pattern remained similar throughout the year. The difference between monthly maximum and minimum ground level concentrations of $PM_{2.5}$ was less compared to other pollutants. As seen in the Table 28, the minimum and maximum monthly predicted $PM_{2.5}$ concentrations were 0.951µg m^{-3} (October) at coordinates 708919m: 5113157m, elevation 32.1m and 1.663 µg m^{-3} (February) at coordinates 708919m: 5113157m, elevation 32.1m respectively. Maximum and minimum monthly ground level $PM_{2.5}$ concentration receptor remained same as other two pollutants.

Figures 55a-l Monthly GLCs of $PM_{2.5}$ due to point and highway emission sources

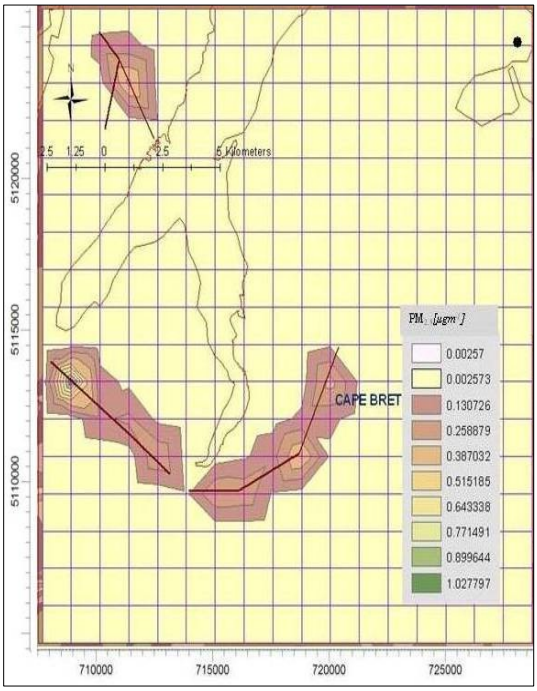

a. January

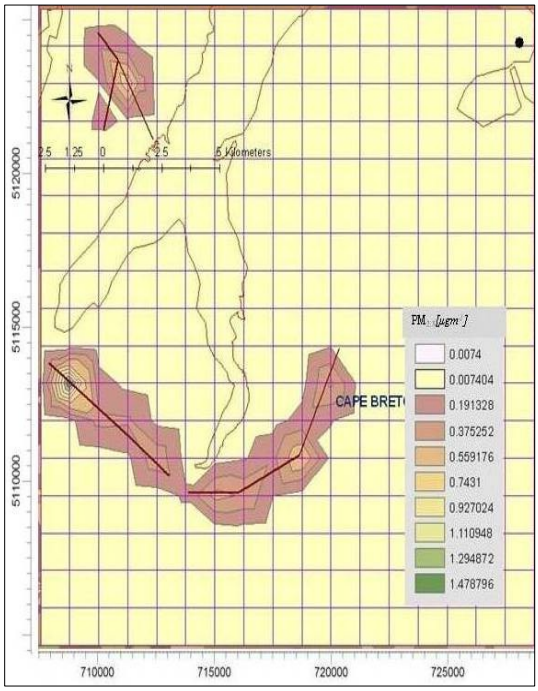

b. February

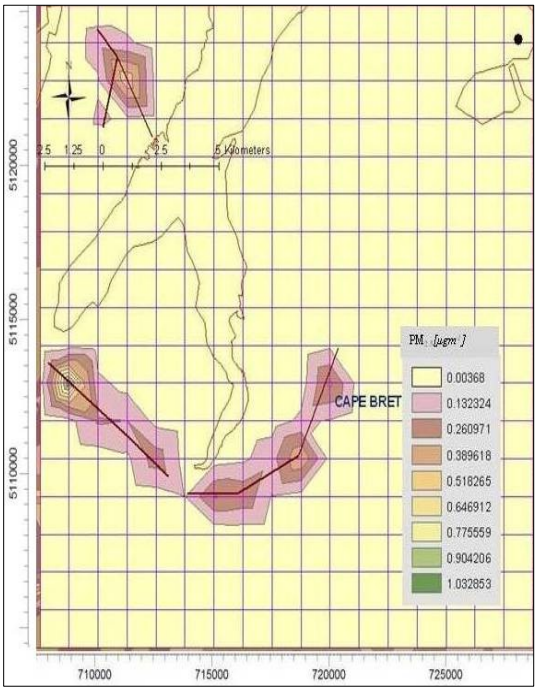

c. March

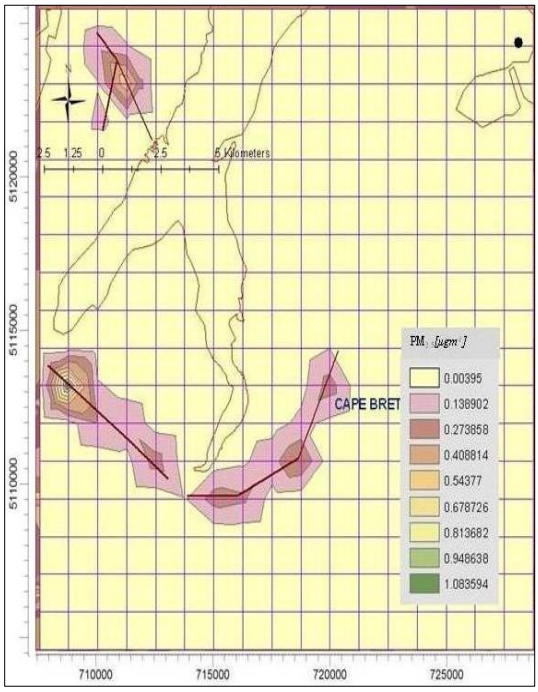

d. April

(Figures Cont'd)

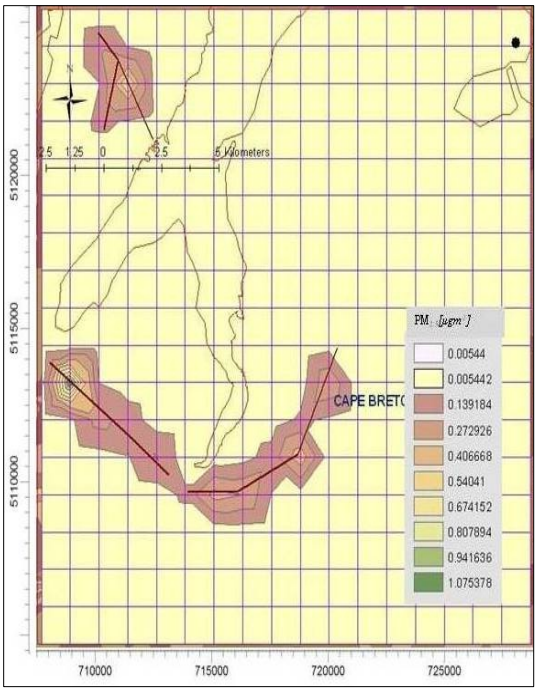

e. May

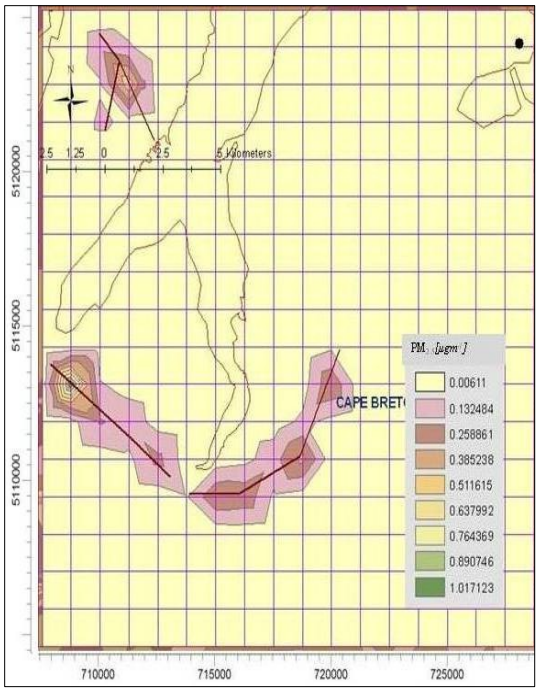

f. June

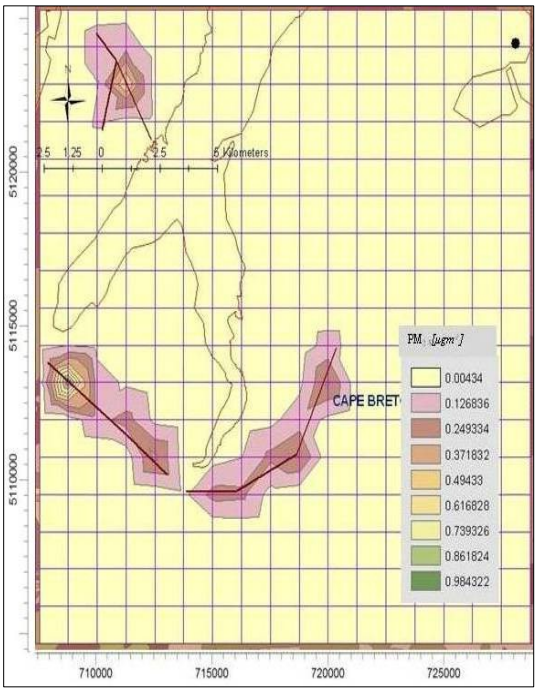

g. July

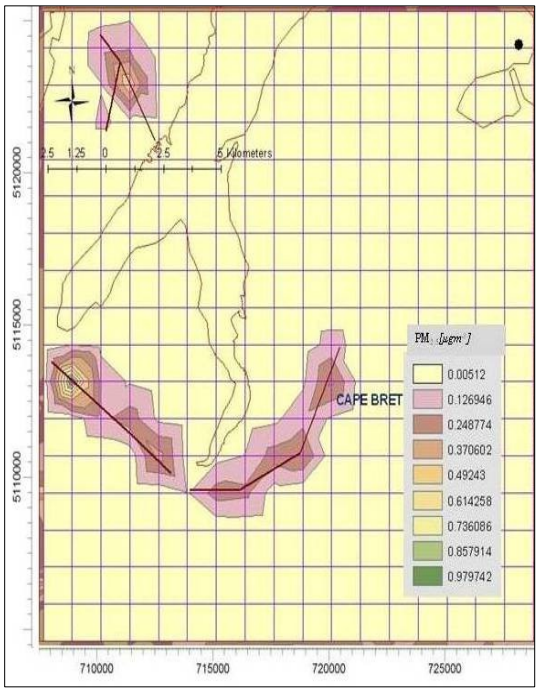

h. August

(Figures Cont'd)

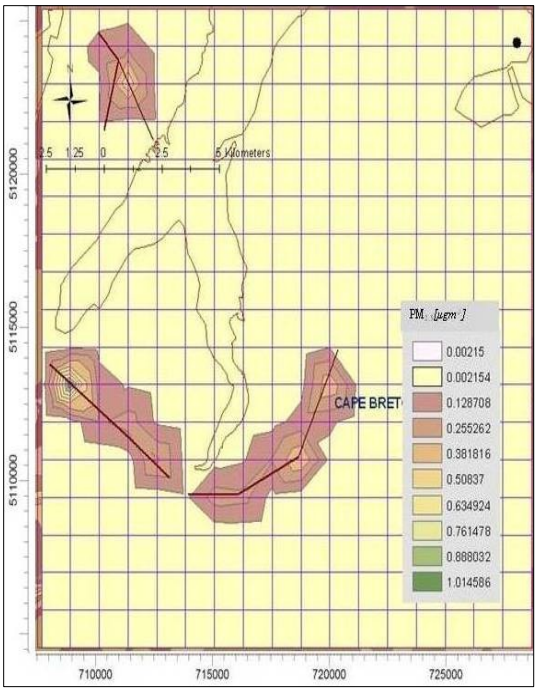

i. September

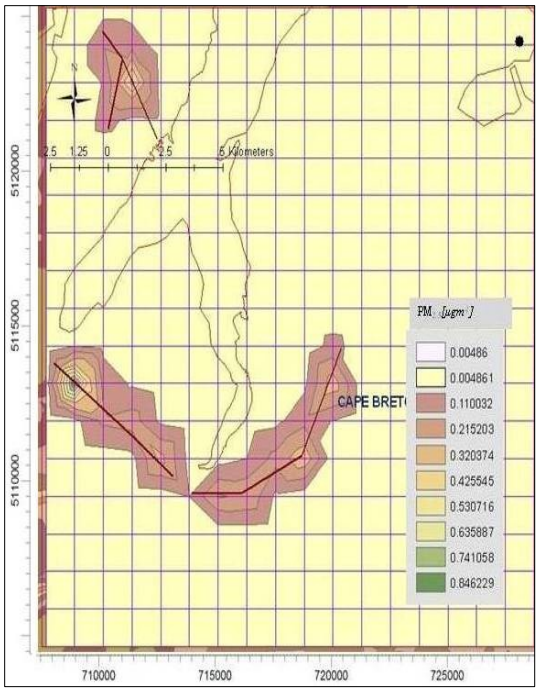

j. October

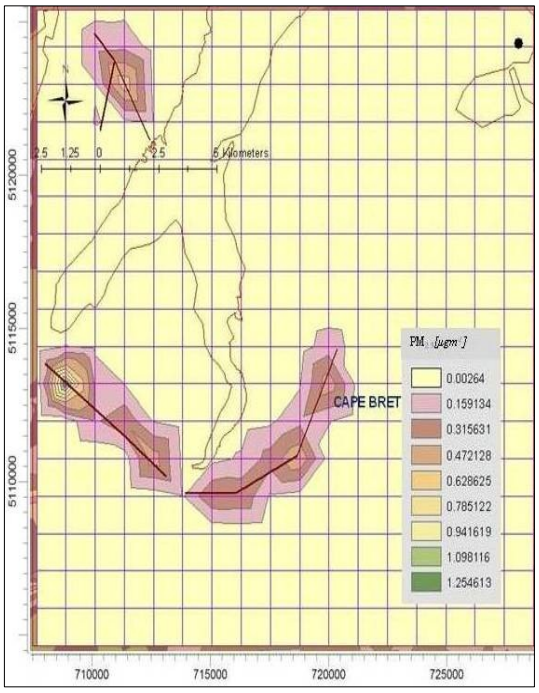

k. November

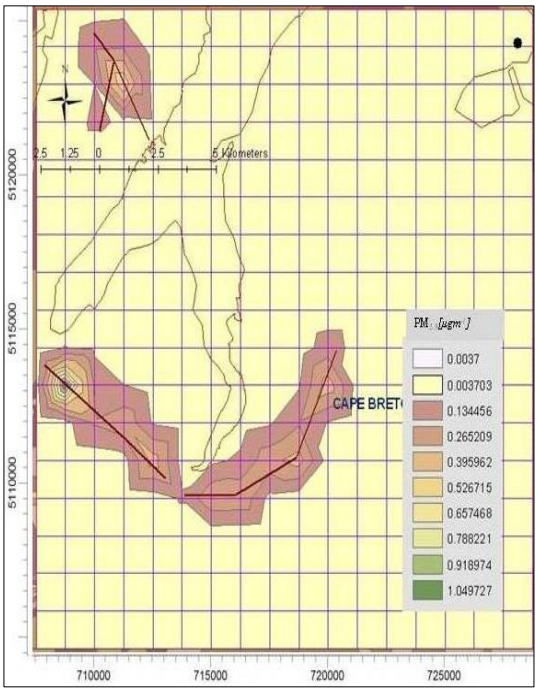

l. December

Table 28 Monthly MAX and MIN GLCs of $PM_{2.5}$

	$PM_{2.5}$	
Month	Monthly Min *[$\mu g\ m^{-3}$]* UTM coordinate (m) Elevation (m)	Monthly Max *[$\mu g\ m^{-3}$]* UTM coordinate (m) Elevation (m)
Jan	0.003 (708919:5106907) 184.1	1.155 (708919:5113157) 32.1
Feb	0.007 (728919:5125657) NA	1.663 (708919:5113157) 32.1
Mar	0.004 (707669:5108157) 145.9	1.161 (708919:5113157) 32.1
Apr	0.004 (708919:5106907) 184.1	1.219 (708919:5113157) 32.1
May	0.005 (708919:5124407) NA	1.209 (708919:5113157) 32.1
June	0.006 (707669:5106907) 161.7	1.143 (708919:5113157) 32.1
July	0.004 (707669:5106907) 161.7	1.107 (708919:5113157) 32.1
Aug	0.005 (707669:5106907) 161.7	1.102 (708919:5113157) 32.1
Sep	0.002 (707669:5106907) 161.7	1.141 (708919:5113157) 32.1
Oct	0.005 (707669:5106907) 161.7	0.951 (708919:5113157) 32.1
Nov	0.003 (708919:5106907) 184.1	1.411 (708919:5113157) 32.1
Dec	0.004 (707669:5106907) 161.7	1.18 (708919:5113157) 32.1

4.3.7.2 Hourly Averaging of $PM_{2.5}$

Figure 56 shows hourly concentration contour maps of $PM_{2.5}$ in SYD domain. As seen from the figure, dispersion patterns were similar with annual and monthly averaging concentration gradients. From Table 29 it is also seen that the highest GLC receptor remained unchanged as above with higher concentration values due to shorter averaging period.

Figures 56a-e Hourly GLCs of $PM_{2.5}$ due to point and highway emission sources

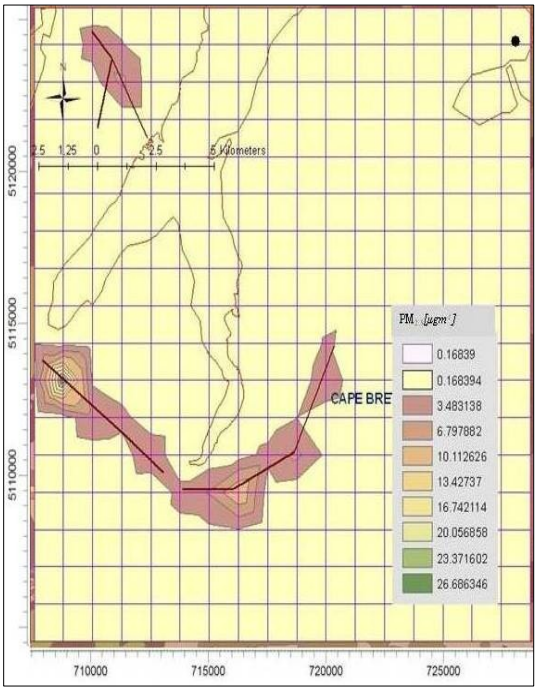

a. 1 hour

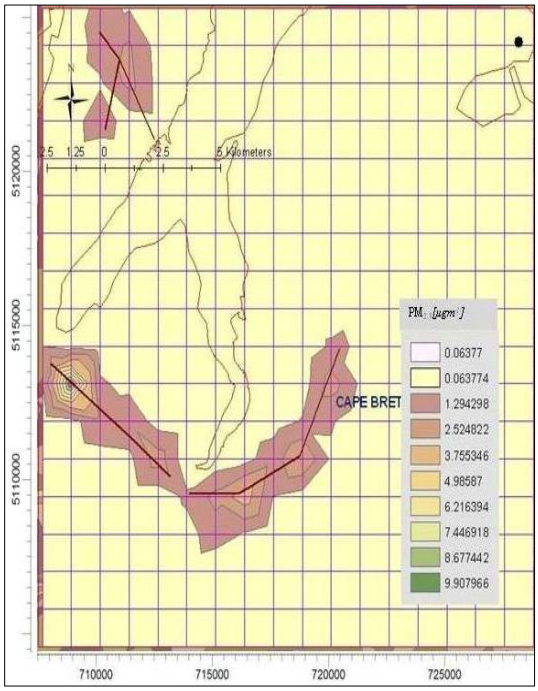

b. 3 hour

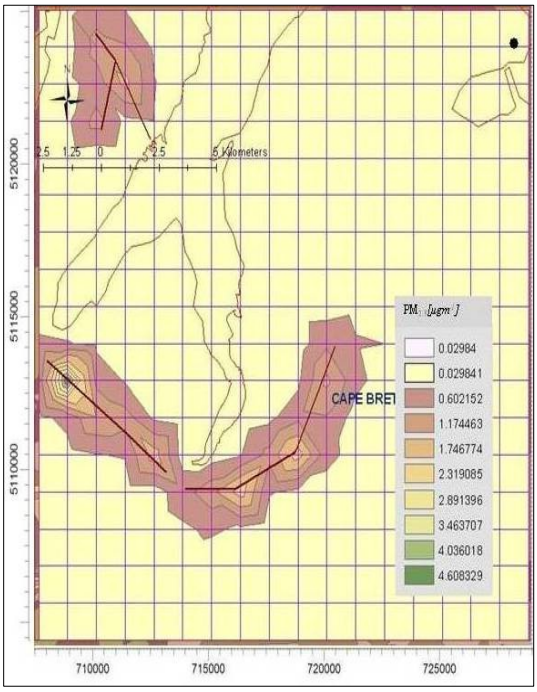

c. 8 hour

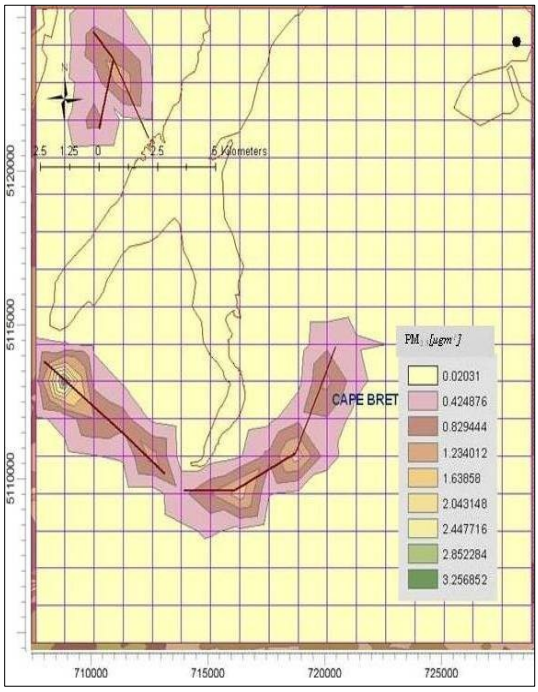

d. 12 hour

(Figure Cont'd)

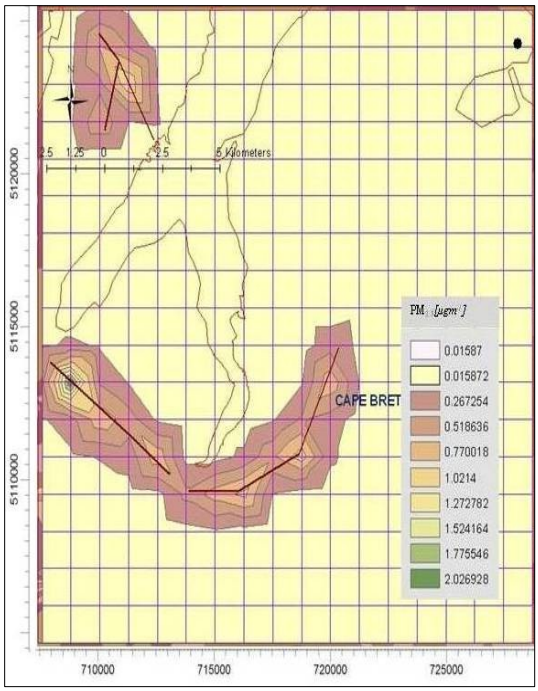

e. 24 hour

Table 29 Hourly MAX and MIN GLCs of $PM_{2.5}$

$PM_{2.5}$		
Hour	Hourly Min *[μg m^{-3}]* UTM coordinate (m) Elevation (m)	Hourly Max *[μg m^{-3}]* UTM coordinate (m) Elevation (m)
1	0.148 (726419:5104407) 52	30.64 (708919:5113157) 32.1
3	0.079 (728919:5116907) 48.3	11.76 (708919:5113157) 32.1
8	0.037 (728919:5124407) NA	7.047 (708919:5113157) 32.1
12	0.029 (726419:5104407) 52	5.175 (708919:5113157) 32.1
24	0.019 (725169:5104407) 60.9	3.602 (708919:5113157) 32.1

4.3.8 Modeling study in PIC domain

Emission of NO_x and SO_2 from Neenah Paper industry and 44.54 km and 19.38 km section length of highways 104 and 106 respectively were used for the dispersion study in PIC domain during 2007.

4.3.8.1 Annual Averaging of NO_x and SO_2

GLC contour maps of NO_x and SO_2 during annual averaging period are shown in Figures 57 and 58. Both point sources and highways contributed high GLCs in this domain. As seen from Figures 57 and 58, the highest annual average NO_x and SO_2 concentration gradients are seen at 13.7 km South East of the Neenah Paper industry. The advection of pollutants was governed by the prevailing wind towards North East. Some high concentrations are seen near the intersection of the highways 104 and 106 due to large number of vehicle flow at the intersection. With reference to Table 30, the minimum and maximum annual average predicted NO_x concentrations were 0.019 $\mu g\ m^{-3}$ located at 504601.09m: 5047573m, elevation 301.8 and 2.32 $\mu g\ m^{-3}$ located at 534293.6m: 5047573m, elevation 66.1 m respectively. The annual minimum and maximum predicted SO_2 concentrations were 0.017 $\mu g\ m^{-3}$ found at 504601.09m: 5047573m, elevation NA and 0.1.226 $\mu g\ m^{-3}$ at 534293.6m: 5047573m, elevation 66.1 m respectively. As seen from Table 30, the highest concentration receptor remained unchanged for both the pollutants.

Figure 57 Annual GLCs of NO_x due to point and highway emission sources

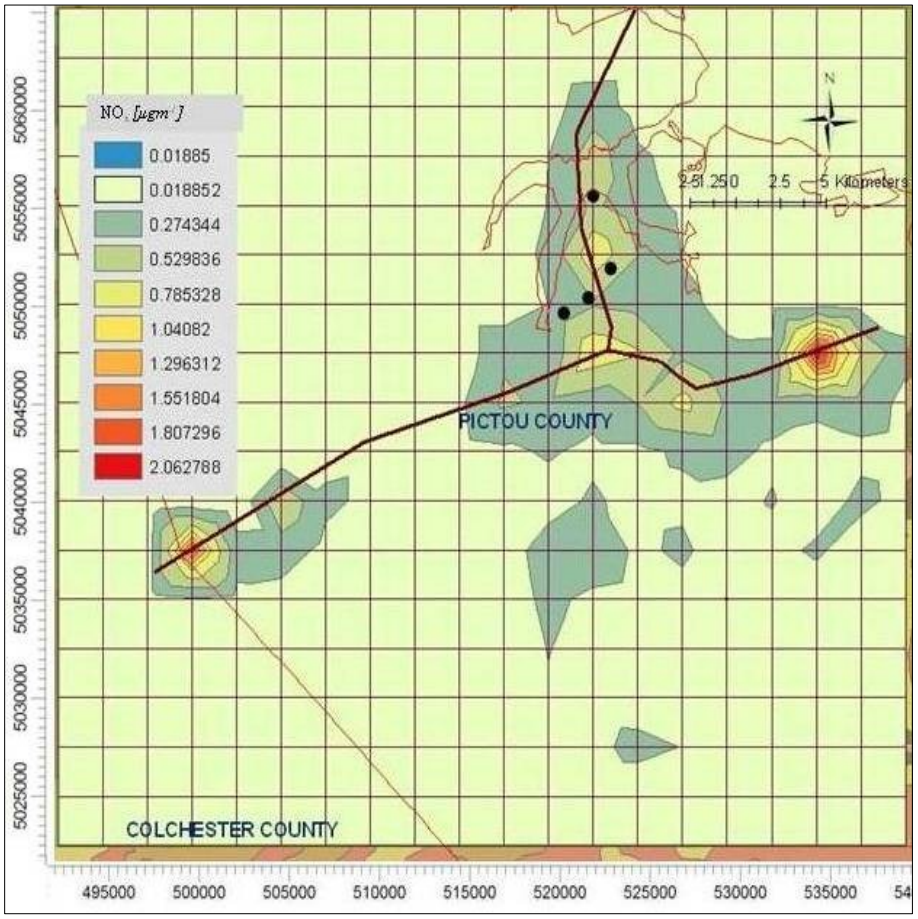

Figure 58 Annual GLCs of SO_2 due to due to point and highway emission sources

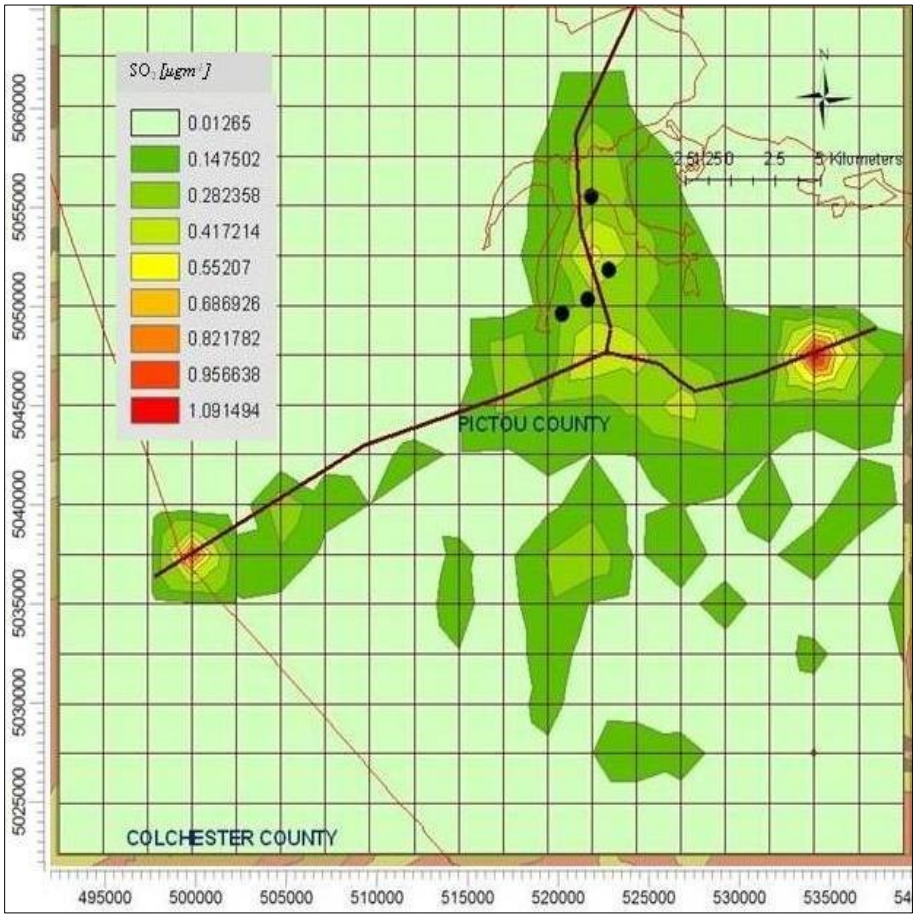

Table 30 Annual MAX and MIN GLCs of NO_x and SO_2

Pollutant	Annual Min *[µg m^{-3}]* UTM coordinate (m) Elevation (m)	Annual Max *[µg m^{-3}]* UTM coordinate (m) Elevation (m)
NO_x	0.019 (504601.09:5047573) 301.8	2.32 (534293.6:5047573) 66.1
SO_2	0.013 (504601.09:5047573) 301.8	1.226 (534293.6:5047573) 66.1

4.3.8.2 Monthly averaging of NO_x and SO_2

Figures 59 and 60 show monthly concentration contour maps of NO_x and SO_2. As seen from Figures 59 and 60, dispersion patterns of NO_x and SO_2 were similar to each other and highways contributed larger amount of pollutants than the point emission sources. From Table 31 it is seen that the minimum and maximum monthly NO_x concentrations were 1.744 μg m^{-3} (March) at coordinates 534293.6m: 5047573m, elevation 66.1 and 3.14 μg m^{-3} (February) at coordinates 534293m.6:5047573m, elevation 66.1m respectively. The minimum and maximum monthly predicted SO_2 concentrations are 0.924 μg m^{-3} (March) at coordinates 534293.6m: 5047573m, elevation 66.1m and 1.653 μg m^{-3} (October) at coordinates 534293m.6:5047573m, elevation 66.1m respectively. Monthly averaging results show that the high concentration values persisted during winter months due to stable atmospheric conditions. There were no significant changes in GLCs during summer months due to lower amount of NO_x and SO_2 release from highway emissions.

Figures 59a-l Monthly GLCs of NO_x due to point and highway emission sources

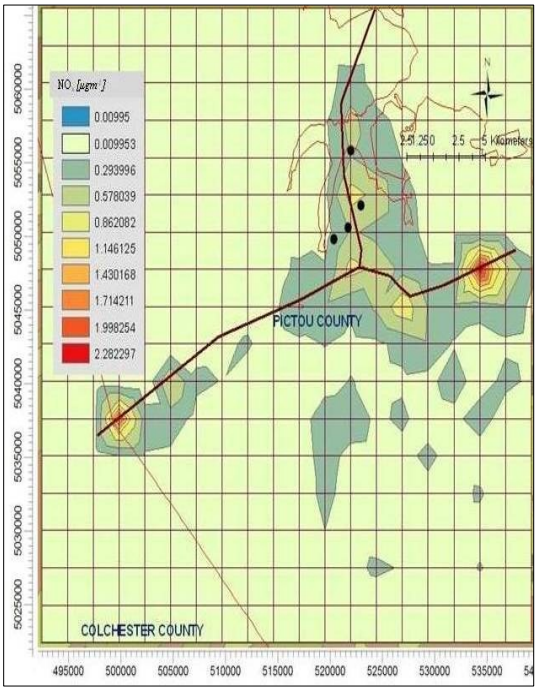

a. January

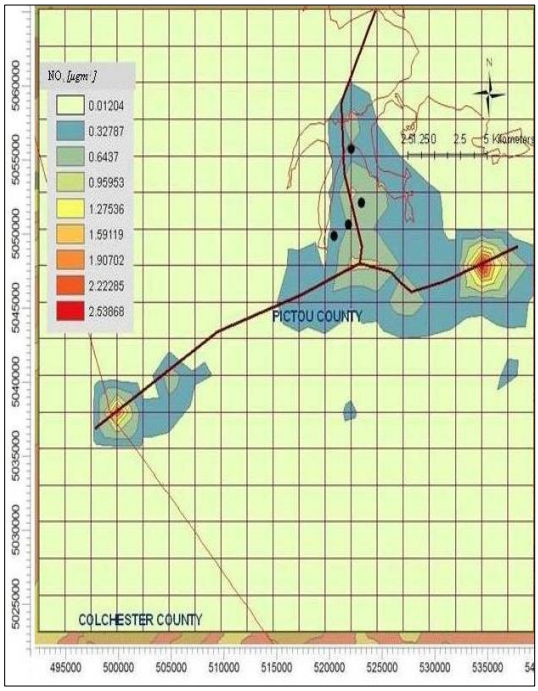

b. February

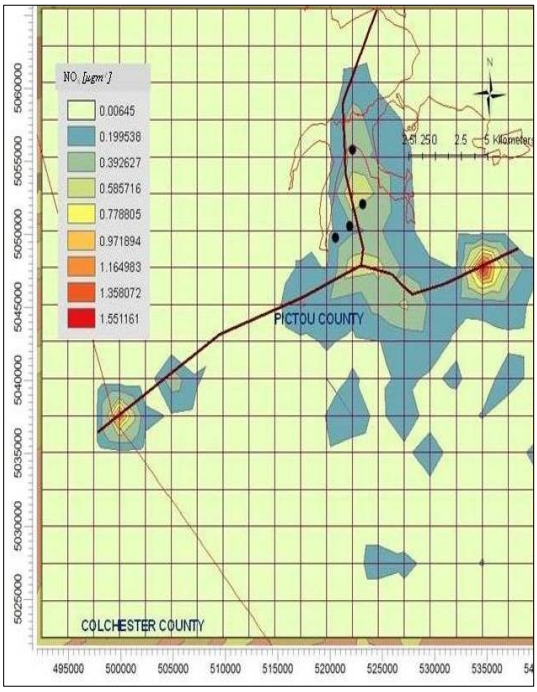

c. March

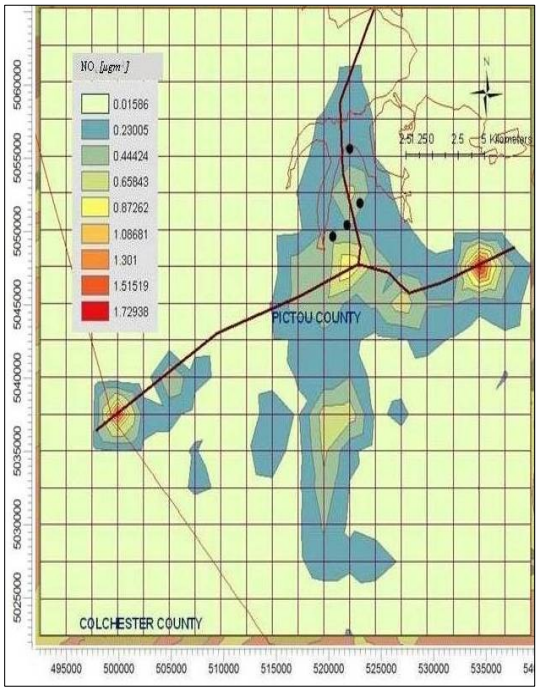

d. April

(Figures Cont'd)

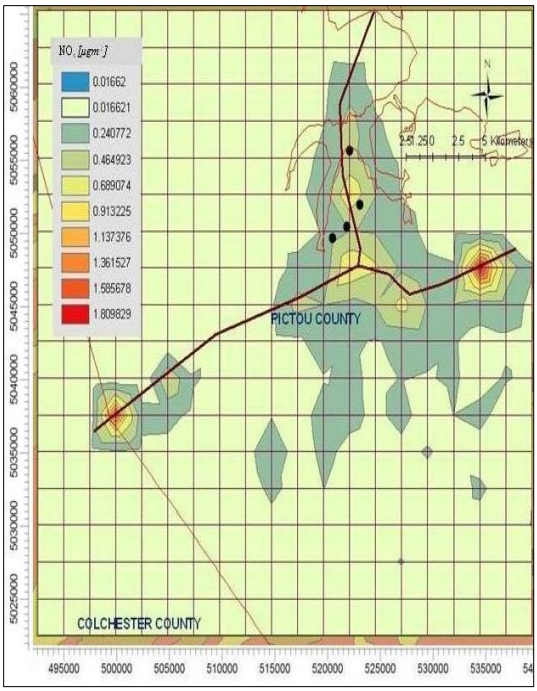

e. May

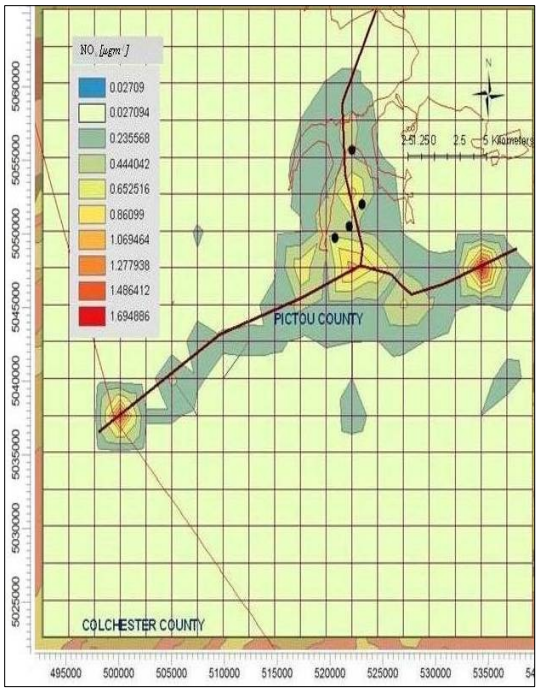

f. June

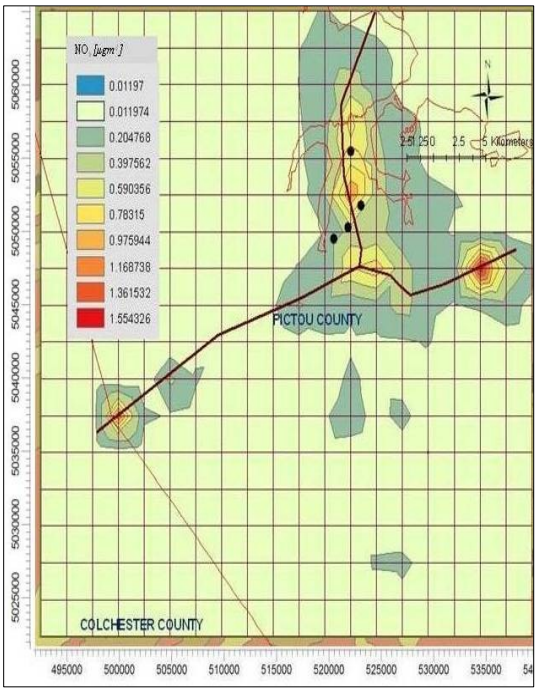

g. July

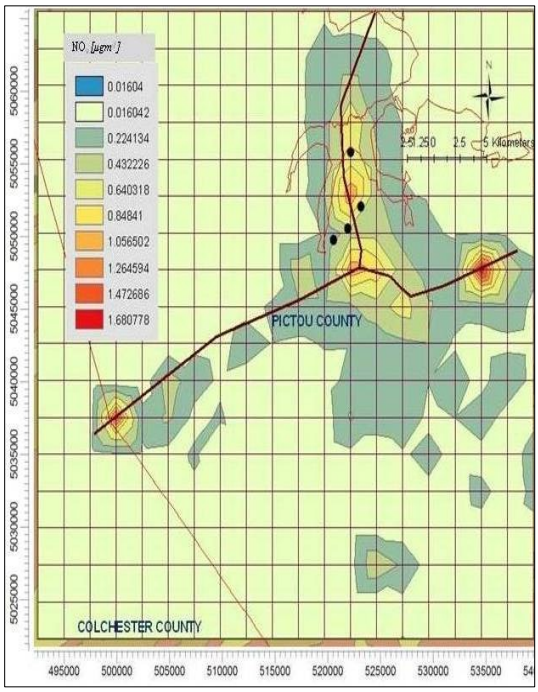

h. August

(Figures Cont'd)

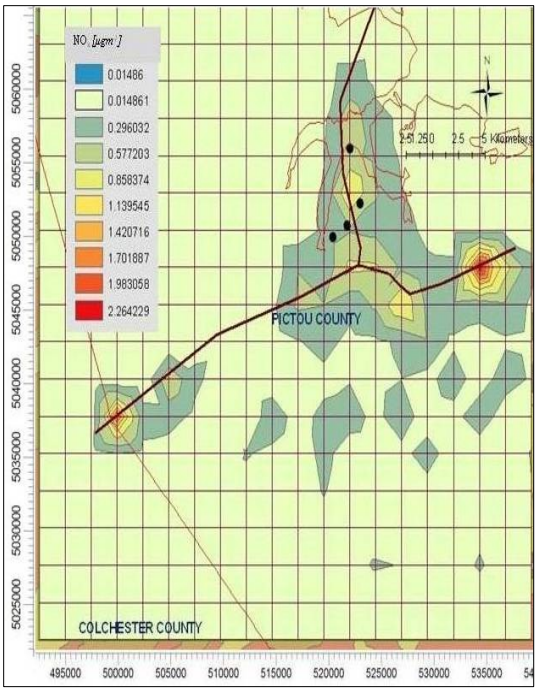

i. September

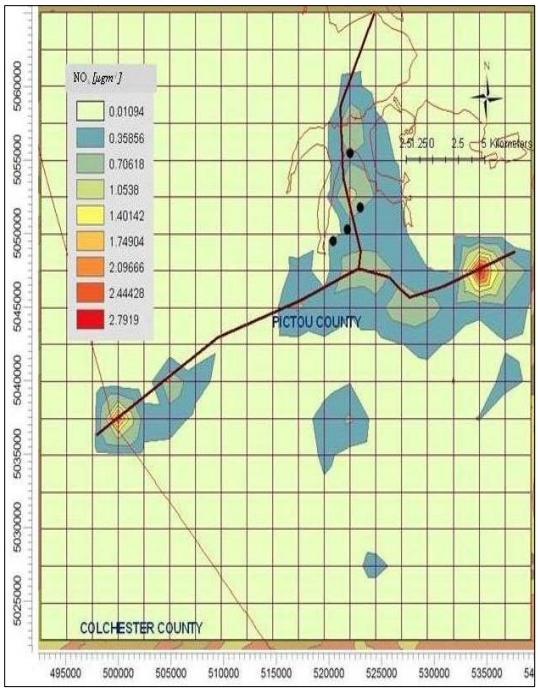

j. October

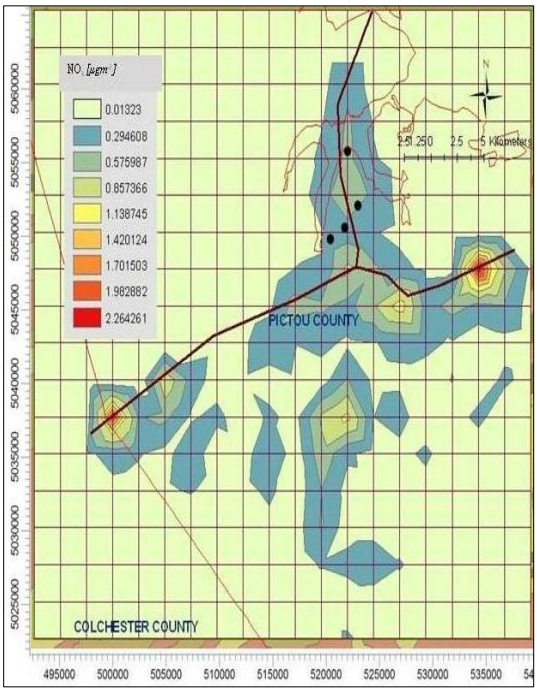

k. November

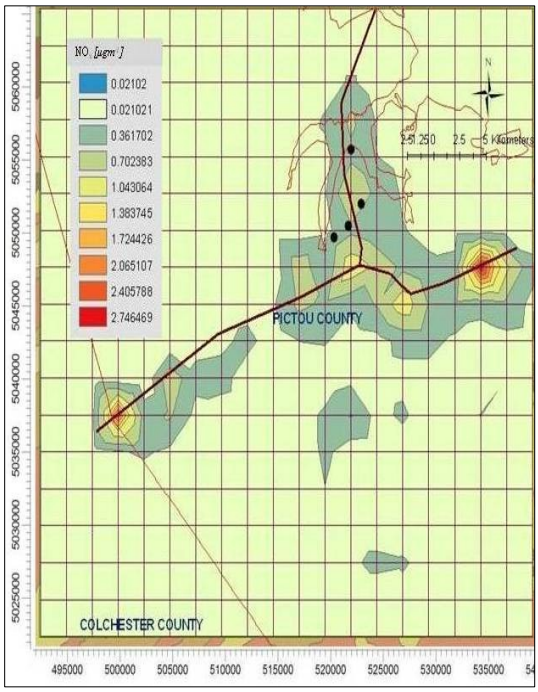

l. December

Figures 60a-l Monthly GLCs of SO_2 due to point and highway emission sources

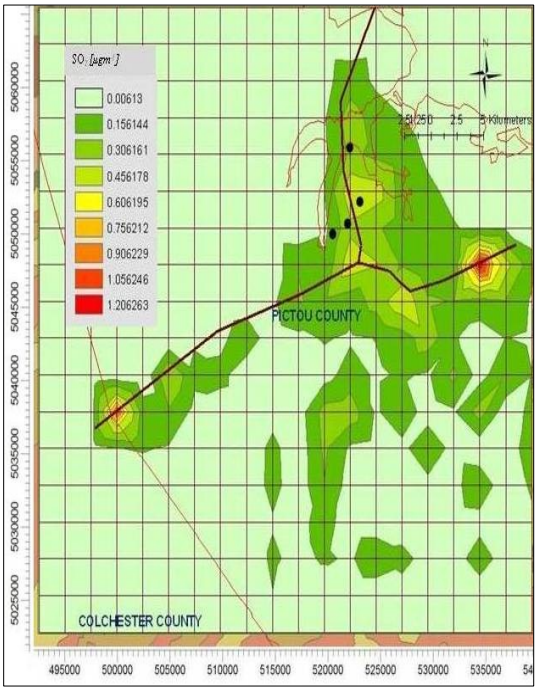

a. January

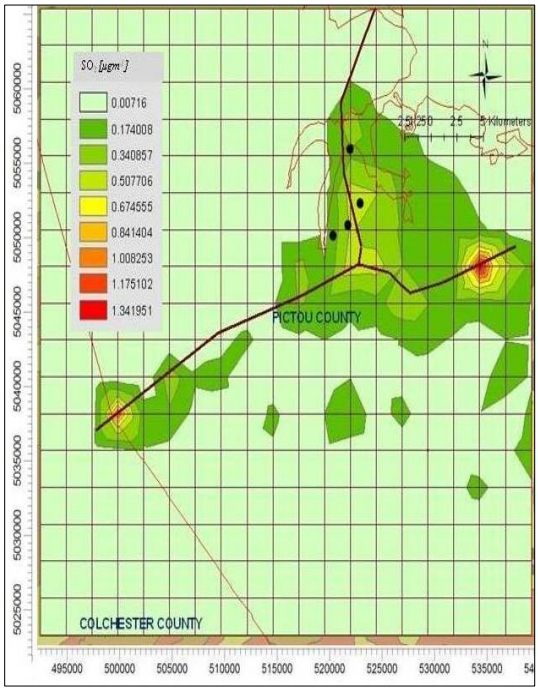

b. February

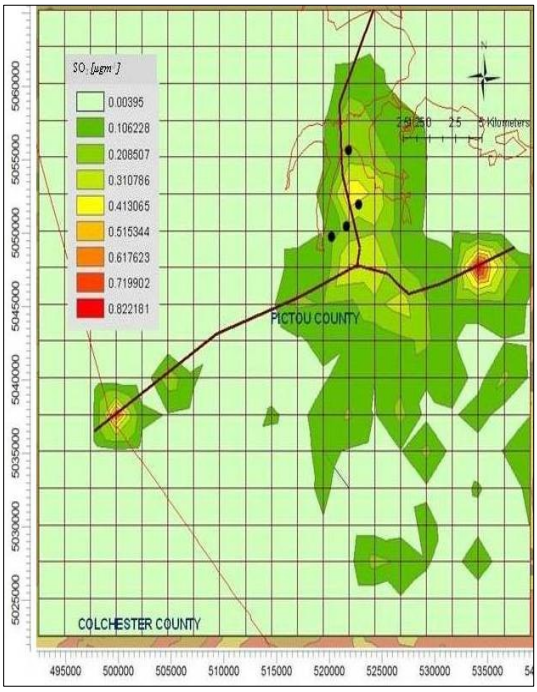

c. March

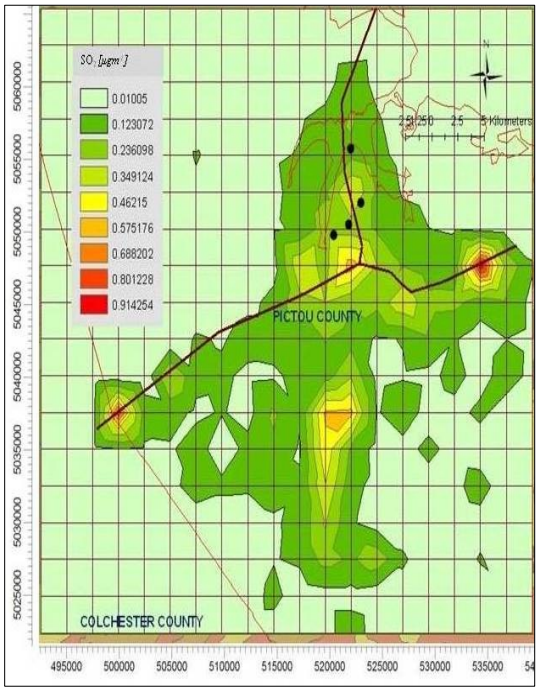

d. April

(Figures Cont'd)

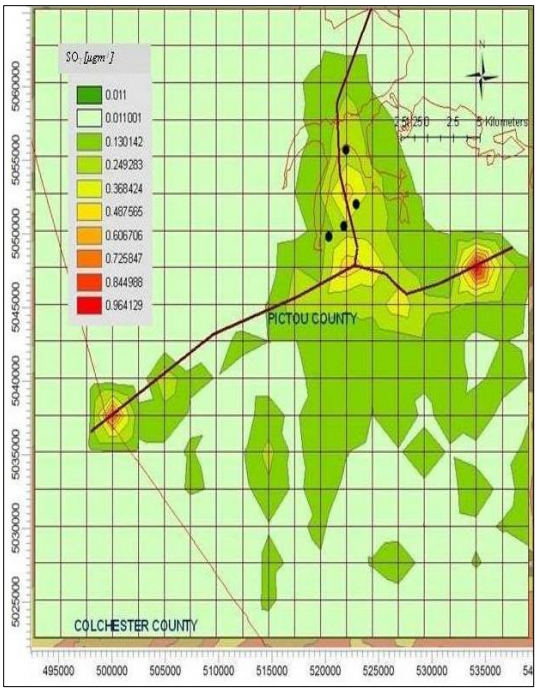

e. May

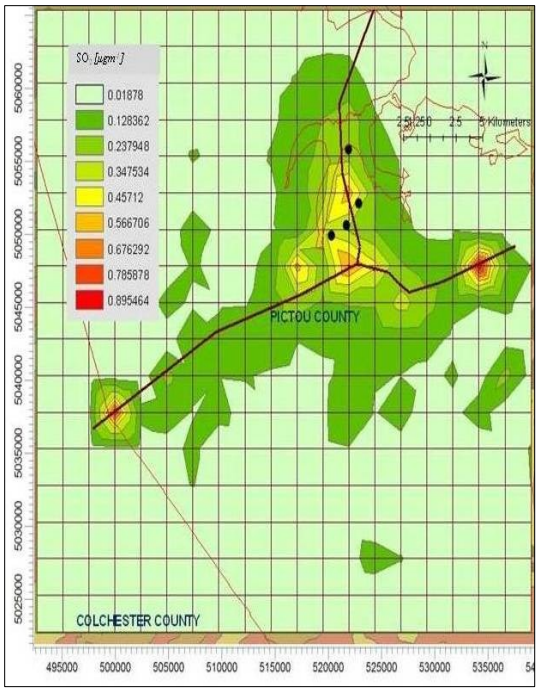

f. June

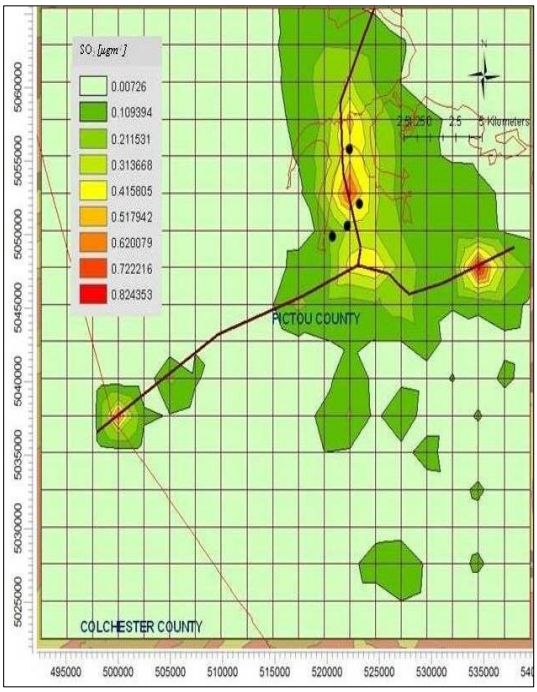

g. July

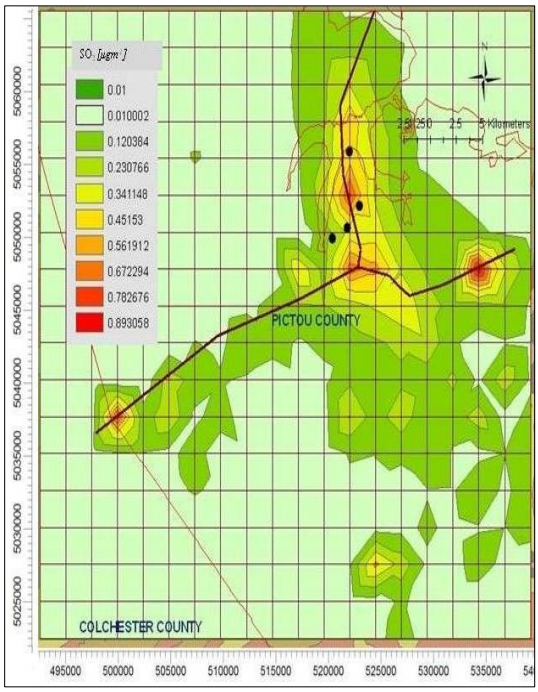

h. August

(Figures Cont'd)

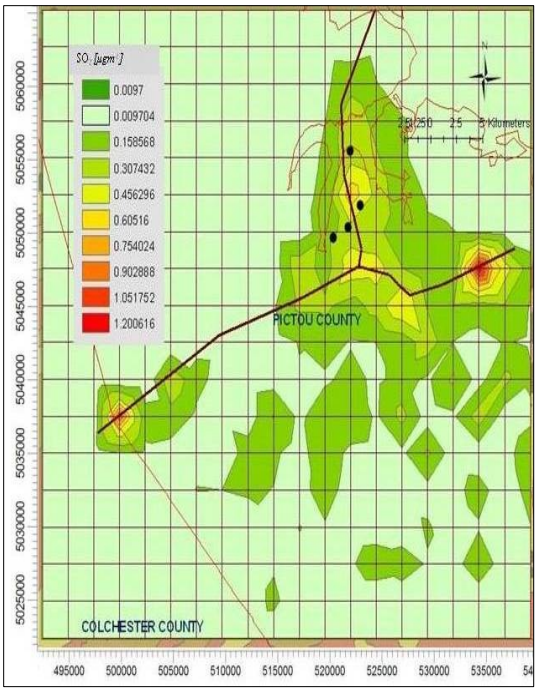

i. September

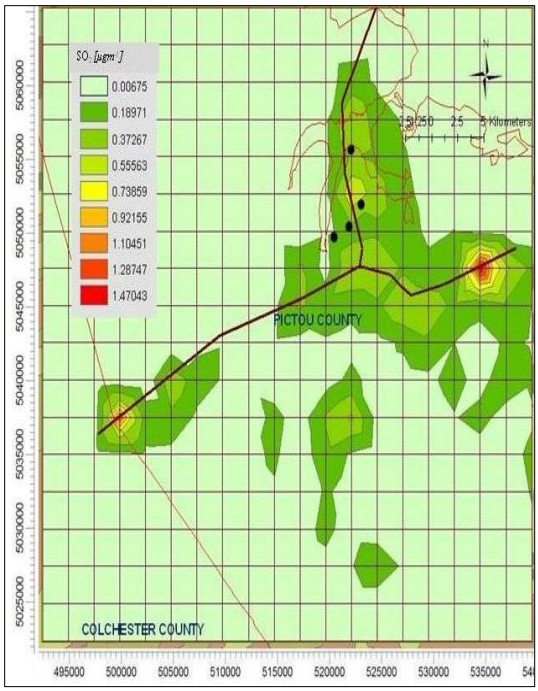

j. October

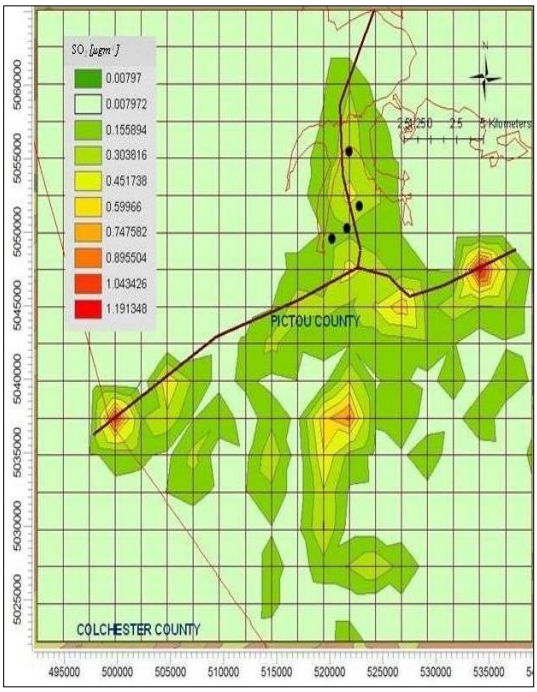

k. November

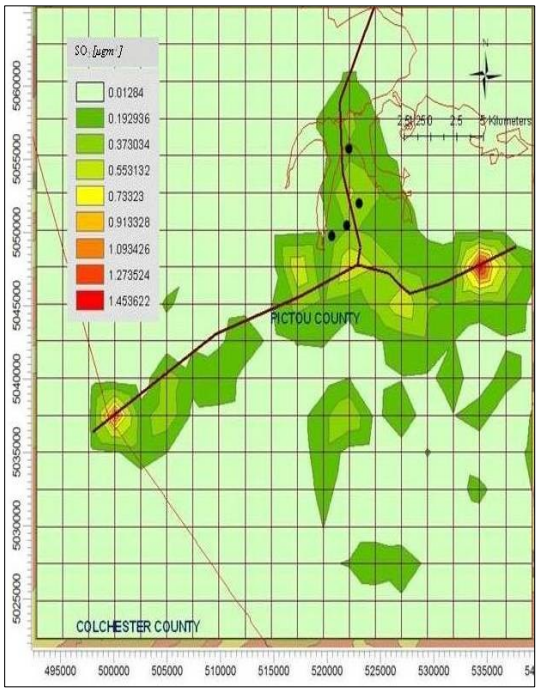

l. December

Table 31 Monthly MAX and MIN GLCs of NO_x and SO_2

	NO_x		SO_2	
Month	Monthly Min *[μg m^{-3}]* UTM coordinate (m) Elevation (m)	Monthly Max *[μg m^{-3}]* UTM coordinate (m) Elevation (m)	Monthly Min *[μg m^{-3}]* UTM coordinate (m) Elevation (m)	Monthly Max *[μg m^{-3}]* UTM coordinate (m) Elevation (m)
Jan	0.01 (499652.31:5047573) 275.4	2.566 (534293.6:5047573) 66.1	0.006 (497178:5045064) 253.4	1.356 (534293.6:5047573) 66.1
Feb	0.012 (502127:5045064) 280.7	2.855 (534293.6:5047573) 66.1	0.007 (502127:5045064) 280.7	1.509 (534293.6:5047573) 66.1
Mar	0.006 (497178:5045064) 253.4	1.744 (534293.6:5047573) 66.1	0.004 (497178:5045064) 253.4	0.924 (534293.6:5047573) 66.1
Apr	0.016 (539242:5065136.5) NA	1.944 (534293.6:5047573) 66.1	0.01 (539242:5065136.5) NA	1.027 (534293.6:5047573) 66.1
May	0.017 (504601.09:5047573) 301.8	2.034 (534293.6:5047573) 66.1	0.011 (504601.09:5047573) 301.8	1.083 (534293.6:5047573) 66.1
June	0.027 (539242:5065136.5) NA	1.903 (534293.6:5047573) 66.1	0.019 (539242:5065136.5) NA	1.005 (534293.6:5047573) 66.1
July	0.012 (492229:5055100.5) NA	1.747 (534293.6:5047573) 66.1	0.007 (492229:5027500.5) NA	0.926 (534293.6:5047573) 66.1
Aug	0.016 (504601.09:5047573) 301.8	1.889 (534293.6:5047573) 66.1	0.01 (504601.09:5047573) 301.8	1.003 (534293.6:5047573) 66.1
Sep	0.015 (499652.31:5047573) 275.4	2.545 (534293.6:5047573) 66.1	0.01 (492229:5052591.5) NA	1.349 (534293.6:5047573) 66.1
Oct	0.011 (504601:5050082.5) 285.9	3.14 (534293.6:5047573) 66.1	0.007 (499652.31:5047573) 275.4	1.653 (534293.6:5047573) 66.1
Nov	0.013 (504601.09:5047573) 301.8	2.546 (534293.6:5047573) 66.1	0.008 (499652.31:5047573) 275.4	1.339 (534293.6:5047573) 66.1
Dec	0.021 (516973:5024991.5) 261.1	3.087 (534293.6:5047573) 66.1	0.013 (516973:5024991.5) 261.1	1.634 (534293.6:5047573) 66.1

4.3.8.3 Hourly Averaging of NO_x and SO_2

Figures 61 and 62 show hourly GLC contours maps of NO_x and SO_2 respectively. As seen from Figures, 61 and 62 South and Eastern areas of the domain receive high GLCs of NO_x and SO_2. This phenomenon could be due to moderately high surface roughness of the cultivated land along with influence of wind direction. As seen from Table 32 the highest concentration values were seen at receptors with high elevations as the AERMOD predicts higher GLC values at higher elevations (US EPA, 1998).

Figures 61a-e Hourly GLCs of NO_x due to point and highway emission sources

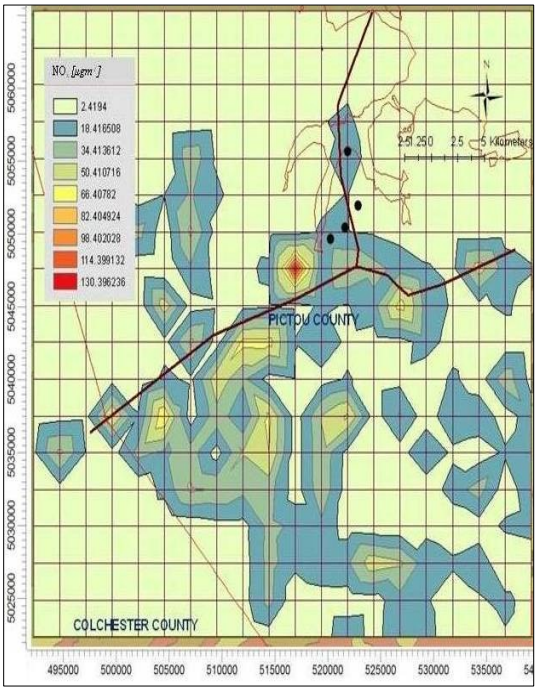

a. 1 hour

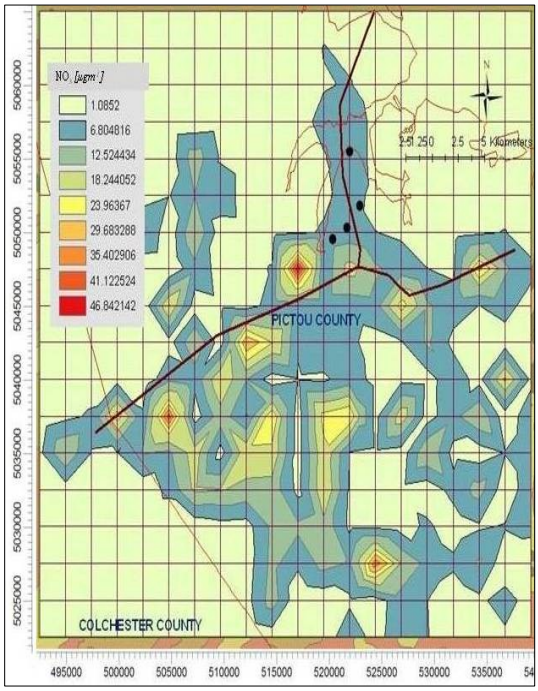

b. 3 hour

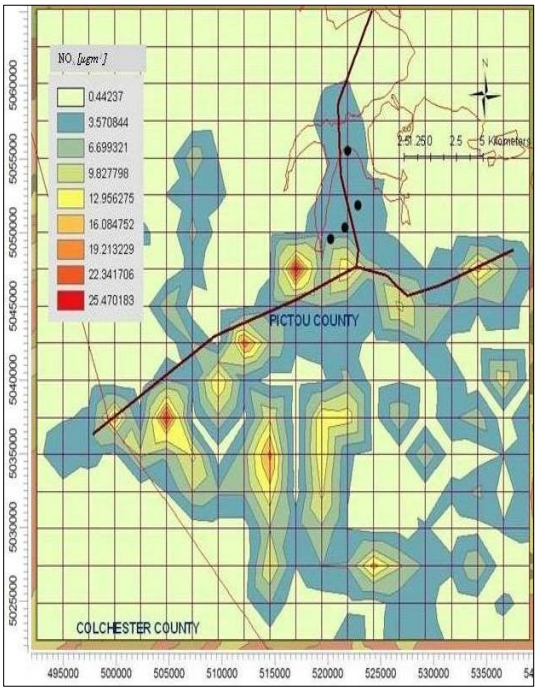

c. 8 hour

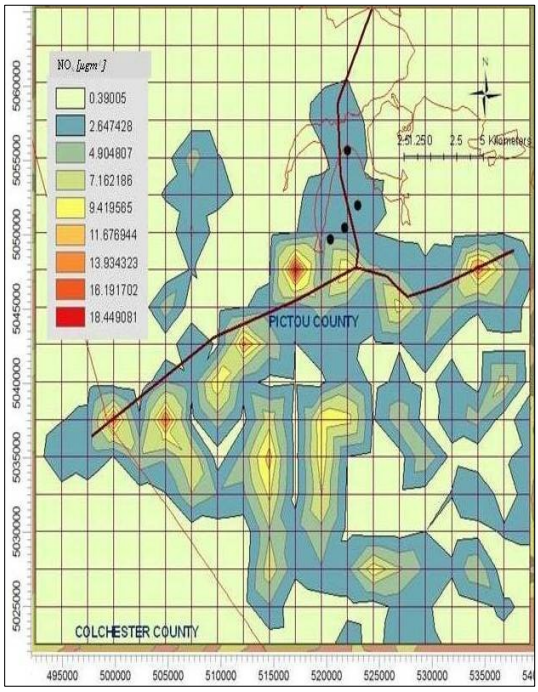

d. 12 hour

(Figure Cont'd)

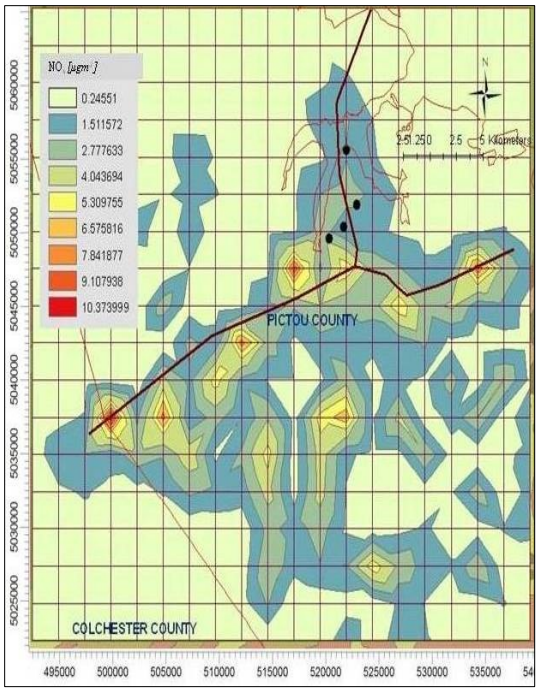
NO2 [µgm-3]
0.24551
1.511572
2.777633
4.043694
5.309755
6.575816
7.841877
9.107938
10.373999
N
2.5 1.25 0 2.5 5 Kilometers
PICTOU COUNTY
COLCHESTER COUNTY
5060000
5055000
5050000
5045000
5040000
5035000
5030000
5025000
495000
500000
505000
510000
515000
520000
525000
530000
535000

e. 24 hour

Figures 62a-e Hourly GLCs of SO_2 due to point and highway emission sources

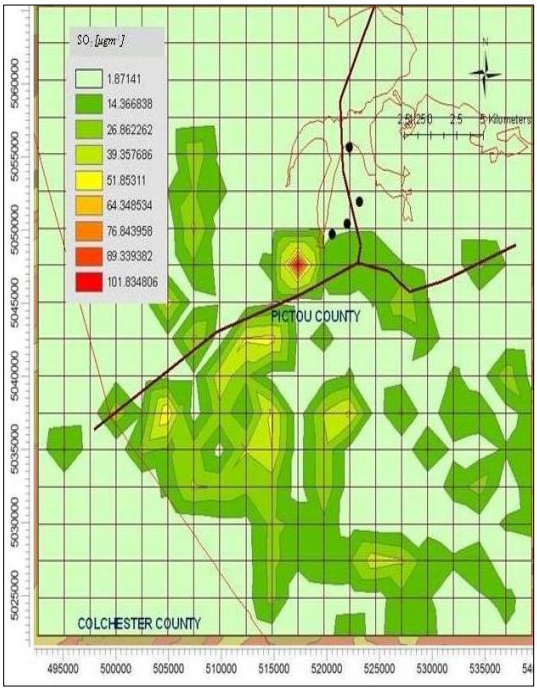

a. 1 hour

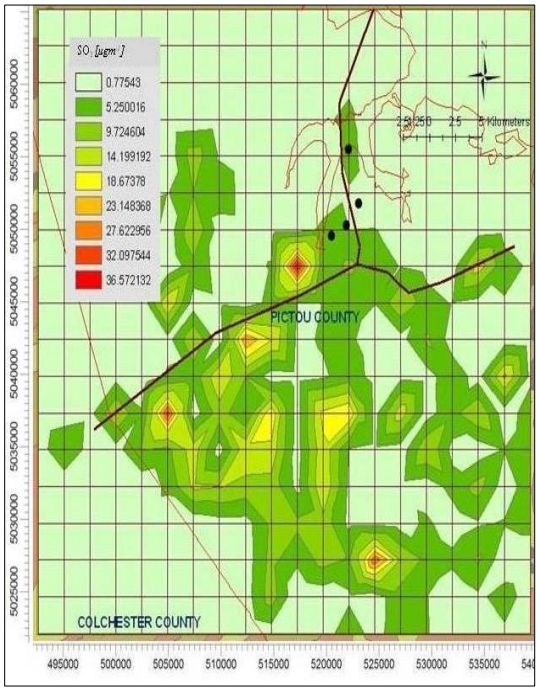

b. 3 hour

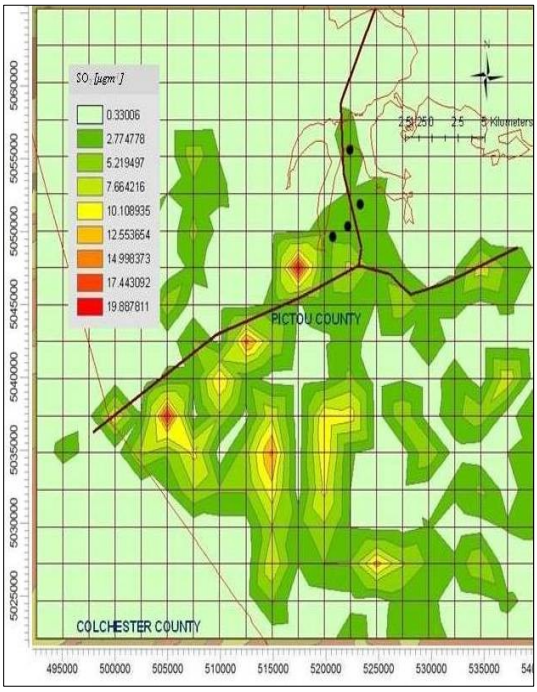

c. 8 hour

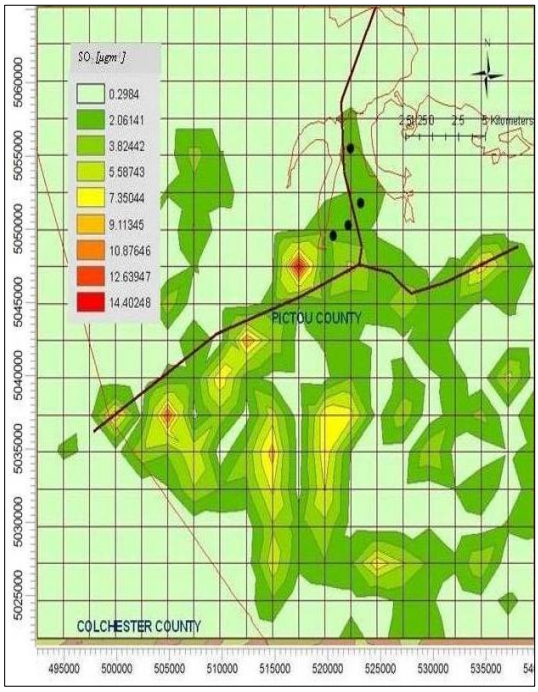

d. 12 hour

(Figure Cont'd)

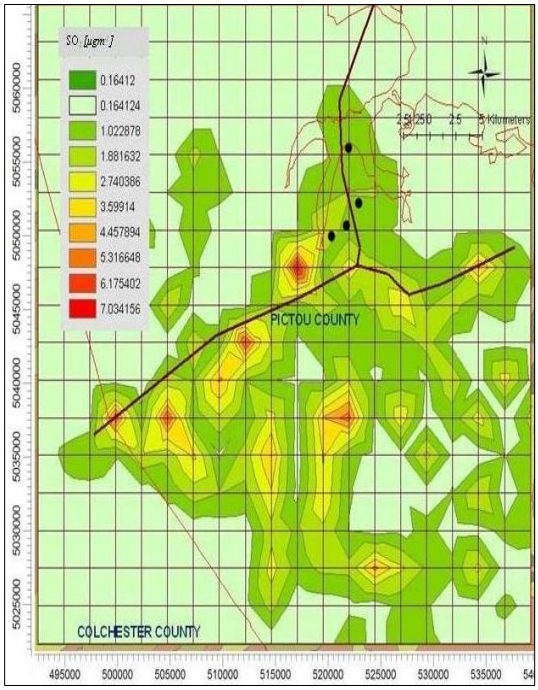

e. 24 hour

Table 32 Hourly MAX and MIN GLCs of NO_x and SO_2

	NO_x		SO_2	
Hour	Hourly Min *[µg m^{-3}]* UTM coordinate (m) Elevation (m)	Hourly Max *[µg m^{-3}]* UTM coordinate (m) Elevation (m)	Hourly Min *[µg m^{-3}]* UTM coordinate (m) Elevation (m)	Hourly Max *[µg m^{-3}]* UTM coordinate (m) Elevation (m)
1	2.419 (539242.38:5065136.5) NA	146.4 (516973:5047573) 148.8	1.871 (539242.38:5065136.5) NA	114.33 (516973:5047573) 148.8
3	1.085 (492229.19:5055100.5) NA	52.562 (516973:5047573) 148.8	0.775 (497177.93:5022482.5) NA	41.05 (516973:5047573) 148.8
8	0.442 (4992229.19:5047573) NA	28.56 (516973:5047573) 148.8	0.33 (492229.19:5047573) NA	22.33 (516973:5047573) 148.8
12	0.39 (539242.38:5060118.5) NA	20.71 (516973:5047573) 148.8	0.298 (534293.63:5065136.5) NA	16.165 (516973:5047573) 148.8
24	0.246 (492229.19:5055100.5) NA	11.64 (499652.3:5037537) 203.9	0.164 (492229.19:5055100.5) NA	7.89 (516973:5047573) 148.8

4.3.9 $PM_{2.5}$ modeling study in PIC domain

Emission of $PM_{2.}$from Neenah Paper industry and 44.54 km and 19.38 km section length of highways 104 and 106 respectively were used for dispersion study in PIC domain during 2004.

4.3.9.1 Annual averaging of $PM_{2.5}$

GLC contour maps of $PM_{2.5}$ in PIC domain during annual averaging period is shown in Figure 63. As seen from the figure, both highways and point sources contributed high GLC in this domain. The advection of pollutant was governed by the prevailing wind blowing towards North East. Some high concentrations are seen near the intersection of the highways 104 and 106 due to more number of vehicles, recorded from the emission inventory (Green, 2008). The annual minimum and maximum predicted $PM_{2.5}$ concentration was 0.017 µg m^{-3} found at 492229.19m: 5045064m, elevation NA and 0.884 µg m^{-3} at the coordinate 521921.8m: 5052592m elevation 30.1m respectively.

Figure 63 Annual GLCs of $PM_{2.5}$ due to due to point and highway emission sources

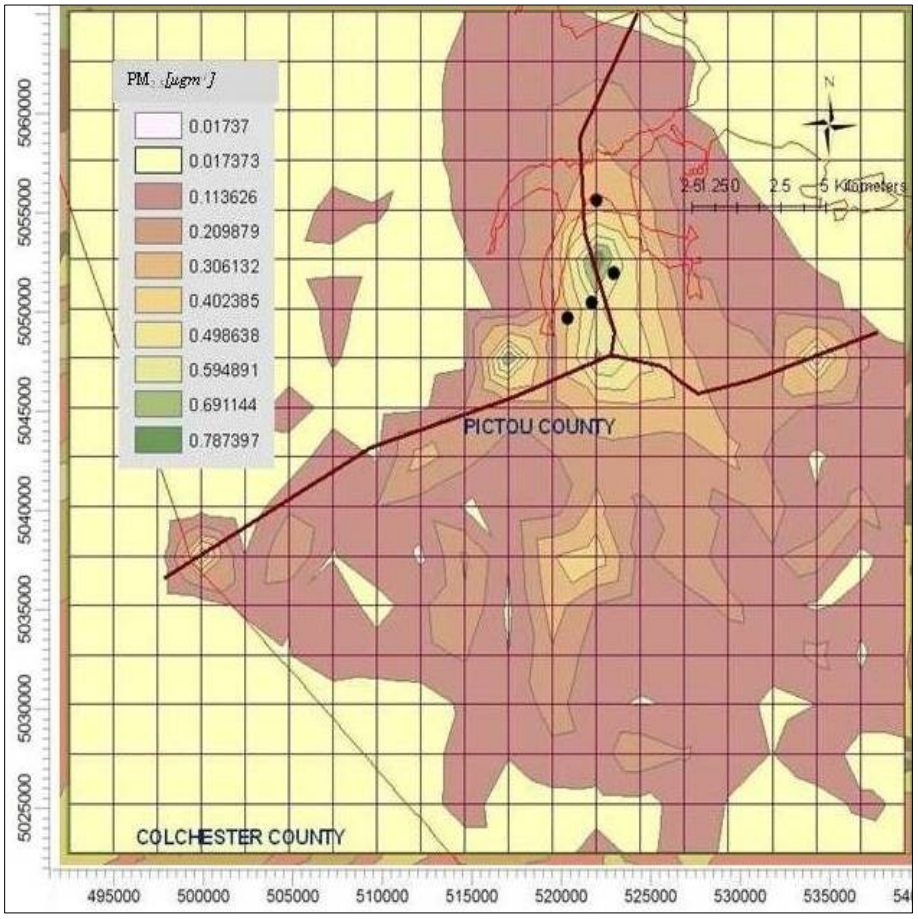

4.3.9.2 Monthly averaging of NO_x and SO_2

Figure 64 shows the monthly maps of ground level $PM_{2.5}$ concentration contours. According to the maps, highest GLC of $PM_{2.5}$ is seen at 1 km downwind of the Neenah Paper industry during most of the months. As seen from the Table 33, the minimum and maximum monthly $PM_{2.5}$ concentrations were 0.855 µg m^{-3} (May) at coordinates 534293.6m: 5047573m, elevation 66.1m and 1.474 µg m^{-3} (January) at coordinates 534293.6m: 5047573m, elevation 66.1m respectively. Monthly averaging results show the high concentrations of the pollutants were found in the winter months due to stable atmospheric conditions. No significant variation was seen in GLCs during summer months. Ground level $PM_{2.5}$ concentration values were found in southern part of the domain due to moderately high surface roughness of the cultivated land.

Figures 64a-k Monthly GLCs of $PM_{2.5}$ due to point and highway emission sources

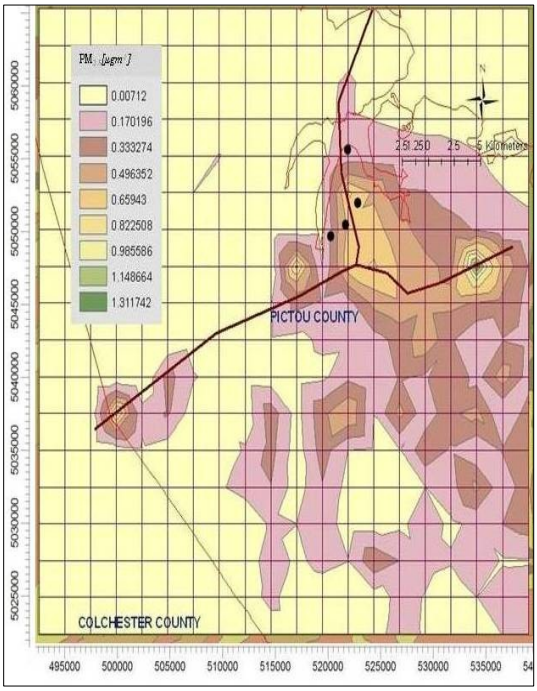

a. January

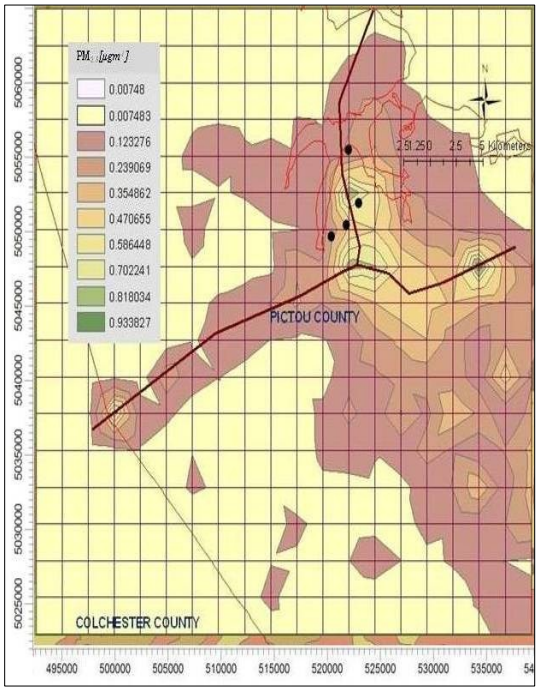

b. February

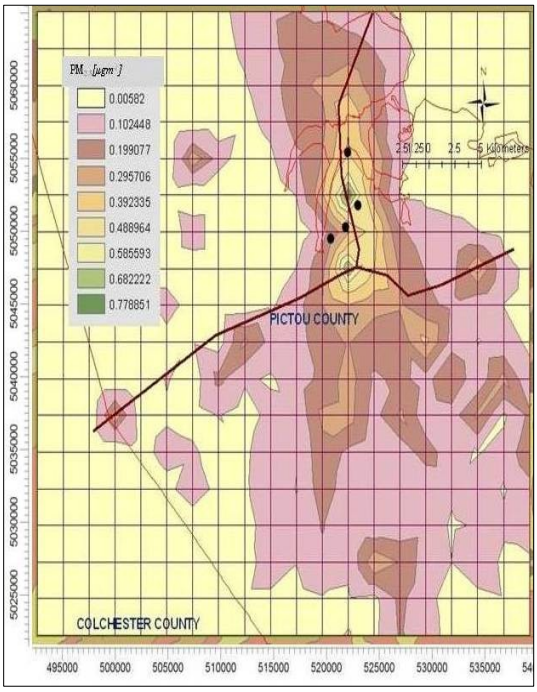

c. April

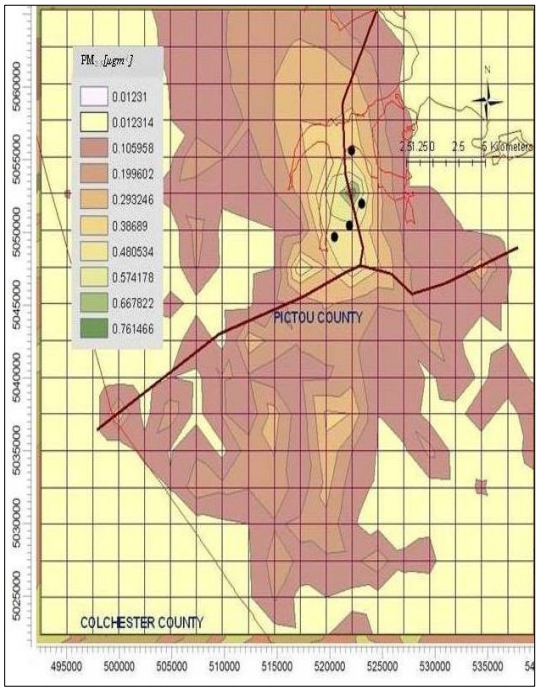

d. May

(Figures Cont'd)

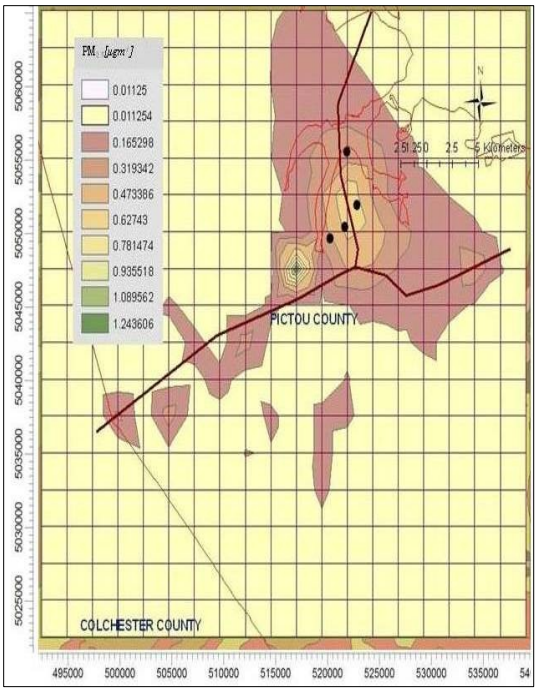

e. June

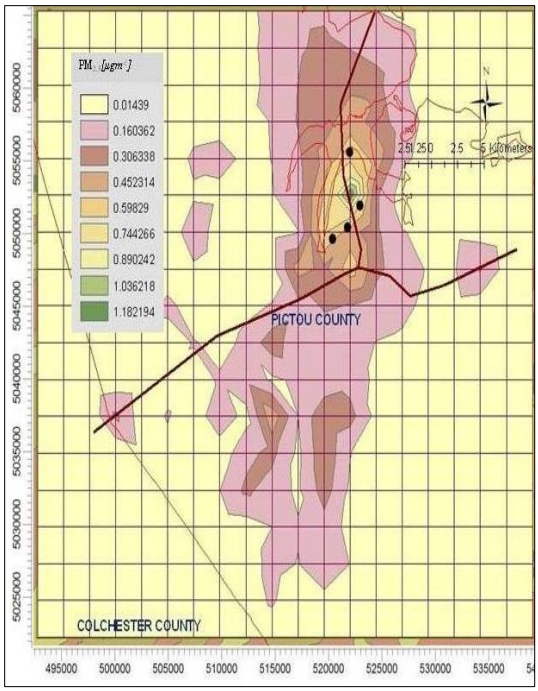

f. July

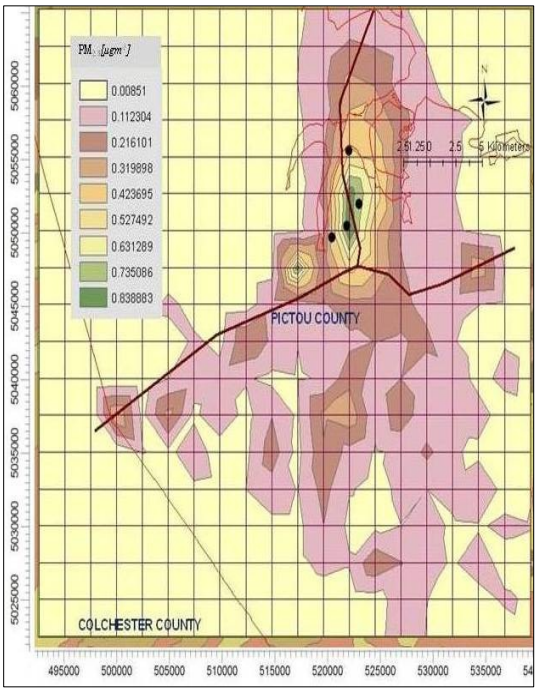

g. August

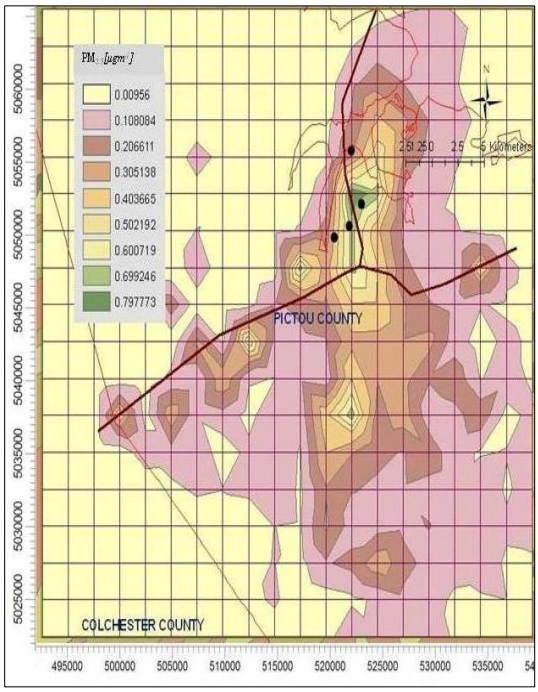

h. September

(Figures Cont'd)

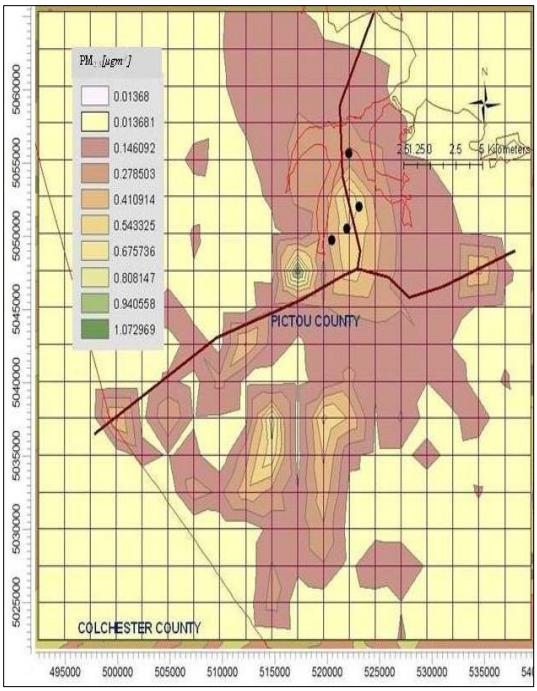

i. October

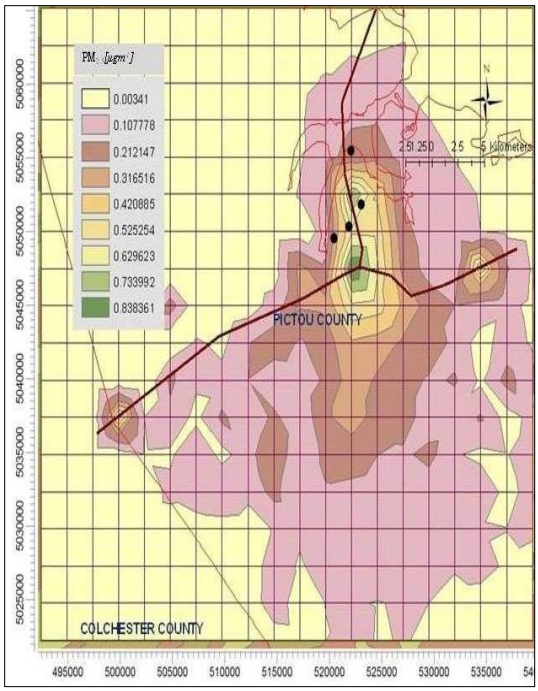

j. November

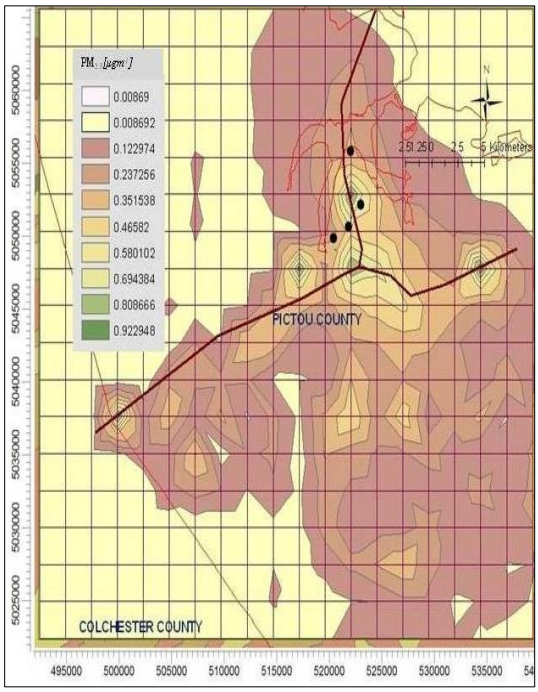

k. December

Table 33 Monthly MAX and MIN GLCs of $PM_{2.5}$

	$PM_{2.5}$	
Month	Monthly Min *[$\mu g\ m^{-3}$]* UTM coordinate (m) Elevation (m)	Monthly Max *[$\mu g\ m^{-3}$]* UTM coordinate (m) Elevation (m)
Jan	0.007 (502127:5045064) 280.7	1.474 (534293.6:5047573) 66.1
Feb	0.007 (499652.31:5047573) 275.4	1.05 (534293.6:5047573) 66.1
Mar	NA NA NA	NA NA NA
Apr	0.006 (494704:5035028) NA	0.875 (521921.8:5052592) 30.1
May	0.012 (492229:5027500.5) NA	0.855 (521921.8:5052592) 30.1
June	0.011 (502127:5022482.5) NA	1.398 (516973:5047573) 148.8
July	0.014 (492229:5042555) NA	1.328 (521921.8:5052592) 30.1
Aug	0.009 (492229:5052591.5) NA	0.943 (521921.8:5050083) 54.8
Sep	0.01 (497178:5045064) 253.4	0.896 (521921.8:5052592) 30.1
Oct	0.014 (492229:5032519) NA	1.205 (516973:5047573) 148.8
Nov	0.003 (499652.31:5047573) 275.4	0.943 (521921.8:5047573) 38.9
Dec	0.009 (504601.09:5047573) 301.8	1.037 (534293.6:5047573) 66.1

4.3.9.3 Hourly Averaging of $PM_{2.5}$

Figure 65 shows hourly maps of GLC contours of $PM_{2.5.}$ With reference to the meteorological data it can be seen that the lower wind speed during early morning hours affected the dispersion. Due to wind speed increasing during the afternoon and evening, $PM_{2.5}$ advected longer distances during later hours of the day. During the 24-hr period, the difference between the highest and lowest GLC was least, which indicates that the larger amount of dispersal took place within late afternoon. As seen from Table 34, highest concentration receptor remained unchanged throughout the day.

Figures 65a-e Hourly GLCs of $PM_{2.5}$ due to point and highway emission sources

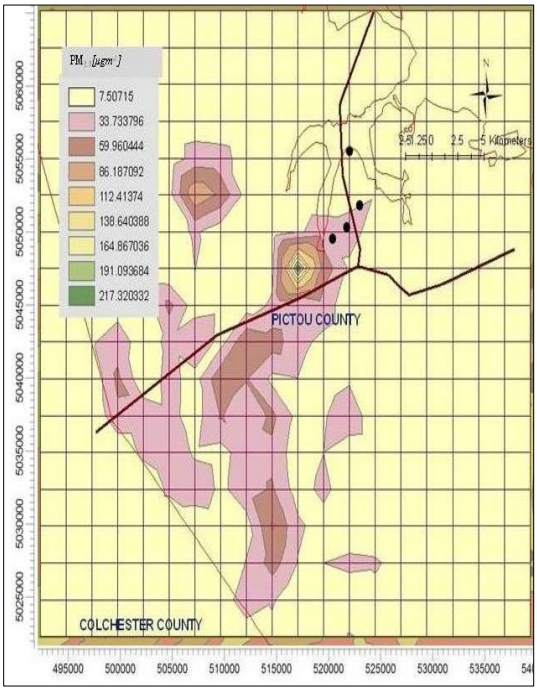

a. 1 hour

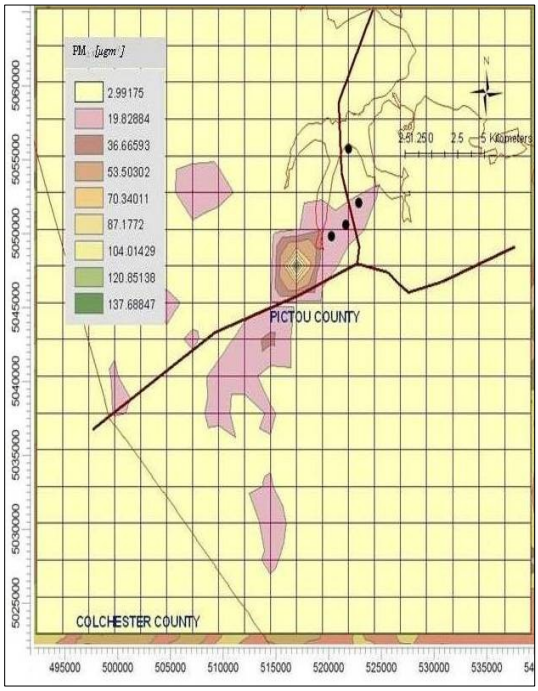

b. 3 hour

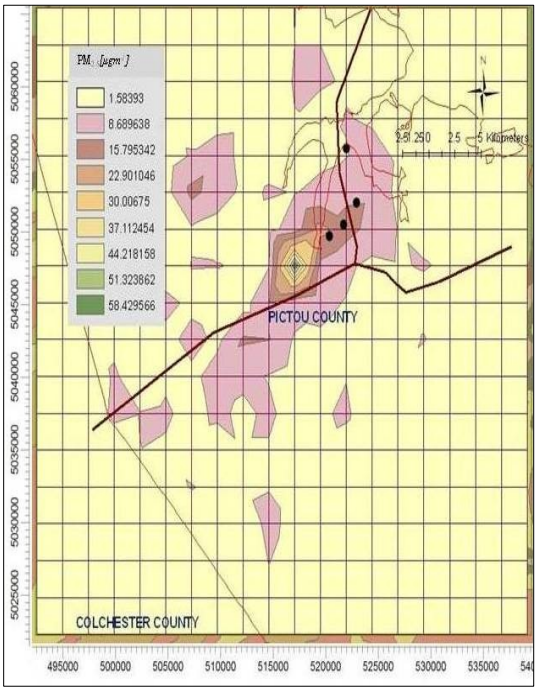

c. 8 hour

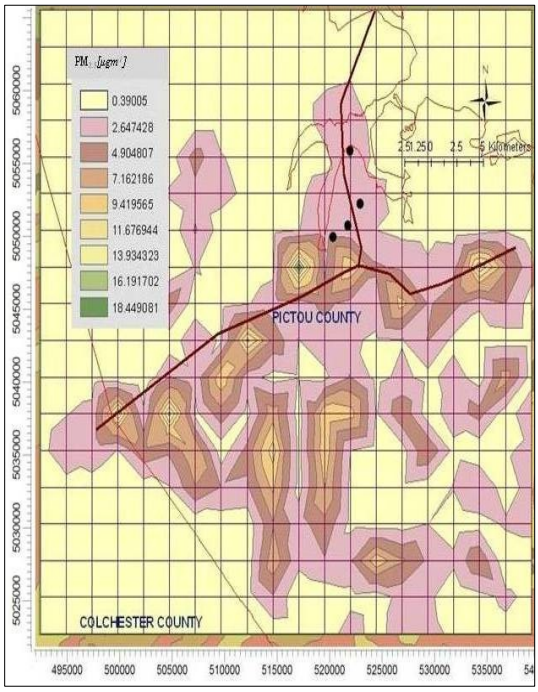

d. 12 hour

(Figure Cont'd)

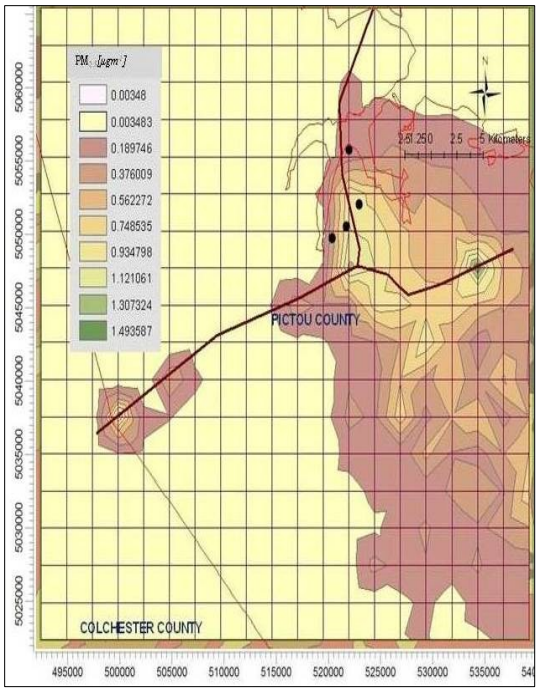

e. 24 hour

Table 34 Hourly MAX and MIN GLCs of $PM_{2.5}$

	$PM_{2.5}$	
Hour	Hourly Min *[µg m^{-3}]* UTM coordinate (m) Elevation (m)	Hourly Max *[µg m^{-3}]* UTM coordinate (m) Elevation (m)
1	7.507 (531819.25:5024991.5) 215.5	243.547 (516973:5047573) 148.8
3	2.992 (499652.31:5022482.5) NA	154.526 (516973:5047573) 148.8
8	1.584 (499652.31:5024991.5) NA	65.535 (516973:5047573) 148.8
12	0.987 (497177.94:5022482.5) NA	43.699 (516973:5047573) 148.8
24	0.003 (499652.31:5047573) 275.4	1.68 (534293.6:5047573) 66.1

4.3.10 Modeling study in HFX domain

Emission of NO_x, SO_2 and $PM_{2.5}$ from Dartmouth oil refinery, Capital Health, Dalhousie University, Tuft's cove power generation station, 56.66 km of highway 101, 57.83 km of highway 102, 12.8 km of highway 103, 36.86 km of highway 107, 9.04 km of highway 111 and 32.65 km of highway 118 were used for conducting the dispersion simulation study in HFX domain during 2004.

4.3.10.1 Annual averaging of NO_x, SO_2 and $PM_{2.5}$

Annual GLC contour maps of NO_x, SO_2 and $PM_{2.5}$, are presented in Figures 66 through 68. It can be seen in Figures 66 and 67, the highest predicted surface concentration gradients for NO_x and SO_2 were centered on, and immediately to the East South East, of the Oil refinery in Dartmouth. Although this spatial pattern is still evident in Figure 68 for $PM_{2.5}$, the highest $PM_{2.5}$ concentrations in the Halifax domain were found at the intersection of highway 102 and the main road 118 at coordinates 457583.4m: 4960726m. From Table 35, the minimum and maximum annual average predicted NO_x and SO_2 concentrations are seen at the same receptor at 460010.9m: 4943021m, elevation 41.7 m. Point sources from Dartmouth oil refinery and Tuft's cove contribute major amount GLCs in this domain compared to highways. Highways and main roads contributed larger amount of $PM_{2.5}$ compared to other two pollutants. In the case of all three pollutants, advection was governed by prevailing wind direction at 265^o.

Figure 66 Annual GLCs of NO_x due to point and highway emission sources

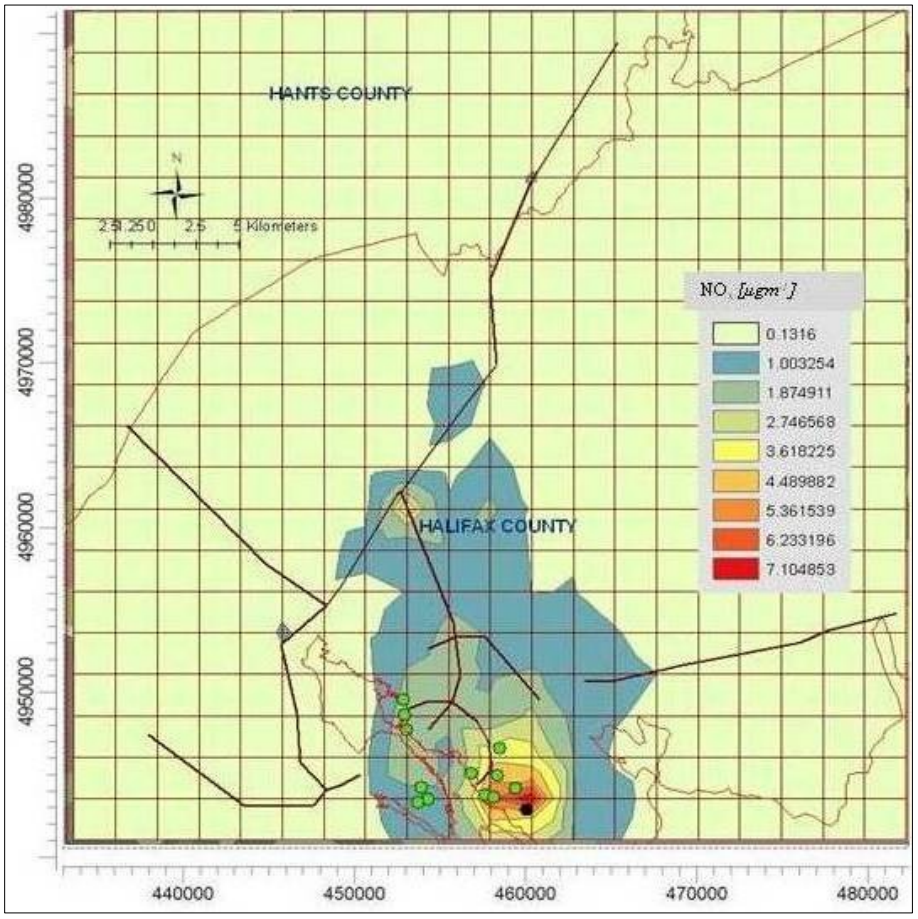

Figure 67 Annual GLCs of SO_2 due to due to point and highway emission sources

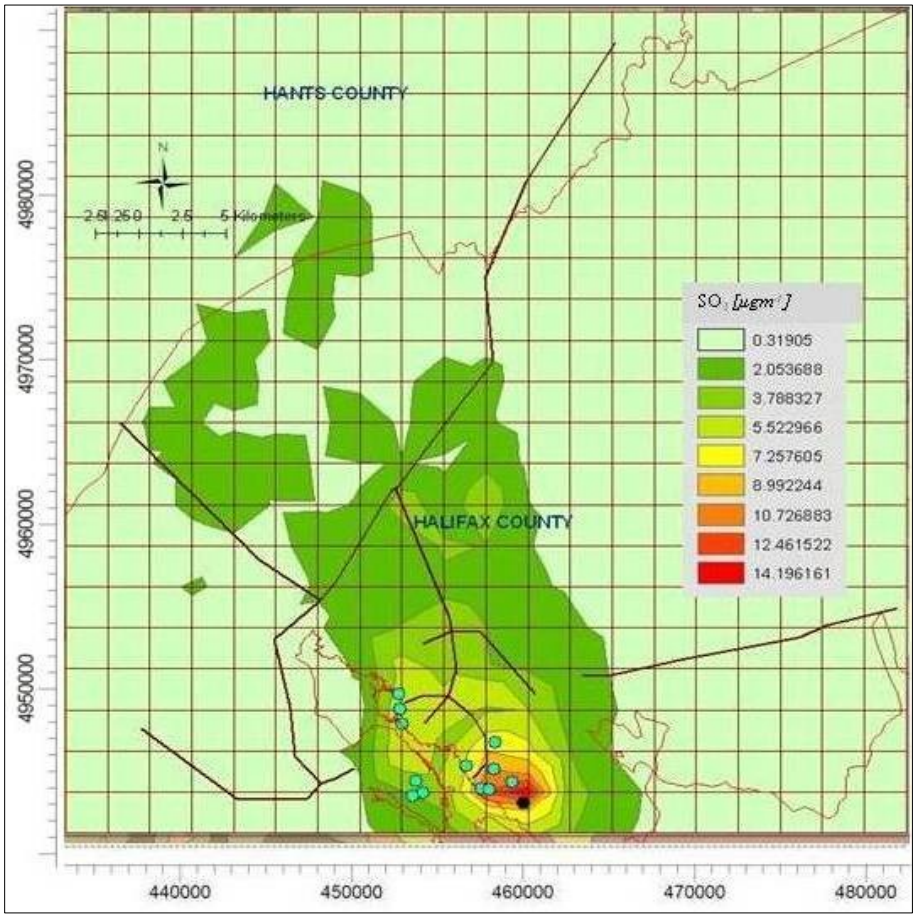

Figure 68 Annual GLCs of $PM_{2.5}$ due to due to point and highway emission sources

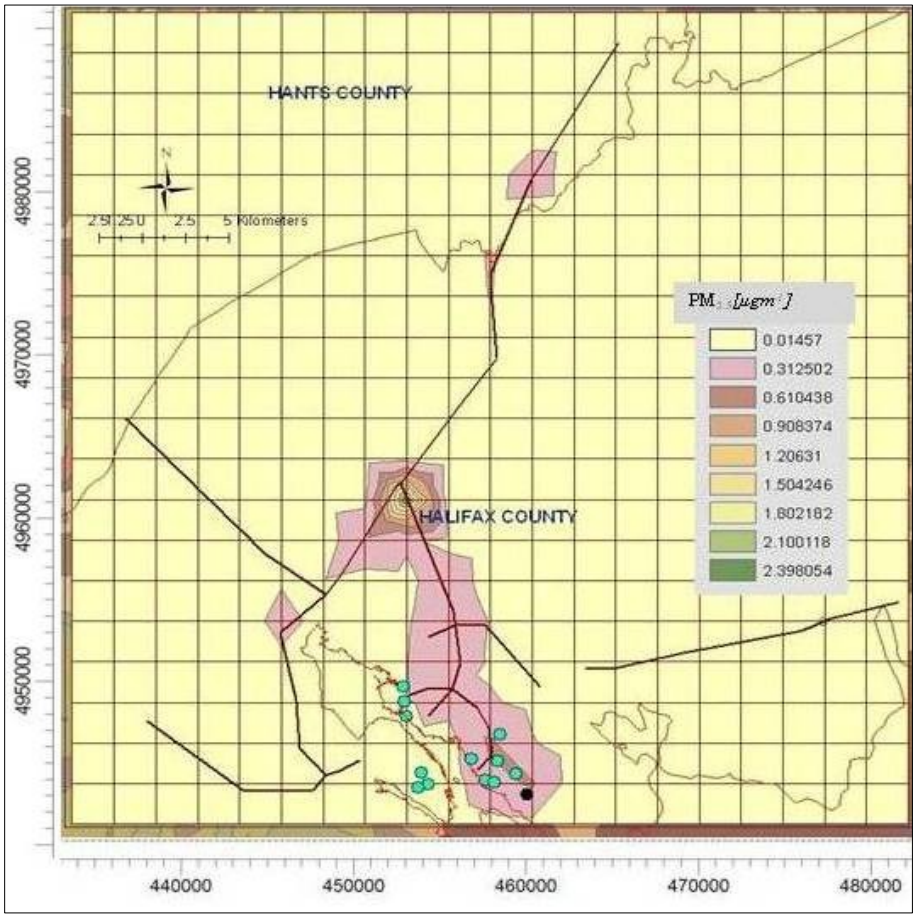

Table 35 Annual MAX and MIN GLCs of NO_x, SO_2 and $PM_{2.5}$

Pollutant	Annual Min *[µg m^{-3}]* UTM coordinate (m) Elevation (m)	Annual Max *[µg m^{-3}]* UTM coordinate (m) Elevation (m)
NO_x	0.136 (479431.09:4991077) NA	8.38 (460010.9:4943021) 41.7
SO_2	0.319 (479431.09:4991077) NA	15.93 (460010.9:4943021) 41.7
$PM_{2.5}$	0.014 (479431.09:4991077) NA	2.67 (457583.4:4960726) 175.3

4.3.10.2 Monthly averaging of NO_x, SO_2 and $PM_{2.5}$

Figures 69 through 71 show monthly GLC gradient maps of NO_x, SO_2 and $PM_{2.5}$ in HFX domain. Monthly averaging shows, GLC of pollutants were high in winter months due to high release height and prevailing wind towards North East. High release height was interfered by the atmospheric stability during winter months with low ambient temperature resulting in high GLCs. From Table 36, it is seen that minimum and maximum concentration values of NO_x and SO_2 were seen at the same receptor which is located at 460010.9m: 4943021m, elevation 41.7 m, 2 km north east of the Dartmouth refinery. Dispersion pattern of $PM_{2.5}$ remain similar for all the months throughout the year and the highest GLCs of NO_x, SO_2 and $PM_{2.5}$ remain unchanged.

Figures 69a-l Monthly GLCs of NO_x due to point and highway emission sources

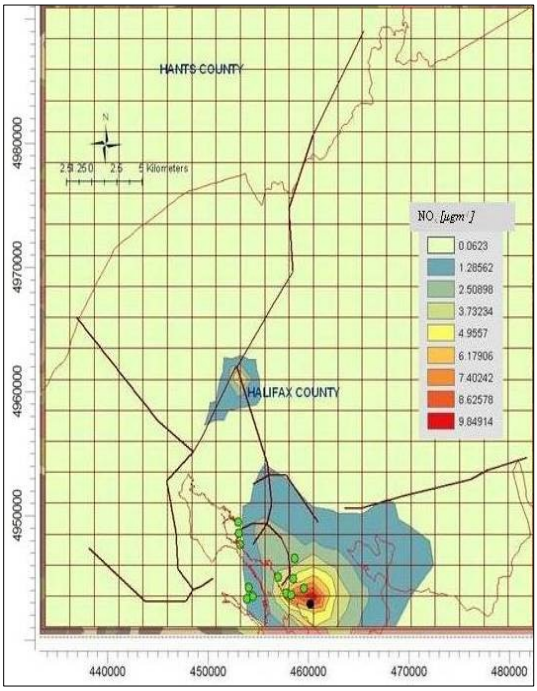

a. January

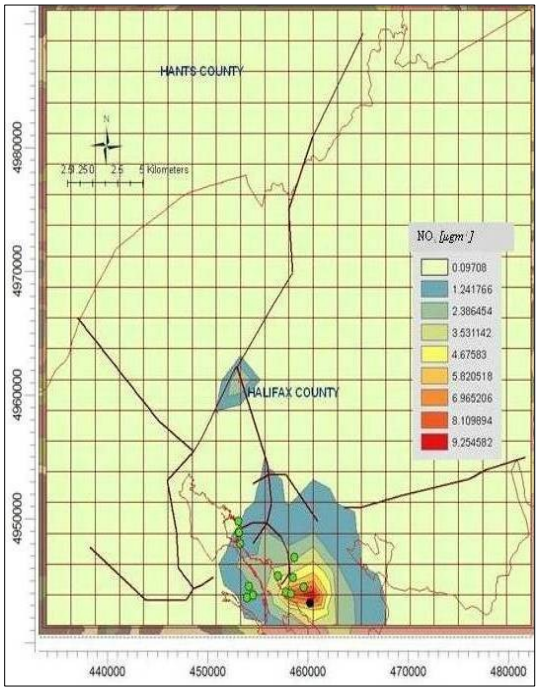

b. February

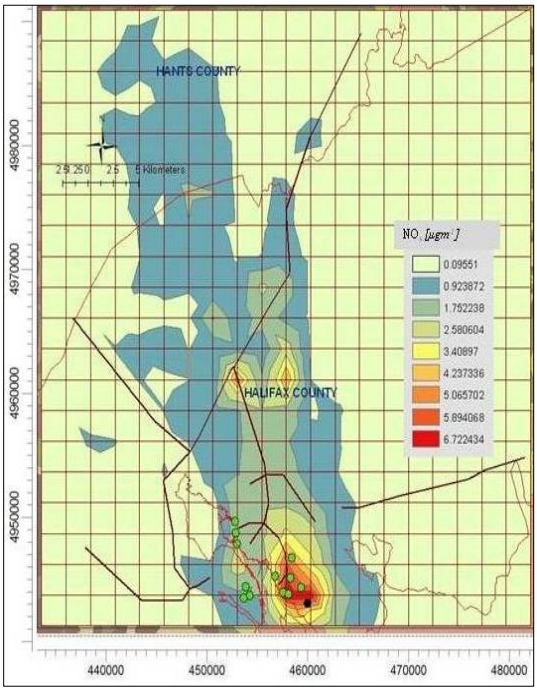

c. March

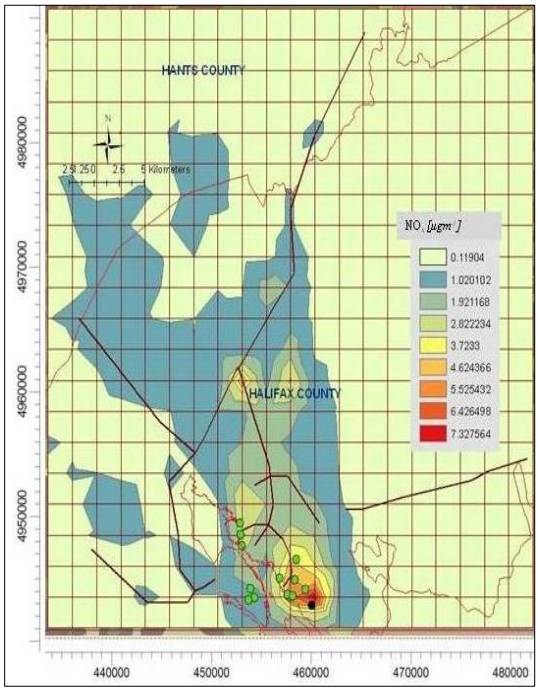

d. April

(Figures Cont'd)

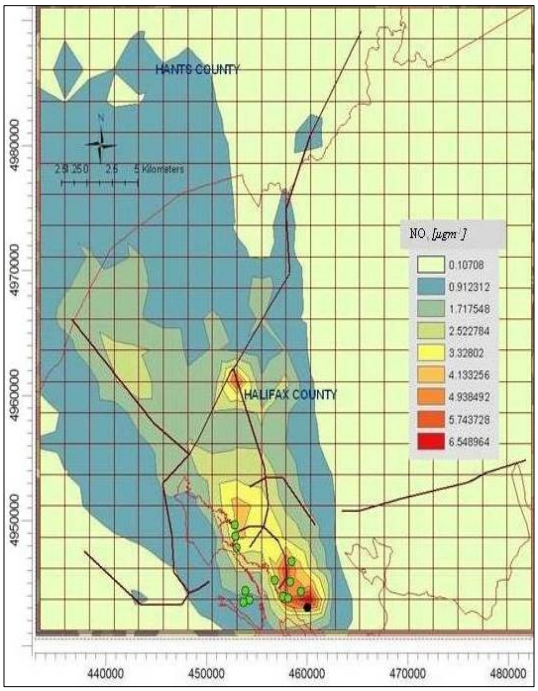

e. May

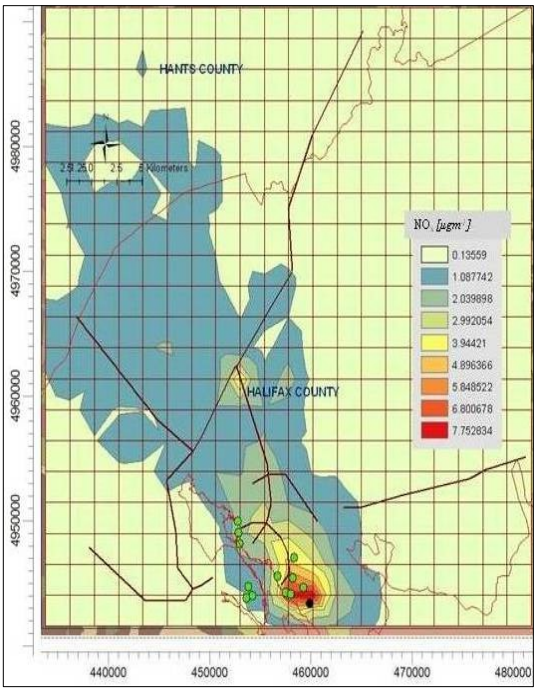

f. June

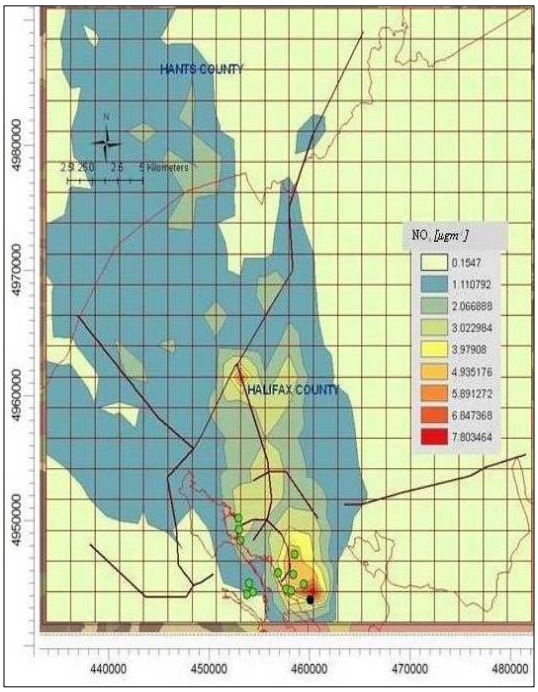

g. July

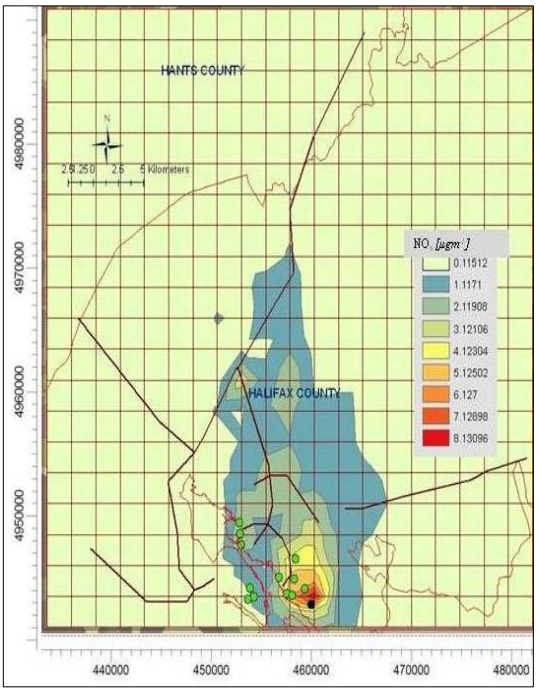

h. August

(Figures Cont'd)

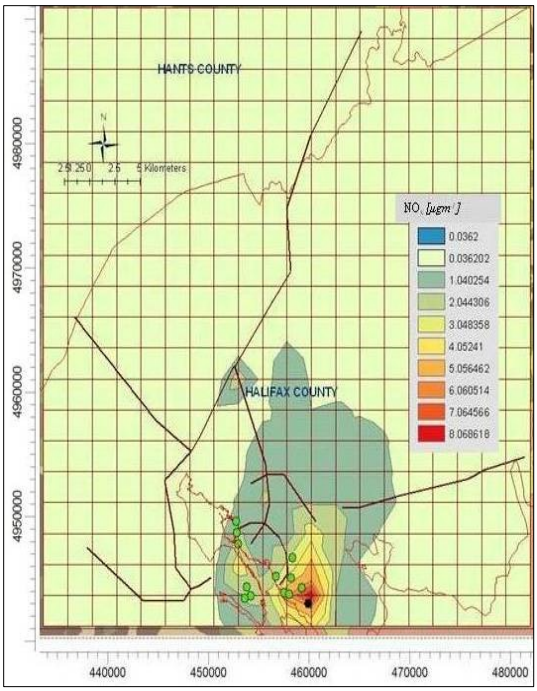

i. September

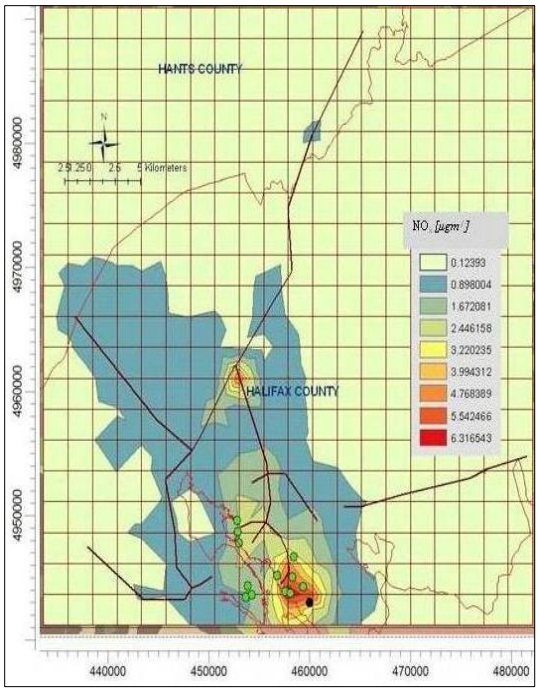

j. October

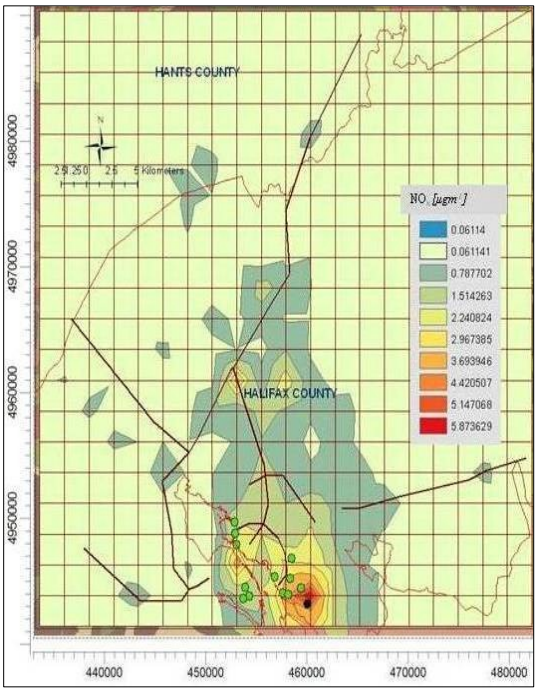

k. November

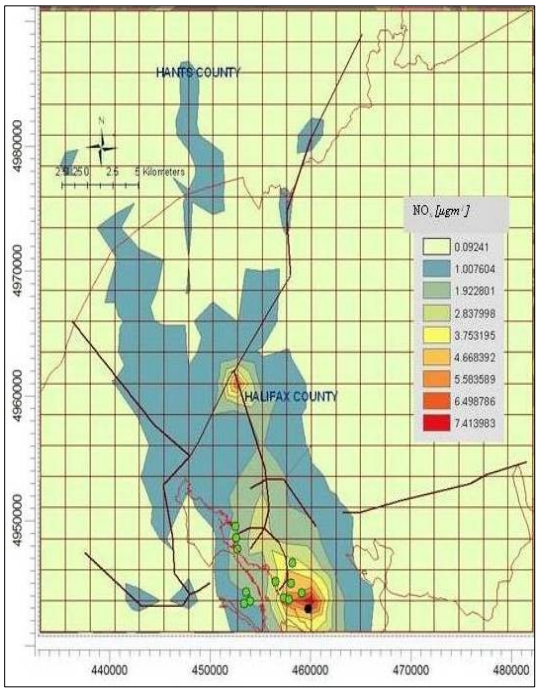

k. December

Figures 70a-l Monthly GLCs of SO_2 due to point and highway emission sources

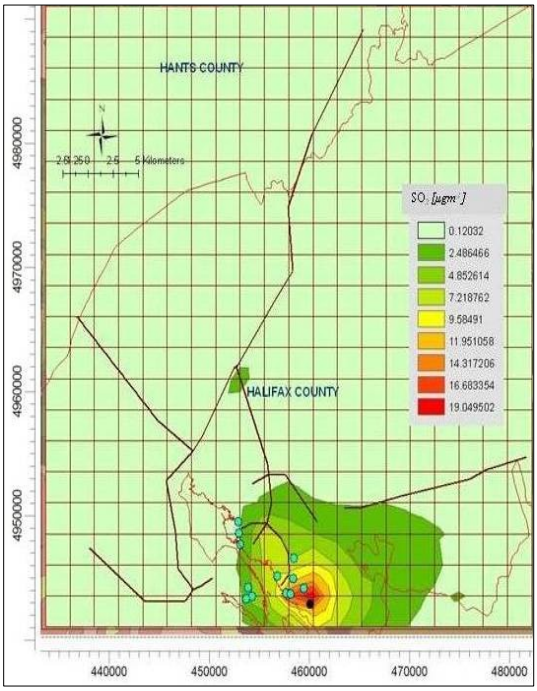

a. January

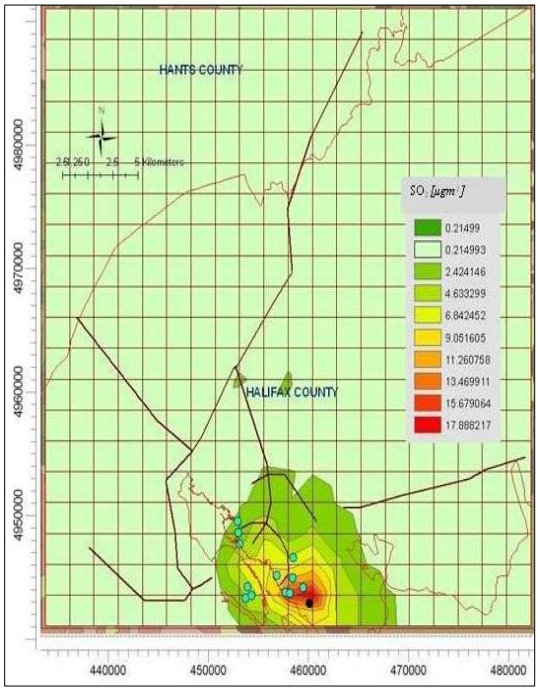

b. February

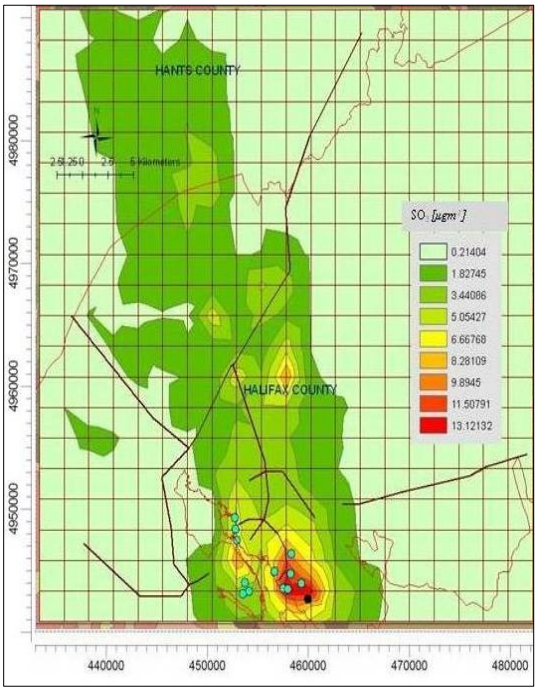

c. March

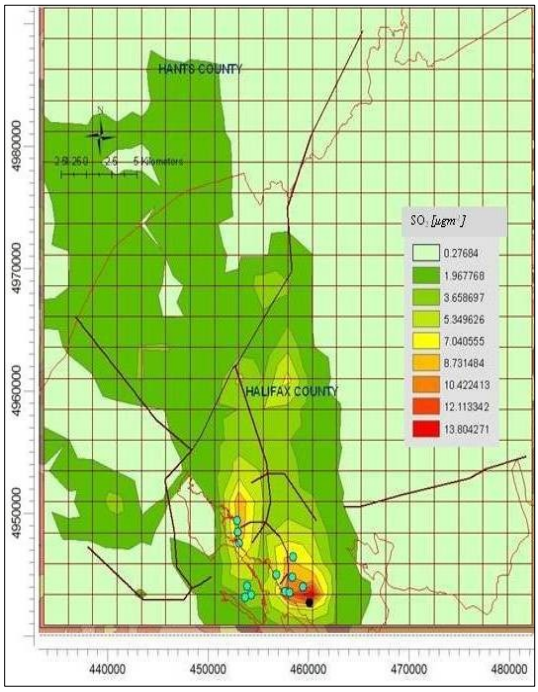

d. April

(Figures Cont'd)

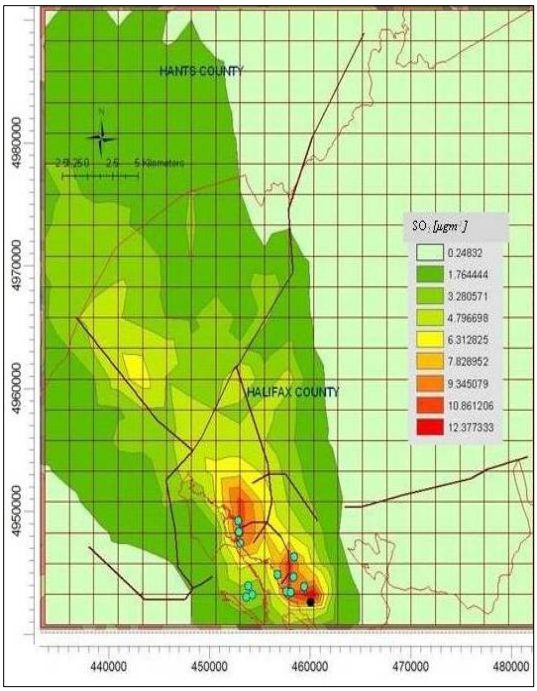

e. May

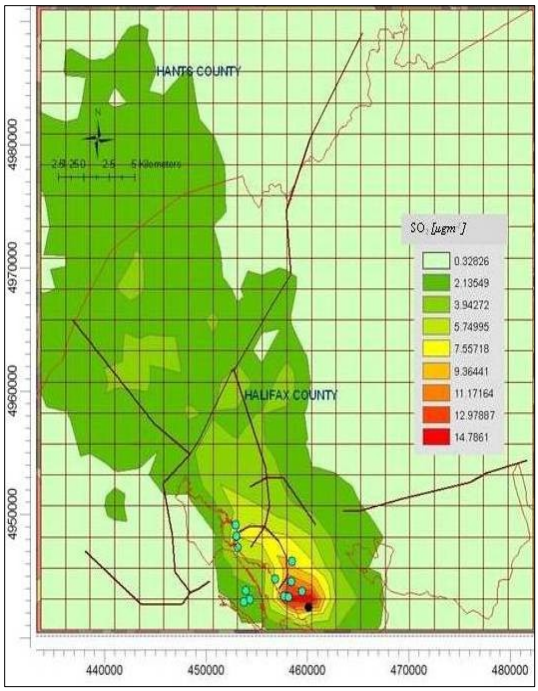

f. June

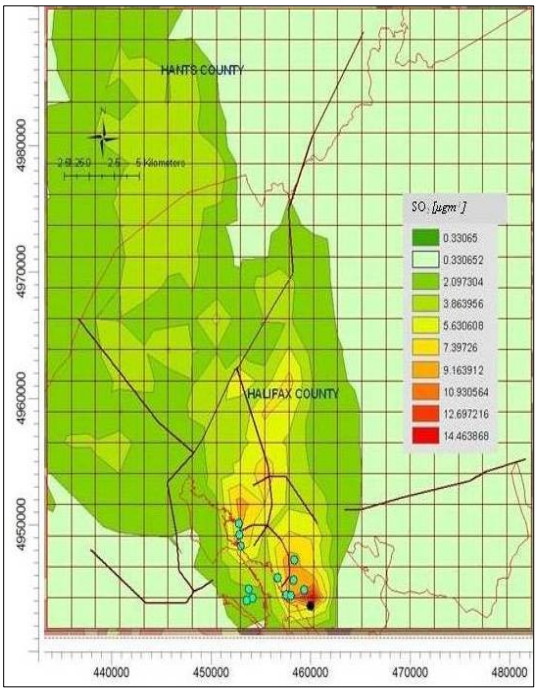

g. July

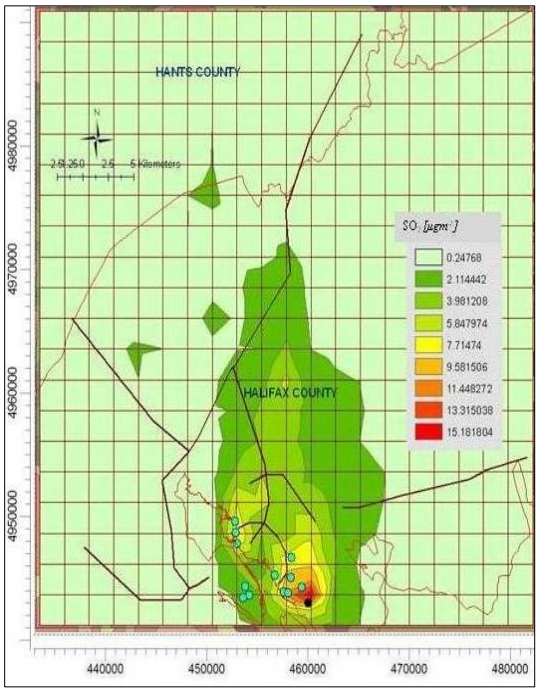

h. August

(Figures Cont'd)

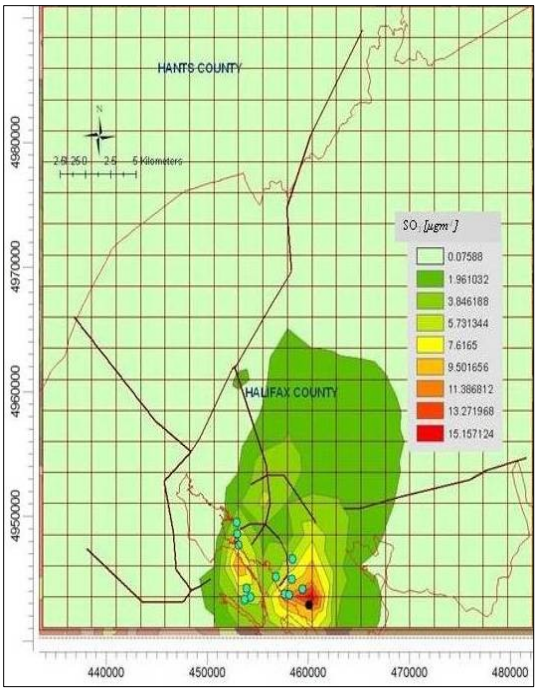

i. September

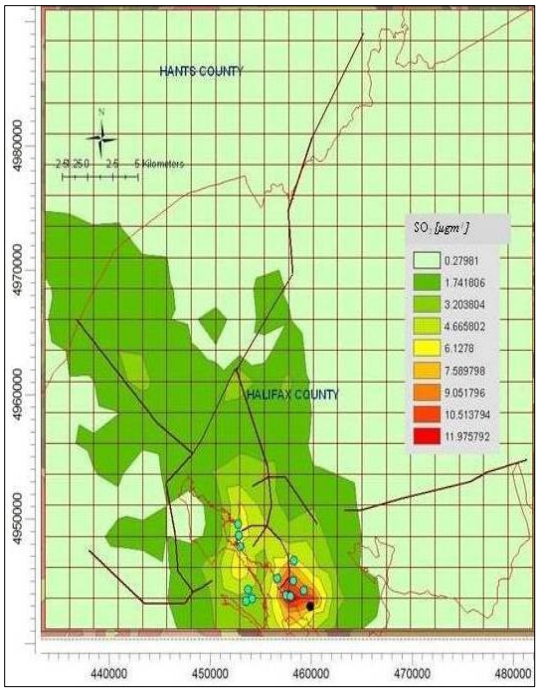

j. October

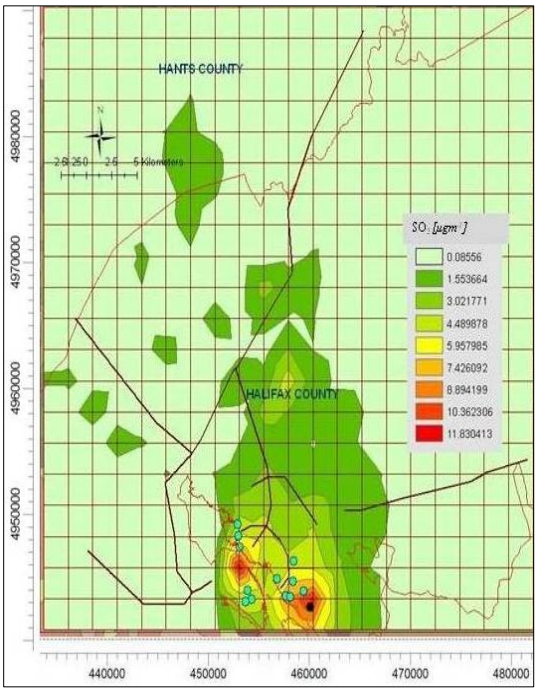

k. November

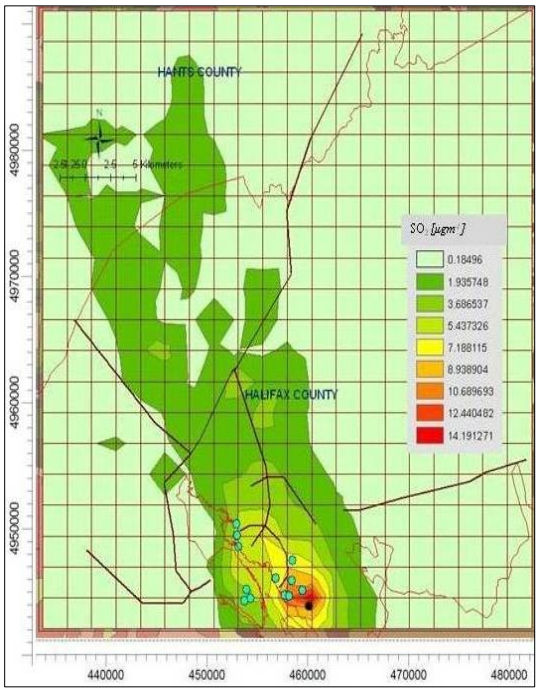

l. December

Figures 71a-l Monthly GLCs of $PM_{2.5}$ due to point and highway emission sources

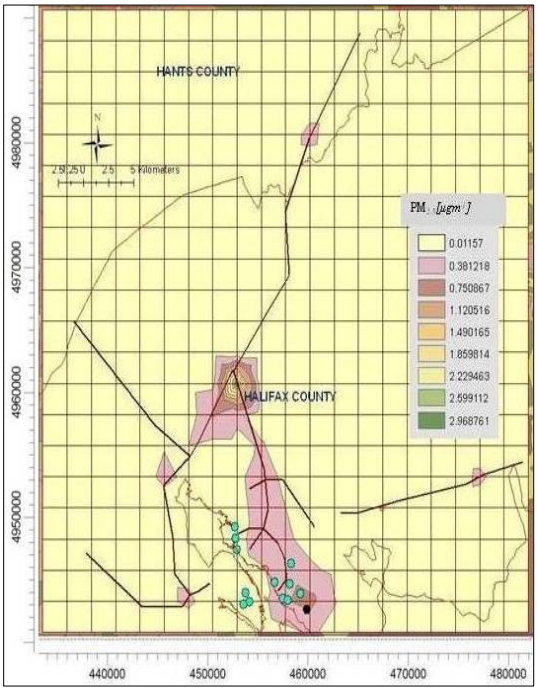

a. January

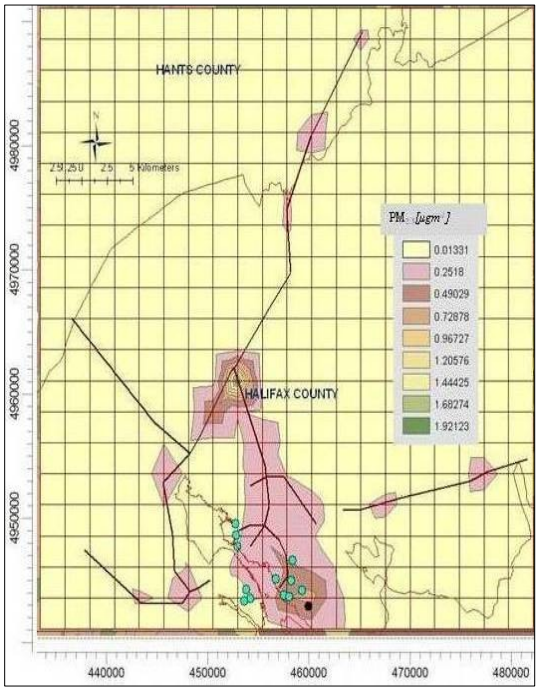

b. February

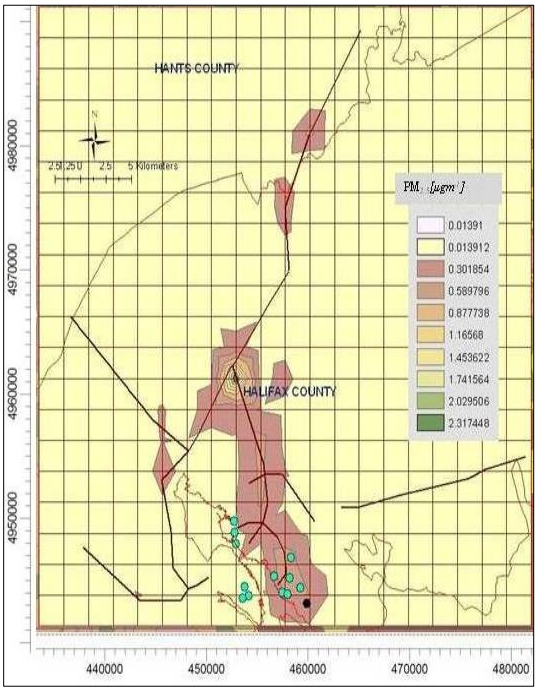

c. March

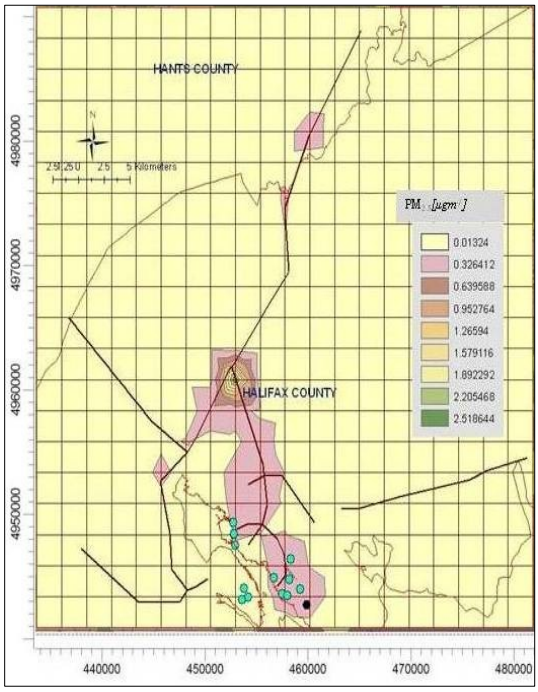

d. April

(Figures Cont'd)

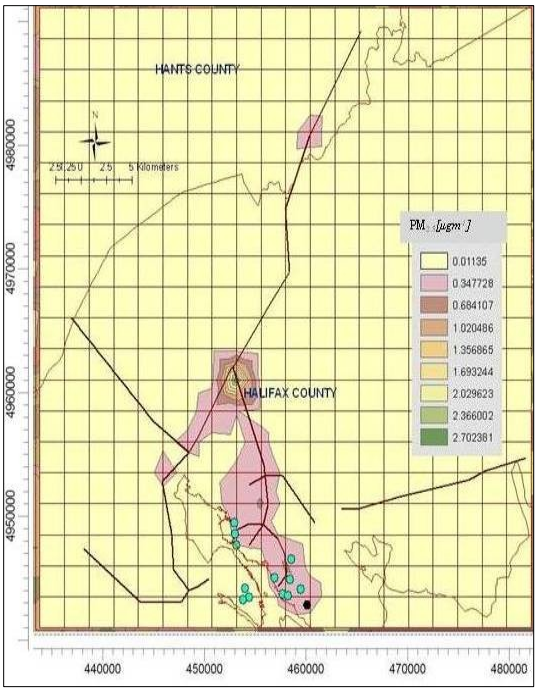

e. May

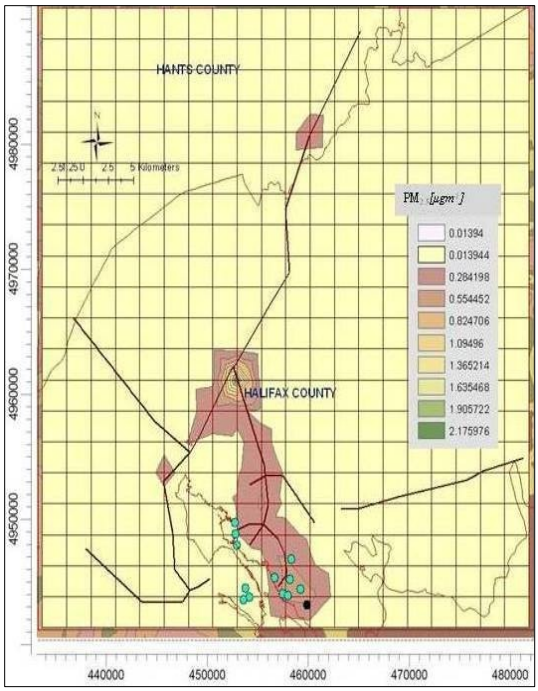

f. June

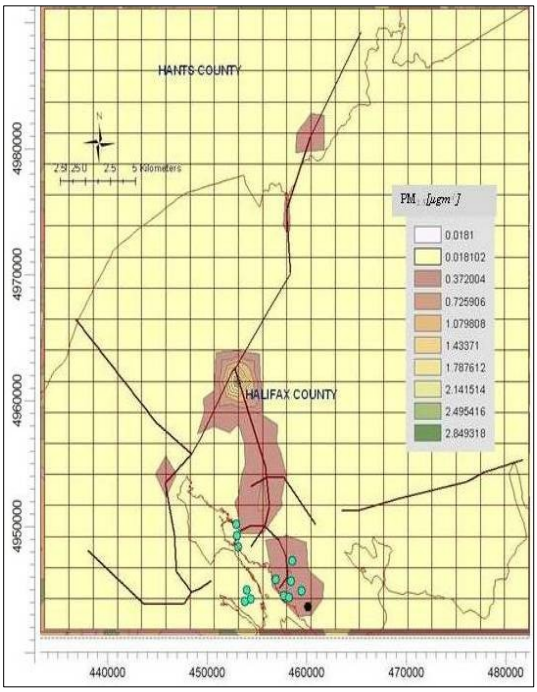

g. July

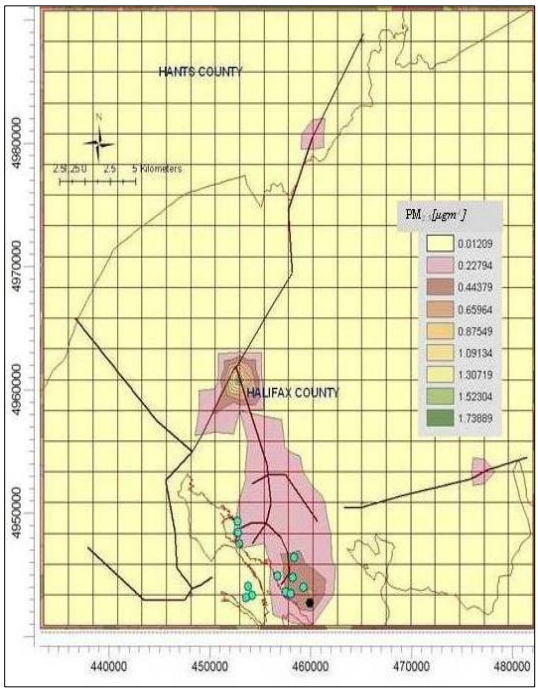

h. August

(Figures Cont'd)

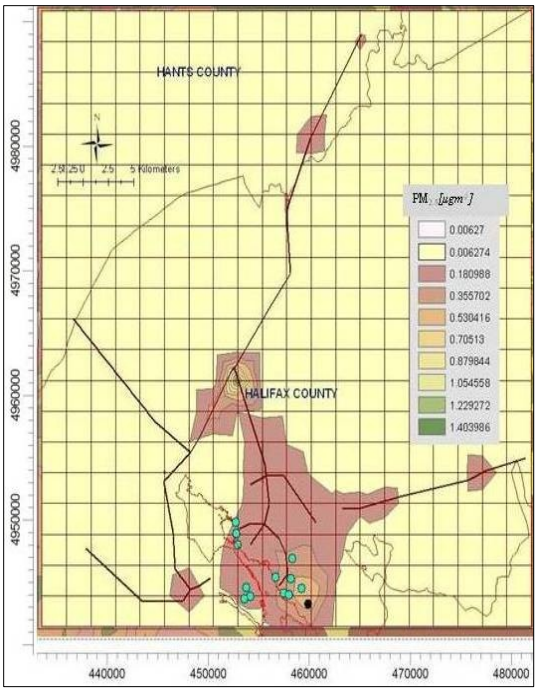

i. September

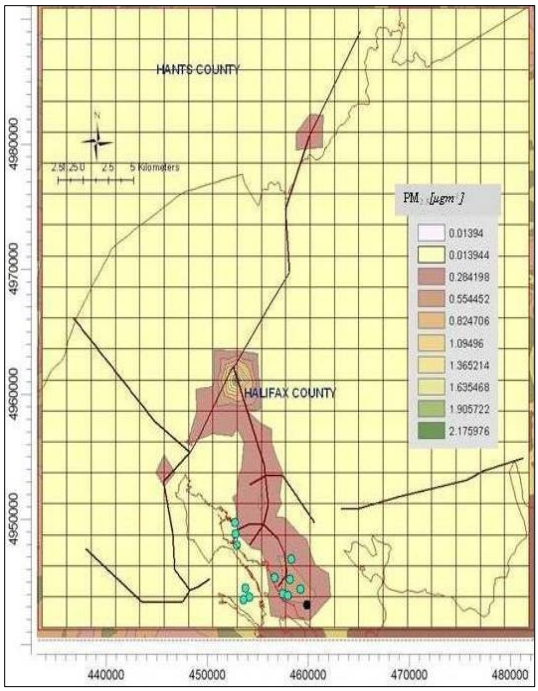

j. October

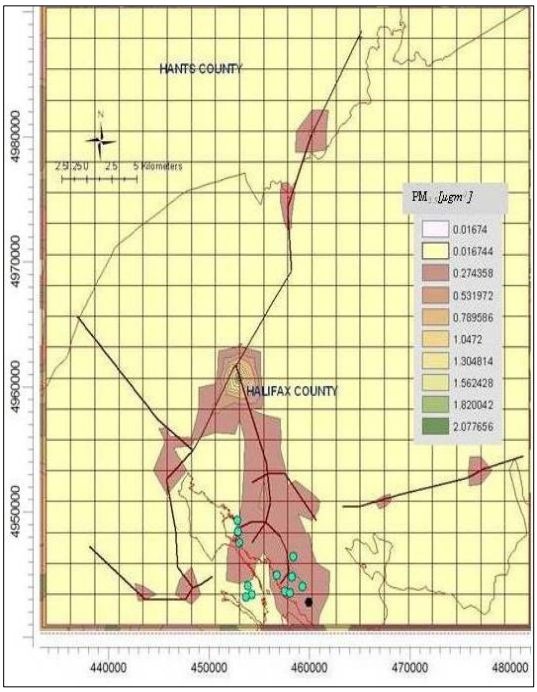

k. November

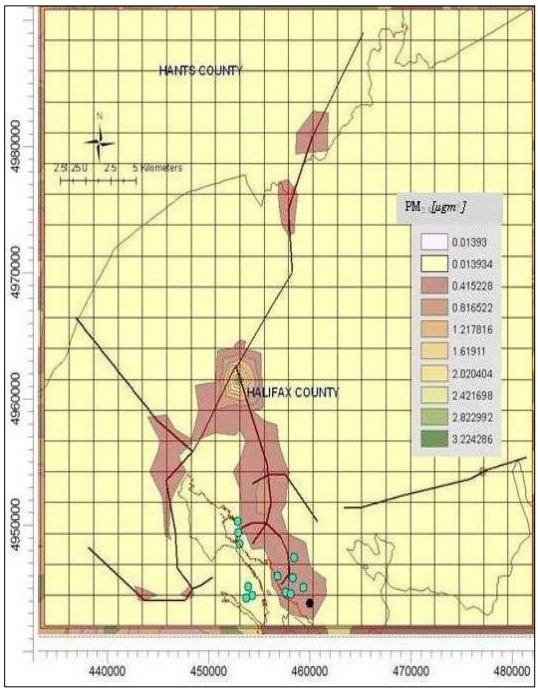

l. December

Table 36 Monthly MAX and MIN GLCs of NO_x, SO_2 and $PM_{2.5}$

	NO_x		SO_2		$PM_{2.5}$	
Month	Monthly Min *[μg m^{-3}]* UTM coordinate (m) Elevation (m)	Monthly Max *[μg m^{-3}]* UTM coordinate (m) Elevation(m)	Monthly Min *[μg m^{-3}]* UTM coordinate (m) Elevation (m)	Monthly Max *[μg m^{-3}]* UTM coordinate (m) Elevation (m)	Monthly Min *[μg m^{-3}]* UTM coordinate (m) Elevation (m)	Monthly Max *[μg m^{-3}]* UTM coordinate (m) Elevation (m)
Jan	0.062 (469721:4991077) NA	11.072 (460010.9:4943021) 41.7	0.12 (469721:4991077) NA	21.42 (460010.9:4943021) 41.7	0.012 (477003.6:4991007) NA	3.338 (457583.4:4960726) 175.3
Feb	0.097 (433308.2:4975901.5) 162.7	10.34 (460010.9:4943021) 41.7	0.215 (433308.2:4973372) 158.7	20.1 (460010.9:4943021) 41.7	0.013 (479431.1:4991077) NA	2.16 (457583.4:4960726) 175.3
Mar	0.096 (433308.2:4940492) 83.8	7.551 (460010.9:4943021) 41.7	0.214 (433308.2:4940492) 83.8	14.73 (457583.4:4943021) 23.1	0.014 (433308.2:4940492) 83.8	2.605 (457583.4:4960726) 175.3
Apr	0.119 (479431.1:4991077) NA	8.23 (460010.9:4943021) 41.7	0.277 (479431.1:4991077) NA	15.5 (460010.9:4943021) 41.7	0.013 (479431.1:4991077) NA	2.832 (457583.4:4960726) 175.3
May	0.107 (479431.1:4991077) NA	7.354 (460010.9:4943021) 41.7	0.248 (479431.1:4991077) NA	13.89 (460010.9:4943021) 41.7	0.011 (479431.1:4991077) NA	3.039 (457583.4:4960726) 175.3
June	0.136 (477003.6:4991077) NA	8.7 (460010.9:4943021) 41.7	0.328 (479431.1:4991077) NA	16.6 (460010.9:4943021) 41.7	0.014 (479431.1:4991077) NA	2.446 (457583.4:4960726) 175.3
July	0.155 (481858.6:4948080) NA	8.76 (460010.9:4943021) 41.7	0.331 (477003.6:4950609) NA	16.23 (460010.9:4943021) 41.7	0.018 (481858.6:4940492) NA	3.203 (457583.4:4960726) 175.3
Aug	0.115 (433308.2:4945550.5) 70.1	9.13 (460010.9:4943021) 41.7	0.248 (433308.2:4945550) 70.1	17.05 (460010.9:4943021) 41.7	0.012 (433308.2:4940492) 83.8	1.955 (457583.4:4960726) 175.3
Sep	0.036 (433308.2:4970843) 189.9	9.073 (460010.9:4943021) 41.7	0.076 (433308.2:4988548) 84.3	17.04 (460010.9:4943021) 41.7	0.006 (433308.2:4983489) 169.2	1.579 (457583.4:4960726) 175.3
Oct	0.124 (469721:4991077) NA	7.1 (460010.9:4943021) 41.7	0.28 (469721:4991077) NA	13.44 (457583.4:4943021) 23.1	0.015 (479431.1:4991077) NA	3.337 (457583.4:4943021) 23.1
Nov	0.061 (435735.8:4940492) 65.7	6.6 (460010.9:4943021) 41.7	0.086 (433308.2:4945550) 70.1	13.3 (452728.4:4945550) 46.1	0.017 (479431.1:4991077) NA	2.335 (457583.4:4960726) 175.3
Dec	0.092 (479431.1:4991077) NA	8.33 (460010.9:4943021) 41.7	0.185 (433308.2:4940492) 83.8	15.942 (460010.9:4943021) 41.7	0.014 (479431.1:4991077) NA	3.626 (457583.4:4960726) 175.3

4.3.10.3 Hourly Averaging of NO_x, SO_2 and $PM_{2.5}$

Figures 72 through 74 show hourly GLC contour maps of predicted NO_x, SO_2 and $PM_{2.5}$. Hourly averaging shows a similar kind of dispersion pattern for NO_x and SO_2 throughout the day. High GLC of the pollutants is seen near highways for shorter averaging periods, one reason could be the high surface roughness of the urban areas. From Table 37, it is seen that minimum and maximum concentration values of NO_x and SO_2 were found at the same receptor which is located at 460010.9m: 4943021m, elevation 41.7 m, 2km North East of the Dartmouth refinery. Dispersion pattern of $PM_{2.5}$ was similar to other two pollutants for shorter averaging periods. As the highway vehicles contributed higher amount of $PM_{2.5,}$ the highest GLC receptor shifted at the intersection of highway 102 and main road 118. Some high GLCs of all three pollutants are seen within 1 km east of Dartmouth refinery and Tufts Cove generation station during 24-hr. This phenomenon indicates calm atmospheric condition during late night hours.

Figures 72a-e Hourly GLCs of NO_x due to point and highway emission sources

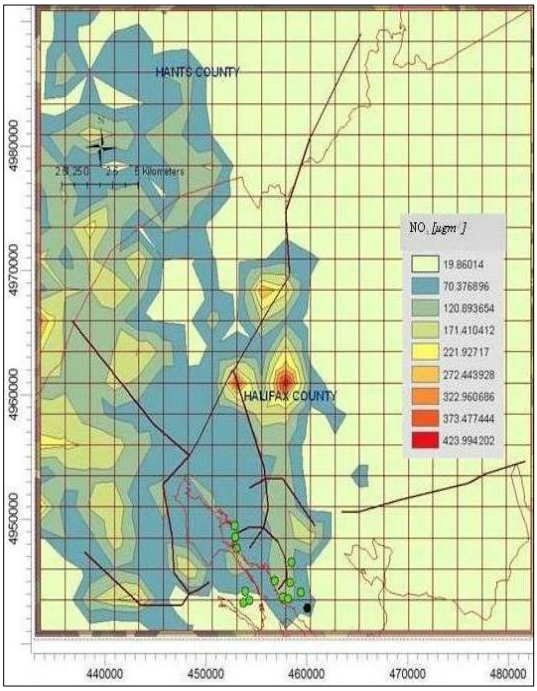

a. 1 hour

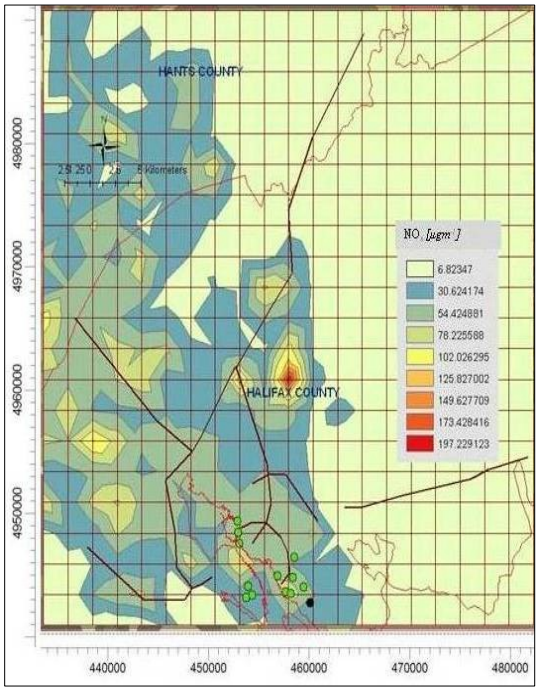

b. 3 hour

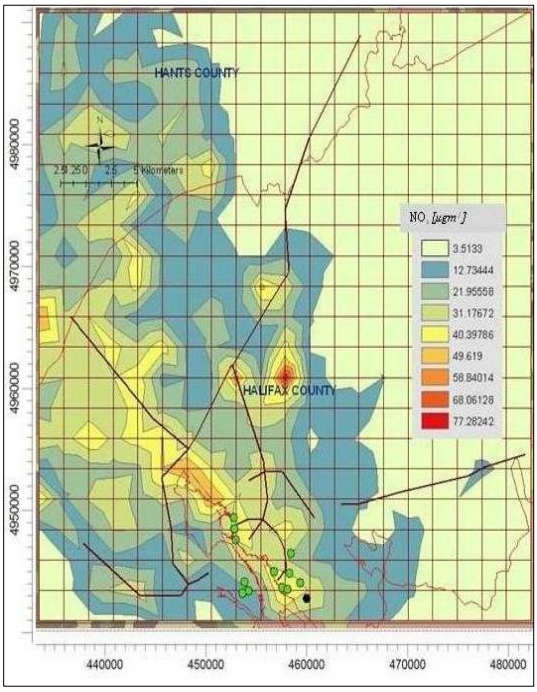

c. 8 hour

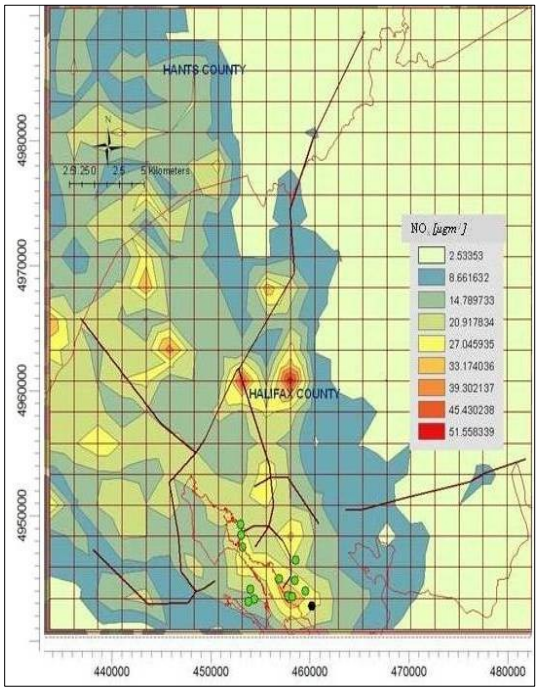

d. 12 hour

(Figure Cont'd)

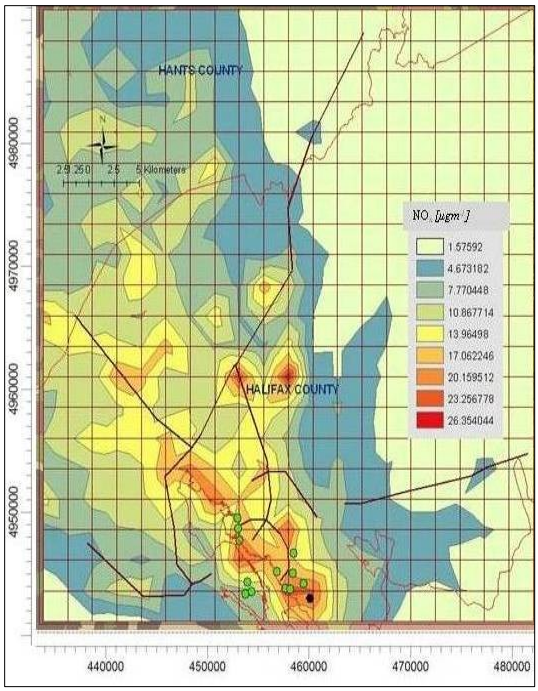
HANTS COUNTY
HALIFAX COUNTY
2.5 0 2.5 5 Kilometers
NO2 [µgm-3]
1.57592
4.673182
7.770448
10.867714
13.96498
17.062246
20.159512
23.256778
26.354044
4960000
4970000
4980000
4990000
440000
450000
460000
470000
480000

e. 24 hour

Figures 73a-e Hourly GLCs of SO_2 due to point and highway emission sources

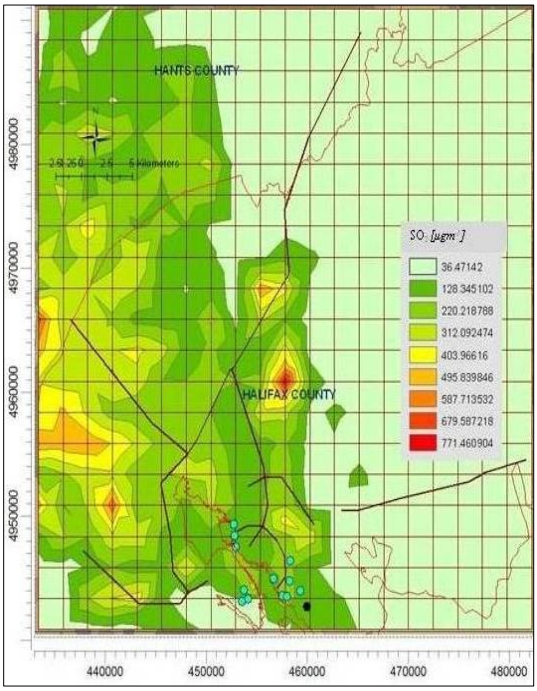

a. 1 hour

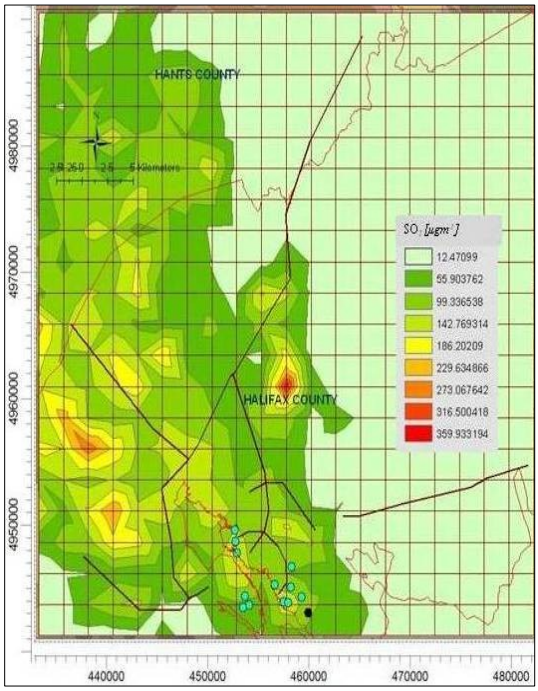

b. 3 hour

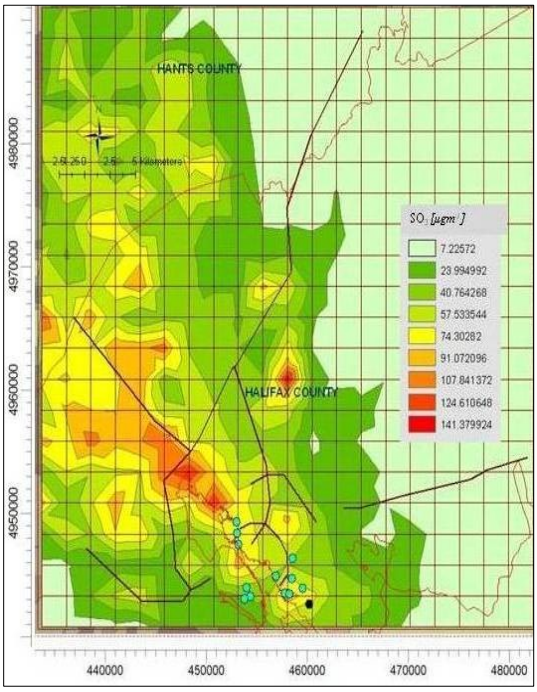

c. 8 hour

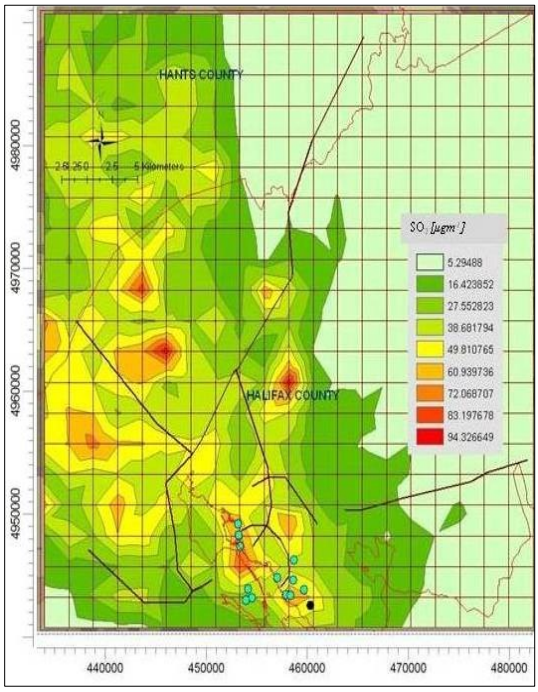

d. 12 hour

(Figure Cont'd)

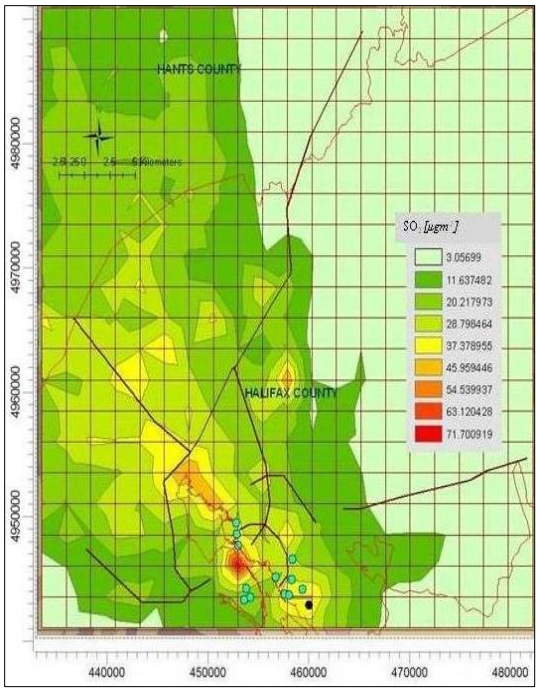
HANTS COUNTY
HALIFAX COUNTY
SO2 [µgm-3]
3.05699
11.637482
20.217973
28.798464
37.378955
45.959446
54.539937
63.120428
71.700919
4980000
4970000
4960000
4950000
440000
450000
460000
470000
480000

e. 24 hour

Figures 74a-e Hourly GLCs of $PM_{2.5}$ due to point and highway emission sources

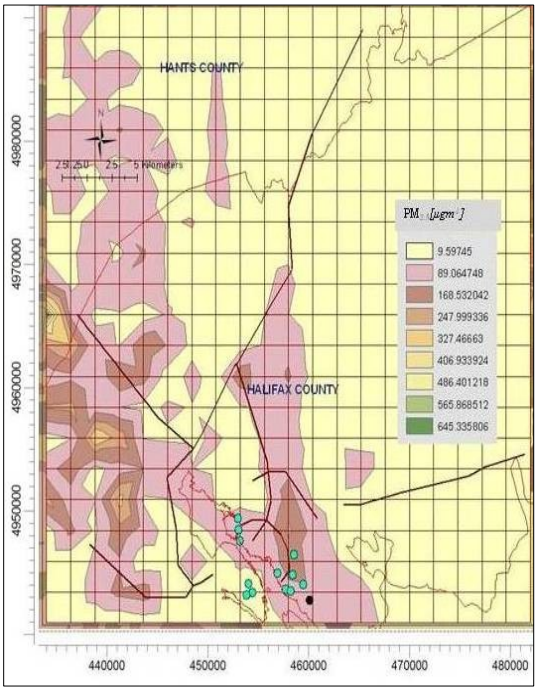

a. 1 hour

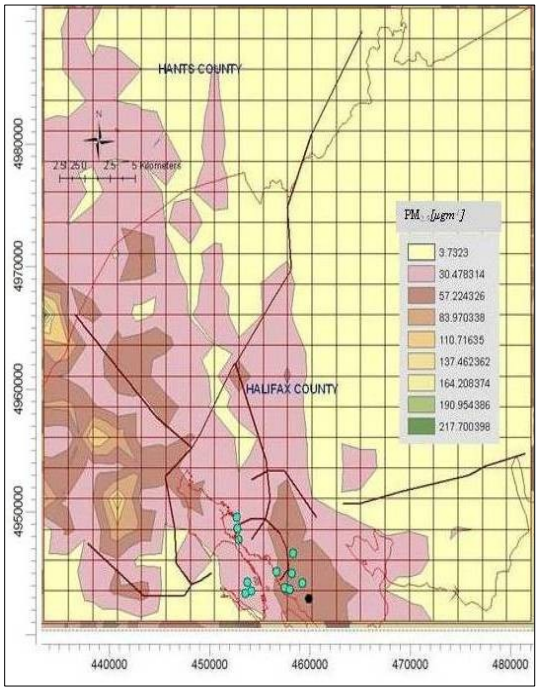

b. 3 hour

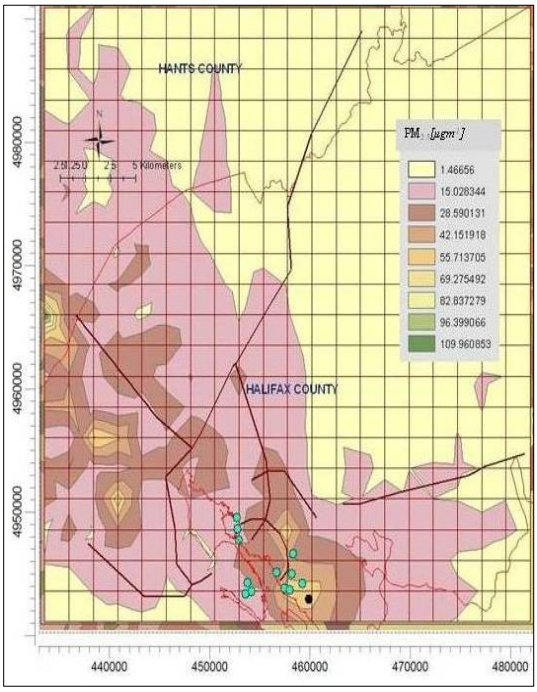

c. 8 hour

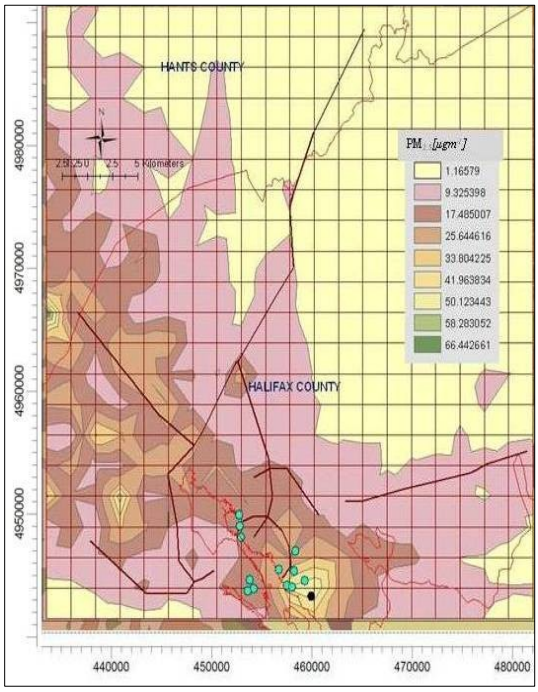

d. 12 hour

(Figure Cont'd)

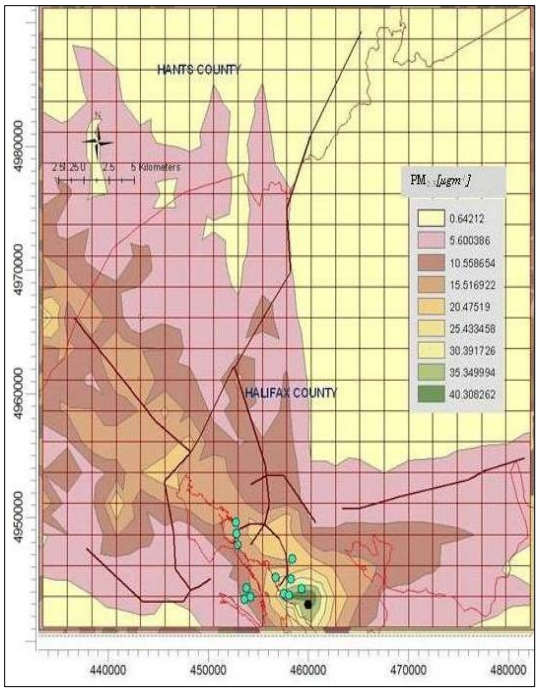

e. 24 hour

Table 37 Hourly MAX and MIN GLCs NO_x, SO_2 and $PM_{2.5}$

Hour	NO_x		SO_2		$PM_{2.5}$	
	Hourly Min *[µg m^{-3}]* UTM coordinate (m) Elevation (m)	Hourly Max *[µg m^{-3}]* UTM coordinate (m) Elevation (m)	Hourly Min *[µg m^{-3}]* UTM coordinate (m) Elevation (m)	Hourly Max *[µg m^{-3}]* UTM coordinate (m) Elevation (m)	Hourly Min *[µg m^{-3}]* UTM coordinate (m) Elevation (m)	Hourly Max *[µg m^{-3}]* UTM coordinate (m) Elevation (m)
1	19.86 (469721.03:4991077) NA	474.51 (457583.4:4960726) 175.3	36.471 (469721.03:4991077) NA	863.33 (457583.4:4960726) 175.3	9.597 (467293.5:4986019) 36.3	724.803 (433308.2:4965785) 217.8
3	6.823 (479431.09:4991077) NA	221.03 (457583.4:4960726) 175.3	12.471 (479431.09:4991077) NA	403.36 (457583.4:4960726) 175.3	3.732 (467293.5:4986019) 36.3	244.44 (433308.2:4965785) 217.8
8	3.513 (469721.03:4991077) NA	86.5 (457583.4:4960726) 175.3	7.226 (469721.03:4991077) NA	158.15 (457583.4:4960726) 175.3	1.467 (467293.5:4988548) 39.2	123.523 (433308.2:4965785) 217.8
12	2.534 (469721.03:4991077) NA	57.68 (457583.4:4960726) 175.3	5.295 (479431.09:4991077) NA	105.456 (457583.4:4960726) 175.3	1.166 (467293.5:4988548) 39.2	74.602 (433308.2:4965785) 217.8
24	1.576 (479431.09:4991077) NA	29.45 (457583.4:4960726) 175.3	3.057 (479431.09:4991077) NA	80.28 (452728.4:4945550) 46.1	0.019 (440590.78:4991077) 197.4	5.164 (452728.4:4960726) 101.7

4.3.11 Use of the simulation data

Simulations results from section 4.2 through 4.3 can be used to prepare database to identify the high GLC of NO_x, SO_2 and $PM_{2.5}$ receiving areas due to mentioned emission sources in seven modeling domains across the province. Therefore it will help in providing information on community exposure to air pollutants and health risk assessment. Also a number of available emission sources can be included in these modeling domains in future to evaluate the dispersion patterns of the pollutants and GLC values to help in airshed management of the province.

4.4 Comparison between AERMOD Predicted and NAPS Observed $PM_{2.5}$, NO_x and SO_2 Data

AERMOD predicted GLCs of $PM_{2.5}$, NO_x and SO_2 were compared with observed concentration values at four NAPS stations in Halifax, Sydney, PortHawksbury and Pictou to evaluate the model performance. Both monthly and hourly observed SO_2 values from Halifax, Sydney and PortHawksbury, NO_x values from Halifax and $PM_{2.5}$ values from Halifax and Pictou during 2004 were available to compare with model predicted values. This comparison can also help in finding input data gaps for better GLC predictions in the future. Five discrete Cartesian receptors were assigned at NAPS station coordinates for comparison purpose.

4.4.1 Monthly and Hourly Comparison

Halifax

Figures 75, 77 and 79 show comparison between the monthly mean of AERMOD predicted and monthly mean of observed $PM_{2.5}$, NO_x and SO_2 values respectively in the HFX domain. Figures 76, 78 and 80 show comparison between the hourly mean of AERMOD predicted and hourly mean of observed $PM_{2.5}$, NO_x and SO_2 values respectively in the HFX domain.

It can be seen from Figure 75 that the lowest NAPS observed $PM_{2.5}$ concentration occurred in January (2.5 $\mu g\ m^{-3}$) with the lowest AERMOD predicted $PM_{2.5}$ concentrations occurring in May (0.11 $\mu g\ m^{-3}$) while the highest observed $PM_{2.5}$ concentration occurred in July (7.1 $\mu g\ m^{-3}$) and

the highest predicted $PM_{2.5}$ concentration in November (0.23 µg m^{-3}). The minimum and maximum monthly $PM_{2.5}$ predicted concentrations were 6.6 µg m^{-3} (November) at coordinates (x-460010.89m: y-4943020.92m), elevation 41.7 and 9.56 µg m^{-3} (July) at coordinates (x-460010.89m: y-4943020.92m), elevation 41.7 m respectively. From Figure 75, it can be seen that the model predicted $PM_{2.5}$ concentration was on an average factor of 25 lower than the observed value. There was also a poor correlation (R^2 = 0.053) between the predicted and observed values over the entire 12-months. However, between March and September 2004 there was an improved correlation ($R^2$of 0.35) between the predicted and observed values. The predicted annual mean $PM_{2.5}$ concentration of 0.16 µg m^{-3} was found at the NAPS site coordinates compared to the NAPS observed concentration of 4.08 µg m^{-3}.

Figure 75 Predicted vs. NAPS observed monthly $PM_{2.5}$ concentrations in HFX domain

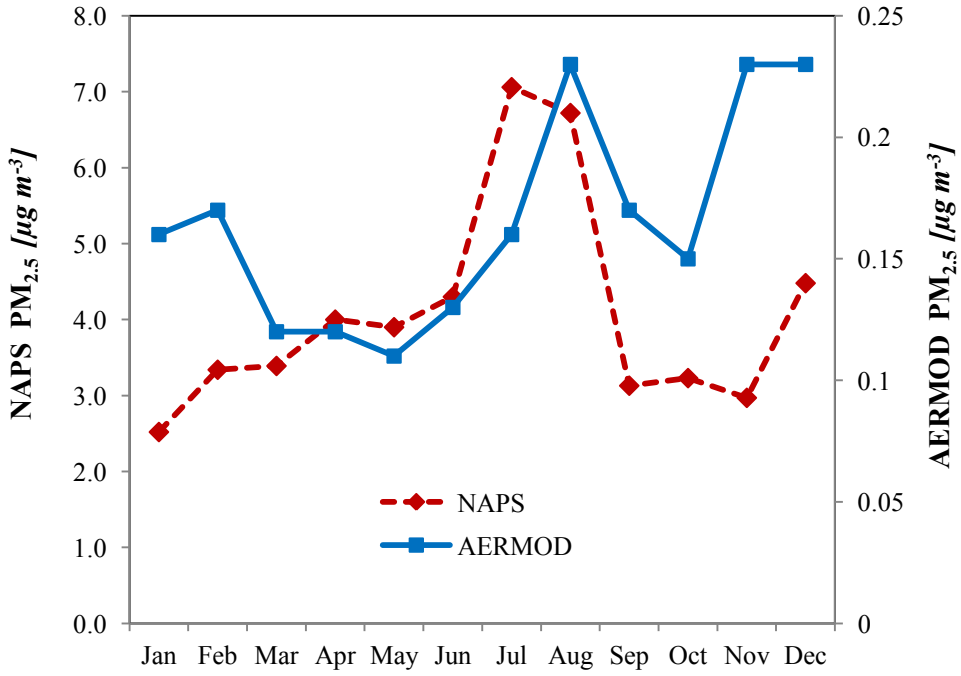

It can be seen from Figure 76 that the NAPS observed $PM_{2.5}$concentrations were higher than the AERMOD predicted $PM_{2.5}$ concentrations during 1-hr, 3-hr, 8hr and 24-hr averaging periods. During 12-hr averaging period the model over predicted the GLC by a factor of 1.25. There was a reasonable correlation (R^2 = 0.68) between predicted and observed concentration values over hourly averaging periods throughout the day.

Figure 76 Predicted vs. NAPS observed hourly $PM_{2.5}$ concentrations in HFX domain

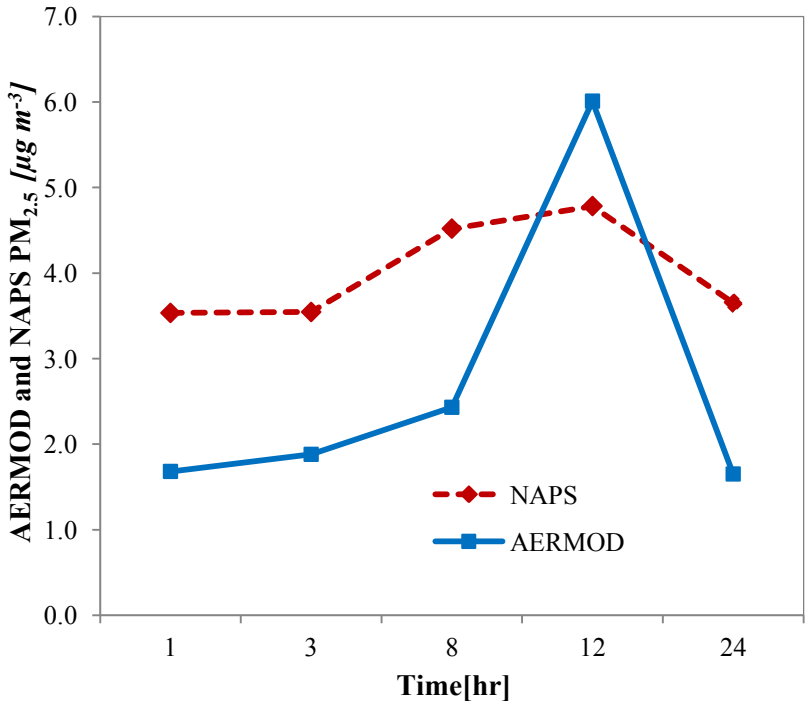

It can be seen from Figure 77 that the lowest NO_x observed concentration occurred in September (33.0 µg m^{-3}) with the lowest predicted NO_x concentrations occurring in August (1.48 µg m^{-3}). The highest observed NO_x concentration occurred in December (45.0 µg m^{-3}) with the highest predicted NO_x concentration occurring in September (2.4 µg m^{-3}) respectively. From Figure 77, it can also be seen that the model predicted NO_x concentration was on average a factor of 21 lower than the observed NO_x values in Halifax. In addition there appeared to be no correlation between the predicted and observed NO_x concentrations ($R^2$of 0.0009). The minimum and maximum monthly NO_x predicted concentrations was 13.4 µg m^{-3} (October) at coordinates (x-457583.37m: y-4960726.02m), elevation 128.2 and 24.1 µg m^{-3} (February) at coordinates (x-460010.89m: y-4943020.92m), elevation 41.7 m respectively. The predicted annual mean NO_x found at the NAPS site coordinates was 0.16 µg m^{-3} compared to the NAPS observed concentration of 4.1 µg m^{-3}.

Figure 77 Predicted vs NAPS observed monthly NO_x concentrations in HFX domain

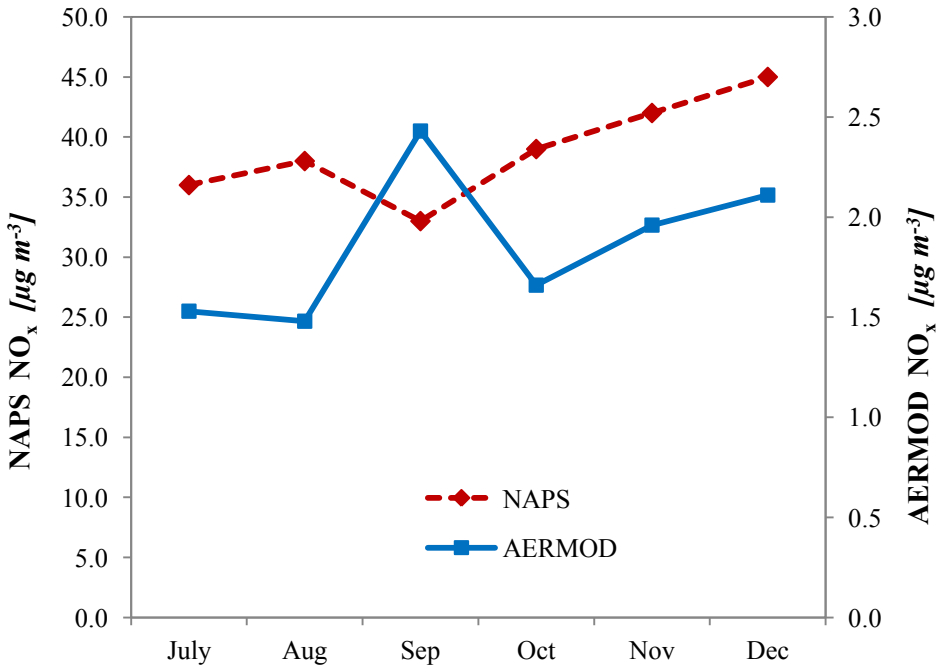

It can be seen from Figure 78 that the NAPS observed NO_x concentration were always higher than AERMOD predicted NO_x concentrations. During 8-hr averaging period, model under predicted the GLC by a factor of 8. There was a poor correlation (R^2 = 0.031) between the predicted and observed over hourly averaging periods throughout the day.

Figure 78 Predicted vs NAPS observed monthly NO_x concentrations in HFX domain

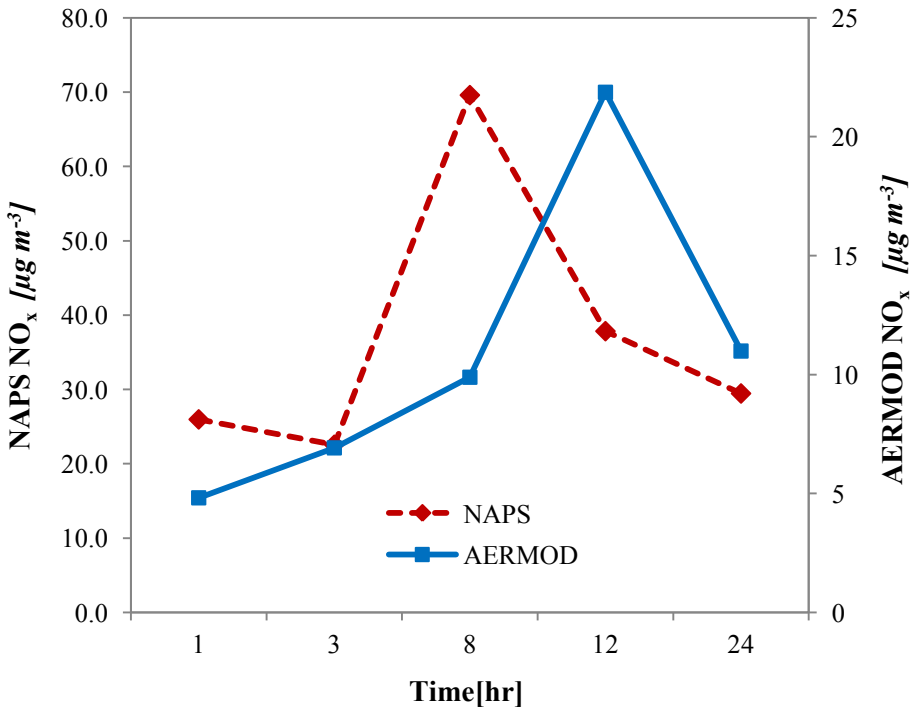

It can be seen from Figure 79 that the lowest observed SO_2 concentration occurred in September (4.5 µg m^{-3}) with the lowest predicted SO_2 concentration was computed in March (3.2 µg m^{-3}) respectively. Figure 79 also shows that the highest observed SO_2 concentration occurred in January (9.81 µg m^{-3}) with highest predicted SO_2 concentrations occurring in September (6.8 µg m^{-3}) respectively. From Figure 79, it can also be seen that monthly predicted SO_2 concentration was a factor of 1.5 lower than the observed SO_2 concentration in HFX domain. There appeared to be a poor correlation (R^2 of 0.16) between the predicted and observed trend in SO_2 values over the 12-month comparison period, but this was due to large over prediction in September. When the September comparative data was removed there was a very good correlation (R^2 = 0.77) between the trend of the predicted and observed SO_2 concentrations in Halifax domain. The minimum and maximum monthly predicted SO_2 concentration of 1.69 µg m^{-3} (January) and 24.9 µg m^{-3} (July) were found at the same coordinates (x-728918.95m: y-5125657.12m), elevation 32.1 m. The predicted annual mean SO_2 found at the NAPS site coordinates was 4.9 µg m^{-3} compared to the NAPS observed concentration of 7.3 µg m^{-3}.

Figure 79 Predicted vs NAPS observed monthly SO_2 concentrations in HFX domain

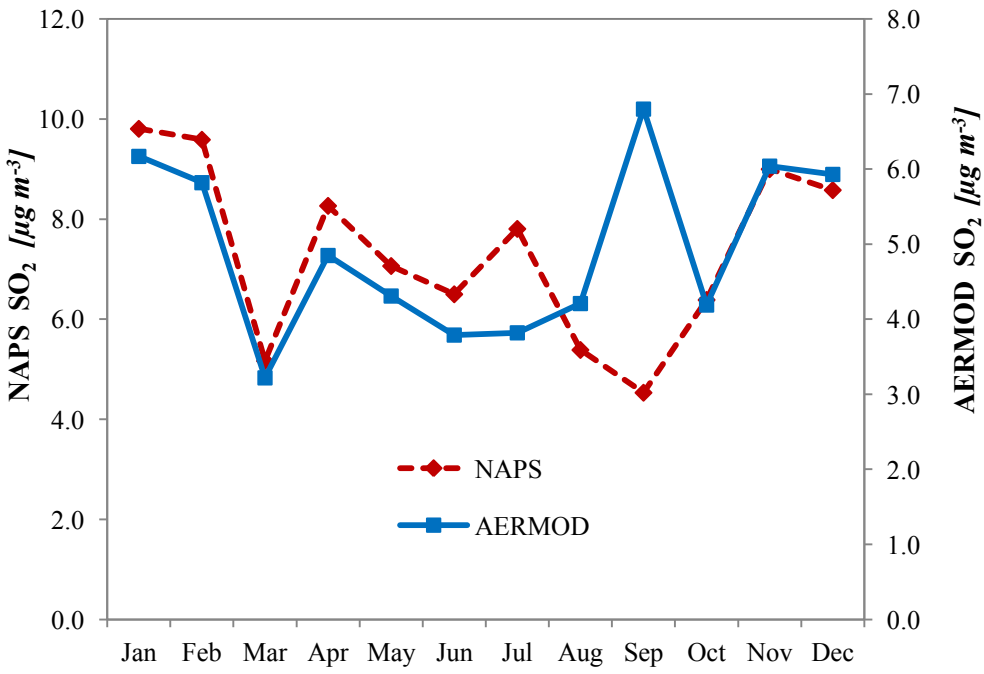

It can be seen from Figure 80 that the NAPS observed SO_2 concentration were higher than the AERMOD predicted SO_2 concentrations during 1hr, 8hr, 12hr and 24hr averaging periods. During 3-hr averaging period, model under predicted the concentration by a factor of 1.2. There was a reasonable correlation (R^2 = 0.58) between the predicted and observed over hourly averaging periods throughout the day.

Figure 80 Predicted vs NAPS observed hourly SO_2 concentrations in HFX domain

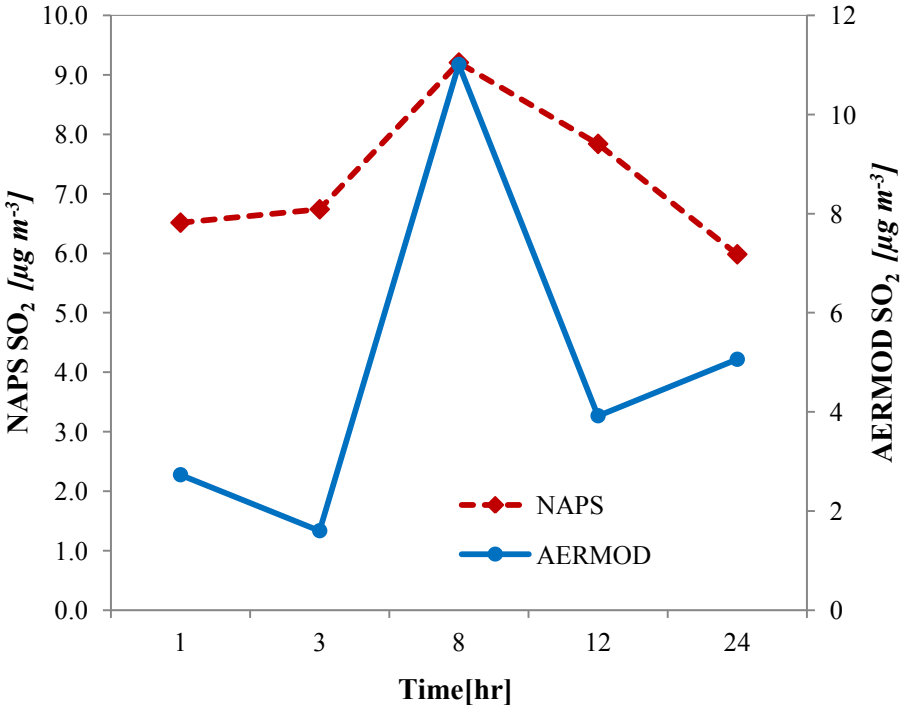

The reason for the increased concentration gradients observed for $PM_{2.5}$, NO_x and SO_2 to the East of the refinery in Figures 66 through 68 is, in all likelihood, due to the Westerly prevailing wind (ref Figure 3.5) advecting the point and line emissions immediately to the East of their source. With reference to figure 68 it can be observed that the average surface $PM_{2.5}$ concentration values over downtown Halifax and peninsula was less than 0.015 µg m^{-3}. This can be considered of low impact when compared to the National Air Quality Objective reference level for 24-hr of 15 µg m^{-3} or the longer term CWS of 30 µg m^{-3} (98^{th} percentile, 3-year

average). Therefore, there was a negligible predicted source contribution to the surface $PM_{2.5}$ values from the major line and point sources modeled in HFX domain. The other known sources of $PM_{2.5}$ in the HFX domain, that were not included in the model simulation may include, but are not limited to, other line sources, domestic emissions, suspended surficial dust, sea salt and long range transport (Waugh, 2006).

From Figure 67 it can be observed that SO_2 does not show a strong association with major line sources. This can be explained by SO_2 being more strongly associated with power generation, the hospitals and universities in Halifax that burn high sulfur fuel compared to line sources that use low sulfur fuel (Hingston, 2005).

With reference to Figure 68, the highest annual average AERMOD predicted $PM_{2.5}$ value was found to be 2.69 $\mu g\ m^{-3}$ at the intersection of highway 102 and 118 (x-452728.48m: y-4960725.93m), elevation 81.5 m. This contrasts with an annual average observed $PM_{2.5}$ concentration at the Lake Major NAPS site of 4.1 $\mu g\ m^{-3}$ for the same period. It was found on average that the AERMOD predicted $PM_{2.5}$ concentration at the Lake Major NAPS site was a factor of 26 lower than the observed $PM_{2.5}$ concentration. The main sources of $PM_{2.5}$ in this area are vehicle emissions from highway 102, 107, 118 and the Forest Hills Extension. Other sources of $PM_{2.5}$ include fossil fuel combustion for domestic space heating, sea salt, fugitive surficial dust, fugitive emissions from a nearby gravel quarry, agricultural activity and long range transport. Only point sources and major line sources (highway 102, 107 and 118) were included in the AERMOD monthly average predictions for Lake Major. The remaining sources mentioned above were not included in the AERMOD model simulation. This probably explains why there was a factor of 25 under prediction by AERMOD of surface $PM_{2.5}$ concentrations at Lake Major. This demonstrates that the point and major line sources in the Halifax domain do not significantly impact surface $PM_{2.5}$ concentrations at the Lake Major NAPS site. Indeed, even the highest predicted $PM_{2.5}$ concentration (2.69 $\mu g\ m^{-3}$) found in the Halifax domain is a factor of 1.3 lower than the annual average observed at Lake Major.

The AERMOD predicted surface NO_x concentrations for the NAPS station were on average a factor of 21 lower than observed value. The reason for the poor correlation and the large difference between the monthly predicted and observed is likely due to AERMOD modeling

only a small portion of the total NO_x emissions in Halifax. The main sources of NO_x in Halifax are from vehicles and AERMOD only modeled emissions from 3 highways and 3 main roads in the Halifax domain. None of the vehicle emissions from the downtown Halifax streets surrounding the NAPS site were modeled. It is known that NO_x is predominately associated with local emission sources such as vehicle emissions. (Hingston, 2005)Ship and domestic heating NO_x emission sources were also not included in the AERMOD model simulations. This likely explains the vast difference between the AERMOD predicted and observed NO_x concentrations shown in Figure 66. However, this result is insightful as it demonstrates that the NO_x emissions from the point and the 6 major lines sources modeled are predicted to have little impact on surface NO_x concentrations in the HFX domain. From Figure 66 it can also be seen that there is good agreement between the predicted and the observed trend in NO_x concentrations ($R^2 = 0.68$).

The comparison between observed and predicted SO_2 illustrated in Figure 4.70 shows that the model under predicts by a factor of 1.5 for the downtown Halifax NAPS station. However, with the exception of September, there was good agreement seen in the trend between the AERMOD predicted and observed the SO_2 ($R^2 = 0.77$). In the month of July the model under predicts by a factor of 2.0. The month of July also corresponds to the height of cruise liner visits to Halifax Harbor (Hingston, 2005). Cruise liners (and Cargo vessels) are known to use "Bunker" fuel high with a high S-content. Therefore, the increased ship SO_2 emissions and the fact these emission were not included in the AERMOD simulations, probably explains the factor of 2.0 model under prediction for July. However, it can be seen in Figure 11 that AERMOD over predicted the observed by SO_2 within a factor of 1.5 in the month of September. It is known that AERMOD can over predict lower observed concentrations and also during stable conditions and this may help to explain the model over prediction for September. {Perry, 2005 #892} It is known that by far the largest SO_2 emission source (81%) in Halifax is from Tuffs Cove Power station, IWK/VG Hospitals and Dartmouth Refinery (Hingston, 2005) (Bryden, 2009). The explanation for the relatively small difference (< factor of 2.0) between the predicted and observed in Halifax is probably due to the fact that these sources were captured by the model.

Hourly averaging show better agreement between the observed and AERMOD predicted ground level concentrations of $PM_{2.5}$, NO_x and SO_2. Over prediction by the model are seen during late morning and afternoons, which could be the effect of albedo.

Sydney

Figure 81 demonstrates a comparison of the AERMOD monthly average (March through October 2004) predicted surface SO_2 concentrations with NAPS observations at the same coordinates. It can be seen in Figure 81 that the lowest SO_2 observed concentration occurs in April (1.4 µg m^{-3}) and the lowest SO_2 predicted concentration occurred in May (1.2 µg m^{-3}). The highest SO_2 observed concentration occurred in July (3.0 µg m^{-3}) and the highest SO_2 predicted concentration also occurred in July (4.62 µg m^{-3}). There was no significant difference (p=0.439) between the monthly averaged AERMOD predicted and observed SO_2 concentrations. It can also be seen in Figure 81 that there is very good agreement (R^2 of 0.68) between the predicted and observed SO_2 in the SYD domain. The predicted annual mean SO_2 found at the NAPS site coordinates was 2.33 µg m^{-3} compared to the NAPS observed concentration of 2.08 µg m^{-3}.

Figure 81 Predicted vs NAPS observed monthly SO_2 concentrations in SYD domain

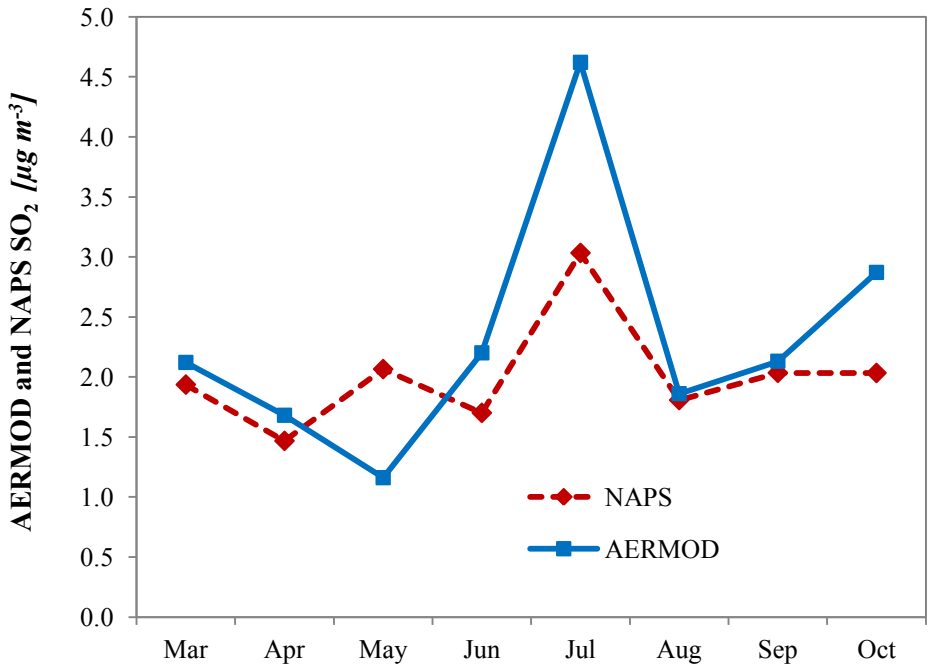

It can be seen from Figure 82 that the NAPS observed SO_2 concentration are higher than the AERMOD predicted SO_2 concentrations during 1-hr, 3-hr, 12-hr and 24-hr averaging periods. During 8-hr averaging period the model under predicted the concentration by a factor of 2.2. There is very poor correlation (R^2 = 0.003) between the predicted and observed over the hourly averaging periods throughout the day.

Figure 82 Predicted vs NAPS observed hourly SO_2 concentrations in SYD domain

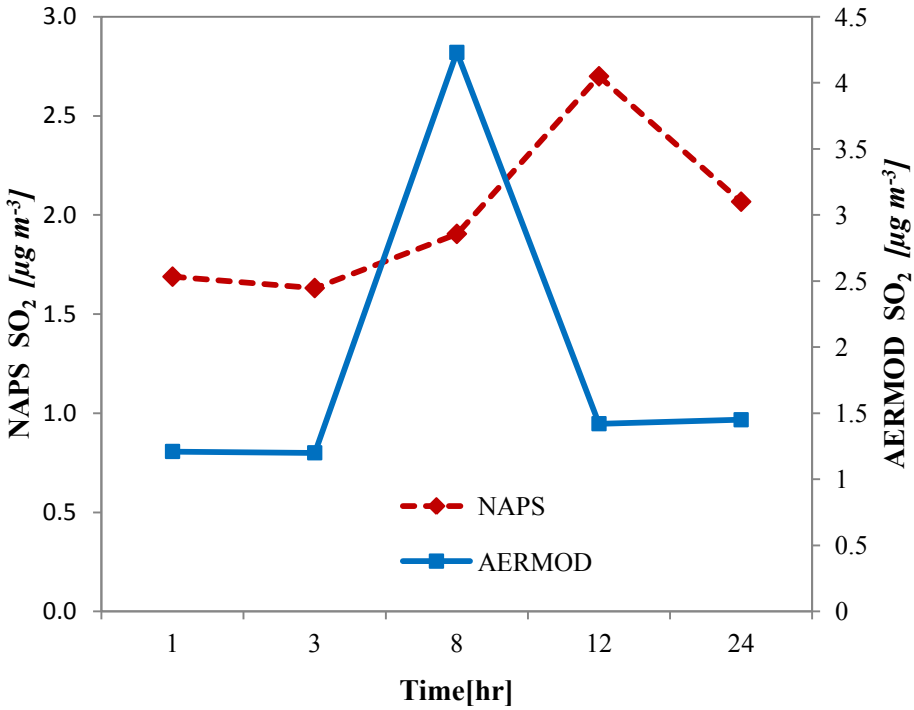

From Figure 81 it can be clearly seen that the dispersion pattern of SO_2 is directly downwind of the Lingan Power Station. AERMOD predicted highest SO_2 concentration of 8.7 µg m^{-3} at a receptor 2.5 km NE (x-729057.69m: y-5121953.62m) of the Lingan Power Station. The chief source of SO_2 emissions in the SYD domain is the Lignan Power Station. The good agreement (R^2 = 0.68) between the predicted (2.3 µg m^{-3}) and observed (2.1 µg m^{-3}) SO_2 at the SYD NAPS site is probably due to the dominant SO_2 emitter (Lingan Power Station) being included in the model simulation for the SYD domain. This result demonstrates that AERMOD can satisfactorily model the dispersion of SO_2 emission in a domain of this size if the major sources are included in the model.

Hourly averaging showed poor performance of the model compared to monthly averaging.

Port Hawkesbury

Figure 83 provides a comparison of the AERMOD monthly average predicted surface SO_2 concentrations with NAPS observations at the same location in the PRTHAWKS domain. It can be seen in Figure 83 that the lowest observed SO_2 concentration occurred in September (0.37 µg m^{-3}) and the lowest predicted SO_2 concentration was in September (0.1 µg m^{-3}). The highest monthly observed SO_2 concentration occurred in April (4.1 µg m^{-3}) and the highest predicted monthly SO_2 concentration also occurred in April (9.3 µg m^{-3}). Over the 12-month comparative period there was on average a factor of 8.8 differences between the predicted and observed SO_2 in PRTHAWKS. It can also be observed from Figure 83 that there was poor agreement between the predicted and observed trend (R^2 = 0.18) with some large over predictions for the months of April, July and November. The predicted annual mean SO_2 found at the NAPS site coordinates was 1.68 µg m^{-3} compared to the NAPS observed concentration of 2.2 µg m^{-3}.

Figure 83 Predicted vs NAPS observed monthly SO_2 concentrations in PRTHWKS domain

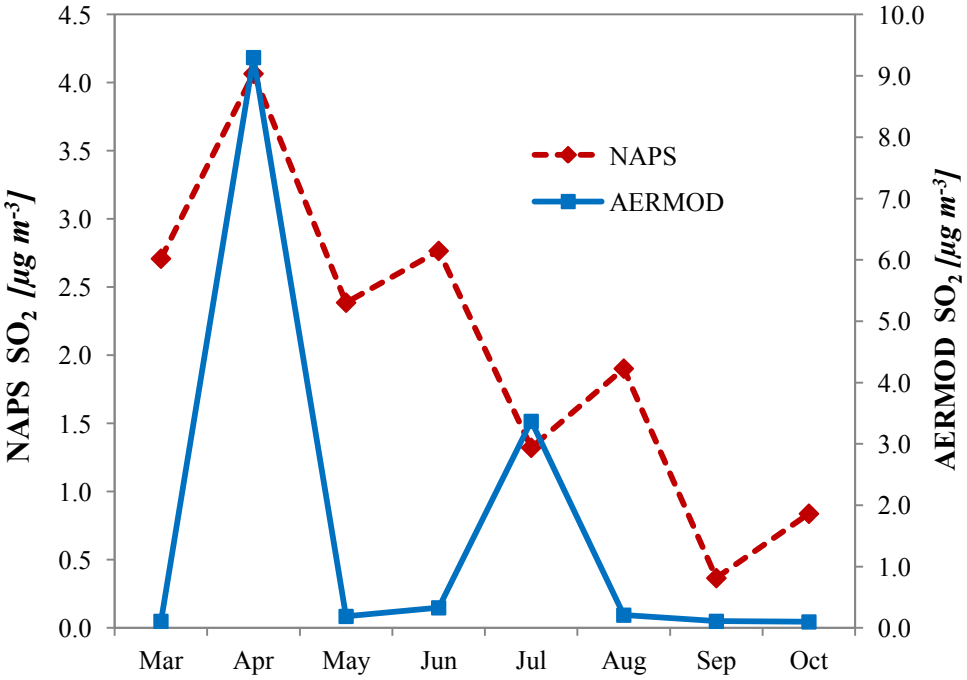

It can be seen from Figure 84 that the NAPS observed SO_2 concentration are higher than the AERMOD predicted SO_2 concentrations during 1-hr, 3-hr, 12-hr and 24-hr averaging periods. During 8hour averaging period the model under predicted the concentration by a factor of 1.2. There is very poor correlation (R^2 = 0.16) between the predicted and observed over the hourly averaging periods throughout the day.

Figure 84 Predicted vs NAPS observed hourly SO_2 concentrations in PRTHWKS domain

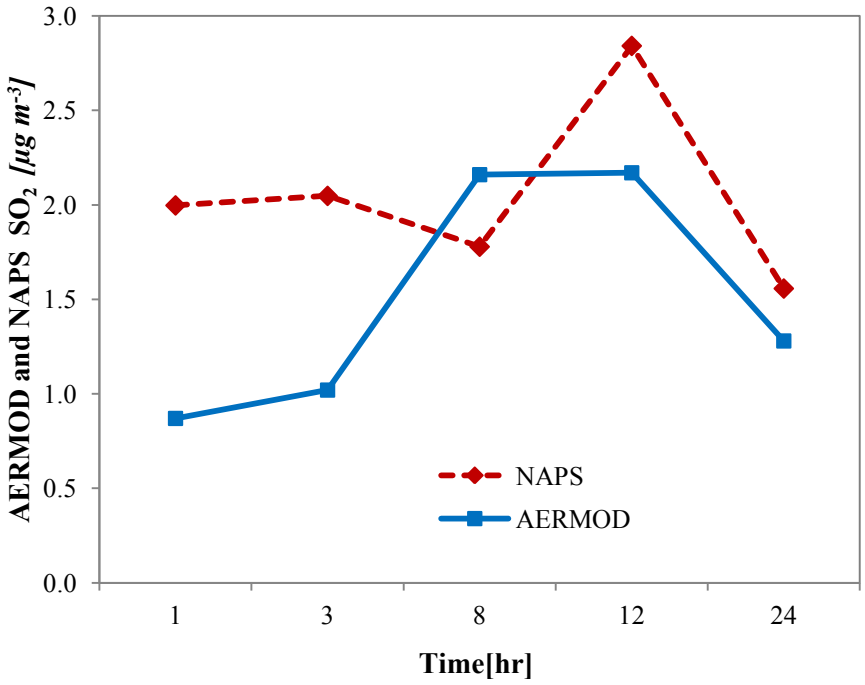

On average the difference between the predicted and observed SO_2 concentrations at Port Hawkesbury NAPS station was factor of 8.6. One possible reason may be SO_2 emissions from shipping in the area that were not included in the AERMOD simulations. From Figure 13 it can be seen that AERMOD over predicted the SO_2 concentrations for months of April, July and November at the NAPS station. Again, it is known that AERMOD can over predict when compared to low ambient concentrations and during stable conditions (A. J. Cimorelli et al., 2005). The chief emission sources in the PRTHWKS domain include the New Page industry and Exxon Mobil Inc. and state highways. With reference to Figure 45, the dispersion pattern from New Page industry can be seen to be influenced by the prevailing wind from the South West. Hourly averaging show better agreement between the observed and AERMOD predicted concentrations compared to monthly averaging (R^2 = 0.16).

Pictou

Figure 85 compares the monthly average AERMOD predicted and monthly averaged observed $PM_{2.5}$ concentration in the PIC domain. It can be seen in Figure 85 that the lowest observed $PM_{2.5}$ concentration occurred in January (5.1 µg m^{-3}) and the lowest predicted $PM_{2.5}$ concentration also occurring in January (0.16 µg m^{-3}). The highest observed $PM_{2.5}$ concentration occurred in July (11.9 µg m^{-3}) and the highest predicted $PM_{2.5}$ concentration was also in July (0.48 µg m^{-3}). Over the 11-month comparative period the predicted $PM_{2.5}$ was found to be a factor of 25 lower than the observed $PM_{2.5}$ in PIC. The observed and predicted $PM_{2.5}$ concentrations at the NAPS site (Figure 4.73) were well correlated (R^2 of 0.65). Predicted annual mean SO_2 found at the NAPS site coordinates was 0.26 µg m^{-3} compared to the NAPS observed concentration of 7.2 µg m^{-3}.

Figure 85 Predicted vs NAPS observed monthly $PM_{2.5}$ concentrations in PIC domain

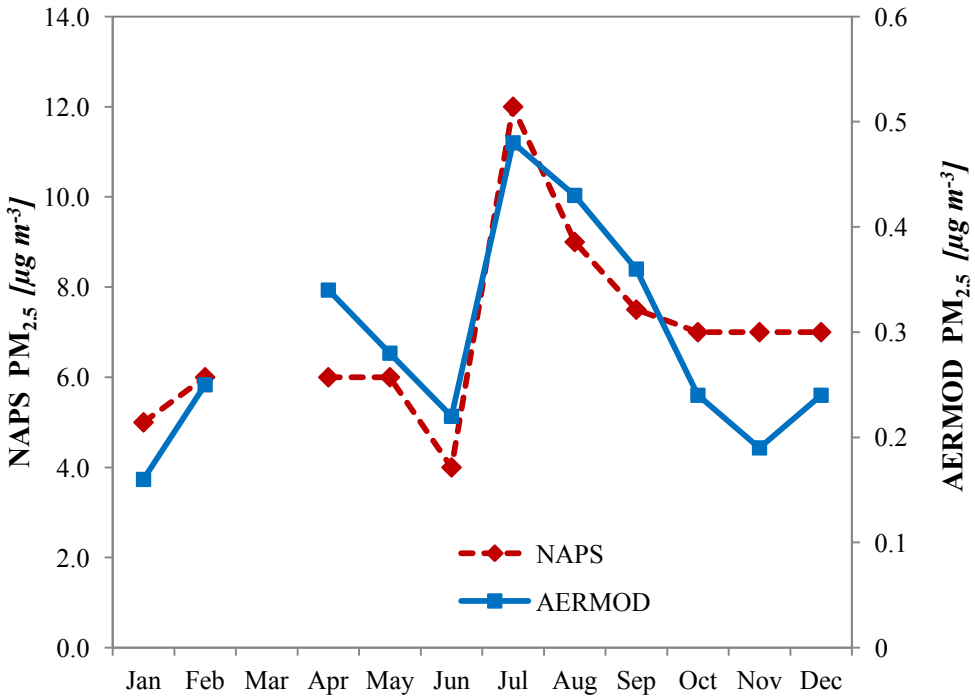

It can be seen from Figure 86 that the NAPS observed $PM_{2.5}$concentration are always higher than the AERMOD predicted $PM_{2.5}$ concentrations. During 24-hr averaging period the

model under predicted the concentration by a factor of 33.3. There is a poor correlation (R^2 = 0.003) between the predicted and observed over the hourly averaging periods throughout the day.

Figure 86 Predicted vs NAPS observed hourly $PM_{2.5}$ concentrations in PIC domain

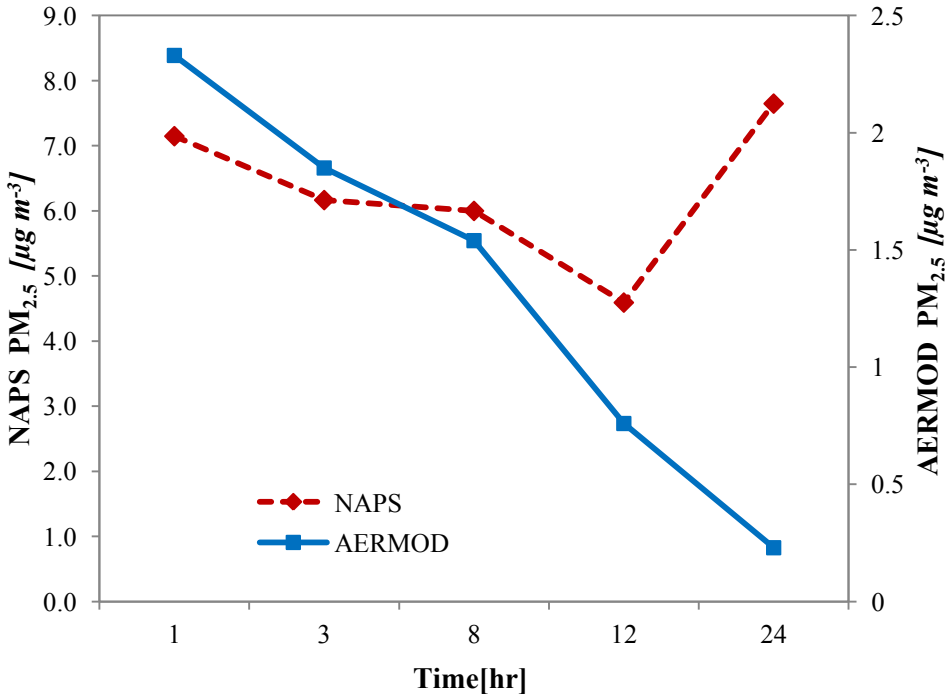

With reference to Figure 85 AERMOD under predicted the annual averaged $PM_{2.5}$ value at Pictou NAPS station by a factor of 25 due to point and highway emission sources included in this study. The major emission sources in this domain include agricultural activity, domestic combustion, small-scale industries and highways. The Neenah paper industry, highways 104 and 106 had little impact on observed surface $PM_{2.5}$ concentrations at the Pictou NAPS station coordinates. It was found that the highest predicted $PM_{2.5}$ was 0.88 µg m^{-3} found 6km west of junction of highways 104 and 106at coordinates(x-521921.73m:y-5052591.37m), elevation 30.1m MSL. Hourly comparison show poor performance of the model.

Hourly averaging indicates higher factor of under prediction by the model than the monthly averaging.

CHAPTER 5: CONCLUSIONS AND RECOMMENDATIONS

Based upon the results of AERMOD simulations conducted in this study and comparison between NAPS monitored ambient NO_x, SO_2 and $PM_{2.5}$ values, the following conclusions can be made.

In all seven domains, air contaminants dispersal was in line with the prevailing wind direction. If the point source, with a release height 100m or greater is situated in the downwind direction, it has negligible effect on GLC within the model domain. In LNN and TRR domains, vehicle emissions tend to have more of a strong local impact than point sources and therefore they are the dominant contributor to GLCs in these domains. The release height of the vehicle emission is very low compared to point sources; as a result higher ground level concentrations are seen in close proximity to the highways.

In HFX domain, the coordinates of AERMOD predicted highest NO_x and SO_2 GLCs indicate that the point source emissions and prevailing wind direction impacted the dispersal of above two pollutants. On the other hand, the coordinates of model predicted highest $PM_{2.5}$ GLC indicates that the highway emission and prevailing wind direction had major influence on the dispersal of $PM_{2.5}$. Model predictions in HFX domain also demonstrated that the GLCs of NO_x, SO_2 and $PM_{2.5}$ were higher in winter months compared to the GLCs in summer months.

AERMOD predicion results showed that the distance between the emission sources and the highest GLC receptor of NO_x, SO_2 and $PM_{2.5}$ was minimum in HFX domain and maximum in PIC domain respectively.

No significant variation was seen in model predicted GLCs of NO_x, SO_2 and $PM_{2.5}$ in summer and winter months in SYD domain. In HFX, PRTHWKS, PIC and SYD domains, maximum dispersal of the pollutants takes place during 8 hour through 12 hour averaging period under unstable atmospheric condition produced by thermally convective solar radiation.

The comparison study between predicted and observed surface concentrations demonstrates that AERMOD has a tendency to over predict the GLCs of NO_x, SO_2 and $PM_{2.5}$ for shorter averaging periods and under predict for longer averaging periods. This study highlights that the point and

major line sources of $PM_{2.5}$ and NO_x had only a negligible contribution to surface concentrations in the Halifax domain when compared to observed values at the NAPS station. AERMOD was able to closely predict the observed surface concentrations of SO_2 in Halifax within a factor of 1.5. Good agreement (R^2 = 0.77) was also seen with the observed monthly trend in SO_2 concentrations in the HFX domain due to the fact that, the main source of SO_2 in Halifax is from point sources which are included in the model. The Lingan Power Station in SYD was shown to be the dominant source of surface SO_2 with simulation results showing very good agreement with the monthly observed SO_2 concentrations.

It can be seen from the dispersion pattern that the main source of SO_2 influencing surface concentrations in PRTHWKS domain is from point sources, showing enhanced concentration gradients directly downwind of these facilities. However, the AERMOD SO_2 predictions in the PRTHWKS domain were on average a factor of 8.6 below the observed concentrations. Although AERMOD predictions followed closely the observed SO_2 concentration trends in the HFX and SYD domains, it appears that this was not the case for PRTHAWKS. The other sources such as ship emissions, of SO_2 may have impacted the airshed.

AERMOD predictions for $PM_{2.5}$ in the PIC domain were a factor 25 lower than observed values, implying that AERMOD did not model all source inputs of $PM_{2.5}$ in this domain. However, it can be seen that the predicted monthly trend in $PM_{2.5}$ closely follows that of the observed $PM_{2.5}$. Perhaps the emission factors may have to be rechecked for this domain.

By comparing the predicted air pollutant concentrations with the observed values it was shown that AERMOD can predict SO_2 within a factor of 2 in Halifax and Sydney. Due to AERMOD not having a complete emissions inventory, the predicted surface concentrations of SO_2 in Port Hawkesbury, $PM_{2.5}$ and NO_x in Halifax and $PM_{2.5}$ in Pictou were far lower than the observed values. Therefore, it is difficult to evaluate the accuracy of the AERMOD simulations for these metrics at those locations when the emission inventories were incomplete. However, AERMOD can provide some insight into the potential source contribution of $PM_{2.5}$, NO_x and SO_2 to surface air quality, at any coordinate with the domain, from the point and major line sources.

In addition, the AERMOD simulation results can also be used to assess community exposure to the air pollutants and to inform airshed management decisions.

Future work is needed to generate more accurate emission rate calculations by gathering information about the actual operation time of the point sources as the industrial units can sometimes be shut down for maintenance resulting in lower emissions than modeled. This in turn would help in specifying the emission factors in the model. More accurate emission rates can be achieved by exacting the vehicle count for each vehicle type e.g. the number of gasoline, diesel, electric vehicle, gasoline vehicle etc. under main categories such as light-duty commercial vehicle, light-duty passenger vehicle, and heavy-duty commercial vehicle on road etc.

Characteristics of the area emission sources such as construction activity and domestic heating have to be made available. The number of meteorological stations has to be increased for collection and documentation of long term meteorological data to increase the efficiency of the model performance. It is strongly recommended to have more upper air data collection sites near to the surface air station. It is recommended that emissions data for roads and streets be also included in the model to better improve predictions of NO_x dispersion in these domains, especially for Halifax. In terms of other point sources in Halifax, it is recommended that ship emissions should also be considered in the model input as this is also recognized as a major point source in Halifax.

GIS database could be prepared with more complete emission inventory. All of the above recommendations will help to improve predictions of the various air pollutant dispersion scenarios across the province in future.

REFERENCES

AERMOD Implementation Workgroup. (2009). *AERMOD IMPLEMENTATION GUIDE.* Retrieved from http://www.epa.gov/scram001/7thconf/aermod/aermod_implmtn_guide_19March2009.pdf

Agarwal, M., & Tandon, A. (2010). Modeling of the urban heat island in the form of mesoscale wind and of its effect on air pollution dispersal. *Applied Mathematical Modelling, 34*(9), 2520-2530. doi:DOI: 10.1016/j.apm.2009.11.016

Anfossi, D., Brusasca, G., & Tinarelli, G. (1990). Tinarelli, G., 1990. simulation of atmospheric diffusion in low wind speed meandering conditions by monte-carlo dispersion model. *Il Nuovo Cimento, 13c*, 995.

Arya, S. P. (1988). *Introduction to micrometerology*. San Diego, California: Academic Press.

Ashrafi, K., & Hoshyaripour, G. A. (2010). A model to determine atmospheric stability and its correlation with CO concentration. *International Journal of Civil and Environmental Engineering, 2*(2)

Atari, D. O., Luginaah, I., Xu, X., & Fung, K. (2008). Spatial variability of ambient nitrogen dioxide and sulfur dioxide in sarnia, chemical valley, ontario, canada. *Journal of Toxicology and Environmental Health, Part-A, 71*, 1572.

Bascom, R. (1996). Environmental factors and respiratory hyper sensitivity: The americas. *Toxicology Letters, 86*(2-3), 115-130. doi:DOI: 10.1016/0378-4274(96)03682-X

Bass, A., Benkley, C. W., Scire, J. S., & Mories, C. S. (1979). No. EPA 600/7-80-056). Research Triangle Park, NC.: US Environmental Protection Agency.

Beelen, R., Hoek, G., van den Brandt, Piet A., Goldbohm, R. A., Fischer, P., Schouten, L. J., . . . Brunekreef, B. (2008). Long-term effects of traffic-related air pollution on mortality in a dutch cohort (NLCS air-study). *, 116*(2)

Bell, M. L., Davis, D. L., & Fletcher, T. (2004). A retrospective assessment of mortality from the london smog episode of 1952: The role of influenza and pollution. *Environmental Health Perspectives, 112*(1)

Bell, M. L., & Davis, D. L. (2001). Reassessment of the lethal london fog of 1952: Novel indicators of acute and chronic consequences of acute exposure to air pollution. *Environmental Health Perspectives, 109*(3)

Bennett, M., & Hunter, G. C. (1997). Some comparisons of lidar estimates of peak ground-level concentrations with the predictions of UK-ADMS. *Atmospheric Environment, 31*(3), 429-439. doi:DOI: 10.1016/S1352-2310(96)00220-8

Benson, P. (1989). *Caline 4 – a dispersion model for predicting air pollution concentrations near roadways.* Sacramento, CA: Division of New Technology and Research, Department of Transportation,.

Boznar, M., Lesjak, M., & Mlakar, P. (1993). A neural network-based method for short-term predictions of ambient SO2 concentrations in highly polluted industrial areas of complex terrain. *Atmospheric Environment.Part B.Urban Atmosphere, 27*(2), 221-230. doi:DOI: 10.1016/0957-1272(93)90007-S

Brunekreef, B., Janssen, N. A. H., de Hartog, J., Harssema, H., Knape, M., & van Vilet, P. (1997). Air pollution from truck traffic and lung function in children living near motorway. *Epidemiology, 8*, 298.

Bryden, B. (2009). The air we breathe. nova scotia's air quality report, 2000 - 2007., 1-48.

Carruthers, D. J., Edmunds, H. A., Bennet, M., Wood, P. T., Milton, M. J. T., Robinson, R., . . . Timmis, R. (1997). Validation of the ADMS dispersion model and assessment of its performance relative to R-91 and ISC using archived LIDAR data. *International Journal of Environment and Pollution, 8*(3-6), 264.

Carslaw, D. C., & Beevers, S. D. (2002). Dispersion modelling considerations for transient emissions from elevated point sources. *Atmospheric Environment, 36*(18), 3021-3029. doi:DOI: 10.1016/S1352-2310(02)00231-5

Cermak, J. E. (1996). Thermal effects on flow and dispersion over urban areas: Capabilities for prediction by physical modeling. *Atmospheric Environment, 30*(3), 393-401. doi:DOI: 10.1016/1352-2310(95)00142-5

Churg, A. (1996). The uptake of mineral particles by pulmonary epithelial cells. *American Journal of Respiratory and Critical Care Medicine, 154*(46), 1124.

Cimorelli, A. J., Perry, S. G., Venkatram, A., Weil, J. C., Paine, R. J., Wilson, R. B., . . . Peters, W. D. (2003). *AERMOD:Description of model formulation.* No. EPA 454/R-03-002d, 85 pp).U.S. Environmental Protection Agency.

Cimorelli, A. J., Perry, S. G., Venkatram, A., Weil, J. C., Paine, R. J., Wilson, R. B., . . . Brode, R. W. (2005). AERMOD: A dispersion model for industrial source applications. part I: General model formulation and boundary layer characterization. *Journal of Applied Meteorology, 44*, 682.

Colls, J. (2002). *Air pollution* (2nd ed.). New York: Clay's Library of Health and the Environment.

De Gouw, J. A., Brock, C. A., Atlas, E. L., Bates, T. S., Fehsenfeld, F. C., Goldan, P. D., . . . Williams, E. J. (2008). Sources of particulate matter in the northeastern united states in summer. *JOURNAL OF GEOPHYSICAL RESEARCH, 113*(D08301)

Dockery, D. W., Arden Pope III, C., Xu, X., Spengler, J. D., Ware, J. H., Fay, M. E., . . . Speizer, F. E. (1993). An association between air pollution and mortality in six U.S. cities. *The New England Journal of Medicine, 329*(24), 1753.

Dongarrà, G., Manno, E., Varrica, D., Lombardo, M., & Vultaggio, M. (2010). Study on ambient concentrations of PM10, PM10–2.5, PM2.5 and gaseous pollutants. trace elements and chemical speciation of atmospheric particulates. *Atmospheric Environment, 44*(39), 5244-5257. doi:10.1016/j.atmosenv.2010.08.041

ESRI, S. (2008). *ArcGIS v9.3* . 380 New York Street , Redlands, CA 92373-8100:

Fedorovich, E., Kaiser, R., Rau, M., & Plate, E. (1996). Wind tunnel of turbulent flow structure in the COnvective boundary layer capped by inversion layer. *Journal of Atmospheric Sciences, 53*(9), 1273.

Gabriel, M., Williamson, D., & Brooks, S. (2005). Atmospheric speciation of mercury in two contrasting southeastern US airsheds. *Atmospheric Environment, 39*, 4947.

Garcia, J. H., Lia, W., Arimotob, R., Okrasinskic, R., Greenleed, J., Waltona, J., . . . Sageb, S. (2004). Characterization and implication of potential fugitive dust sources in the paso del norte region. *The Science of the Total Environment, 325*, 95-112.

Gibson, M. D., Bache, D. H., Hursthouse, A. S., Beverland, I. J., Craig, S. E., Clark, C. F., . . . Jones, C. (2009). Using mass reconstruction along a four-site transect as a method to interpret 1 PM10 in

west

central scotland, UK. *Journal of the Air and Waste Management Association, 59*(12), 1429-1436.

Gibson, M. D., Guernsey, J. R., Beauchamp, S., Waugh, D., Heal, M. R., Brook, J. R., . . . Terashima, M. (2009). Quantifying the spatial and temporal variation of ground-level ozone in the rural annapolis valley, nova scotia, canada using nitrite-impregnated passive samplers. *Journal of Air & Waste Management. Association, 59*, 310-320.

Gibson, M., Potter, R., Guernsey, J., Ward, T., Wheeler, A., Stieb, D., . . . Bazinet, P. (2010). Woodsmoke source apportionment in the rural annapolis valley, nova scotia, canada. Calgary.

Gildemeister, A., Graney, J., & Keeler, G. (2005). Source proximity reflected in spatial and termporal variability in particle and vapor phase hg concentrations in detroit, MI. *Atmospheric Environment, 39*(8), 53.

Green, W. A. (2008). *Nova scotia comprehensive air pollutant emission source inventory.*Nova Scotia Environment, Air Quality Branch.

Grosch, T. G., & Lee, R. F. (1998). *Sensitivity of the AERMOD air quality model to the selection of land use parameters.* Retrieved 1st May, 2009, 2009, from http://www.environmental-expert.com/Files%5C20658%5Carticles%5C4842%5Ctp_wessex99.pdf

Hanna, S. R., Chang, J. C., & Fernau, M. E. (1998). Monte carlo estimates of uncertainties in predictions by a photochemical grid model(UAM-IV) due to uncertainties in input variables. *Atmospheric Environment, 32*, 3619.

Harrison, R. M., Andrew, R. D., & Jones, M. R. (1997). SOURCES AND PROCESSES AFFECTING CONCENTRATIONS OF PMlo AND PM2.5 PARTICULATE MATTER IN BIRMINGHAM (U.K.). *Atmospheric Environment, 31*(24), 4103.

Hingston, M. (2005). *An assessment of marine vessel emissions and their contribution to air quality in halifax harbour for the year 2002.*

Hoare, A., Regan, D. G., & Wilson, D. P. (2008). Sampling and sensitivity analyses tools (SaSAT) for computational modelling . *Theoretical Biology and Medical Modelling, 5*(4)

Holmes, N. S., & Morawska, L. (2006). A review of dispersion modelling and its application to the dispersion of particles: An overview of different dispersion models available. *Atmospheric Environment, 40*(30), 5902-5928. doi:10.1016/j.atmosenv.2006.06.003

Holzworth, G. C. (1972). Mixing heights, wind speeds and potential for urban pollution throughout the contiguous united states. *AP-101,* , 118.

James, K. J., Cherry, M., & Stack, M. A. (1995). Assessment of chemical plant emissions on an urban environment: A new approach to air quality measurements. *Chemosphere, 31*(7), 3741-3751. doi:DOI: 10.1016/0045-6535(95)00223-U

Jesse, L., Cristiane, L., & Michael, A. (2000). *User's guide ISCAERMOD view.* No. Volume I & Volume II). Ontario, Canada: Lakes Environmental Pt. Ltd.

Johnson, M., Isakov, V., Touma, J. S., Mukerjee, S., & Özkaynak, H. (2010). Evaluation of land-use regression models used to predict air quality concentrations in an urban area. *Atmospheric Environment, 44*(30), 3660-3668. doi:10.1016/j.atmosenv.2010.06.041

Kampa, M., & Castanas, E. (2008). Human health effects of air pollution. *Environmental Pollution, 151*(2), 362-367. doi:DOI: 10.1016/j.envpol.2007.06.012

Katsouyanni, K. (2003). Ambient air pollution and health. *Br Med Bull, 68*(1), 143.

Kellerhals, M., Beauchamp, S., Belzer, W., Blanchard, P., Froude, F., Harvey, B., . . . Tordon, R. (2003). Temporal and spatial variability of total gaseous mercury in canada: Results from the canadian atmospheric mercury measurement network (CAMNet). *Atmospheric Environment, 37*, 1003.

Kesarkar, A. P., Dalvi, M., Kaginalkar, A., & Ojha, A. (2007). Coupling of the weather research and forecasting model with AERMOD for pollutant dispersion modeling. A case study for PM10 dispersion over pune, india. *Atmospheric Environment, 41*(9), 1976-1988. doi:DOI: 10.1016/j.atmosenv.2006.10.042

Krautstrunk, M., Neumann-Hauf, G., Schlager, H., Klemm, O., Beyrich, F., Corsmeier, U., . . . Kotzian, M. (2000). An experimental study on the planetary boundary layer transport of air pollutants over east germany. *Atmospheric Environment, 34*(8), 1247-1266. doi:DOI: 10.1016/S1352-2310(99)00124-7

Krewski, D., Burnett, R. T., Goldberg, M., Hoover, K., Siemiatycki, J., Abrahamowicz, M., . . . White, W. (2005). Reanalysis of the harvard six cities study, part II: Sensitivity analysis. *Inhalation Toxicology, 17*, 343.

La Spina, A., Burton, M., & Salerno, G. G. (2010). Unravelling the processes controlling gas emissions from the central and northeast craters of mt. etna. *Journal of Volcanology and Geothermal Research, 198*(3-4), 368-376. doi:10.1016/j.jvolgeores.2010.09.018

Lakes Environmental. (2008). *AERMOD course guide*

Lee, S., & Keener, T. C. (2008). Dispersion modeling of mercury emissions from coal-fired power plants at coshocton and manchester, ohio.*108*(n4), 65.

Lee, D. S., Dollard, G. J., & Pepler, S. (1998). Gas-phase mercury in the atmosphere of the united kingdom. *Atmospheric Environment, 32*(5), 855-864. doi:DOI: 10.1016/S1352-2310(97)00316-6

Lu, G., Brook, J. R., Alfarra, M. R., Anlauf, K., Leaitch, W. R., Sharma, S., . . . Phinney, L. (2006). Identification and characterization of inland ship plumes over vancouver, BC. *Atmospheric Environment, 40*, 2767.

Manolopoulos, H., Snyder, D., Schauer, J., Hill, J., Turner, J., Olson, M., & Krabbenhoft, D. (2007). Sources of speciated atmospheric mercury at a residential neighborhood impacted by industrial sources. *Environmental Science & Technology, 41*, 5626.

Masters, G. M. (1997). Introduction to environmental engineering and science. In (2nd ed.,). Upper Saddle River, New Jersey, 07458: Prentice Hall.

Mazur, M., Mintz, R., Lapalme, M., & Wiens, B. (2009). Ambient air total gaseous mercury concentrations in the vicinity of coal-fired power plants in alberta, canada. *Science of the Total Environment, 408*(2), 373-381. doi:DOI: 10.1016/j.scitotenv.2009.10.006

Mehdizadeh, F., & Rifai, H. S. (2004). Modeling point source plumes at high altitudes using a modified gaussian model. *Atmospheric Environment, 38*(6), 821-831. doi:DOI: 10.1016/j.atmosenv.2003.10.041

Moore, D. J. (1969). The distributions of surface concentrations of sulphur dioxide emitted from tall chimneys. *Philosophical Transactions of the Royal Society, 265*, 245.

National Round Table on the Environment and the Economy. (2008). *Developing ambient air quality objectives for canada.* No. TD883.7.C3D48).

Neupane, B., Jerrett, M., Burnett, R. T., Marrie, T., Arain, A., & Loeb, M. (2010). Long-term exposure to ambient air pollution and risk of hospitalization with community-acquired pneumonia in older adults. *AMERICAN JOURNAL OF RESPIRATORY AND CRITICAL CARE MEDICINE, 181*, 47.

Okamoto, S., & Shiozawa, K. (1978). Validation of an air pollution model for the keihin area. *Atmospheric Environment (1967), 12*(11), 2139-2149. doi:DOI: 10.1016/0004-6981(78)90169-5

Oke, T. R. (1978). Boundary layer climates. In (pp. 372) John Wiley and Sons.

Otte, T. L., Pouliot, G., Pleim, J. E., Young, J. O., Schere, K., Wong, D. C., . . . Seaman, N. L. (2005). Linking the eta model with the community multiscale air quality (CMAQ) modeling system to build a national air quality forecasting system. *NCEP Notes,* , 367.

Pearson, R. L., Watchel, H., & Ebi, K. L. (2000). Distance-weighted traffic density in proximity to a home is a risk factor for leukemia and other childhood cancers. *Journal of the Air and Waste Management Association, 50*, 175.

Perry, S. G., Cimorelli, A. J., Lee, R. F., Paine, R. J., Venkatram, A., Weil, J. C., & Wilson, R. B. (1994). AERMOD: A dispersionmodel for industrial source applications. *, 94-TA2.3.04, 16 pp*

Petersen, R. L., & Parce, D. K. (1993). EFFECT OF A NEARBY HILL ON GOOD ENGINEERING PRACTICE STACK HEIGHT. *86th Annual AWMA Conference,*

Pope, C. A. I. (2000). What do epidemiological findings tell us about health effects of environmental aerosols? *Journal of Aerosol Medicine, 13*(4), 335-354.

Pope, C. A. (1996). Adverse health effects of air pollutants in a nonsmoking population. *Toxicology, 111*(1-3), 149-155. doi:DOI: 10.1016/0300-483X(96)03372-0

Pöschl, U. (2005). Atmospheric aerosols: Composition, transformation, climate and health effects.*44*(46), 7520.

Raman, S. S., & Cermak, J. E. (1975). Physical modeling of flow and diffusion over an urban heat island. In F.N. Frenkiel and R.E. Munn (Ed.), *Advances in geophysics* (pp. 223-240) Elsevier. doi:DOI: 10.1016/S0065-2687(08)60582-8

Rao, S. T., Sistla, G., Keenan, M. T., & Wilson, J. S. (1980). An evaluation of some commonly used highway dispersion models. *Atmospheric Environment, 20*, 1095.

Riga-Karandinos, A., & Saitanis, C. (2005). Comparative assessment of ambient air quality in two typical mediterranean coastal cities in greece. *Chemosphere, 59*(8), 1125-1136. doi:10.1016/j.chemosphere.2004.11.059

Schnelle, K. B. J., & Dey, R. P. (2000). *Atmospheric dispersion modeling compliance guide*. 11 West 19th Street, New York, NY 10011: Mc Graw-Hill.

Schulman, L. L., Strimaitis, D. G., & Scire, J. S. (2000). Development and evaluation of the PRIME plume rise and building downwash model. *Air and Waste Management Association, 50*, 378.

Seinfeld, J. H., & Pandis, S. N. (2006). Atmospheric chemistry and physics - from air pollution to climate change. In (2nd ed.,) John Wiley & Sons.

Simpson, M., Raman, S., Lundquist, J. K., & Leach, M. (2007). A study of the variation of urban mixed layer heights. *Atmospheric Environment, 41*(33), 6923-6930. doi:DOI: 10.1016/j.atmosenv.2006.08.029

Snyder, D., Dallmann, T., Schauer, J., Holloway, T., & Kleeman, M. (2008). Direct observation of the break-up of a nocturnal inversion layer using elemental mercury as a tracer. *Geophysical Research Letters, 35*(L1), 7812.

Snyder, W. H., Thompson, R. E., Eskridge, R. E., Lawson, I. P., Castro, J. T., Lee, J. C., . . . Ogawa, Y. (1985). The structure of the strongly stratified flow over hills: Dividing streamline concept. *The Journal of Fluid Mechanics, 152*, 249.

Stern, A. (1976). *Air pollution* (3rd ed.). New York: Academic Press.

Stieb, D. M., Evans, G. J., Sabaliaukas, K., Chen, L., Campbell, M. E., Wheelar, A. J., . . . Guay, M. (2008). A scripted activity study of the impact of protective advice on personal exposure to ultra-fine and fine particulate matter and volatile organic compounds. *Journal of Exposure Science and Environmental Epidemiology, 18*, 495.

Stieb, D. M., Judek, S., & Burnett, R. T. (2002). Meta-analysis of time-series studies of air pollution and mortality: Effects of gases and particles and the influence of cause of death, age, and season. *Journal of Air & Waste Management. Association, 52*, 470.

Taylor, H. J., Ashmore, M. R., & Bell, J. N. B. (1986). *Air pollution injury to vegetation.* London: Institute of Environmental Health Officers.

Temme, C., Blanchard, P., Steffen, A., Banic, C., Beauchamp, S., Poissant, L., . . . Wiens, B. (2007). Trend, seasonal and multivariate analysis study of total gaseous mercury data from the canadian atmospheric mercury measurement network (CAMNet). *Atmospheric Environment, 41*(26), 5423-5441. doi:DOI: 10.1016/j.atmosenv.2007.02.021

Thad, G. (2004). *Air quality*. Boca Raton, Florida 33431: Lewis Publishers.

Tidblad, J., Kuvera, V., & Mikhailov, A. A. (1988). *Statistical analysis of 8 year material exposure and acceptable deterioration and pollution levels.* No. 30). Stockholm, Sweden: Swedish Control Institute.

Tie, X., Brasseur, G., & Ying, Z. (2010). Impact of model resolution on chemical ozone formation in mexico city: Application of the WRF-chem model [Abstract]. *Atmospheric Chemistry and Physics, 10*(18) 8629.

Transport Canada. (May 2008). *USER GUIDE FOR URBAN TRANSPORTATION EMISSIONS CALCULATOR (UTEC).*Transport Canada.

U.S. EPA. (1998). *Revised draft User's guide for the AERMOD meteorological preprocessor (AERMET).*

Valko, M., Leibfritz, D., Moncol, J., Cronin, M. T. D., Mazur, M., & Telser, J. (2007). Free radicals and antioxidants in normal physiological functions and human disease. *International Journal of Biochemistry and Cell Biology, 39*(1), 44.

Venegas, L. E., & Mazzeo, N. A. (2006). Modelling of urban background pollution in buenos aires city (argentina). *Environmental Modelling & Software, 21*(4), 577-586. doi:DOI: 10.1016/j.envsoft.2004.08.013

Venkatram, A. (1980). Dispersion in the stable boundary layer. *American Meteoreological Society,* , 229.

Venn, A. J., Lewis, S. A., Cooper, M., Hubbard, R., & Britton, J. (2001). Living near a main road and the risk of wheezing illness in children. *American Journal of Respiratory Care Medicine, 164*, 2177.

Vijay Bhaskar, R. V., Jeba, R., P, M., & Amit P, K. (2008). Measurement and modeling of respirable particulate (PM10) and lead pollution over madurai, india. *Air Quality, Atmosphere & Health, 1*(1), 45.

Wagstrom, K. M., & Pandis, S. N. (2011). Sourceereceptor relationships for fine particulate matter concentrations in the eastern united states. *Atmospheric Environment, 45*, 347.

Waugh, D. L. (2006). *Particulate matter climatology for atlantic canada* . No. En57-36/2006-4E).

Wikipedia, e. (2011). *Nova scotia.* Retrieved August 3rd, 2011, from http://en.wikipedia.org/wiki/Nova_Scotia

Zannetti, P. (1986). A new mixed segmented-puff approach for dispersion modeling. *Atmospheric Environment, 20*, 1121.

Zhou, Y., Levy, J. I., Hammitt, J. K., & Evans, J. S. (2003). Estimating population exposure to power plant emissions using CALPUFF: A case study in beijing, china. *Atmospheric Environment, 37*(6), 815-826. doi:DOI: 10.1016/S1352-2310(02)00937-8

Zou, B., Benjamin Zhan, F., Gaines Wilson, J., & Zeng, Y. (2010). Performance of AERMOD at different time scales. *Simulation Modelling Practice and Theory, 18*(5), 612-623. doi:DOI: 10.1016/j.simpat.2010.01.005